



**Aufbau und Charakterisierung eines Knochenmark-Stammzellnischen-Modells**  
**Development and characterization of a bone marrow stem cell niche model**

Doctoral thesis for a doctoral degree  
at the Graduate School of Life Sciences,  
Julius-Maximilians-Universität Würzburg,  
Section Biomedicine

submitted by

**Davide Confalonieri**

from

**Castel San Giovanni (PC), Italy**

Würzburg, 2017

**Submitted on:** .....

Office stamp

**Members of the *Promotionskomitee*:**

**Chairperson:** .....

**Primary Supervisor: Prof. Dr. Heike Walles**.....

**Supervisor (Second): Prof. Dr. Franz Jakob**.....

**Supervisor (Third): Dr. Dipl.-Ing. Jan Hansmann**.....

**Date of Public Defence:** .....

**Date of Receipt of Certificates:** .....

# Davide Confalonieri

## PhD Candidate

Würzburg, DE | 97070, Sanderring 7 | [davide.confalonieri@uni-wuerzburg.de](mailto:davide.confalonieri@uni-wuerzburg.de)

## Professional Experience

### PhD Researcher

2014-2017

Fraunhofer IGB, University Hospital (Würzburg, DE)

- **Exemplary teamwork** as demonstrated by the development of a cell-based therapy to enter the market for the regeneration of critical-size bone defects within the 7 partners of the Marie Curie BIO-Inspire European consortium, leading to the publication of 2 papers, the development of a GMP-compliant medium and the deposition of a patent;
- **Excellent international scientific communication** as evidenced by frequent traveling and monthly stays at collaborating institutions (FUJIFilm, NL; ISTECC, IT), including presentation of scientific results at 6 international conferences in Europe and U.S.;
- **Creative and application-oriented thinking** as evidenced by the development of several collaborations leading to the discovery of a possible drug target, supervision of 6 Master and Bachelor students shared with research partners and the coordination of a project for the funding of a start-up.

### Internship

2012-2013

Fondazione IRCCS Istituto Nazionale dei Tumori, Milan (IT); Ospedali Riuniti di Trieste, Trieste (IT)

- **Experience with clinical practice** through research and diagnostic activity in the Haematology and Bone Marrow Transplant Unit of the National Cancer Institute.

## Education

### PhD, Tissue Engineering and Regenerative Medicine

2014-2017

University of Würzburg, Würzburg (DE), Graduate School of Life Sciences

- Courses and seminars in Good scientific practice, Intercultural communication, Intellectual property, Scientific writing, Grant Proposal Writing, Time management, Poster design and Oral presentation, Animal trial planning and performing (FELASAC), Statistics, Quality Management and GMP-compliance.

### Center for Innovation and Entrepreneurship

2016–2017

IGZ Würzburg

- Courses in Entrepreneurship and Start-up founding, Project management, Business model canvas, Development of medicinal products and medical devices

**MSc, Medical Biotechnology and Molecular Medicine** 2011 - 2013

University of Milan, Milan (IT)

- Courses in Tissue engineering, Immunobiotechnology, Transplantology, Physiopathology, Pharmacology, Genetics, Nanotechnology, Bioinformatics

**BSc, Biotechnology** 2008 – 2011

University of Pavia, Pavia (IT)

- Courses in Molecular biology, Biochemistry, Genetics, Microbiology

## Language Proficiencies

Italian	●	●	●	●	●
English	●	●	●	●	●
German	●	●	●	●	○
French	●	●	●	○	○
Spanish	●	●	○	○	○

## Social Involvement

- **Awards:** Travel Award (TERMIS International Meeting, Washington 2015); Marie Skłodowska Curie Scholarship INT, BIO-Inspire (2014), Career Development Fellowship (Graduate School of Life Science, Würzburg 2017).
- **Societies:** Tissue Engineering and Regenerative Medicine International Society (TERMIS); Junior Editor (Early Stage Researcher Journal, ESR).

## Patents

**Confalonieri D, Hansmann J, Krzimirski S, Walles H.** Hybrid cell detachment-free cell expansion system for adherent cell culturing and related proceeding protocol. *Deposited.*

## Publications

**Confalonieri D, La Marca M, van Dongen EMWM, Walles H, Ehlicke F.** An Injectable Recombinant Collagen I Peptide - based Macroporous Microcarrier Allows Superior Expansion of C2C12 and Human Bone Marrow - derived Mesenchymal Stromal Cells and Support Deposition of Mineralised Matrix. *Tissue Engineering Part A, (2017) Epub ahead of print*

**Pawelec KM, Confalonieri D, Ehlicke F, van Boxtel HA, Walles H, Kluijtmans SG.** Osteogenesis and Mineralization of Mesenchymal Stem Cells in Collagen Type I Based Recombinant Peptide Scaffolds. *Journal of Biomedical Material Research Part A, (2017) Epub ahead of print*

**Confalonieri D, Ehlicke F, Walles H.** Different Osteopontin Variants are Involved in the Maintenance of the Bone Marrow Niche in an in vitro Niche Model. *(Abstract) 18th Meeting of the European Association of Haematopathology (EAHP), Basel (CH), 03-08.09.2016*

**Confalonieri D, Ehlicke F, Walles H.** Influence of Hematopoietic Components of the Bone Marrow on In Vitro Bone Formation Assays. (Abstract) *TERMIS World Conference, Boston (USA), 08.09.2015*

**Confalonieri D, Ehlicke F, Knychala J, La Marca M, Walles H.** A new In-Vitro Bone Formation Assay Starting from a Collagen-Based Granular Scaffold. (Abstract) *WITE Conference, Würzburg (DE), 26.06.2015*

**Carniti C, Gimondi S, Vendramin A, Recordati C, Confalonieri D, Bermema A, Corradini P, Mariotti J.** Pharmacologic Inhibition of JAK1/JAK2 Signaling Reduces Experimental Murine Acute GVHD While Preserving GVT effects. *Clinical Cancer Research, (2015) 21(16):3740-9*

**Ficial M, Antonaglia C, Chilosi M, Santagiuliana M, Tahseen AO, Confalonieri D, Zandonà L, Bussani R, Confalonieri M.** Keratin-14 Expression in Pneumocytes as a Marker of Lung Regeneration/Repair during Diffuse Alveolar Damage. *American Journal of Respiratory and Critical Care Medicine, (2014) 189(9): 1142-45*

**Carniti C, Gimondi S, Vendramin A, Confalonieri D, Recordati C, Bermema A, Mariotti J, Corradini P.** In vivo Jak1/Jak2 inhibition protects from acute GvHD while maintaining robust antitumor activity. (Abstract) *American Society of Hematology Annual Meeting, 09.12.2013*

**Santagiuliana M, Confalonieri D, Bonin S, Antonaglia C, Confalonieri M.** Preliminary study to evidence potential adult pulmonary stem cells on endoscopic transbronchial biopsy. (Abstract) *European Respiratory Society, Barcellona, 08.09.2013*

## Affidavit

I hereby confirm that my thesis entitled “Development and characterization of a bone marrow stem cell niche model” is the result of my own work. I did not receive any help or support from commercial consultants. All sources and / or materials applied are listed and specified in the thesis.

Furthermore, I confirm that this thesis has not yet been submitted as part of another examination process neither in identical nor in similar form.

Würzburg, 29.08.2017

Place, Date

Signature

## Eidesstattliche Erklärung

Hiermit erkläre ich an Eides statt, die Dissertation „Aufbau und Charakterisierung eines Knochenmark-Stammzellnischen-Modells“ eigenständig, d.h. insbesondere selbständig und ohne Hilfe eines kommerziellen Promotionsberaters, angefertigt und keine anderen als die von mir angegebenen Quellen und Hilfsmittel verwendet zu haben.

Ich erkläre außerdem, dass die Dissertation weder in gleicher noch in ähnlicher Form bereits in einem anderen Prüfungsverfahren vorgelegen hat.

Würzburg, 29.08.2017

Ort, Datum

Unterschrift

## **Zusammenfassung:**

Kritische Knochendefekte stellen heutzutage ein ungelöstes Problem in der klinischen Praxis dar, da die verfügbaren prothetischen Optionen oft die mechanische Anpassung an das Gewebe nicht gewährleisten oder zu wichtigen immunologischen und Implantat-bedingten Komplikationen führen.

In diesem Kontext ermöglichen Tissue Engineering-Ansätze neue Strategien, um *in vitro* Zell-Material Interaktionen zu untersuchen und so die Implantatmaterialien zu optimieren.

In dieser Arbeit habe ich Zell-Material Interaktionen eines neuen Kollagen-basierten Scaffolds untersucht, das langfristig als Trägerstruktur für eine zellbasierte Therapie für kritische Knochendefekte entwickelt werden soll. Im Rahmen der Dissertation konnte ich belegen, dass die Kollagen-basierten makroporöse Mikrocarrier für die Zellvermehrung humaner mesenchymaler Stammzellen (MSC) und deren osteogene Differenzierung unter GMP Bedingungen verwendet werden können. Außerdem habe ich die Kokultur von hämatopoietischen Stammzellen des Knochenmarks und multiplen Myelomzellen funktionell charakterisiert. Ich konnte erstmals Kulturbedingungen etablieren, die die Langzeitkultur ohne die Verwendung von Zytokinen ermöglicht. Mittels dieser Kokultur konnte ich ein Knochenmarknischen-Modell etablieren und die Untersuchung der Expression von zentralen Signalkaskaden der Homöostase dieser Nische untersuchen. Ich konnte die Expression von zwei verschiedenen Isoformen von Osteopontin nachweisen, die in Tiermodellen nicht gefunden werden. Diese Isoformen des Osteopontins habe ich kloniert und die rekombinanten Isoformen exprimiert und ihre Rollen in der Homöostase der Knochenmarknische untersucht.

## **Summary:**

Critical size bone defects represent nowadays an unresolved problem in the clinical practice, where the available prosthetic options often lack adequate mechanical matching to the host tissue or lead to important immunological and implant-related complications.

In this context, Tissue Engineering approaches promise more effective strategies to study cell-material interactions *in vitro* and consequently optimize implant materials.

In this work, I investigated the cell-scaffold interactions of a new collagen-based scaffold for a putative cell-based therapy for critical size defects to be developed. In the context of this thesis, I could demonstrate that the collagen-based macroporous microcarriers could be employed for the expansion and osteogenic differentiation of human mesenchymal stromal cells (MSCs) under GMP-compliant conditions. Moreover, I functionally characterized the co-culture of bone marrow hematopoietic stem cells and multiple myeloma cells. I was for the first time able to establish culture conditions allowing

their long-term culture in absence of externally supplemented cytokines. Using this co-culture, I was able to establish a bone marrow niche model to investigate the expression of key signaling pathways involved in the niche's homeostasis. I was able to demonstrate the expression of two different isoforms of Osteopontin, that could not previously be detected in animal models. Finally, I cloned these Osteopontin isoforms, expressed recombinant versions of the isoforms, and investigated their roles in the homeostasis of the bone marrow niche.



*To Brigitte,  
love of my life, source of inspiration and  
motivation through all this work*

*To my parents,  
who followed me into this journey and  
gave all they could to support me in every moment*

*To my grandparents,  
for their unconditional love and their prayers in all my choices.*

*A Brigitte,  
amore della mia vita, fonte di ispirazione e  
motivazione per tutto questo lavoro*

*Ai miei genitori,  
che mi hanno seguito in questo percorso e  
mi hanno dato tutto quello che potevano per supportarmi in ogni momento*

*Ai miei nonni,  
per il loro amore incondizionato e le loro preghiere in tutte le mie scelte.*

*Look wide, and even when you think you are looking wide - look wider still.*

*Guardate lontano, e anche quando credete di star guardando lontano, guardate ancora più lontano!*

*Robert Baden-Powell*

## LIST OF CONTENT:

ABBREVIATIONS	1
1 INTRODUCTION	3
1.1 A cell therapy approach for bone tissue engineering: bone structure and the mineralization process	3
1.1.1 Mesenchymal stromal cells and their role in bone tissue engineering	8
1.1.2 Microcarrier technology and advantages over 2D cell expansion systems	10
1.2 Mesenchymal stromal cells to investigate the bone marrow niche	12
1.2.2 Regulation of the Stem Cell Niche Dynamics	16
1.2.3 The diseased bone marrow niche and the role of Osteopontin	19
1.2.4 Osteopontin	20
2 AIM OF THE STUDY	24
3 MATERIALS AND METHODS	25
3.1 Human Bone Marrow Mesenchymal Stromal Cells characterization and biobanking	25
3.2 Optimization of a GMP-compliant medium for hBMSCs expansion and differentiation	27
3.3 Optimization of the macroporous microcarriers for hBMSCs expansion and delivery	29
3.3.1 Cell seeding on Cellnest™ and related procedures	30
3.3.2 Live/Dead Staining, DAPI staining, DNA quantification and RT-Real Time PCR on Cellnest™	31
3.4 Investigation of strategies for hBMSCs differentiation and mineralization of the microcarriers	31
3.5 Establishment of a Bone Marrow Niche model	33
3.6 Recombinant OPNa and OPNb are differently produced and deposited	35
3.7 Possible applications of a bone marrow niche model: the case of multiple myeloma	36
3.8 Statistical analysis	37
4 RESULTS	38
4.1 Human bone marrow mesenchymal stromal cells characterization and biobanking	38
4.2 Optimization of a GMP-compliant medium for hBMSCs expansion and differentiation	40
4.3 Optimization of the macroporous microcarrier for hBMSCs expansion and delivery	44
4.4 Investigation of strategies for hBMSCs differentiation and mineralization of the microcarriers	50
4.5 Establishment of a Bone Marrow Niche model	55
4.6 Recombinant OPNa and OPNb are differently produced and deposited	60
4.7 Possible applications of a bone marrow niche model: the case of multiple myeloma	63
5 CONCLUSION	73
6 BIBLIOGRAPHY	74
7 APPENDIX	88

## ABBREVIATIONS

**μCT** = Micro-Computed Tomography

**AGM** = Aorto-gonad-mesonephros region

**ALL** = Acute lymphoblastic leukemia

**ALP** = Alkaline Phosphatase

**AML** = Acute myelocytic leukemia

**ANG** = Angiogenin

**Ang-1** = Angiopoietin

**ANOVA** = Analysis of variance

**bFGF** = Basic Fibroblast Growth Factor

**BFU-E** = Burst Forming Unit Erythroid

**BGLAP/BGP** = Osteocalcin

**BMP2** = Bone Morphogenetic Protein 2

**BSA** = Bovine Serum Albumin

**BSP I** = Bone sialoprotein I

**BSP II** = Osteopontin

**CAR** = CXCL12-abundant reticular cells

**CD** = Cluster of differentiation

**cDNA** = Complementary DNA

**CFU-E** = Colony Forming Unit Erythroid

**CFU-G** = Colony Forming Unit Granulocyte

**CFU-GEMM** = Colony Forming Unit Erythrocyte Macrophage Megakaryocyte

**CFU-GM** = Colony Forming Unit Granulocyte-Macrophage

**CFU-M** = Colony Forming Unit Macrophage

**CLL** = Chronic Lymphocytic Leukemia

**CLP** = Common Lymphoid Progenitor

**CML** = Chronic Myelocytic Leukemia

**CMP** = Common Myeloid Progenitor

**Col1a1** = Collagen type I

**CXCL12** = C-X-C motif Chemokine Ligand 12

**CXCL4** = C-X-C motif Chemokine Ligand 4

**CXCR4** = C-X-C motif Chemokine Receptor 4

**DAPI** = 4',6-diamidino-2-phenylindole

**DARC** = Duffy antigen receptor for chemokines

**DHT** = Dehydrothermal

**DMEM** = Dulbecco Modified Eagle's minimal Essential Medium

**DMEM-F12** = DMEM/ Ham-F12 50-50 mixture

**DMSO** = Dimethyl sulfoxide

**DNA** = Deoxyribonucleic acid

**DPBS** = Dulbecco's Phosphate-buffered Saline

**dsDNA** = Double Strand DNA

**ECM** = Extracellular Matrix

**EDC** = 1-Ethyl-3-(3-dimethylaminopropyl)-carbodiimide

**Eta-1** = Osteopontin

**FCS** = Fetal Calf Serum

**FGF-1** = Fibroblast Growth Factor -1

**FI** = Fold Increase

**FLT3L** = FMS-like Tyrosine Kinase 3 Ligand

**G-CSF** = Granulocyte Colony Stimulating Factor

**GMP** = Good Manufacturing Practice

**GMP<sub>1</sub>** = Granulocyte Macrophage Progenitor

**hBMSCs** = Human Bone Marrow-derived Mesenchymal Stromal Cells

**HIF-1** = Hypoxia-Inducible Factor 1

**HLA-DR** = Human Leukocyte Antigen- antigen D Related

**HMDIC** = hexamethylene diisocyanate

**HSCs** = Hematopoietic Stem Cells

**ICAM-1** = Intercellular Adhesion Molecule 1

**IGF** = Insulin-like Growth Factor

**JNK** = c-Jun N-terminal Kinase

**Lepr1** = Leptin Receptor 1

**LMPP** =Lymphoid Primed Multipotent Progenitor

**LT** = Long Term

**MCs** = Microcarriers

**MEP** = Megakaryocyte-Erythroid Progenitor

**MM** = Multiple Myeloma

**MMP** = Matrix Metalloprotease

**MPL** = Myeloproliferative Leukemia Protein

**MPP** = Multipotent Progenitor Cells

**MSCs** = Mesenchymal Stromal /Stem Cells

**NG2** = Neuron-Glial antigen 2

**NK** = Natural killer

**OPG** = Osteoprotegerin

**OSX** = Osterix

**PDL** =Platelet-Derived Lysate

**PDs** = Population Doublings

**PTH** = Parathyroid Hormone

**PTM** = Post-Translational Modification

**RCP** = Collagen I-based recombinant peptide, Cellnetst™

**RCP-HA** = Collagen I- based recombinant peptide and hydroxyapatite composite microbeads

**RGD** = Arginin, Glycin, Aspartic acid

**RNA** = Ribonucleic Acid

**ROS** = Reactive Oxygen Species

**RPMI** = Roswell Park Memorial Institute Medium

**RT-Real Time PCR** = Retro transcribed Real Time Polymerase Chain Reaction

**Runx2** = Runt-related transcription factor 2

**Sca-1** = Stem Cells Antigen -1

**SCF** = Stem Cell Factor

**SD** = Standard Deviation

**SDS-PAGE** = Sodium Dodecyl Sulfate Polyacrylamide Gel Electrophoresis

**SEM** = Scanning Electron Microscopy

**SOP** = Standard Operating Protocol

**Sp7** = Osterix

**SPARC** =Osteonectin

**SPP1** = Osteopontin

**ST** = Short Term

**TBS** = Tris-Buffered Saline

**TCP** = Tricalciumphosphate

**TGF-β1** = Transforming Growth Factor β 1

**Tie2** = TEK Tyrosine Kinase

**TLR** = Toll-Like Receptor

**TPO** = Thrombopoietin

**VCAM-1** = Vascular Cell Adhesion Molecule 1

**VE-cadherin**= Vascular Endothelial Cadherin

**VEGF** = Vascular Endothelial Growth Factor

## 1 INTRODUCTION

Tissue Engineering and Regenerative Medicine are multidisciplinary fields focusing on the development of artificial organs, biomimetic tissues and engineered cells in order to restore or maintain tissue and organ function. They combine principles of biology, material science, biomolecular engineering and medicine among others to produce organs, tissues, methods and devices suitable for implantation, clinical application and drug testing.

Millions of people worldwide suffer from trauma-, cancer- or age-related orthopedic diseases, often resulting from poorly treated bone or cartilage defects. Although autologous and allogeneic bone transplantation are nowadays considered the gold standards for bone repair, autologous transplantation can lead to chronic pain at the donor site and suffer of limited availability, while allogeneic transplantation maintains potential risks for complications such as graft rejection and disease transfer. On the other hand, synthetic substitutes and prosthesis employed in the clinic often lack an adequate mechanical match to the defect to be cured and important biological properties for large defect regeneration<sup>1-3</sup>.

For these reasons, bone tissue engineered constructs may represent a promising and alternative approach<sup>4</sup> with the potential to overcome the limitations of the current therapeutic strategies. Since the bone tissue lies in tight contact or functional relationship with several organs and physiological systems, among whom the hematopoietic system plays a role of utmost importance for the homeostasis of the organism, the following chapters of this introduction will be dedicated to the illustration of the concepts underlying (1) bone physiology, (2) a cell-therapy-based tissue engineering approach for regeneration of bone critical size defects, and (3) a possible application of the engineered bone for the reconstitution of an *in vitro* bone marrow niche model.

### 1.1 A cell therapy approach for bone tissue engineering: bone structure and the mineralization process

The human bone is composed of 80% cortical bone (lamellar bone), constituting the external part of the bone and occupying the marrow space at the diaphysis, and 20% trabecular bone (spongy or woven bone), constituting the inner region of the epiphysis and metaphysis of the long bones. The cortical bone is composed mainly, except for the last external layers, of haversian systems composed of concentric layers of perpendicularly oriented lamellae surrounding haversian canals containing nerves and blood vessels<sup>5</sup> (Figure 1). One single system of lamellae surrounding one haversian canal is called osteon, and the terminally differentiated bone cells (osteocytes) embedded at the interface between two lamellae are responsible for the deposition of new mineralized bone upon reabsorption from osteoclasts, a macrophage-derived bone-specific cell type responsible of initiating bone remodeling.

Different canals are linked together by perpendicular channels, called Volkmann's channels, containing blood vessels, allowing a better blood circulation of the bone. At the molecular level, the bone appears to have a remarkably hierarchical structure, composed of two major constituents: the collagen, assembled into fibrils and constituting the most abundant protein in the organic phase of the bone extracellular matrix; and the hydroxyapatite, whose crystals deposit and elongate on the collagen fibrils<sup>6</sup>, constituting the main component of the bone mineral phase. This hierarchical structure enables the bone to be a light-weight material that can carry large loads by combining the toughness of inorganic materials and the flexibility of protein-based tissues<sup>7</sup>.

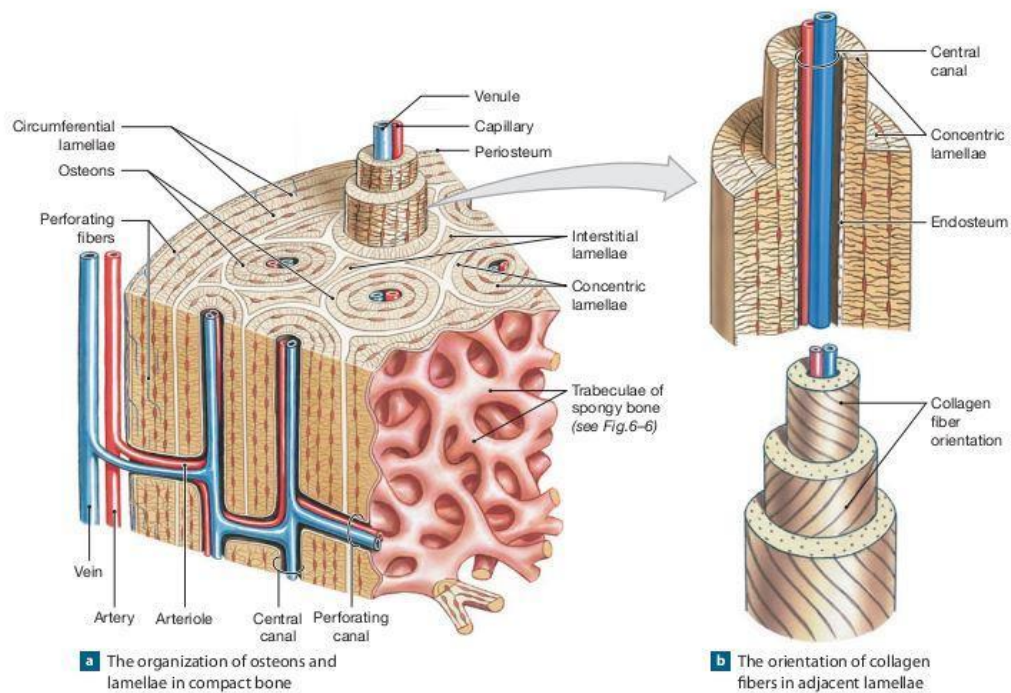


Figure 1: Structure of the bone, with focus on the haversian system and the disposition of the collagen fibers<sup>8</sup>

*In vivo*, nucleation and growth of the hydroxyapatite crystals can be heavily affected by matrix proteins following different mechanisms, and the composition of the matrix may facilitate or retard crystal nucleation and elongation<sup>9</sup> at different time points during maturation of the mineralized tissue<sup>10</sup>. The bulk of the mineral is constituted by poorly crystalline, carbonate-containing hydroxyapatite and, apart from collagen<sup>11</sup>, more than 200 other proteins can be found in the bone, of which only few are involved in mineralization<sup>12</sup>. Those can be grouped in different families as presented in Table 1:

Table 1: Classification of the proteins of the mineralized tissues<sup>13</sup>

<i>Protein</i>	<i>Location**</i>
Phosphorylated glycoproteins	
Bone sialoprotein I/osteopontin/secreted sialophosphoprotein/2ar	B, C, N
Bone sialoprotein II/bone sialoprotein/BSP/secreted sialoprotein II	B
Osteonectin/culture heat shock protein/SPARC	B, N
BAG-75	B
Bone phosphoprotein	B
Phosphorylated proteins	
Dentin phosphophoryn/dentin phosphoprotein	D
24-kD-phosphoprotein/N-propeptide type I collagen	B
Proteins with $\gamma$ -carboxyglutamic acid	
Osteocalcin/bone Gla protein/BGP	B
Matrix Gla protein	B, C
Proteins with glycosaminoglycan side chains	
Cartilage proteoglycan (monomer & aggregate)	C
Bone proteoglycan I/biglycan/HAPG1	B, C, N
Bone proteoglycan II/decorin/HAPG2	B, C, N
HAPG3	B, ?
Proteins derived from procollagen	
Chondrocalcin	C
24-kD bone phosphoprotein	B
Glycosylated proteins and others	
Thrombospondin	B, C, N
SCAB 1-3	B, ?

*\*Proteins separated by / have extensive homology, or are identical proteins being given different names by different researchers.*

*\*\*B = found in bone and /or synthesized by osteoblasts; C= found in cartilage and /or synthesized by chondrocytes; D= found in dentin or synthesized by odontoblast; N= found in other nonmineralizing tissues and synthesized by cells other than osteoblasts, odontoblasts and chondrocytes; ?= of unknown origin.*

The single procollagen monomers form triple helices after pairing of the N- and C-terms, that are later removed to form a molecule of collagen. This can assemble in semiflexible rods<sup>14</sup> by arranging in a linear fashion with other collagen molecules, leaving a separation between adjacent ends and forming the so-called quarter-staggered array. This packing pattern results in a gap zone and an overlap zone. The gap region is the proposed site for initial mineral deposition<sup>15</sup>. X-ray and neutron diffraction studies demonstrated that the mineral crystals are arranged in a pattern that follows the periodicity of the collagen fibrils, lying exclusively in the gap<sup>15</sup> (Figure 2). Several noncollagenous proteins in the matrix localize adjacent to or are associated with the hydrophobic domains of the collagen fibril and immobilize mineral-binding proteins to the collagen and enable the binding to particular face of apatite crystals. While some of these proteins such as Osteocalcin, Bone sialoprotein and Osteonectin have been reported to enhance or enucleate mineral deposition on the collagen fibrils, the role of other proteins in bone mineralization, such as Osteopontin, has long been discussed because of its strong binding capability to hydroxyapatite and the consequent ability to inhibit mineralization *in vitro*, suggesting a role in regulating the elongation of the hydroxyapatite crystals<sup>11</sup>.

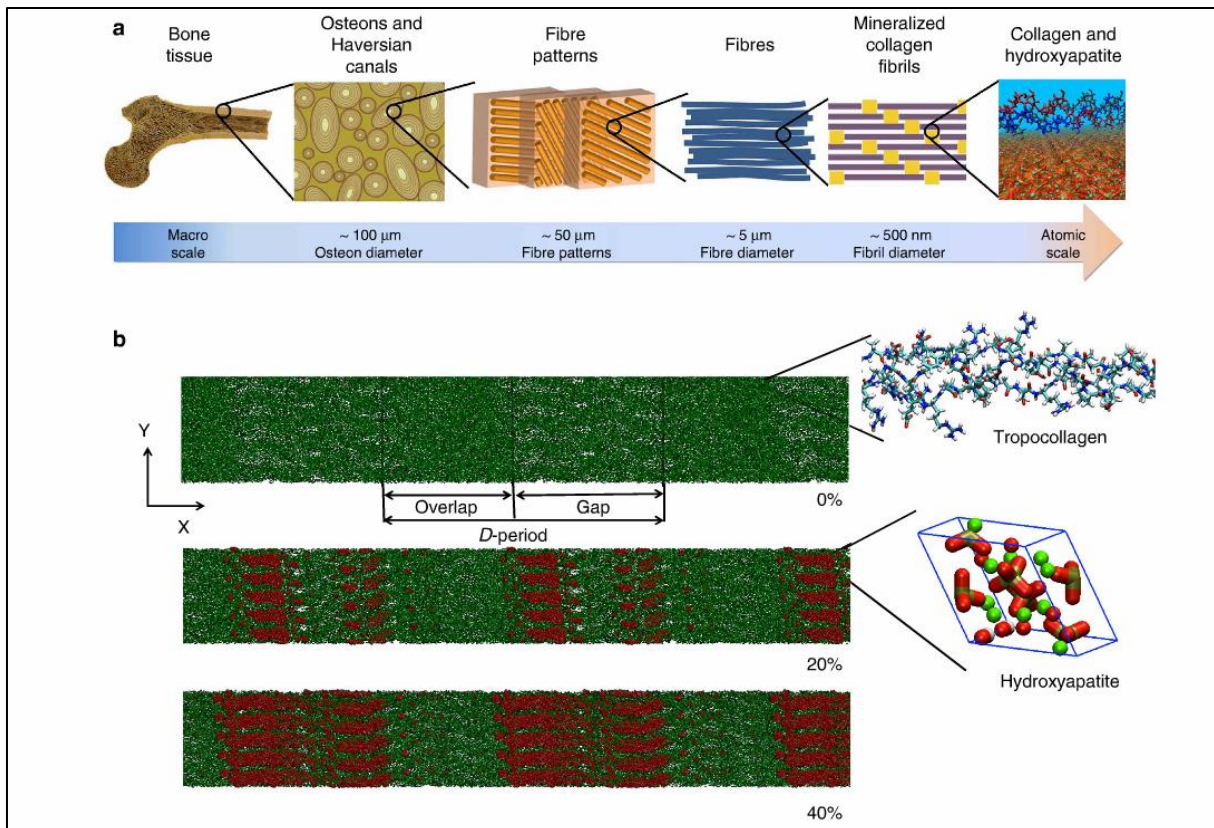


Figure 2: Structure of the collagen and mineralization model. Single collagen triple helices assemble to form collagen microfibril in the staggered-quarter assay. Hydroxyapatite-binding proteins deposit into the gap region and enucleate mineral formation and deposition<sup>16</sup>.

During development and natural reparative processes, bone is formed via two distinct processes occurring in proximity of a vascular network<sup>17</sup>, called endochondral and intramembranous ossification. During endochondral ossification (Figure 3, upper panel), blood vessels enter the cartilaginous template of the bones and stimulate the differentiation of the chondrocytes into hypertrophic chondroblasts, that gradually substitute collagen II with collagen X<sup>13</sup> and undergo apoptosis to leave space to lacunae hosting osteo-progenitors, that would ultimately mineralize the existing cartilaginous template and substitute the existing collagen with collagen I<sup>11</sup>. Similarly, following fracture, the disrupted vascular supply creates a hypoxic environment that recruits<sup>16</sup> a first vascular network to the site of inflammation.



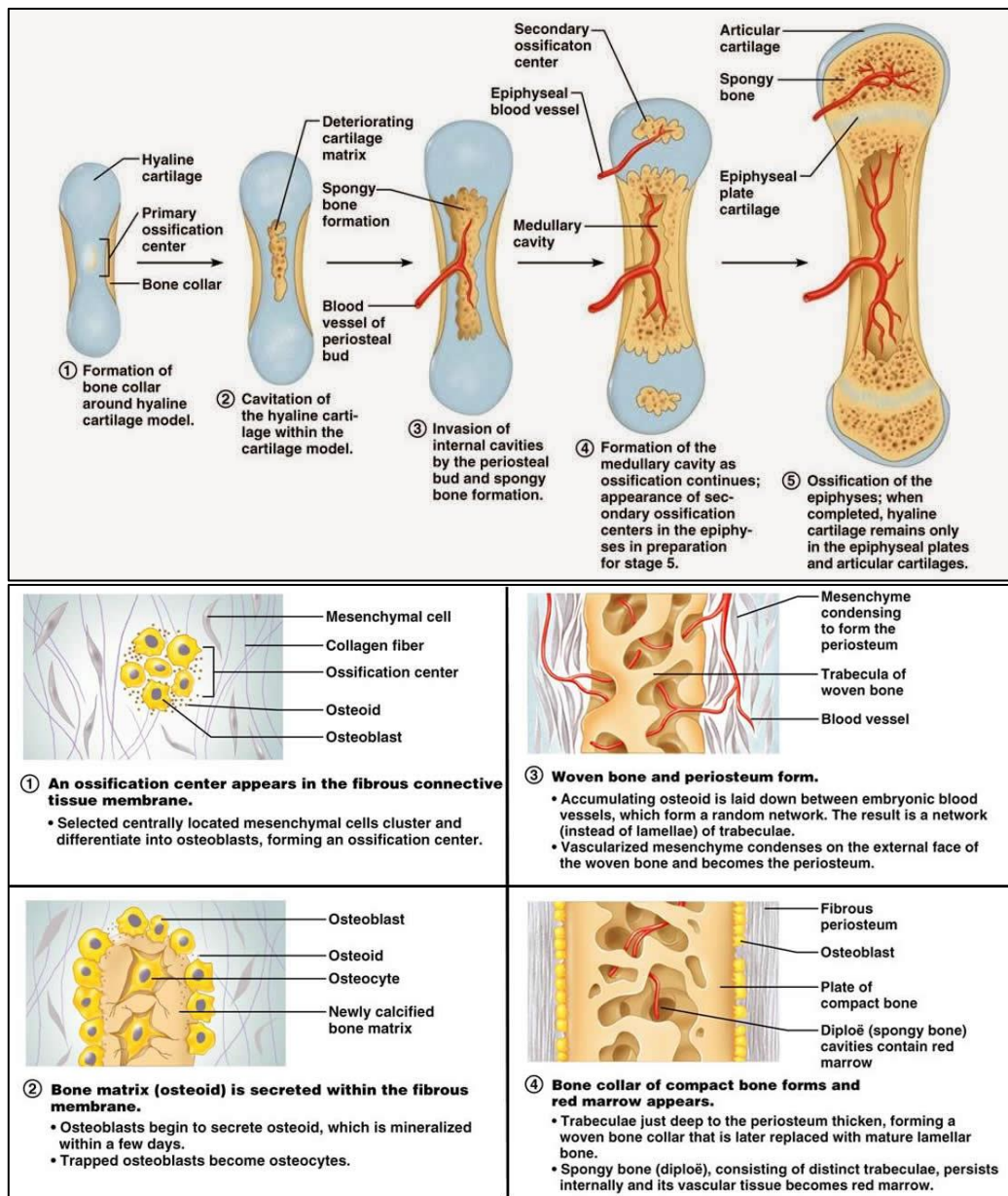


Figure 3: Graphical representation of endochondral (**upper panel**) and intramembranous (**lower panel**) ossification<sup>18</sup>.

The inflammatory cascade subsequently initiates the endochondral ossification by recruiting resident mesenchymal stromal cells (MSCs), that form a cartilaginous callus being gradually resorbed and mineralized following formation of a vascular network. On the other hand, intramembranous ossification (Figure 3, lower panel) occurs through direct assembling and differentiation of MSCs present in the medullary cavity without formation of a cartilaginous callus during the reparative process. In this context, the activation of the hypoxia-inducible factor 1 (HIF-1) pathway in an hypoxic microenvironment triggers the upregulation of angiogenic factors such as the vascular endothelial growth factor (VEGF)<sup>19</sup> and the recruitment of a vascular network.

Besides vascularization, several other biochemical and biomechanical factors are involved in bone formation and remodeling. During physical activity the skeletal system is subject to biomechanical forces including compressive, bending and torsional loads, that push interstitial fluid through the lacunae and canaliculi connecting adjacent osteocytes embedded in the bone matrix<sup>20</sup>. The shear stress generated by the flowing interstitial fluid is able to influence mechanical transduction pathways on bone cells during bone formation and remodelling, and while mechanical stress favours the formation of bone, bone loss typically occurs under non-weight bearing circumstances.

During fracture healing, several surrounding tissues concur to the healing process, providing progenitor cells and the needed blood supply. Among these tissues, the periosteum plays a role of utmost importance<sup>21</sup>. It is a thin and highly vascularized<sup>22</sup> bilayered tissue membrane attached to the external surface of the bone by collagenous fibre known as Sharpeys fibres, and while the outer layer consists of fibroblasts, the inner layer is rich in MSCs able of directing bone and cartilage differentiation<sup>23</sup>. Furthermore, while musculo-osteal and fascio-osteal vessels connect muscles and periosteum, capillary anastomoses link the periosteum with the intramedullary circulation in the bone cortex<sup>22</sup>. Thanks to this connections, it has been suggested that the periosteum serves as a local source of osteo-progenitors for bone healing and remodelling<sup>24</sup>, and its absence in fracture healing was shown to lead to decreased fracture healing capability<sup>21</sup>.

### **1.1.1 Mesenchymal stromal cells and their role in bone tissue engineering**

Mesenchymal stromal cells (MSCs) constitute a heterogeneous population of spindle-shaped cells that can be isolated from many tissues including adipose tissue<sup>25</sup>, bone marrow<sup>26</sup>, umbilical cord blood<sup>25,26</sup>, skeletal muscle<sup>27</sup>, deciduous dental pulp<sup>28</sup>, synovia<sup>29</sup>, Wharton's jelly<sup>30</sup>, and skin<sup>31</sup>. Three minimal criteria, according to the International Society for Cellular Therapy, must be fulfilled in order to identify human MSCs: plastic adherence; surface antigen expression (presence of CD73 (Sh3/4), CD90 (Thy1), CD105 (SH2), absence of CD14 or CD11b, CD19 or CD79a, CD34, CD45 and HLA-DR); and *in vitro* differentiation into mesodermal lineages (adipogenic, chondrogenic and osteogenic)<sup>32</sup>.

miRNA and mRNA analysis of differentiation markers of MSCs extracted from different sources revealed an "environmental-niche memory" for these cells, resulting in a better differentiation in the cellular types characteristic of the original host tissue<sup>33,34</sup> despite their similar morphology and surface antigen expression. For this reason, it appears that bone marrow-derived MSCs constitute the best candidate for bone tissue engineering. This difference could be due to the influence of interacting neighboring populations, to the exposure to proteases or to different oxygen pressures in the tissues of origin, that could result in differentially regulated intracellular responses able to direct MSCs' function and fate<sup>35</sup>.

Within the bone marrow, MSCs constitute a heterogeneous population expressing several markers shared by other cell types of the bone marrow such as CD146<sup>36</sup>, C-X-C motif Chemokine Ligand 12 (CXCL12)<sup>37</sup>, Nestin<sup>38</sup>, Leptin Receptor 1 (Lepr1)<sup>39</sup>, Prx-1<sup>40</sup>, Osterix (SP7)<sup>40</sup> and Mx-1<sup>41</sup>, and stromal cells expressing these markers have been shown to support hematopoietic stem cell (HSCs) maintenance. Because of this, the ontogenic identity of this cell population is still largely discussed, and appears to be partly overlapping with other cell populations involved in the maintenance of HSCs in the bone marrow niche and hematopoiesis. CXCL12-abundant “reticular” cells (CAR) constitute a cell type located adjacent to the sinusoids and that was first shown to reside near HSCs in the bone marrow<sup>37</sup>. Their ablation depletes HSCs and severely impairs the adipogenic and osteogenic capability of bone marrow cells<sup>42</sup>. Similarly, CD146<sup>+</sup> skeletal stem cells localize adjacent to bone marrow sinusoids and support HSC maintenance<sup>36</sup>.

Bone-forming mesenchymal stromal cells appear to be hosted in regulatory niches defined by blood vessels<sup>43</sup> expressing the pericyte markers Neuron-glia antigen 2 (NG2) and nestin<sup>38,44</sup> and supporting long-term repopulating HSCs<sup>38</sup>. In these vessels, nestin<sup>+</sup> Sca-1<sup>+</sup> (Stem Cell Antigen -1) VE-cadherin<sup>+</sup> (Vascular Endothelial cadherin) bone marrow endothelial cells constitute precursor cells able to give rise to both endothelial and mesenchymal lineages<sup>45</sup>. The hematopoiesis-supporting function of bone marrow MSCs is further underlined by the fact that bone-forming mesenchymal progenitors transplanted in mice are sufficient to create bony ossicles which are progressively infiltrated by host vasculature and that can host HSCs<sup>36,46</sup>. This suggests that, even if osteo-progenitor cells cannot directly promote HSC maintenance, they can promote the formation of HSC niches by recruiting vasculature, and recent studies point out that specific subsets of MSCs may play different functions throughout the bone marrow. In this context, it appears that Sca1<sup>+</sup>CD146<sup>+</sup> progenitors localize mainly to the perivascular regions, while CD166<sup>+</sup>Sca1<sup>-</sup> cells localize mainly to the endosteal surface and may preferentially support lymphopoiesis or suppress myelopoiesis<sup>47</sup>.

While the traditional approaches for bone repair are autologous transplantation or allogeneic transplantation from cadaveric donor, bone tissue engineering approaches with the use of MSCs are either based on the delivery of the cells alone or of a cell-scaffold combination. While the applications for MSCs in maxillofacial reconstruction are widely reported, applications of MSCs for the reconstruction of critical size bone defects are still lacking or under experimentation, being more focused on the management of osteonecrosis of the femur<sup>48</sup>, and having difficulties in landing the clinical practice. For maxillofacial applications, expanded MSCs<sup>49</sup> or bone marrow concentrates<sup>50</sup> are often co-implanted with  $\beta$ -tricalciumphosphate or hydroxyapatite synthetic scaffolds<sup>51</sup>, decellularized bone powders or granules<sup>50</sup>, or embedded in platelet-rich plasma derivatives<sup>52</sup>.

Opposite to autologous and allogeneic bone graft, both posing significant risks to the patient, MSCs do constitute a relatively safe therapeutic option<sup>53</sup>, with no reports of immunological-related side effects<sup>54</sup> or tumorigenic tendencies<sup>55</sup> of MSCs alone<sup>56</sup> or when seeded in tissue engineering constructs for human application<sup>35</sup>. Furthermore, MSCs hold the potential to reduce graft versus host disease<sup>57</sup>, increase cell engraftment<sup>58</sup> and migrate to inflamed tissues where they modulate inflammation and recruit host cells leading to tissue repair<sup>53</sup>.

Taken together, these characteristics make these cells extremely appealing for bone tissue engineering, and their clinical application promises to overcome the issue of limited availability of healthy primary differentiated cells from patients. Several technical solutions have in fact be found to this problem, including expansion in specifically designed bioreactor setups or the employment of chemically defined or non-chemically defined Good Manufacturing Practice (GMP)-compliant cell culture media. Among the best alternatives available, platelet-derived lysate (PDL) constitutes a promising alternative to the fetal calf serum (FCS)<sup>59,60</sup> for MSCs expansion and osteogenic differentiation.<sup>61</sup>

Osteogenic differentiation of MSCs can be easily divided in two phases, namely an early and a late differentiation phase. Typical of the early differentiation phase is the expression of early differentiation markers such as alkaline phosphatase (ALP), collagen 1 (col1a1) and the master regulation gene Runx2 (Runt-related transcription factor 2) regulating osteo-chondrogenic commitment, whose expression increases until the start of the late differentiation phase. Typical of the late differentiation phase is the expression of markers such as bone morphogenetic protein 2 (BMP2), Osteonectin (SPARC), Osteopontin (SPP1), Osteocalcin (BGLAP), Osteoprotegerin (OPG), and the master gene of osteogenic differentiation Osterix (OSX)<sup>62</sup>.

### **1.1.2 Microcarrier technology and advantages over 2D cell expansion systems**

Several materials have been employed so far for bone tissue engineering. These materials are intended to mimic either the organic phase<sup>63-65</sup> or the mineral phase of the bone matrix. While the initial aim of materials employed for the reconstruction of hard tissues is the maintenance of physical stability and stiffness, these materials should also hold enough porosity to allow cell infiltration, proliferation and vascularization<sup>66</sup>. Scaffold porosity in particular has been proved crucial for bone formation, which occurs at the lining surface of the pores. Different kinds of ceramics<sup>67</sup>, such as  $\beta$ -tricalciumphosphate ( $\beta$ -TCP)<sup>68</sup>, calcium-deficient hydroxyapatite<sup>69</sup> and  $\beta$ -CaSiO<sub>3</sub><sup>70</sup>, and bioactive glasses<sup>71</sup>, can be manufactured to present either porous macrostructures<sup>72</sup> or well-defined concavities presenting diameters of 100-500 $\mu$ m and to possess a final porosity up to 90%.

Several approaches combining synthetic materials with hydroxyapatite<sup>73</sup> and/or  $\beta$ -TCP<sup>74</sup> have furthermore been employed in order to compromise between the request for initial stability of the implant and the ability to support further mineral deposition. Among these approaches, de-mineralized<sup>75</sup> and re-mineralized<sup>76</sup> bone matrix provided promising results in terms of MSCs differentiation and mineral deposition, but their production remains exceedingly laborious. Moreover, the correct proportion between organic and mineral phase, together with scaffold architecture, is necessary for proper bone regeneration, contributing in providing the cells with the needed signals for osteogenic differentiation. The cytoskeleton of adhering cells is in fact normally maintained in a state of tension called tensegrity, pulling on the cell membrane through focal adhesions and resulting in degradation of the extracellular matrix (ECM). ECM degradation causes cell spreading and development of tensile forces, which in turn initiate proliferation and tissue formation. Application of tension enhances osteoblastic gene expression including the calcitonin receptor,  $\beta$ -catenin, Runx2, and Wnt-8<sup>77</sup>. Consequently, MSCs grown on stiff substrates exhibit extensive production of stress fibers and tend to differentiate toward the osteogenic and chondrogenic lineages, while cells on collagen gels show less spreading, fewer stress fibers but more filopodia<sup>78</sup> and tend to differentiate toward the adipogenic lineage<sup>79,80</sup>.

New scaffold formulations mimicking the organic phase of the bone matrix are not just aimed at the reconstitution of the physical stability of the implant, but also at the development of a vascularized network and achievement of a more natural spatial cell distribution into the matrix, that may in turn result in better support of bone formation over time. Among the scaffolds employed for bone tissue engineering the most employed are cellulose sponges<sup>65</sup>, electrospun fibers<sup>73</sup>, multilayered scaffolds for vascularization<sup>81,82</sup> and collagen microcarriers<sup>63,83</sup>.

Microcarrier (MCs) technology is an emerging field of interest, allowing to expand different adherent cell types in a suspension culture on a small three-dimensional substrate for a wide range of applications<sup>84</sup>. While classical two-dimensional cell culture methods provide data that are poorly translatable to the *in vivo* situation<sup>85</sup>, three-dimensional porous scaffolds support cell proliferation by allowing cell ingrowth and by mimicking the cells-matrix and cell-cell interactions in a more physiological way<sup>86</sup>. Initially proposed by van Wezel in 1967<sup>87</sup>, suspension systems such as the MCs technology add several advantages to other three-dimensional porous scaffolds, such as a higher surface-to-volume ratio<sup>88</sup>, eventually leading to higher cell yields<sup>89</sup>; higher gas and nutrient exchange when compared to static systems<sup>90</sup>; the possibility to subject the cells to physical stimuli<sup>91</sup>; and ultimately the possibility to scale up the expansion process<sup>89</sup>. Several micro- and macro- carriers are nowadays commercially available, being characterized by distinct features such as size, porosity, density, surface charge and adhesion properties<sup>92</sup>. Although several of these microcarriers are constituted of or coated with animal-derived proteins of the extracellular matrix, the use of

recombinant – ECM-inspired materials such as recombinant collagen would allow for a significant animal-free scaling up of scaffold production, reducing the costs of the therapies while providing the cells with a physiological microenvironment and a potentially higher flexibility in their application range. The choice of the appropriate crosslinking strategy and the specific formulation of the synthetic material would in fact allow to tune scaffold stability, degradation rate and surface properties in order to adapt them to the selected application, cell type of interest or target tissue<sup>93</sup>. Ultimately, the conformity of the material with GMP regulations will influence its applicability as cell delivery system for tissue engineering clinical applications. In this regard, the possibility to employ MCs for cell culturing without the need for enzymatic cell detachment makes the MCs technology particularly suited for cell-based therapeutic applications<sup>94</sup>, holding potential for the use of MCs as injectable cell carriers only requiring minimal invasive surgical procedures.

## **1.2 Mesenchymal stromal cells to investigate the bone marrow niche**

As previously introduced, MSCs do not only play an important role in bone regeneration and bone tissue engineering, but constitute one of the most important protagonists of the bone marrow niche, contributing to the regulation of hematopoiesis and to the maintenance of hematopoietic stem cells (HSCs) throughout the bone marrow. Therefore, an *in vitro* model comprising both MSCs and a bony matrix may hold the potential to provide with important insights (1) in the bone marrow stem cell niche homeostasis and regulation and (2) in the development of several hematological malignancies. For this reason, the following chapters will be dedicated to the illustration of the current theories underlying the conceptualization of the bone marrow stem cell niche microenvironment, its dynamics, and its behavior under physiological conditions and disease. Finally, I will provide a clearer focus on Osteopontin, a protein studied for its involvement in the maintenance of the bone marrow niche and in the mineralization process.

### **1.2.1 Hematopoiesis and the bone marrow microenvironment**

The hematopoietic system is responsible for the production and maintenance of the blood. The blood is involved in several important functions, such as providing nutrition to the cells and tissues of the body by vehiculating glucose, oxygen and other substances; it fosters the interaction between different organs such as kidneys, bone and liver by transporting hormones and other signaling molecules; it participates in important processes such as coagulation during wound healing; and it provides progenitor cells for the immune system.

Hematopoiesis is the process of formation of blood cells starting from a population of hematopoietic stem cells in the bone marrow. It is a hierarchical process (Figure 4), and it can be pictured as a series of branchings in which more lineage-restricted progenitors originate through asymmetric division from HSCs and eventually form terminally differentiated cell populations. This system is highly dynamic<sup>95</sup> and it is possible to argue that important underlying mechanisms such as stem cell differentiation, lineage fate and niche competition are better explained in the light of population biology, by considering the complex set of interactions within and between cell lineages and the extent of the environmental influences<sup>96</sup>.

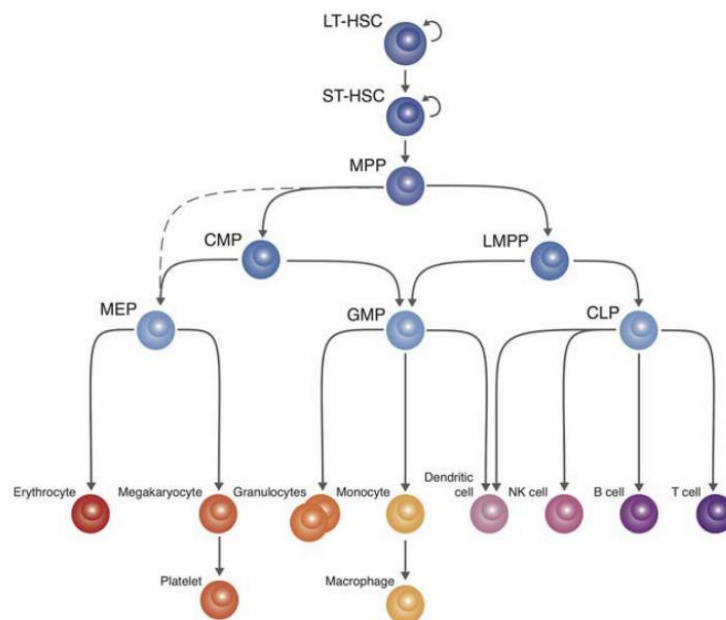


Figure 4. Schematic representation of hematopoiesis. Dashed arrow denotes a putative transition.

**CLP:** common lymphoid progenitor; **CMP:** common myeloid progenitor; **GMP<sub>1</sub>:** granulocyte-macrophage progenitor; **HSC:** hematopoietic stem cells; **LMPP:** lymphoid-primed multipotent progenitor; **LT:** long term; **MEP:** megakaryocyte-erythroid progenitor; **NK:** natural killer; **ST:** short term<sup>97</sup>

The bone marrow produces in fact approximately 500 billion cells a day into the peripheral circulation<sup>98</sup>. Such a high production rate requires cells able to self-renew, creating differentiated cells while maintaining their stemness for a lifetime. Since highly proliferating cells undergo a higher number of genetic alterations comparing to resting cells, it is intuitive to think that stem cells need a particular environment in which they can maintain their stemness while regulating proliferation and differentiation. The existence of such a microenvironment within the bone marrow, called “bone marrow niche” or “stem cell niche”, was formally proposed by Schofield in 1978<sup>99</sup>. The term “niche” was later defined as the local tissue microenvironment that directly maintains and regulates a particular kind of stem or progenitor cell<sup>100</sup>.

During early development, hematopoiesis begins in the yolk sac<sup>101</sup> starting from a precursor cell type of endothelial and hematopoietic cells called “hemangioblast”<sup>102</sup>. On the other hand, long-term reconstituting HSCs originate from the intra-embryonal aorto-gonad-mesonephric region (AGM) in mice and humans<sup>102</sup>. Later in the development, HSCs migrate to the fetal liver<sup>103</sup>, and dramatic postnatal changes in the portal vessel after closure of the umbilical inlet at birth leads to the migration of HSCs to the bone marrow, wherein long-term hematopoiesis persists postnatally. Here HSCs are identified as a CD150<sup>+</sup> CD48<sup>-</sup> CD41<sup>-</sup> cell population, and all serially transplantable HSCs, including the most quiescent HSCs, are contained within the CD150<sup>+</sup> CD48<sup>-</sup> CD41<sup>-</sup>/CD41<sup>low</sup> population<sup>104</sup>.

Hematopoiesis-supporting bone marrow or red marrow resides in the axial skeleton in the flat bones, such as pelvis, sternum, skull, ribs, vertebrae, and the metaphyseal and epiphyseal ends of long bones, while a bone marrow with a higher fat content also called yellow marrow can be found in the diaphyseal portion of long bones. Several arteries enter the bone marrow through the bone cortex, terminating in the endosteum, the connective tissue lining the inner surface of compact bone, and branching in the metaphysis or diaphysis of long bones<sup>105</sup>. In proximity to the bone, arterioles anastomose with a plexus of venous sinusoids that drain the bone marrow via collecting venules that lead back to the central longitudinal vein<sup>43</sup>. The arterioles run close to the endosteal region and are surrounded by rare NG2<sup>+</sup> nestin<sup>bright</sup> pericytes, while sinusoids are thin-walled, consisting of a layer of flat endothelial cells with little to no basement membrane, and surrounded by leptin receptor<sup>+</sup> or nestin<sup>dim</sup> perivascular cells and CAR cells<sup>39,44,106</sup>.

Because of the abundance of draining sinusoidal vessels, the bone marrow does not have a lymphatic system, and all vessels are interspersed within the trabecular bone, establishing a circular blood flow pattern from the center of the marrow cavity towards the periphery and back again<sup>107</sup>. This particular configuration led to the hypothesis that more than one spatially distinct niches are indeed present in the bone marrow, and recent evidences showed that two microenvironments, respectively the arteriolar and the sinusoidal-megakaryocyte niche, play important roles in the regulation of hematopoiesis (Figure 5). Both these niches localize to the endosteal region in proximity to osteolineage cells<sup>104,108</sup>, while a subset of HSCs is located in the central marrow<sup>109</sup>. Frenette et al. showed that quiescent HSCs preferentially localize to arterioles in the endosteal-arteriolar region<sup>44</sup>. On the other hand, Itkin et al. observed that haematopoietic cell rolling and adhesion and transendothelial migration of mature leukocytes and immature HSPCs occurs exclusively via sinusoids<sup>110</sup>. Among the factors influencing HSC behavior in the two niches, the higher permeability and lower shear rates in sinusoidal vessels<sup>111</sup> allow penetration of plasma through the fenestrated endothelium from the peripheral blood. This in turn increases the intracellular levels of reactive oxygen species (ROS) in HSCs<sup>110</sup>, hampering their quiescence, accelerating their differentiation and exhaustion<sup>112</sup> and promoting their mobilization by activating their motility machinery<sup>113</sup>.



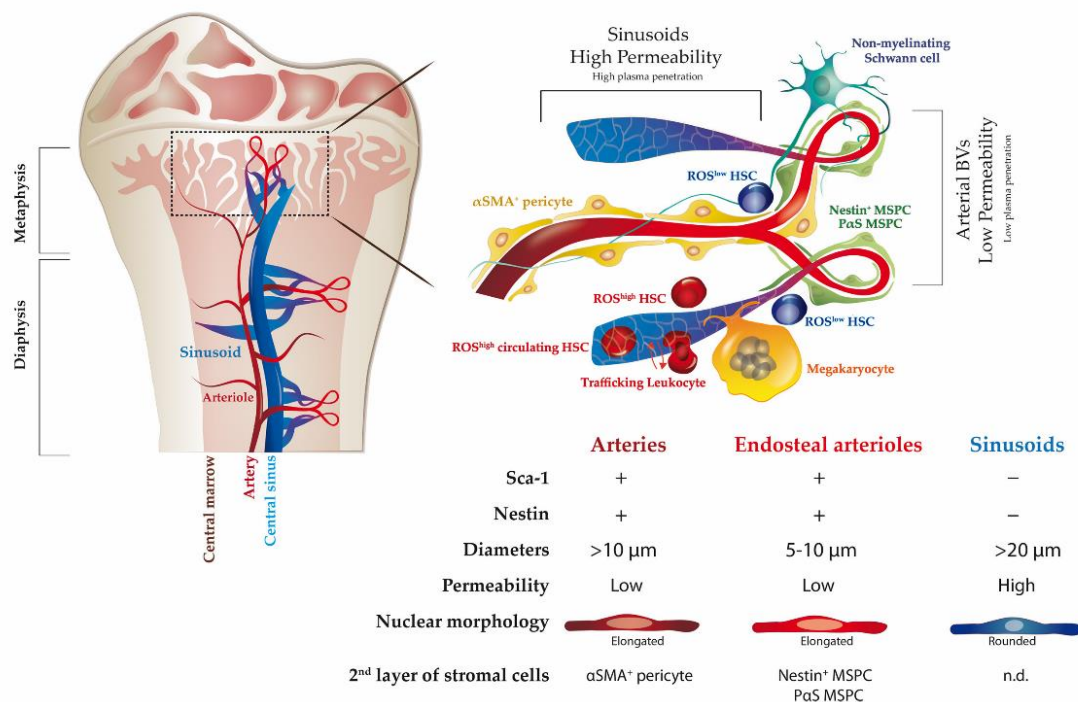


Figure 5: Representation of a proposed bone marrow blood vessels model and regulation of haematopoiesis by arterial bone marrow endothelial, sinusoidal endothelial cells, megakaryocytes, mesenchymal stem and progenitor cells and innervating Schwann cell nerve fibres <sup>110</sup>.

Several cell types of the bone marrow concur to the equilibrium of the niche. As previously mentioned, endothelial cells play an important role in defining the identity of the two bone marrow niches, and while endothelial cells are reported to promote HSC maintenance<sup>114</sup>, bone marrow sinusoidal endothelial cells promote long-term reconstituting HSC expansion in culture<sup>115</sup>. This process is likely mediated by the production from endothelial cells and MSCs-like cells of high levels of angiopoietin-like protein-3, E-Selectin<sup>116</sup>, stem cell factor (SCF)<sup>39</sup> and CXCL12<sup>40,106</sup>, and regeneration of sinusoidal endothelial cells is required for HSC homing and recovery of hematopoiesis after myeloablation<sup>117</sup>.

This important angiogenetic process, is regulated by different populations of pericytic cells. Although not completely characterized, sinusoidal pericytes likely functionally and morphologically overlap with several mesenchymal stromal cell populations, including CAR cells, leptin-receptor 1 stromal cells and nestin<sup>+</sup> stromal cells<sup>39,42</sup>, while arteriolar pericytes express high levels of CXCL12, SCF and NG2. Transplantation of mesenchymal stromal cells from the bone marrow has been shown to form chimeric “ossicles” supporting a functional hematopoietic microenvironment with blood vessels ingrowth upon transplantation at heterotopic sites<sup>36</sup>, while mesenchymal cells from non-bone tissues and differentiated osteoblasts interestingly failed to establish bone and hematopoiesis in the same experimental setup<sup>36,118</sup>.

Osteoblasts were long thought to play a central role in the formation of the bone marrow niche<sup>119</sup>, but following experiments showed that, unlike osteolineage cells<sup>120,121</sup>, alterations in the number of osteoblasts *in vivo* have no acute effects on HSC frequency<sup>122</sup> but may play an important role in lymphopoiesis and in lymphoid tissue function<sup>106</sup>.

Another cell type reported to reside in close proximity to ROS<sup>low</sup> early HSCs in sites distant from arteries are megakaryocytes. These cells have been reported to help maintaining HSC quiescence in the endosteal-arteriolar niche<sup>109,123</sup> through a mechanism mediated by Transforming Growth Factor  $\beta$ 1 (TGF- $\beta$ 1)<sup>123</sup> and C-X-C motif Chemokine Ligand 4 (CXCL4)<sup>109</sup> signaling and by thrombopoietin (TPO) availability<sup>124</sup>. Moreover, megakaryocytes support indirectly the bone marrow niche by stimulating proliferation of osteoblastic cells through fibroblast growth factor-1 (FGF-1) production<sup>123</sup>, inhibiting osteoclast formation<sup>125</sup> and interacting with long-lived plasma cells<sup>126</sup>.

Finally, CD169<sup>+</sup> macrophages constitute another cell type involved in the equilibrium of the bone marrow niche by regulating erythroid maturation<sup>127</sup> and promoting HSC retention in the bone marrow through stimulation of CXCL12 expression by nestin<sup>+</sup> cells upon circadian stimulation by sympathetic nerve fibers<sup>128</sup>.

### 1.2.2 Regulation of the Stem Cell Niche Dynamics

Despite the relatively recent identification of the major players of the bone marrow niche and their role in the regulation of hematopoiesis, important questions regarding the regulation of the balance between symmetric and asymmetric differentiation and the response to perturbations such as infection, anemia or inflammation by HSCs still remain unanswered. Several mathematical models propose to define HSCs' stemness based on lineages rather than single cells<sup>129</sup>, proposing that HSCs are "primed" before differentiation, with only 15-45% of HSCs in an active state dividing every 24-36 days and the rest comprising a dormant subset dividing every 110-193 days<sup>130</sup>. However, it is not yet clear whether HSC self-renewal and differentiation actually occur within the same niche or if regulation of hematopoiesis involves local mobilization of a HSC subset to neighboring niches followed by asymmetric division<sup>131</sup>. In fact, dividing cells residing into the niche have the potential to originate daughter cells remaining in contact with the niche microenvironment or to result in half of the daughter cells residing in the niche and half at a distance from the niche<sup>132</sup>.

Maintenance of this dynamic equilibrium is regulated by different signaling axes including secreted factors, cell-cell contact signaling and cell-matrix mediated systems. Among the secreted factors, CXCL12 produced from perivascular mesenchymal stromal cells, endothelial cells and osteoblasts<sup>37,40,106</sup> binds to the C-X-C motif Chemokine Receptor 4 (CXCR4) on the HSCs' membrane

and plays an important role for HSC retention into the niche<sup>40,106</sup>, maintenance of quiescence<sup>37,133</sup> and for the reduction of vascular permeability<sup>110</sup> by limiting oxidative stress injury in HSCs<sup>134</sup>. In this context, circadian fluctuations in CXCR4 and CXCL12 may allow HSCs and multipotent progenitor cells (MPPs) to uncouple from other niche signals promoting quiescence or lymphoid lineage commitment and allow for cell division, self-renewal and commitment to the myeloid lineage<sup>37,133</sup>.

Another signaling pathway involved in cell fate decision in the bone marrow niche is the Wnt signaling pathway. Wnt ligands can be divided in “canonical” - involving  $\beta$ -catenin, such as Wnt1, Wnt3A, and Wnt8 - or “noncanonical” - using  $\text{Ca}^{2+}$  signals or JNK kinases, such as Wnt5A and Wnt11<sup>135</sup>, which are mutually exclusive as a result of competition for receptor binding. While noncanonical Wnt signaling is required to maintain HSC quiescence, canonical Wnt is activated during stress conditions to induce HSC self-renewal and differentiation<sup>136</sup>. Among the other signals maintaining HSC quiescence, Angiopoietin 1 (Ang-1) promotes HSC interaction with the extracellular matrix and the cellular components of the niche<sup>137</sup> through  $\beta$ 1-integrin and N-cadherin, and activates several cell cycling regulators through the phosphatidylinositol 3-kinase/Akt signaling pathway<sup>121</sup>. Lastly, other two secreted factors, interleukin 18 (IL-18) and TGF- $\beta$  may play a role in maintenance of HSC quiescence *in vitro*<sup>138</sup> but may not be enough to maintain the HSC stem pool *in vivo*<sup>139</sup>.

Although maintenance of HSCs quiescence is important for long-term hematopoiesis, self-renewal and differentiation are important processes developed during evolution allowing mobilization of HSCs to the peripheral blood to react to injury and stress situation. The number of HSCs in the blood cycles in a circadian fashion, and mobilization of HSCs into the blood circulation can be stimulated by several hematopoietic cytokines, including granulocyte colony-stimulating factor (G-CSF), granulocyte-macrophage colony-stimulating factor, FMS-like Tyrosine Kinase 3 Ligand (Flt3L), kit ligand and TPO<sup>140</sup>. Moreover, other signaling molecules such as Hedgehog<sup>141</sup>, pleiotropin<sup>142</sup>, endothelial growth factor<sup>143</sup>, ANG ribonuclease<sup>144</sup>, parathyroid hormone (PTH)<sup>145</sup> and fibroblast growth factor<sup>146</sup> play important roles in the maintenance and expansion of long-term repopulating HSCs and in the regulation of endothelial integrity<sup>147</sup> upon irradiation. Finally, production of a number of different molecules such as lipopolysaccharide, single-stranded RNA and peptidoglycans during infection can stimulate HSC mobilization. These molecules are in fact ligands of Toll-like receptors (TLR), a family of pattern recognition receptors expressed on HSCs<sup>148</sup>, endothelial cells<sup>149</sup> and MSCs<sup>150</sup>, and activation of TLR4<sup>151</sup> and TLR5<sup>152</sup> signaling can lead to increased granulopoiesis, production of G-CSF and decrease of CXCL12 expression.

Secreted factors are important regulators of the bone marrow niche dynamics, acting both at local and systemic level for the coordinated response to external stimuli and for the preservation of normal hematopoiesis. Nevertheless, the absence of a physical barrier in the bone marrow, able to separate

the different microenvironments contained therein, makes it appealing to hypothesize that other mechanisms involved in the constraint of HSCs within the niche space are better able to maintain the different hematopoietic progenitors in their respective niches.

SCF constitutes one of the most important membrane-bound proteins expressed perivascularly by Lepr<sup>+</sup> mesenchymal stromal cells located around bone marrow sinusoids and at low levels by endothelial cells, and its deletion in these cell types depletes the bone marrow from HSCs<sup>39</sup>. Notch, a membrane protein present on HSCs' membrane, is particularly important during development, and loss of Notch signaling leads to HSC exhaustion and depletion over time<sup>153</sup>. Moreover, arteriolar endothelial cells express high levels of the adhesion molecules VCAM-1, ICAM-1, P-selectin and JAM-A<sup>154</sup>, while sinusoidal endothelial cells preferentially express E-selectin, which is involved in HSC homing to the bone marrow<sup>155</sup> and in the negative regulation of HSC quiescence<sup>116</sup>. Finally, Duffy antigen receptor for chemokines (DARC /CD234) is a transmembrane protein expressed on macrophages whose interaction with CD82/KAI1 on HSCs maintains the dormancy of long-term HSCs<sup>156</sup>.

Although signaling with the cellular microenvironment has been shown to largely determine cell fate in HSCs, the migration of hematopoiesis to the bone marrow suggests that further signals from the bone matrix are indeed able to partly drive or regulate essential mechanisms such as quiescence maintenance or residence in the niche. A local increase in pO<sub>2</sub> due to plasma infiltration into the marrow microenvironment and the consequent increase in intracellular reactive oxygen species (ROS) may in fact impair maintenance of quiescence in HSCs<sup>157</sup>, while calcium release upon remodeling of the bone matrix plays an important role for HSC homing to the endosteal niche<sup>158</sup>. Finally, several proteins of the extracellular matrix, such as heparan sulfate<sup>159</sup> and Osteopontin<sup>160</sup>, are crucial for the interaction and adhesion of HSCs to the niche microenvironment. Most interestingly, while molecules expressed on the HSCs' surface such as  $\beta$ 1-integrin<sup>121</sup>, N-cadherin<sup>121</sup> are downstream targets in Tie2 (TEK Tyrosine Kinase 2)/Ang-1 signaling<sup>161</sup> and TPO/myeloproliferative leukemia protein (MPL) signaling<sup>162</sup> in HSCs respectively, Osteopontin (OPN) has been shown to negatively regulate HSC number in the bone marrow niche<sup>163</sup> by maintaining the quiescence of long-term HSCs<sup>164</sup>. Taken together, these studies suggest that proteins mediating cell-matrix adhesion may not only contribute to the anchoring of HSCs inside the niche microenvironment, but may also regulate cell-cycle quiescence of HSCs in the bone marrow.

### 1.2.3 The diseased bone marrow niche and the role of Osteopontin

The bone marrow constitutes a microenvironment characterized by a great variety of functions, such as maintenance of cell stemness through quiescence, regulation of cell differentiation and cell fate, regulation of cell mobilization or retention in the bone marrow. Moreover, despite their abundance in the bone marrow, immune cells present in this microenvironment are at most progenitor cells which do not possess the terminal commitment required to exert a full immune response, making the bone marrow a *de facto* immune sanctuary. All these properties make the bone marrow niche an ideal microenvironment for the infiltration and proliferation of several hematopoietic cancers and metastasizing solid tumors.

Following malignant transformation of hematopoietic progenitors, leukemia can arise and disrupt normal hematopoiesis by competing with HSCs for the bone marrow niche. Leukemia stem cells can drastically alter the niche microenvironment by interacting with healthy hematopoietic cell types<sup>165</sup> and affecting mesenchymal stromal cells and osteoblast function<sup>166</sup>. By adapting the niche microenvironment to their need, leukemia stem cells can enter quiescence, acquiring drug resistance, while occasionally originating fast cycling daughter cells.

Leukemia can be classified on the base of which hematopoietic lineage is affected from the disease, either lymphocytes or myelocytes, and of the progression dynamics, either acute or chronic. The four main types of leukemia include therefore acute lymphocytic leukemia (ALL)<sup>167</sup>, chronic lymphocytic leukemia (CLL)<sup>168</sup>, acute myelocytic leukemia (AML)<sup>169</sup> and chronic myelocytic leukemia (CML)<sup>170</sup>. In the context of leukemia, Osteopontin has been associated to disease progression, contributing for instance to ALL progression and acquisition of chemotherapy resistance or insensitivity<sup>171</sup>, or binding to molecules such as CD44<sup>172</sup>, suggested to play an important role in CLL survival signaling<sup>173</sup>.

Beside leukemia, several hematopoietic malignancies affect the bone marrow niche. Among them, the induction of marrow fibrosis through the secretion of TGF- $\beta$  from immature or dysplastic megakaryocytes has been reported in myeloproliferative neoplasms such as myelofibrosis<sup>174</sup>, and the involvement of Osteopontin has been shown to be an important activator of large B-cell lymphoma<sup>175</sup> and non-Hodgkin's lymphoma<sup>176</sup>.

Moreover, Multiple Myeloma (MM) is a malignant disease of the bone marrow characterized by the clonal proliferation of malignant plasma cells which is of particular interest in the clinic, accounting for approximately 1% of all cancers and being the second most common hematologic malignancy after non-Hodgkin's lymphoma. Typical signs of MM are osteolytic bone lesions and bone pain, hypercalcemia, renal insufficiency, reduced hematopoiesis, reduced polyclonal immunoglobulin production and increase in bone marrow angiogenesis. MM cells profoundly change the niche

microenvironment by altering MSCs and osteoblasts both phenotypically and functionally<sup>177</sup>, with MSCs being expanded inside the bone marrow at the expense of osteogenesis. The clinical significance of MM derives to the fact that a subset of CD138<sup>-</sup> MM cells resides in the endosteal/osteoblastic region and enters quiescence, acquiring drug resistance and insensitivity to treatment<sup>178</sup>. Upon migration outside the niche, these cells are characterized by a higher heterogeneity comparing to a previous stage of the disease and by a higher drug resistance, leading to a 5-year disease-free survival rate of 49% and a 10-year survival virtually near to zero.

As previously reported, the bone marrow niche constitutes a rich microenvironment ideal for the long-term maintenance of stem cells. It is therefore not surprising that not just hematopoietic malignancies, but also other cancer types metastasize and home into the bone marrow. Among them, it has been shown that breast cancer-derived osteolytic bone metastases activate osteoblast and lead to tumor growth in the bone marrow<sup>179</sup>. Moreover, prostate cancer metastases can home to the bone marrow and even directly compete with normal HSCs for niche support<sup>180</sup>. Tumor cells from solid tumors often produce VEGF in order to promote angiogenesis. However, VEGF production results in a loss of sinusoidal vasculature in the bone marrow<sup>181</sup>, causing HSCs to mobilize to peripheral blood. Unfortunately, circulating HSCs are recruited to the tumor site, where they promote metastasis by developing into myeloid immunosuppressive cells upon G-CSF stimulation from cancer cells within the premetastatic site, leading to tumor progression and lower progression-free survival<sup>182</sup>.

This process may be partially mediated by Osteopontin (OPN), which is often found in the plasma of tumor patients and which is associated with increased metastatic risk<sup>183</sup>. Although OPN does not appear to influence the primary tumor size or the ability to incorporate bone-marrow derived cells, it influences the growth of distant metastatic lesions by activating the bone marrow<sup>184</sup> and mediating macrophage migration, activation and survival<sup>185</sup>. It is therefore possible to assume, that OPN indirectly affects HSC proliferation in cancer by inducing macrophage chemotaxis and cytokine production in the niche.

#### **1.2.4 Osteopontin**

Osteopontin (OPN) was initially described as a secreted phosphoprotein, identified together with BSP as one of the most abundant after collagen in the bone extracellular matrix<sup>186</sup>. Its name reflects the potential of this protein to serve as a bridge between cells and the hydroxyapatite on the bone surface<sup>187</sup>, but several names are actually reported in the literature depending on the function described for the very same protein, including Bone Sialoprotein II (BSP-II), early T-lymphocyte activation gene 1<sup>188</sup>(Eta-1) and secreted phosphoprotein 1 (SPP1).

OPN is a 34kDa protein expressed from a single-copy gene<sup>189</sup> on the long arm of chromosome 4 (4q13) and is extensively subject to post-translational modifications (PTM), with different variations of the protein residing in the same or different tissues. The reported size of the secreted protein varies from 44kDa to 75kDa due PTM differences that greatly influence its behavior on normal SDS-PAGE gels. Moreover, five different splice variants are reported for OPN, namely OPNa, OPNb, OPNc, OPNd and OPNe, resulting in five different isoforms lacking each one or more exons. OPNa is considered the full-length version of the protein, and a comprehensive scheme of the structure of the different isoforms and of the PTM sites is presented in Figure 6.

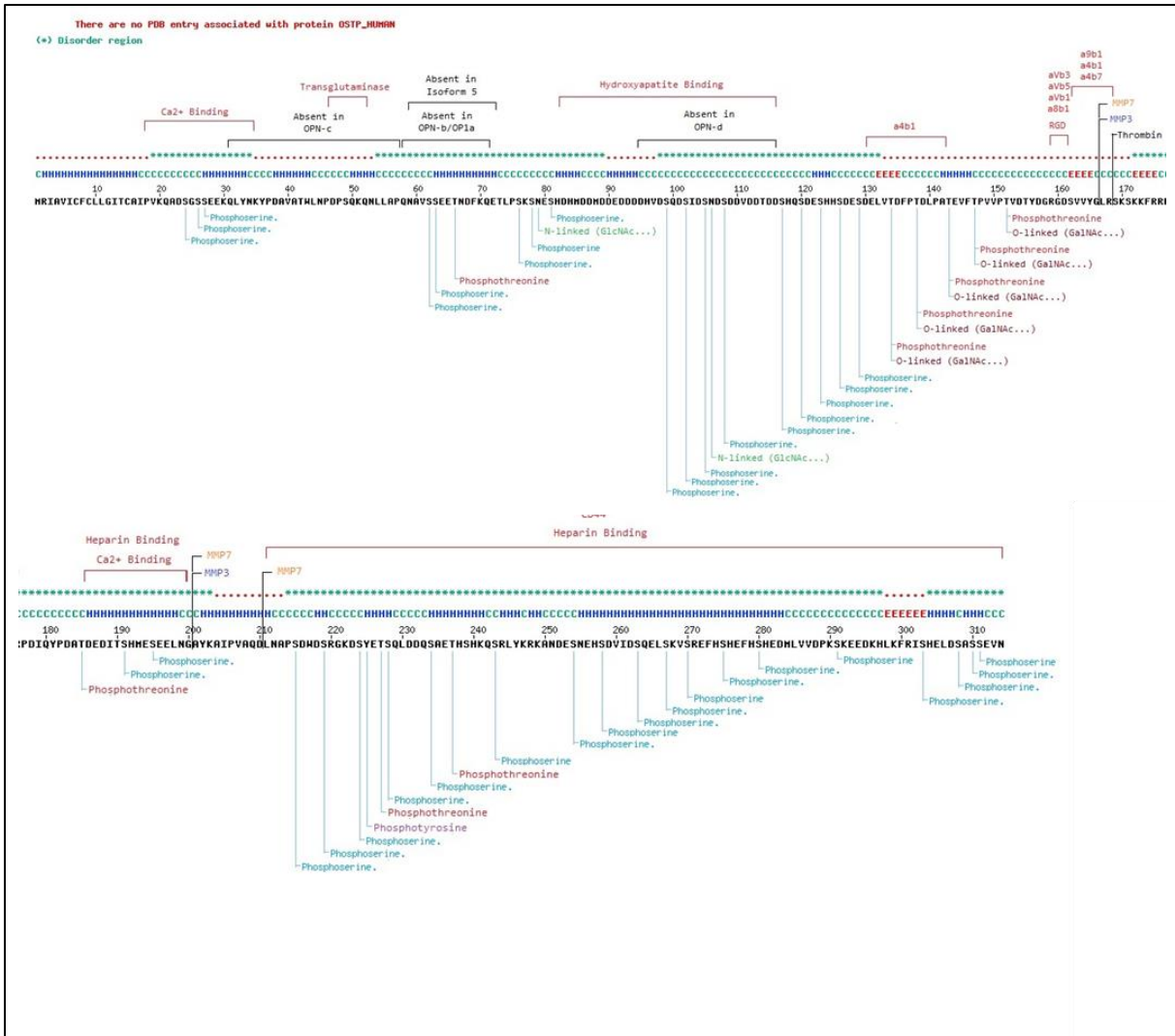


Figure 6: Schematic representation of the structure, splice variants and PTM of Osteopontin

OPN contains a polyaspartic acid motif<sup>190</sup> mediating the binding with hydroxyapatite and calcium ions<sup>187</sup>, and a RGD sequence (arginin, glycin, aspartic acid) mediating cell attachment. The RGD

sequence is flanked by a thrombin cleavage site, and OPN is also substrate of the matrix metalloproteases MMP3 and MMP7<sup>191</sup> at several sites. Upon thrombin cleavage, OPN exhibits an enhanced ability to stimulate cell adhesion and migration.

OPN contains multiple sites for serine and threonine phosphorylation by casein kinase II, Golgi-casein kinase, mammary gland casein kinase, cyclic adenosine monophosphate- and guanosine monophosphate- dependent kinases, protein kinase C or ectokinases<sup>190,192</sup>. In addition >33% of the weight of the protein is estimated to account for the glycosylation<sup>187</sup>, and sites for both N- and O-linked glycosylation have been reported<sup>193</sup>. Although OPN glycosylation may prevent OPN phosphorylation in transformed cells<sup>194</sup>, studies of bone formation *in vitro* indicate that sulphation of the oligosaccharidic chains predominantly occurs in the highly phosphorylated form of OPN<sup>195</sup>. Moreover, OPN presents a transglutaminase crosslinking site<sup>196</sup>, and has been shown to crosslink intra- and intermolecularly with fibronectin<sup>197</sup>, collagen, and compete for osteocalcin binding with transglutaminase<sup>198</sup>. Finally, it presents a potential site for N-myristylation which can attach proteins to membrane structures.

Despite and due to the great variability in the properties of this protein, given by splice variant isoforms and PTM, structural studies found that the protein does not present a folded structure apart from local 2D folding<sup>199</sup> (Figure 7). Because of this, immunodetection methods able to distinguish between the different splice variants and the different PTM *in vivo* and *in vitro* are still largely lacking, and few studies were able to reconstruct a specific OPN variant to its function. Therefore, the almost ubiquitous distribution of this protein and the wide range of functions described most likely reflect the high variability of this protein, unfortunately simplified with a single name.

OPN is in fact reported to be expressed in bone by osteoblasts<sup>200</sup> osteocytes<sup>201</sup> and osteoclasts<sup>202</sup>, dentin, cementum, hyperthrophic cartilage, kidney, brain, bone-marrow-derived stromal cells, vascular tissues and cytotrophoblasts of the chorionic villus in the uterus and decidua, ganglia of the inner ear, brain cells and specialized epithelia of mammary, salivary and sweat glands, bile and pancreatic ducts, distal renal tubules and gut, inactivated macrophages and lymphocytes<sup>193,203</sup>, fibroblasts during wound healing<sup>204</sup>, blood, milk (lactopontin), urine (uropontin) and seminal fluid<sup>205,206</sup>. Its expression is characteristically observed in pathological conditions such as atherosclerosis<sup>207</sup>, restenosis<sup>208</sup>, ventricular hypertrophy<sup>209</sup>, kidney diseases<sup>210</sup> and in various carcinomas and adenocarcinomas in which it is implied in the progression of the transformation process<sup>211</sup> and metastasis<sup>206</sup>.

Several functions are described for OPN in different tissues. The calcium and hydroxyapatite binding properties of OPN and its enrichment in biological fluids characterized by elevated levels of calcium salts is indicative of OPN's function as inhibitor of calcium salts<sup>210</sup>, hydroxyapatite<sup>212</sup> or calcium oxalate precipitation<sup>213</sup>. This function is highly dependent on PTM, as recombinant human OPN lacking PTM or



dephosphorylated cannot inhibit crystal formation<sup>214</sup>. OPN can mediate cell attachment, migration, chemotaxis, opsonizing activity<sup>215</sup> and intracellular signalling in various cells through the interaction between the RGD sequence and the  $\alpha_5\beta_1$ ,<sup>216, 217</sup>,  $\alpha_9\beta_1$ <sup>218</sup> and  $\alpha_8\beta_1$ <sup>219</sup> on the surface of endothelial muscle cells<sup>217</sup>, kidney cells<sup>219</sup>, platelets and macrophages<sup>204</sup> - where OPN inhibits the induction of inducible nitrogen oxide synthase (iNOS)<sup>220</sup>, osteoblasts<sup>187</sup> and osteoclasts<sup>216</sup>. Moreover, OPN binds extracellularly the hyaluronic acid receptor CD44<sup>221</sup> on the membrane of hematopoietic cells. The recruitment of macrophages and lymphocytes through local expression of OPN is employed by cancerous cells at a very early stage to suppress their cytotoxic activity<sup>220</sup> and to initiate autocrine signaling loops able to convert benign tumor cells into highly metastatic cells<sup>206</sup>. Consequently, tumor cells not expressing OPN are eliminated, and OPN-producing clones are selected in secondary metastases<sup>222</sup>. Most importantly, OPN has been particularly studied because of its role in hematopoiesis. In this context, OPN serves as a mediator for the specification between T helper type 1 and 2, their growth and differentiation, and for the regulation of the bone marrow niche<sup>163,164</sup>. Inside the niche in fact, OPN maintains constant the HSCs pool size, and lack of OPN results in expansion and ageing of the HSCs<sup>163,164</sup>. HSCs ageing, in turn, can be attenuated by treatment with thrombin-activated OPN<sup>223</sup>, which has been shown to interact with  $\alpha_9\beta_1$  integrin to regulate CD42 activity and control HSCs polarity.

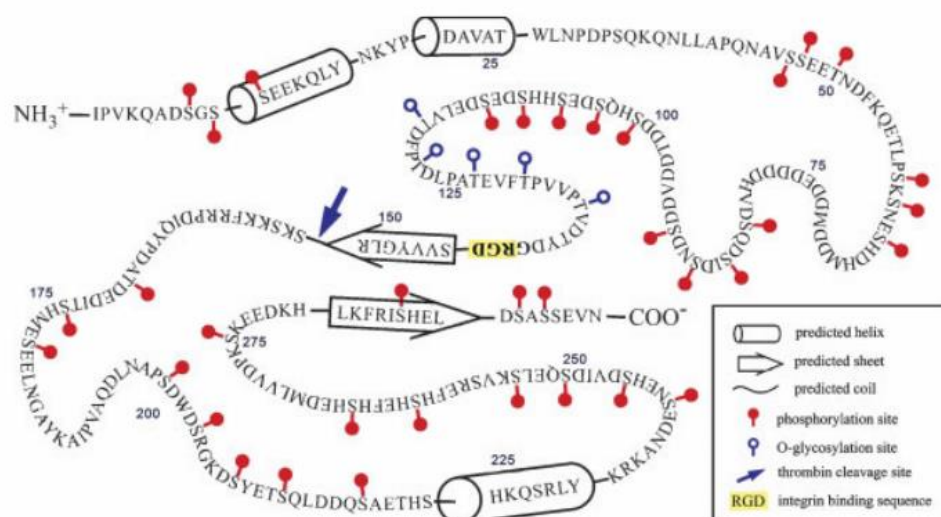


Figure 7: A model of the structure of the human Osteopontin based on prediction of secondary structure prediction<sup>192</sup>.

## 2 AIM OF THE STUDY

Tissue engineering represents a promising alternative approach with the potential to overcome the limitations of the therapeutic strategies, allowing for the *in vitro* reconstruction of bone through a combination of cells and scaffolds, and the implantation of a product derived from the patient's own material and characterized by low immunogenicity, tunable physical stability and virtually no side effects.

Primary aim of this study is therefore the development of a cell therapy for the cure of critical size bone defects based on an injectable mixed formulation comprising human bone marrow-derived mesenchymal stromal cells (hBMSCs) and recombinant collagen I-based macroporous microcarriers (Cellnest™-MCs). Important phases of the cell therapy development include (1) the optimization of a GMP-compliant culture medium for the expansion and osteogenic differentiation of hBMSCs, (2) the optimization of a scaffold for the culturing and expansion of hBMSCs and (3) the exploration of strategies for the mineralization of the scaffold and investigation on the possibility of mineral deposition on the synthetic matrix.

Moreover, the bone tissue lies in tight contact and functional relationship with the bone marrow, hosting and supporting hematopoiesis in adult and playing a role in homeostasis regulation.

Secondary aim of this study is therefore the demonstration of the functionality of the developed bone substitute through the establishment of a bone marrow model based on the co-culture of hematopoietic stem cells and osteogenically differentiated hBMSCs in the macroporous scaffold and the identification of key bone marrow niche factors within the model.

### 3 MATERIALS AND METHODS

The following section will illustrate the different material and methods employed for the different experiments, and the sequence of the experiments will mirror the structure of the results and discussion sessions. Since the Chair of Tissue Engineering and Regenerative Medicine can benefit from a well-organized pool of standard operating protocols (**SOPs**), the different methods will be referred to the relevant SOP whenever significant overlapping between the employed procedure and the relative SOP are present, and eventual discrepancies or adaptation of the SOP, alongside with the structure of the experiments, will be reported in the first part of this section. Frequently used methodologies will be referred to internally by directly citing the paragraph where the methodology has first been reported. Finally, the employed SOPs will be attached as an Appendix in alphabetic order at the end of this Thesis for better clarity.

#### 3.1 Human Bone Marrow Mesenchymal Stromal Cells characterization and biobanking

Human Bone Marrow Mesenchymal Stromal Cells (hBMSCs) were isolated from 15 osteoarthritic patients undergoing total hip replacement surgery according to the SOP **“Isolation und Kultivierung humaner mesenchymaler Vorläuferzellen (hMSC) aus Spongiosa”** and expanded in MSCGM-CD (Lonza) supplemented with 2% v/v FCS (10082147, Gibco) and 1% v/v Penicillin /Streptomycin (10378016, Gibco). Once 80% confluence were reached, cells were passaged according to the SOP **“Passaging Cells”** and aliquots were frozen at -80°C according to the SOP **“Freezing and Unfreezing of Cells”** in FCS 10% v/v dimethyl sulfoxide (DMSO) and later transferred to liquid nitrogen at -196°C. Cells between passage 1 and 2 were thawed according to the same SOP and seeded for characterization. This step was performed in order to subject the cells to further selective pressure and eliminate eventual contaminant macrophages in the culture. A list of the biobanked donors is reported in Table 2.

*Table 2: Anagraphical data of the biobanked donors.*

CODE	GENDER	AGE	CODE	GENDER	AGE
P1	F	62	P51	F	71
P44	M	65	P53	F	61
P45	M	77	P54	M	65
P46	M	73	P55	F	79
P47	M	70	P56	F	75
P48	F	37	P57	F	73

<b>P49</b>	M	64	<b>P58</b>	F	70
<b>P50</b>	F	51			

Expression of the surface-antigen markers CD29-PE (clone WM59, BD Pharmingen), CD44-FITC (clone G44-26; BD Pharmingen), CD73-PE (clone 55-7H1, BD Pharmingen), CD90-PE (clone MOPC-21; BD Pharmingen), CD105-PE (clone 266, BD Pharmingen) and negative markers CD14-FITC (clone 61D3, eBioscience) and CD45-PE (clone J33; Beckman Coulter) was verified by flow cytometry using a FACSCalibur (BD Biosciences) on cells passage 2-3.  $2 \cdot 10^5$  cells for each marker were resuspended in 100 $\mu$ l Dulbecco's Phosphate-buffered Saline (DPBS) (14190144, Gibco) 2% v/v FCS and marked with the previously reported antibody or with antihuman IgG1-PE (clone 679.1Mc7, Beckman Coulter) or antihuman IgG1-FITC (clone 679.1Mc7, Beckman Coulter) control isotypes. After washing once with DPBS, cells were resuspended in 200 $\mu$ l DPBS 2% v/v FCS and at least  $10^4$  events/sample were counted.

Characterization of the differentiation potential of the hBMSCs towards the osteogenic, chondrogenic or adipogenic lineage was performed through culturing of cells between passage 2 and 4 in the respective differentiation media according to the SOP "**Differentiation of mesenchymal precursor cells (hMSCs)**". Cells differentiation was confirmed histologically by staining of the mineral matrix deposited by osteogenically differentiated cells (SOP "**Alizarin Red Staining**"), of the proteoglycans deposited by chondrogenically differentiated cells (SOP "**Alcianblau-Färbung**"), or of the intracellular lipid droplets produced by adipogenically differentiated cells (SOP "**Ölrot-Färbung**"). Of note, Alizarin Red staining is really sensitive to variations in pH, that should be maintained in a range between 4.1 and 4.3. For this reason, counterstaining with hematoxylin cannot be easily performed on these samples, and quantitation of the percentage of osteogenically differentiated cells is not possible, although inter-donor variations in the deposited mineral material can be detected.

Furthermore, cell differentiation was investigated by RT-Real Time PCR of the expression of adipogenic, chondrogenic and osteogenic markers in differentiated cells at 14, 21 or 28 days respectively post differentiation and compared with cell cultured in TheraPEAK MSCGM-CD (190632, Lonza) 2% v/v FCS. RNA was extracted with the RNeasy Micro Kit (Qiagen) after disruption of the membranes with QIAshredder columns (Qiagen) following the manufacturer's instruction<sup>224</sup>, and was retro-transcribed to cDNA following the SOP "**cDNA-Synthese qRT-PCR**". Optimal annealing temperature for all the employed primers was determined by gradient qPCRs in a range comprising the melting temperature ( $T_M$ ) as indicated by the manufacturer. Efficiency of each primer couple was determined with the CFX Manager software (Bio-Rad) by performing a qPCR on serially 1:10 diluted samples using the determined optimal annealing temperature. qPCRs of the differentiation markers were then performed according to SOP "**qRT-PCR**" and data were analyzed following the  $\Delta\Delta C_t$  method by

comparing the different samples with the average of the housekeeping genes EF1 $\alpha$ , GAPDH and HPRT1, displaying a coefficient of variation of normalized reference gene-relative quantities <0.5 and M-value <1. The full sequence of the employed primers is reported in Table 3.

*Table 3: Primers employed for PCR and RT-Real Time PCR*

Gene	Forward	Reverse	Efficiency	Tm (°C)
<b>Col1a1</b>	CACACGTCTCGGTCATGGTA	AAGAGGAAGGCCAAGTCGAG	88.5%	60
<b>Runx2</b>	GAATGGCAGCAGCTATTAATCC	GCCGCTAGAATTCAAACAGTTGG	95.1%	60
<b>BMP2</b>	GCTGTACTAGCGACCCAC	TCATAAACCTGCAACAGCCAACTCG	90.6%	60
<b>BGLAP</b>	TTGGACACAAAGGCTGCAC	CTCACACTCCTCGCCCTATT	86.7%	50
<b>BSP</b>	GCAGTAGTGACTCATCCGAAGAA	GCCTCAGAGTCTTCATCTTCATTC	97%	60
<b>ALP</b>	CTTGACCTCCTCGGAAGACACTC	GCCTGGTAGTTGTTGTGAGCATAG	101.6%	60
<b>OSX</b>	CATCTGCCTGGCTCCTTG	GCCATAGTGAACCTCCTCCTCA	90.7%	53
<b>OPN</b>	TTGCAGTGATTTGCTTTTGCT	TTGGAAGGGTCTGTGGGGCTA	104.8%	50
<b>SPARC</b>	GGCGAGTTTGAGAAGGTGTG	GGATGTATTTGCAAGGCCCG	98.9%	50
<b>OG</b>	GCGCTCGTGTCTGACAT	ACACGGTCTTCCACTTTGCT	95.6%	50
<b>Col2a1</b>	CGGCTTCCACACATCCTTAT	CTGTCTTCCGGTGTGAGGG	88.1%	60
<b>Col10a1</b>	GCTGAACGATACCAATGCC	GTGGACCAGGAGTACCTTGC	92.3%	60
<b>Aggrecan</b>	GGTCTCACTGCCAACTACC	TCGAGGGTGTAGCGGTAGAGA	93.6%	60
<b>Sox9</b>	GCTCAGCAAGACGCTGGGCA	TCCGTGGCCTCCTCTGCCTC	94.9%	60
<b>FABP4</b>	GACAGGAAAGTCAAGAGCACCA	CGCTTTCATGACGCATTCC	100.1%	50
<b>PPAR<math>\gamma</math>2</b>	CATTACGGAGAGATCCACGG	CCAGAAAGCGATTCTTCAC	89.6%	60
<b>LPL</b>	CCGCCGACCAAGAAGAGAT	TAGCCACGGACTCTGCTACT	96.8%	60
<b>Glut4</b>	CCAGTATGTTGCGGAGGCTAT	AAGGCAGCTGAGATCTGGTC	98.8%	60
<b>CD90</b>	CTAGTGGACCAGAGCCTTCG	TGGAGTGCACACGTGTAGGT	99.5%	60
<b>EF1<math>\alpha</math></b>	AGGTGATTATCCTGAACCATCC	AAAGTGGATAGTCTGAGAAGC	91.9%	60
<b>HPRT1</b>	TGACCTTGATTTATTTGCATACC	CGAGCAAGACGTTTCAGTCCT	90.1%	60
<b>GAPDH</b>	TGACGCTGGGGCTGGCATTG	GCTCTTGCTGGGGCTGGTGG	88.6%	60
<b>RPS27A</b>	TCGTGGTGGTGCTAAGAAAA	TCTCGACGAAGGCGACTAAT	90.1%	60
<b>OPNiso</b>	ATGAGAATTGCAGTGATTTGCTTTGCCT	CATGGTCATCATCATCTTCATCATC	/	57

### 3.2 Optimization of a GMP-compliant medium for hBMSCs expansion and differentiation

Preliminary media testings were performed by culturing hBMSCs at 1.500 or 3.000 cells/well for 1, 3, 5 or 7 days in 96-well plates and detecting living cells through measurement of the ATP activity with the CellTiterGlo reagent (Promega) according to SOP “Zytotoxizitätstest\_CellTiterGlo”. The same protocol was performed to investigate the effect of FCS substitution with PDL in the following conditions:

Condition	Medium
<b>1</b>	MSCGM-CD
<b>2</b>	MSCGM-CD 2% FCS
<b>3</b>	Basal Medium (Evonik) + 50ng/ml basic FGF (bFGF) + 2mM alanyl-glutamine
<b>4</b>	Basal Medium + 50ng/ml bFGF + 2.5% Advanced Platelet Lysate
<b>5</b>	Basal Medium + 2.5% Filtered PDL

6	Basal Medium + 10ng/ml PDGF-BB + 2mM alanyl-glutamine
7	Basal Medium + 1ng/ml bFGF + 2mM alanyl-glutamine

Expression of surface markers through flow cytometry and histological analysis of the differentiation potential of the cells after 14 days of culture in MSCGM-CD, MSCGM-CD 2%FCS or Basal Medium 5%PDL was performed following the same protocols as described in the previous section (*3.1 Human Bone Marrow Mesenchymal Stromal Cells characterization and biobanking*).

In-house production of PDL was performed according to the protocol published by Schallmoser et al.<sup>59</sup>. Briefly, 500ml blood bags were collected at 10 different time points from a blood collection center of the Bavarian Red Cross in the proportion of 4 bags from blood group O donors and 1 bag from blood group AB donors. This strategy was adopted in order to avoid exposure of blood group-specific antigens, eventually present on the remnants of membranes of platelet and erythrocytes, to the cells to be cultured, and to avoid administration of antibodies directed against group A or B antigens as present in the plasma of donors of blood group A, B or O. A total of 50 bags were pooled together to form the final product. 40ml of blood were poured from the bags in 50ml tubes and centrifuged at 4250g for 13 minutes without break in order to separate a red blood cell fraction at the bottom of the tube, a supernatant comprising plasma, and a buffy coat at the interface containing mononuclear cells. The buffy coat of 4 blood group O bags was then mixed with the plasma from one blood group AB bag and realiquoted in 50ml tubes to be centrifuged at 300g for 6 minutes without break. This second step was performed in order to separate a red blood cell containing fraction at the bottom of the tube from the plasma and platelets containing fraction in the supernatant. Platelets-containing fractions were collected, aliquoted in 50ml tubes and stored at -80°C. This step was performed in order to lyse the platelets and release the growth factors contained in the platelets into the plasma. Once collection of the donors was completed, the platelet-containing fractions were thawed, pooled together in order to standardize the resulting product, and re-aliquoted for storing at -20°C. Before use, PDL fractions were thawed, centrifuged at 4000g for 15min and the supernatant was filtrated with 0.02µm nylon syringe filters in order to remove eventual cell membrane remnants. In order to test the functionality of the isolated platelets, 1ml of platelet-rich-plasma obtained after the second centrifugation was reconstituted with 10, 20, 50 or 100µl of 10% w/v CaCl<sub>2</sub>. Functionality of the isolated platelets could be detected by precipitation of the platelet and the formation of a fibrin-rich gel.

In order to evaluate possible differences in morphology, hBMSCs of passage 2-4 were cultured in MSCGM-CD 2%FCS, DMEM-F12 (Gibco) 2.5%PDL, DMEM-F12 5%PDL or DMEM-F12 5%PDL 50ng/ml bFGF for 1, 3, 5 and 7 days at 3.000cells/cm<sup>2</sup> in 12-well plates. Differences in morphologies were evaluated after analysis of the images acquired with a Zeiss Axio Vert.A1 cell culture microscope in

brightfield. The proliferation potential of MSCGM-CD 2%FCS, DMEM-F12 5%PDL, DMEM-F12 10%FCS and DMEM-F12 alone were tested by seeding hBMSCs of passage 1-2 at 1.500cells/cm<sup>2</sup> according to SOP **“Growth curve in 24-well plate”** in the different media. Once cells of one case reached 80% confluence, all cells were trypsinized, manually counted and passaged to another 24-well-plate (SOP **“Passaging Cells”**). Medium was changed every second day (SOP **“Medium Change”**) and cells not reaching confluence after 14 days were considered senescent and were not passaged further.

Testing of the influence of FCS substitution with PDL in osteogenic differentiation media on osteogenic differentiation was performed on hBMSCs from passage 2-4. For testing in 2D conditions, cells were seeded in 24-well plates and cultured either in osteogenic medium with 10% FCS or with 5% PDL according to SOP **“Differentiation of mesenchymal precursor cells (hMSCs)”** or in MSCGM-CD 2%FCS (Negative control). Detection of the osteogenic differentiation was then performed according to the SOP **“Alizarin Red Staining”**. For testing in 3D conditions, 10<sup>5</sup> cells were seeded into 200µl of rat tail collagen I gel created by mixing 2 parts of 9.6µg/ml collagen solution in 0.1% v/v acetic acid (506007, Sigma) with 1 part of GNL solution (SOPs **“Making Gel Neutralization Solution “GNL” for Establishing Skin Models”**, **“Isolation von Kollagen Typ I aus Rattenschwänzen”**) and differentiated towards the osteogenic lineage by culturing in MSCGM-CD 2%FCS (Negative control) or osteogenic medium with either 10%FCS or 5%PDL according to the SOP **“Differentiation of mesenchymal precursor cells (hMSCs)”**. At the end of the differentiation period, samples were snap-frozen in liquid nitrogen and embedded in OCT embedding medium (4583, Tissue-Tek). Samples were then later cut in 10µm-thick slices with a Leica cryotome and mineral deposition was detected by Alizarin Red staining (SOP **“Alizarin Red Staining”**) and cells were detected with Hematoxylin counterstaining (SOP **“HE-Färbung”**).

### **3.3 Optimization of the macroporous microcarriers for hBMSCs expansion and delivery**

Collagen I-based recombinant peptide (RCP) is commercially available as Cellnest™ (Fujifilm Manufacturing Europe B.V.) originated through sequential in-tandem cloning of RGD-containing fragments of the human collagen type I molecule, and it results in a gelatin-like material that can be dehydrated and stored for longer periods in solid form, to be then resuspended into double distilled water for scaffold fabrication. It is characterized by molecular weight of 51.7 kDa and isoelectric point of ≈ 10.02. Cellnest™ microcarriers (Cellnest™-MCs) were prepared via a double emulsification method as described by Goosens in patent WO2016063935. Briefly, a first emulsion containing 3% v/v Cellnest™, 2% v/v Tween 80 (P1754-1L, Sigma), 30% v/v water and 65% v/v corn oil (47112-U, Sigma) was heated at 60°C and stirred at 535rpm. A second emulsion was prepared via addition of corn oil to the first emulsion and subsequent cooling to 4°C while stirring at 350rpm. The solution was transferred

in cool acetone (439126, Sigma) under stirring for 5min and at room temperature for an hour. MCs were finally washed four times in acetone and filtered with a void pump before being dried out at 60°C overnight. MCs were either crosslinked for 4 days with the dehydrothermal (DHT) method at 160°C under vacuum conditions, or for 24h in presence of 1-Ethyl-3-(3-dimethylaminopropyl)-carbodiimide (EDC) (03449-25G, Sigma) in 100% ethanol (K928.4, Roth) or hexamethylene diisocyanate (HMDIC)(52649-100ML, Sigma) in 100% ethanol. Standard commercially available CultiSpher® G (M9418-10G, Percell) or in-house manufactured crosslinked Cellnest™-MCs were swelled in DPBS overnight and autoclaved, then washed once with DPBS and thrice with culture medium before cell seeding. Sieved particles of 100-400µm diameter were used for the experiments.

Crosslinked microcarriers were dehydrated in a 70-100% alcohol gradient with increasing concentration followed by 10min incubation in hexamethyldisilazane (379212-100ML, Sigma). Samples were left drying overnight and prepared for Scanning Electron Microscopy (SEM) imaging. Microscopy was performed with a Jeol JSM-6330F Field Emission Scanning Electron Microscope under established conditions and the average pore dimension was calculated by measurement of the larger pore diameter in randomly selected pores performed with Fiji (Image J 1.51g). Micro-Computed Tomography (µCT) analysis was done with a Bruker Skyscan 1172. Image analysis and computer simulation was carried out with Volume Graphics software VGStudio Max. The average diameter of the internal pore interconnections was calculated by plotting the accessible void volume against the diameter of the penetrating particle in the computer simulation for each individual microcarrier and by calculating the diameter of a hypothetical particle accessing 50% of the total accessible volume. In this way, I assumed that the average diameter of interconnections between internal pores would allow a particle of the same diameter to access 50% of the void volume of the microcarrier.

### **3.3.1 Cell seeding on Cellnest™ and related procedures**

The seeding protocol was modified starting from the report by Chen et al.<sup>63</sup> and from CultiSpher®'s protocol<sup>225</sup>. Autoclaved 25ml Spinner Flasks (Wheaton) were washed once with 10ml DPBS, then 30mg of MCs were seeded in each Spinner Flask in 8ml medium. Spinner Flasks were maintained for 30 minutes in a standard cell incubator before seeding  $2.5 \times 10^5$  cells/ flask in 2ml volume. Uniform cell seeding on the MCs was achieved by repeating 4 cycles of 5 minutes stirring at 80rpm and 55 minutes resting at 37°C in a humidified atmosphere of 5%CO<sub>2</sub>. At the end of the seeding, 10ml of medium were added to the culture and continuous stirring at 85rpm was started. Half of the total medium volume was changed every day, and the culture was maintained up to 7 or 28 days. Cell adhesion to the scaffold was evaluated through DNA quantification after 24h. SEM microscopy of colonized beads was



performed as described at 3.3 *Optimization of the macroporous microcarriers for hBMSCs expansion and delivery* after fixation of 1mg of MCs for 10min with 4% paraformaldehyde (47608-1L-F, Sigma).

### **3.3.2 Live/Dead Staining, DAPI staining, DNA quantification and RT-Real Time PCR on Cellnest™**

At day 2, 4 and 7 after seeding 0.5mg of MCs were collected from each Spinner Flask, washed with DPBS and incubated with Live/Dead Cell Double Staining Kit (04511-1KT-F, Sigma) at 37°C for 20 minutes<sup>226</sup>. Living cells were detected using a fluorescence microscope with 490nm emission filter, while dead cells were detected using a 545nm emission filter. For the DAPI staining (D9542-50MG, Sigma), MCs were washed with DPBS, fixed in 4% paraformaldehyde for 10 minutes and incubated with the 29mg/ml DAPI in dH<sub>2</sub>O for 45min on a rocking shaker. Cell nuclei were detected using an Olympus BX60 fluorescence microscope with 420nm emission filter. For the DNA content quantification, 0.5mg of MCs were collected from each Spinner Flask, washed with DPBS, pelleted and frozen at -80°C for a minimum of 6 hours. After thawing, samples were incubated at 60°C overnight with 300µl of papain (1495005-1G, Sigma) 5U/ml. Quantification of DNA content was performed after establishment of the appropriate titration curves with Quant-iT™ PicoGreen® dsDNA Assay Kit (P7589, Thermo Fisher) following the manufacturer's instructions<sup>227</sup>. Measurement of the fluorescent signal was performed at 520nm with a BioTek FLx800 reader. Cell proliferation was evaluated assuming similar DNA content between cells of the same population, and population doublings (PDs) were calculated following the formula:  $PDs = 3.32 \cdot \log(\text{DNA content at the sampling time point} / \text{DNA content at day 1})$ . Extraction of RNA from the hBMSCs cultured on the different microcarriers, retro-transcription of the RNA in cDNA and RT-Real Time PCR of the early differentiation markers Runx2 and Col1a1 were performed as described in the section 3.1. *Human Bone Marrow Mesenchymal Stromal Cells characterization and biobanking*.

### **3.4 Investigation of strategies for hBMSCs differentiation and mineralization of the microcarriers**

In order to investigate the differentiation capability of hBMSCs on DHT-, HMDIC- or EDC-Cellnest™-MCs and CultiSpher®, cells were seeded on the microcarriers as described in 3.3.1 *Cell seeding on Cellnest™ and related procedures* and, after expansion for 7 days in MSCGM-CD 2%FCS, they were differentiated in osteogenic medium (SOP "**Differentiation of mesenchymal precursor cells (hMSC)**"). Negative controls were cultured in MSCGM-CD 2%FCS. After 28 days of differentiation, qPCR analysis of the expression of the differentiation markers Runx2 and Osterix (OSX) was performed as described in 3.3.2 *Live/Dead Staining, DAPI staining, DNA quantification and RT-Real Time PCR on Cellnest™*. Alternatively, whole constructs were embedded in resin (SOPs "**Embedding in Technovit 9100**",

**“Sectioning of polymer embedded tissues”, “Ponal Coating”**) and stained for collagen type 1 (BP8028, Acris Antibodies) (SOP **“Immunofluorescence with fluorochrome”**) or Alizarin Red (SOP **“Alizarin Red Staining”**). In order to test the possibility to assemble Cellnest™-MCs into a solid construct, hBMSCs were seeded on the microcarriers as described in 3.3.1 *Cell seeding on Cellnest™ and related procedures* and seeded in a perfusion bioreactor equipped with 500µm mesh-filters at the extremities, as described by Kleinhans et al.<sup>228</sup>, after 7 days of expansion. During the 7 days of expansion the growth of the hBMSCs allows in fact to join different microcarriers into bigger clusters that can be retained in the perfusion chambers by the filters at the two extremities. After 14 of perfusion with either osteogenic medium or with MSCGM-CD 2% FCS, the samples were embedded in resin (SOPs **“Embedding in Technovit 9100”, “Sectioning of polymer embedded tissues”, “Ponal Coating”**) and stained for collagen type 1, OPN (ab69498, Abcam), Runx2 (ab76956, Abcam) or vimentin (ab8069, Abcam) (SOP **“Immunofluorescence with fluorochrome”**). Fluorescent signal was then detected after marking with anti-rabbit (A-31573, Invitrogen) or anti-mouse (A-31571, Invitrogen) secondary antibodies conjugated with Alexa-647

In order to test the effect of Cellnest™ (RCP) or Cellnest™-hydroxyapatite (RCP-HA) microbeads on hBMSCs differentiation, microbeads were produced in-house at ISTECCNR (Istituto di Scienza e Tecnologia dei Materiali Ceramici, Consiglio Nazionale delle Ricerche). Briefly, for the RCP production a 36% w/w solution of recombinant collagen peptide Cellnest™ in double distilled water was emulsified in corn oil at 45°C for 20 minutes and then cooled down at 5.5°C. The solution was then transferred in cool acetone under stirring for 5 minutes and stirred at room temperature for an hour. The particles were finally washed three times for 10 minutes in acetone and filtered with a void pump before being dried out at 40°C overnight. For the RCP-HA production, a 36% w/w solution of Cellnest™ in double distilled water was added to a H<sub>2</sub>PO<sub>4</sub> solution (W290017-1KG-K, Sigma) and added dropwise to a Ca(OH)<sub>2</sub> solution (450146-25G, Sigma) in order to obtain a Ca:PO<sub>4</sub> molar ratio of 1.67. The solution was left to mineralize at room temperature overnight and emulsified as described for the RCP. Both for RCP and RCP-HA, particles were crosslinked for 2 days with the DHT method at 160°C. Crosslinked beads were resuspended in PBS and sterilized through autoclaving. Sieved particles of 50-75µm were used for the experiments. Influence of RCP and RCP-HA microbeads on hBMSCs vitality and morphology was tested in 2D conditions. hBMSCs were seeded at 2.500cells/cm<sup>2</sup> in 24-well plates on mouse collagen 1 (5162-1G, Sigma) coated round coverslips and cultured for 24 hours in 500µl DMEM Low Glucose 10% FCS 1% Pen/Strep at 37°C in a humidified atmosphere of 5% CO<sub>2</sub>. The following day, RCP or RCP-HA were seeded in each well at the concentration of 0.4mg/ml, and the cells were cultured in this conditions for 1, 3 or 7 days without medium exchange. Cells alone without microbeads were used as negative controls. At day 1, 3 or 7 the samples were retrieved and treated either for Live /Dead staining or for Actin staining. For the Live/Dead staining, culture medium was removed and cells were

washed with PBS and stained with Live/Dead Viability/Cytotoxicity kit (L3224, Invitrogen) following the manufacturer's instruction<sup>229</sup>. The coverslips were then removed from the wells and microscoped using the FITC filter for living cells and the TRITC filter for the dead cells on a LAS X Widefield Leica microscope. For the Actin staining, cells were fixed for 10 minutes in 4% paraformaldehyde and washed in PBS. After blocking with 5% FBS and permeabilization for 7min with 0.1% Triton (X100-500ML, Sigma) in DPBS cells were stained with FITC-conjugated phalloidin (P5282-.1MG, Sigma). Coverslips were retrieved and fixed on a glass slide Entellan (1079600500, EMD Millipore). For the 3D assay, hBMSCs at the concentration of  $5 \cdot 10^6$  cells/ml with RCP or RCP-HA beads at the final concentration of 0.4mg/ml were embedded in rat tail collagen type I-gels as described in *3.2 Optimization of a GMP-compliant medium for hBMSCs expansion and differentiation*, and cultured for 7, 14, 21 and 28 days in either DMEM low glucose 10%FCS or in osteogenic medium with medium exchange every second day. For Live/Dead staining, collagen gels were washed once with DPBS and stained with Live/Dead Viability/Cytotoxicity kit for 20 minutes. Gels were then washed with DPBS, transferred on a glass slide and covered with mounting medium before being microscoped. Alternatively, gels were snap-frozen in liquid nitrogen and embedded in OCT compound. 10 $\mu$ m-thick slices of the gels were finally cut with a Leica microtome and stained with Alizarin Red (SOP "Alizarin Red Staining").

### **3.5 Establishment of a Bone Marrow Niche model**

The Bone Marrow Niche model was established starting from the protocol presented for the differentiation of hBMSCs towards the osteogenic lineage as reported in *3.4 Investigation of strategies for hBMSCs differentiation and mineralization of the microcarriers*. Specifically, microcarriers seeded with hBMSCs at day 21 of differentiation were transferred in 8 $\mu$ m mesh transwell inserts (BR782960, BRAND) at the concentration of 105cells/insert. Subsequently,  $2 \cdot 10^4$  CD34<sup>+</sup> freshly thawed bone marrow-derived HSCs (2M-101B, Lonza) were resuspended in HPGM medium (PT-3926, Lonza) without addition of any further cytokine and seeded in each transwell. Complete medium exchange was performed every 3 days. At day 7 of co-culture, constructs were retrieved for analysis. In other experiments, anti-OPN antibody (ab69498, Abcam) were injected in the constructs at the concentration of 0.125 $\mu$ g/ml or 1.25 $\mu$ g/ml in two different doses at the beginning of the co-culture and at the first medium exchange to achieve a total concentration of 0.25 $\mu$ g/ml or 2.5 $\mu$ g/ml. At day 7 of the co-culture, the colonized microcarriers containing the osteo-hBMSCs- or hBMSCs-HSCs co-cultures were transferred to 15 ml tubes and beads were lysate with 2.5% w/v Trypsin (37289.01, Serva Electrophoresis) for 10min at 37°C. Cells retrieved after trypsinisation of the constructs were separated into a CD34<sup>+</sup> fraction containing hHSPCs and a CD34<sup>-</sup> fraction containing hBMSCs using the CD34 MicroBead Kit UltraPure (130-100-453, Miltenyi Biotec) following the manufacturer's instructions<sup>230</sup>.

Half of the CD34+ fraction was resuspended in RLT buffer (Qiagen) and processed for RNA extraction. RNA extraction, cDNA retro-transcription and RT-Real Time- PCR for Alkaline phosphatase (ALP), collagen type 1 (Col1a1), bone morphogenetic protein 2 (BMP2), Runx2, Osteoprotegerin (OG), Osteocalcin (BGLAP), Osteonectin (SPARC), Osteopontin (OPN) and Osterix (OSX) were performed as reported in *3.1 Human Bone Marrow Mesenchymal Stromal Cells characterization and biobanking*. Primers are listed in Table 3. Alternatively, cells were resuspended in Cell Resuspension Media (HSC003, R&D) and mixed with a Methylcellulose Complete Media (HSC003, R&D) to create a solution of 1.27% Methylcellulose. This is a semi-solid medium containing a cocktail of cytokines intended to propel the differentiation of hematopoietic progenitor cells to a more differentiated and committed stage during the course of 14-16 days. The cell suspension was then injected with a syringe on a 35mm Petri dish. Finally, two 35mm Petri dishes with cells and one with 3ml sterile dH<sub>2</sub>O without lid were placed into a 100mm Petri dish and incubated at 37°C 5%CO<sub>2</sub> for 14-16 days. Upon appearance of colonies on the plate, the colonies were counted with a light microscope on a transparent grid, and 4 different fields were counted for each individual plate. Colonies were differentially classified as BFU-E (burst forming unit erythroid) and CFU (colony forming unit) –E (erythroid), -G (granulocyte), -GM (granulocyte-macrophage), -M (macrophage) and –GEMM (granulocyte erythrocyte macrophage megakaryocyte).

Constructs that were not lysed for RNA isolation or methylcellulose assay were fixed in paraformaldehyde and prepared for SEM microscopy (as reported in *3.3 Optimization of the macroporous microcarriers for hBMSCs expansion and delivery*) or embedded in resin (SOPs **“Ponal Coating”**, **“Embedding in Technovit 9100”**, **“Sectioning of polymer embedded tissues”**). 5µm-thick sections of the samples were then stained either for Hematoxylin & Eosin (SOP **“HE-staining”**), or for Alizarin Red (SOP **“Alizarin Red Staining”**) or for immunofluorescence marking of Osteopontin (SOP **“Immunofluorescence with fluorochrome”**) (ab69498, Abcam). Osteopontin splicing variants detection was performed by PCR with Pfu DNA-polymerase (in-house produced) with OPNiso primers (Table 3) as reported by Phillips et al.<sup>231</sup>. The PCR consisted in a first denaturation step of 3min at 95°C, 20 cycles of 10 sec 95°C – 30sec 57°C – 30sec 72°C, and a final elongation step for 30sec 72°C. PCR samples for splicing variants identification with OPNiso primers were run on a 1.5% Agarose gel (840004, Biozym) with GelRed (41001 - 41003-T, Biotium) and images of the gels were acquired with a UV Transluminator (Vilber Lourmat). Corresponding bands were isolated using the Wizard SV Gel and PCR clean-up system (Promega) and sequenced.

### 3.6 Recombinant OPNa and OPNb are differently produced and deposited

Plasmids pDest490-OPN-a and pDest490-OPN-b were purchased from Addgene (#17590 and #17591)<sup>232</sup> as stab agar colonies. Colonies were plated on Ampicillin-containing LB medium (SOP **“Agar Plates”**), and single colonies were picked for a pre-expansion in 5ml liquid LB-Medium overnight. After expansion, plasmidic DNA was then isolated with PureYield™ Plasmid Miniprep System (A1223, Promega) and sequenced, and 1ml of the sequenced colony was transferred in 4ml of liquid LB medium for a pre-expansion and later to a 200µl liquid LB medium for expansion. Plasmidic DNA was then isolated with a PureYield™ Plasmid Maxiprep System (A2392, Promega) and quantified using a NanoQuant Plate on an Infinite M200 plate reader (Tecan).

hFOB 1.19, HEK293 and CaCo2 cells were expanded until confluence for the transfection experiments. hFOB 1.19 were cultured in DMEM-F12 without phenol red (21-041-025, Gibco) 10%FCS 0.3 mg/ml G418 (A1720-5G, Sigma). HEK293 cell line was cultured according to SOP **“Transfektion von 293T Zellen zur Virusproduktion”**. CaCo2 cell line was cultured according to SOP **“Zellkultur der Caco-2-Zelllinie”**. The three cell lines were transfected with either pDest490-OPN-a or pDest490-OPN-b using the FuGene HD Transfection Reagent (11814443001, Roche) at a plasmid:reagent ratio of 1:3 following the manufacturer’s instructions<sup>233</sup>. For detection of the transfected OPNa, OPNb or the endogenous OPN, cells were cultured on chamberslides (177437, Thermo Fisher) and were marked with either anti-FLAG (F3165-.2MG, Sigma) or anti-OPN antibody (ab69498, Abcam) respectively after fixation for 10min with paraformaldehyde and blocking with TBS 5% FCS. Primary antibodies were detected with an Alexa647-conjugated anti-mouse secondary antibody and microscoped with a Keyence microscope. For detection of the transfected OPNa and OPNb with Western Blot, culture medium was collected after 48h from the transfection. The protein fraction in the medium was concentrated using Amicon® Ultra -15 (UCF901024, Millipore) and resuspended in RIPA modified cell lysis buffer (SOP **“Lysepuffer”**). Similarly, the cell fraction was lysed with RIPA modified cell lysis buffer and the protein concentration of the two fractions was determined according to SOP **“Cell lysis and protein concentration determination”**. Western Blot of the protein fractions was performed according to SOP **“SDS-Gel und Western Blotting”** and the two isoforms were detected with an anti-FLAG antibody followed by an anti-mouse secondary antibody. In order to better isolate the two OPN isoforms, a 6-Histidine tag-containing insert was cloned into the pDest490 plasmids replacing the pre-existent FLAG tag to create the pDest490-OPNa-6His and pDest490-OPNb-6His plasmids. Briefly, the amplicon expanded with the following forward 5′-CAAGAAGGTACCGGATCACAAGTTTG-3 and reverse 5′-TTGTTTCGCTCGACTTAATGTGTATGTGTATGTATTGACCTCAGAAGATGCACTATC-3′ primers was inserted in the original plasmids after cutting with Asp718 (000000011175050001, Sigma) and Sall (000000010348783001, Sigma) on both the original plasmid and the insert. hFOB1.19 cells were transfected with either pDest490 OPNa-6His or pDest490-OPNb-6His using the FuGene HD

Transfection Reagent at a plasmid: reagent ratio of 1:3 following the manufacturer's instructions<sup>233</sup>, and proteins were isolated from either the medium or the cell layer as previously described. Recombinant OPNa-6His and OPNb-6His fusion proteins were purified through affinity chromatography by binding to nickel-agarose microbeads (Ni-NTA Agarose) (1018240, Qiagen) and eluting with a gradient of imidazole (I5513-100G, Sigma). The collected fractions were then run on a SDS-PAGE gel and stained for Coomassie staining according to the SOP "**SDS-Gel und Coomassie-Färbung**". Eluted fractions contained the purified proteins were then pooled together and proteins were quantified according to SOP "**Cell lysis and protein concentration determination**".

For the methylcellulose assay, 20.000 CD34<sup>+</sup> freshly thawed HSCs were seeded in methylcellulose assays as described in 3.5 *Establishment of a Bone Marrow Niche model* after 16 hours of incubation in HPGM 50ng/ml TPO (CYT-115, Prospecbio), 50ng/ml FLT3L (CYT-706, Prospecbio), 25ng/ml SCF (CYT-111, Prospecbio) and 10ng/ml IL-3 (CYT-096, Prospecbio) with either 40ng/ml of in-house produced OPNa, OPNb or a commercially available full length OPN (OPN-FL) (120-35, PreproTech) as described by Guidi et al.<sup>223</sup>. After 14 days, colony counting and characterization was performed and samples were compared to HSCs not incubated with any OPN isoform.

### **3.7 Possible applications of a bone marrow niche model: the case of multiple myeloma**

In order to test the applicability of the Bone Marrow Niche model for the study of hematologic malignancies, the protocol as reported in 3.5 *Establishment of a Bone Marrow Niche model* was adapted for the culturing of the interleukin-6 -dependent multiple myeloma cell line INA6, replacing HSCs in this adapted version of the model. INA6 cells, kindly given from Prof. Franziska Jundt were cultured in RPMI 1640 10%FCS 2.5µg/ml IL-6 and were IL-6 starved for 24 hours and marked for 1 hour with Vybrant™ DiD Cell-Labeling Solution (V22887, Thermo Fisher) before injection in the model at day 21 of hBMSCs's osteogenic differentiation. Medium was changed to a 50%-50% mixture of osteogenic medium and RPMI 1640 10%FCS and medium exchange was performed every 3 days. After 3, 5 or 7 days of co-culture, microbeads were lysate for 10min in 2.5% Trypsin and released cells were spotted on a glass slide, fixated for 10min in paraformaldehyde and stained with an anti-vimentin (ab8069, Abcam) antibody followed by an Alexa488-conjugated anti-mouse secondary antibody (A-21202, Invitrogen). Stained cells were covered with Fluoromount -G with DAPI (00-4959-52, Invitrogen) and microscopied with a Keyence microscope.

### **3.8 Statistical analysis**

All experiments were repeated using hBMSCs of at least three different donors (n=3) between passage 2 and 4. Cell lines employed for the experiments (C2C12, hFOB1.19, HEK293, CaCo2, INA6) were used between passage 1 and 12. OriginPro 8.6 was used to perform the statistical analyses. Statistical differences between groups were determined using two-tailed Welch test for normally distributed samples, or using Mann-Whitney-U Test for not normally distributed samples. Comparison between two or more experimental groups was performed with one-way ANOVA for normally distributed samples or Kruskal Wallis for non-normally distributed samples, followed by Tukey's post-hoc test. Differences were considered statistically significant when p-values  $\leq 0.05$ , and very statistically significant when p-values  $\leq 0.01$ . All values are reported as mean  $\pm$  SD.

## 4 RESULTS

### 4.1 Human bone marrow mesenchymal stromal cells characterization and biobanking

hBMSCs from passage 2-4 were characterized for the expression of surface markers through flow cytometry. All donors presented expression of the positive markers CD29, CD44, CD73 (Sh3/4), CD90 (Thy1) and CD105 (SH2) and lacked the expression of the negative markers CD14 and CD45 (Figure 8). Although no characterization was performed on cells from passage 0 and 1 in order to minimize eventual macrophage contaminants, a certain degree of variability could be detected between donors in the percentage of cells expressing the different markers.

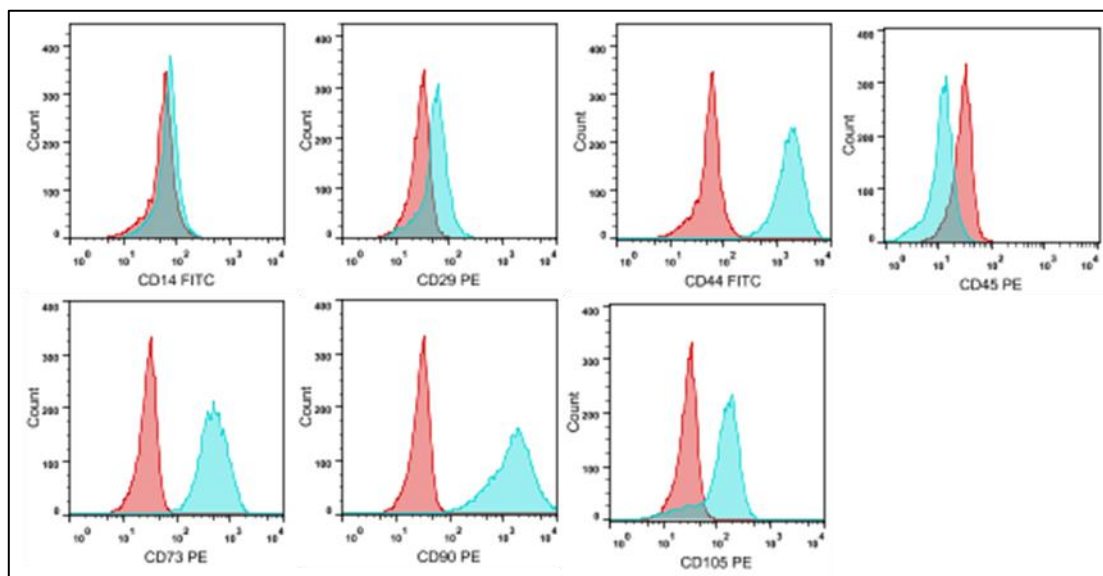


Figure 8: Expression of surface antigen markers by hBMSCs from passage 2-4 isolated from osteoarthritic patient P44

Moreover, hBMSCs from passage 2-4 were cultured until confluence on Permanox chamberslides for adipogenic and osteogenic differentiation or in pellet culture after centrifugation and 24h pellet assembling in a 15ml Falcon tube for chondrogenic differentiation before being differentiated in the respective differentiation media. Differentiation of hBMSCs towards the adipogenic lineage was detected through staining with Oil Red O of the intracellular lipid droplets, and cell nuclei were detected through Hematoxylin staining of the chromatin. Oil Red O staining detected the presence of multiple lipid droplets in variable percentage ranging from as little as 50% to 80-90% of the cultured cells depending on the donor (Figure 9A, B). In contrast, Alcian Blue staining allowed to detect the deposition of glycosaminoglycans characteristics of the cartilage tissue in hBMSCs (identified through Nuclear Fast Red counterstaining) pellet cultures of all donors, indicating successful chondrogenic differentiation of hBMSCs after stimulation with TGF- $\beta$ 3 (Figure 9C, D). Finally, Alizarin Red staining of



the deposited calcium phosphate allowed to detect deposition of mineralized material from osteogenically differentiated hBMSCs, confirming their potential to differentiate towards the osteogenic lineage for all donors (Figure 9E, F).

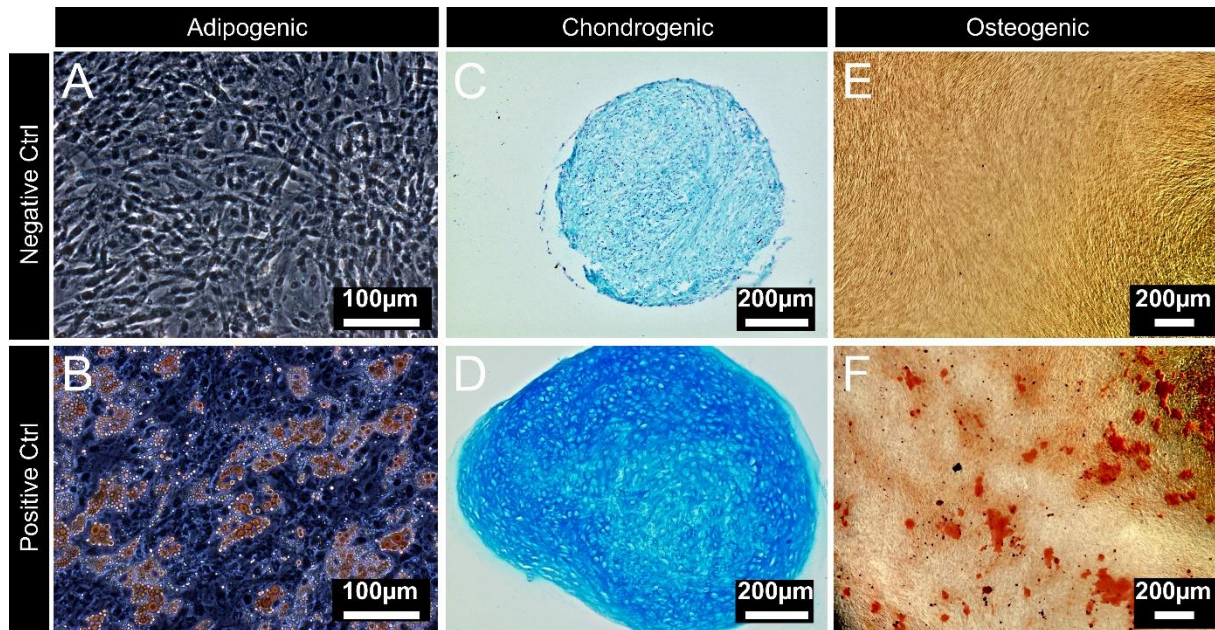


Figure 9: Differentiation of BMSCs toward the adipogenic (A, B), chondrogenic (C, D) and osteogenic (E, F) lineages (P44). **Upper row:** Negative control; **Lower row:** Differentiated samples.

In order to provide a better characterization of the biobanked donors, RT-Real Time PCRs of key differentiation markers were performed on RNA extracted from the differentiated hBMSCs after retro-transcription into cDNA and compared with undifferentiated negative controls cultured in the proliferation medium MSCGM-CD at the same time point. Interestingly, although histological detection of hBMSCs osteogenic differentiation revealed significant production of mineralized material, quantification of the expression of osteogenic differentiation markers such as the early differentiation markers alkaline phosphatase (ALP), collagen 1 (col1a1), bone morphogenetic protein 2 (BMP2) and Runx2, and the late differentiation markers bone sialoprotein (BSP), osteoprotegerin (OPG), osteocalcin (BGLAP), osteonectin (SPARC), osteopontin (SPP1) and osterix (OSX) didn't allow to confirm any significant upregulation of these genes in several donors when compared to the negative controls, although a general upregulation trend could be detected (Figure 10).

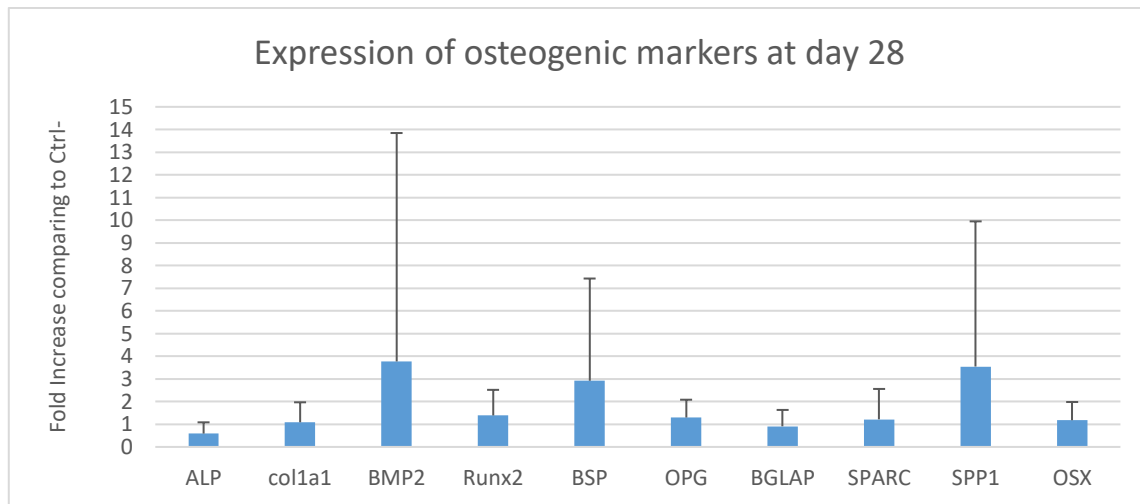


Figure 10: RT-Real time PCR analysis of the expression of osteogenic differentiation marker genes after 28 days of differentiation, compared to hBMSCs cultured in MSCGM-CD (n=15)

#### 4.2 Optimization of a GMP-compliant medium for hBMSCs expansion and differentiation

Since the development of a cell-based therapy requires conformity to GMP-regulations, I explored the possibility to develop a GMP-compliant medium for the expansion of hBMSCs and their differentiation towards the osteogenic lineage.

During preliminary experiments, I compared different commercially available basal media employed for the expansion of hBMSCs and I identified DMEM-F12 as the best competitor to the MSCGM-CD chemically defined medium. However, supplementation of MSCGM-CD medium with 2% FCS led to a 2.8 increase in the total cell yield over the course of 7 days (data not shown), and I therefore focused the following experiments on the replacement of fetal bovine serum with recombinant or human-derived components including human albumin and bovine serum albumin (BSA), bFGF and Insulin-like Growth Factor (IGF). Although supplementation of DMEM-F12 with BSA and a combination of bFGF and IGF led to a 1.5-fold-increase in cell yield over the course of 5 days, this increase didn't prove to be significantly different from supplementation of bFGF alone, and cell yield still resulted to be 10 times lower than MSCGM-CD 2% FCS. Further preliminary experiments were then conducted in order to explore the possibility to replace FCS with other GMP-compliant, non-chemically defined substitutes. In these experiments, we compared the effect of supplementation of a basal medium produced by EVONIK Industries with a commercially available advanced platelet-derived lysate with or without bFGF, a combination of PDGF and alanine-glutamine or bFGF and alanine-glutamine, and the MSCGM-CD medium with or without FCS on hBMSCs proliferation. These experiments pointed out that, although supplementation of PDL to a basal medium could not provide the same cell yield of the MSCGM-CD + 2% FCS, optimally performing for cell proliferation but not anymore chemically defined, it could lead to a 1.9-fold increase in the cell number as compared to MSCGM-CD without FCS (Figure

11A). Moreover, hBMSCs cultured in EVONIK's basal medium + 5% PDL retained the expression of all the MSCs-specific surface antigens (Figure 11B) and the potential to differentiate towards the adipogenic and osteogenic lineages (Figure 11C).

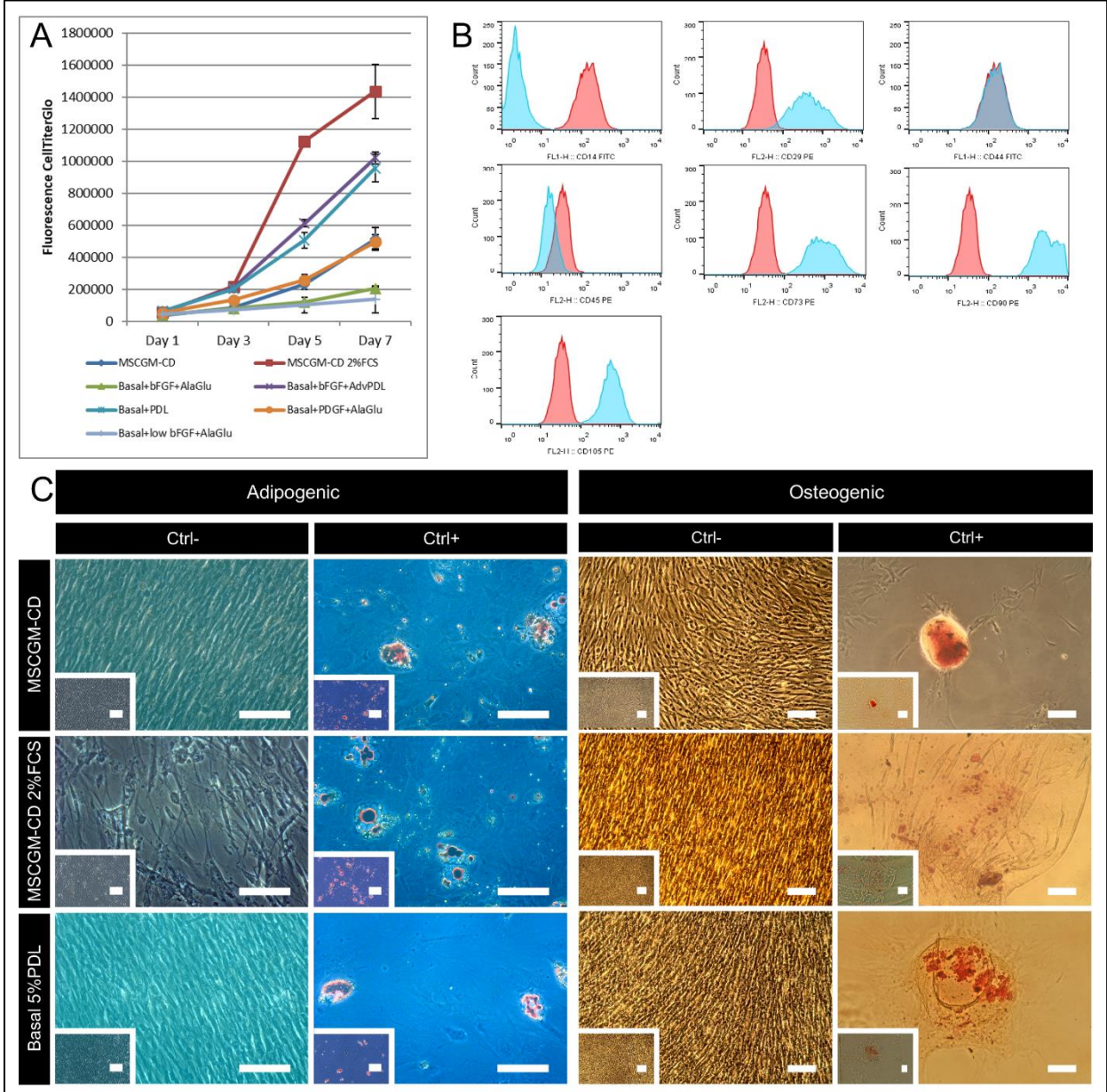


Figure 11: Characterization of cells expanded in Evonik Medium + 5% PDL. Cells expanded with Evonik Medium + PDL **A)** proliferate better than MSCGM-CD without FCS, **B)** retain surface antigen marker expression and **C)** adipogenic and osteogenic differentiation potential. **Scalebar:** 100µm (n=2)

Having identified PDL as a promising GMP-compliant candidate for the replacement of FCS for hBMSCs expansion, I established a protocol for the in-house production of PDL starting from peripheral blood following the protocol indicated by Schallmoser et al.<sup>59</sup>. The plasma fraction obtained with this method contains viable platelets that can be activated to produce a fibrin-rich gel upon reconstitution with

CaCl<sub>2</sub> (Figure 12A), and the final product ready for cell culture application can be produced after further processing.

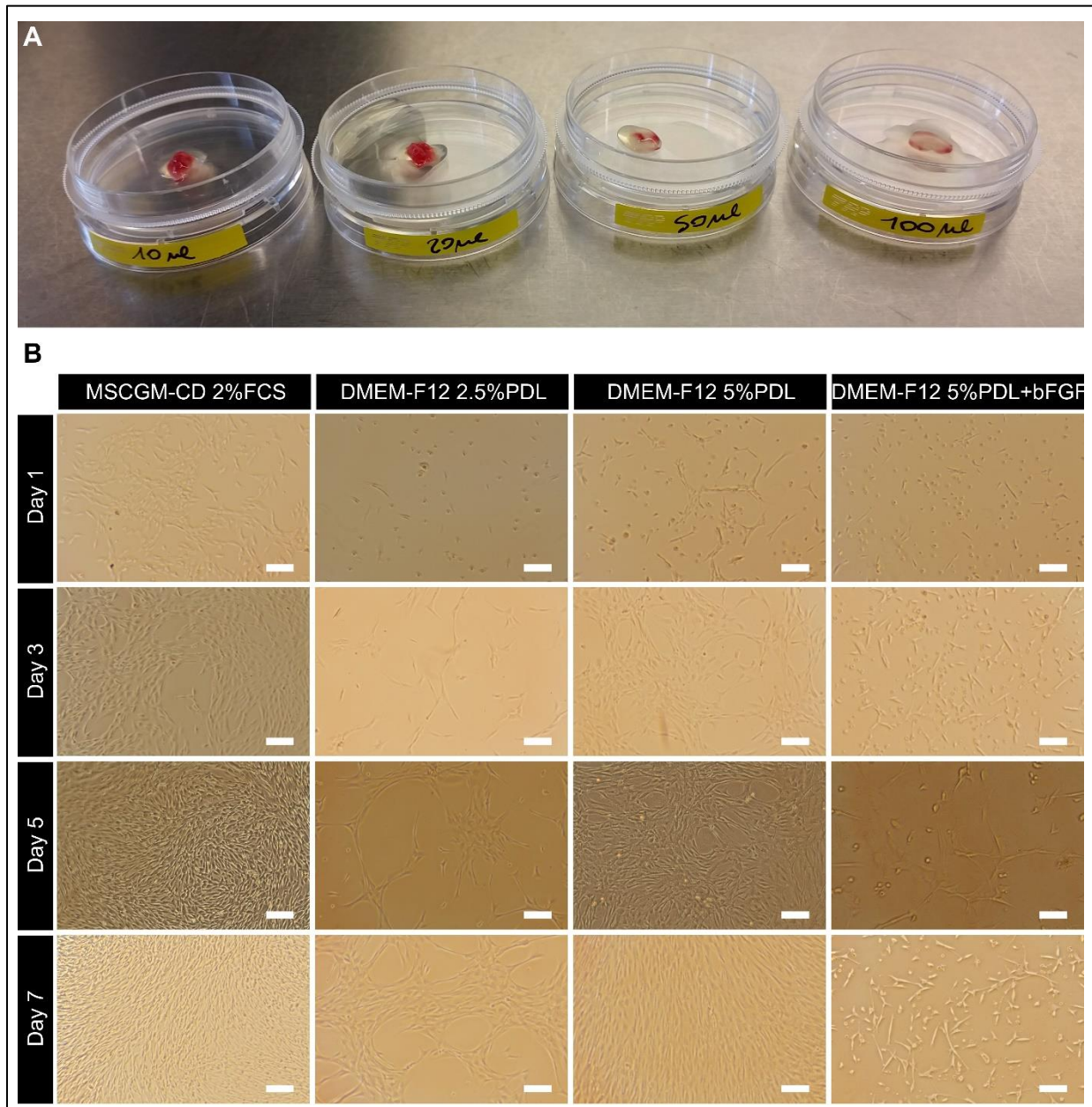


Figure 12: **A)** PDL produced in house retain the potential to form fibrin-rich gel upon CaCl<sub>2</sub> reconstitution. **B)** hBMSCs cultured DMEM-F12 5% PDL proliferate well overtime and retain good morphology. **Scalebar:** 100µm (n=3)

In order to test the potential of PDL as a FCS substitute for hBMSCs proliferation, I therefore supplemented DMEM-F12 with either 2.5% or 5% PDL and compared it with MSCGM-CD +2% FCS in order to compare the effect of PDL on cell morphology (Figure 12B). In all conditions, hBMSCs assumed a fibroblast-like morphology and established cell-cell contacts after few days of culture. Interestingly,

while cells cultured in MSCGM-CD formed a thick collagen layer and started growing to overconfluence, occasionally forming thick clusters that were contracting and disrupting the cell layer, cells cultured in DMEM-F12 + PDL formed a nice monolayer. While cells cultured in DMEM-F12 5%PDL reached 100% confluence after 7 days, cells cultured in DMEM-F12 2.5% only reached 50% confluence during the same timeframe. Moreover, when adding bFGF to DMEM-F12 5%PDL, shown in preliminary experiments to provide an advantage in hBMSCs proliferation, cells started detaching from the culturing surface and didn't reach confluence (Figure 12B).

On the basis of the cell morphology analysis, I performed further proliferation studies on four different donors to compare the effect of DMEM-F12 5% PDL with DMEM-F12 10% FCS and MSCGM-CD 2% FCS, using DMEM-F12 alone as a negative control (Figure 13). The cells were grown in 12-well plates and for practical reasons all cells were passaged when one of the 4 cases reached confluence. The experiment was stopped once the cells couldn't reach confluence within 14 days after passaging. Although a strong difference in the final population doublings could be observed in different donors, the MSCGM-CD 2% FCS medium appeared to perform better, yielding  $8 \pm 2$  population doublings ( $n=4$ ) more comparing to DMEM-F12 5% PDL over the course of 60 days. However, DMEM-F12 5% PDL performed significantly better ( $p<0.05$ ) when compared to DMEM-F12 10% FCS and DMEM-F12 alone, yielding  $17 \pm 5$  population doublings ( $n=4$ ) more. This result shows that, although the DMEM-F12 5% PDL can be improved for hBMSCs expansion purposes, it holds the potential as effective GMP-compliant medium.

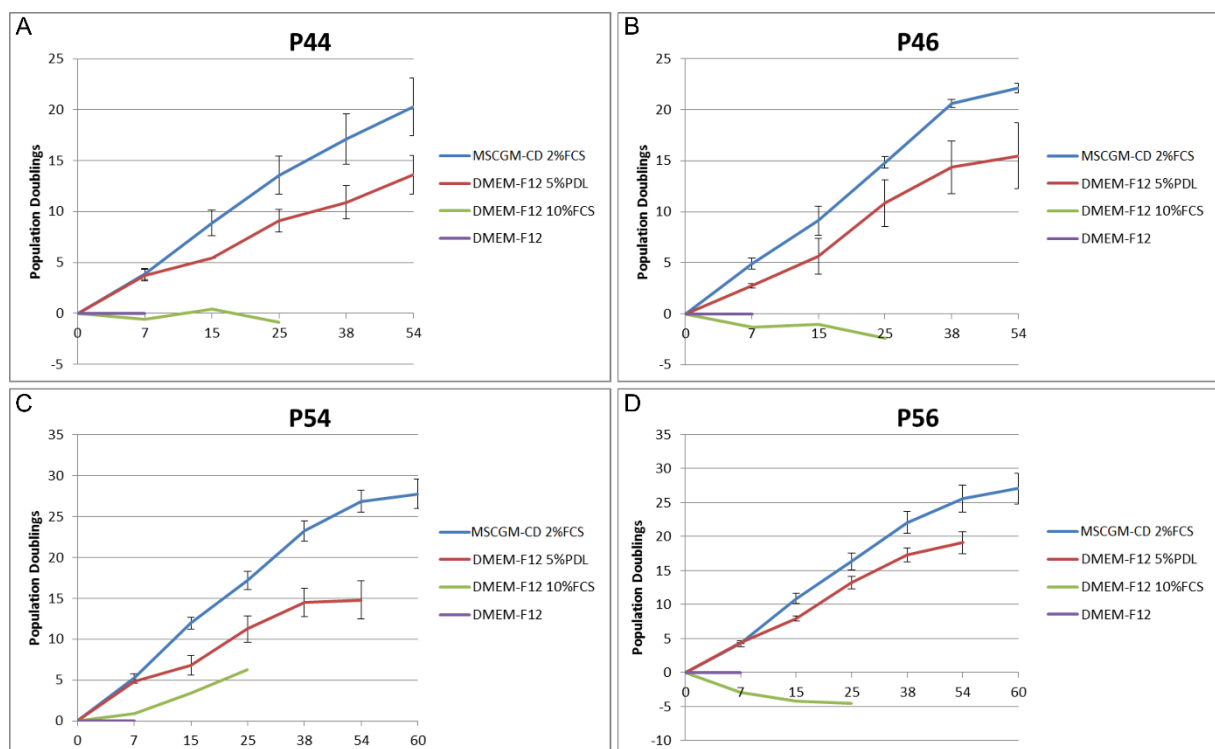


Figure 13: Proliferation curves of hBMSCs of donors P44, P46, P54 and P56 expanded in MSCGM-CD 2% FCS, DMEM-F12 5% PDL, DMEM-F12 10% FCS and DMEM-F12 alone.

After demonstrating the efficacy of PDL in expanding hBMSCs, we therefore investigated the effect of substitution of 10% FCS with 5% PDL in the commonly reported osteogenic medium containing ascorbate-2-phosphate, dexamethasone and  $\beta$ -glycerophosphate. We cultured the hBMSCs in 24-well plates or in a rat tail collagen I-hydrogel for 28 days in either osteogenic medium with FCS or PDL and compared it to MSCGM-CD 2% FCS (2D conditions) or DMEM 10% FCS (3D conditions) as negative controls (Figure 14). In 2D conditions (n=5), hBMSCs cultured in osteogenic medium supplemented with PDL deposited a thick layer of mineralized material covering the whole surface of the well, with a significant increase in the quantity of deposited material starting already from day 7-14, while hBMSCs cultured in standard differentiation medium supplemented with FCS started depositing mineralized material from day 14-21 in sparse isolated spots. Interestingly, when staining the mineralized material deposited by hBMSCs cultured in rat tail collagen I hydrogels (n=3), this dramatic difference was only partially detectable, with an increase in the overall staining starting from day 14 (Figure 14).

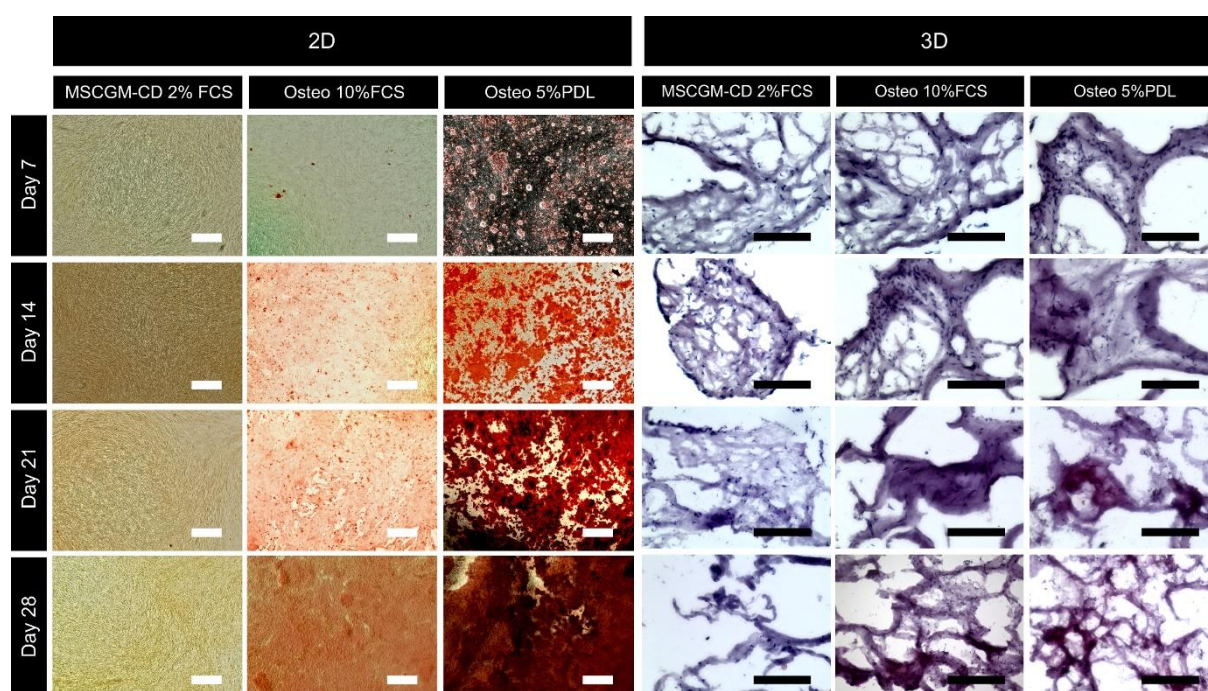
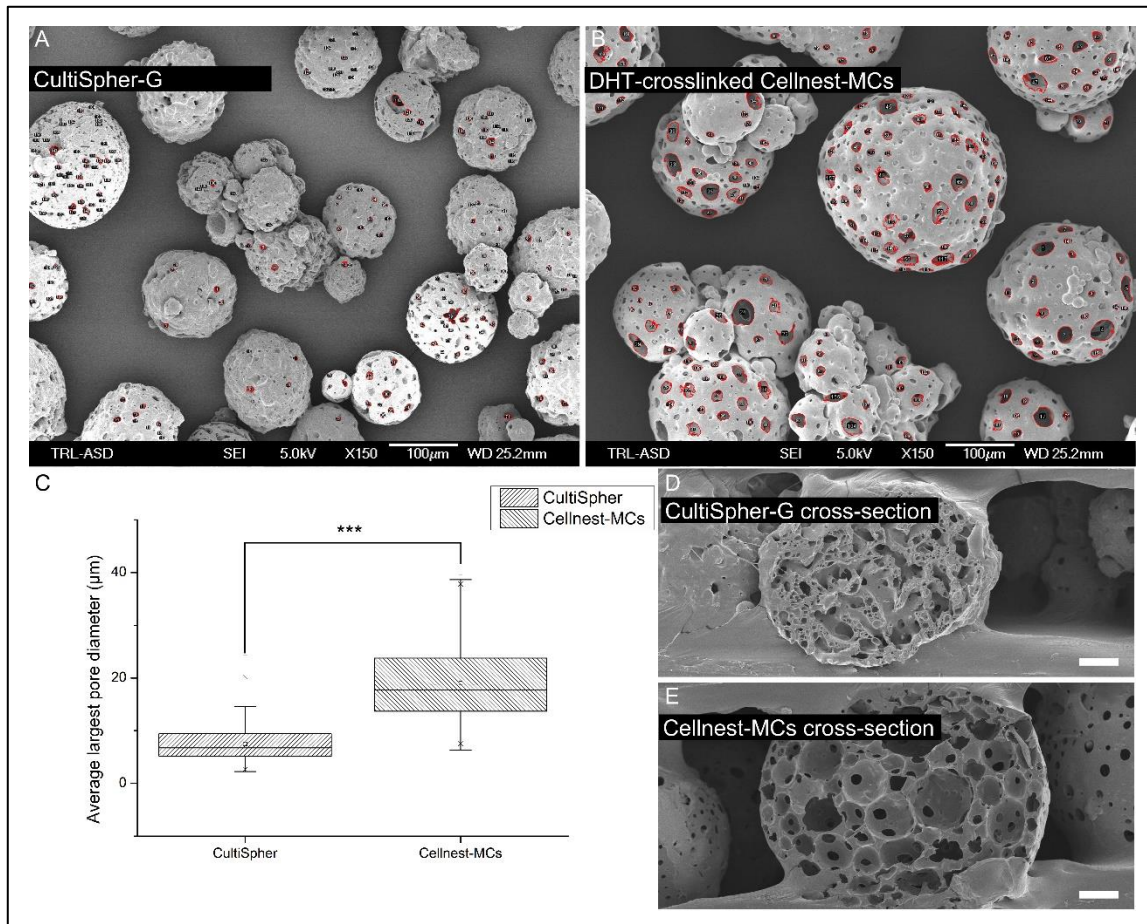


Figure 14: PDL Improves mineralization in 2D (**left panel**) and in a rat tail collagen I hydrogel (**right panel**). **Scalebar 2D: 200 $\mu$ m. Scalebar 3D: 100 $\mu$ m.** Images in collagen hydrogels acquired by Anika Pritzl

#### 4.3 Optimization of the macroporous microcarrier for hBMSCs expansion and delivery

Together with FUJIFilm, we optimized a strategy for the crosslinking of a new kind of macroporous microcarrier based on a recombinant collagen I-based peptide (Cellnest™)<sup>234</sup> for the expansion of BMSCs. Measurements of the average pore diameter of random pores identified from SEM images of Cellnest™-MCs and of CultiSpher-G®, a commercially available alternative porous microcarrier,

revealed that Cellnest™-MCs present significantly larger external pores ( $19\pm 7\mu\text{m}$ ,  $n=312$ ,  $p<0.0001$ ) when compared to Cultispher-G® ( $7\pm 3\mu\text{m}$ ,  $n=318$ ) (Figure 15C).



**Figure 15: Comparison of the architectural characteristics of Cultispher®-G and Cellnest™-MCs. Upper panel: Measurement of external pores of A) Cultispher®-G and B) Cellnest™-MCs. Lower panel: Left) Representation of the distribution of the largest diameter of the external pores in Cultispher®-G and Cellnest™-MCs (\*\*\*:  $p<0.0001$ ). Right) Cross-section of D) Cultispher®-G and E) Cellnest™-MCs. Scalebar:  $100\mu\text{m}$ . SEM images acquired at FUJIFilm Manufacturing Europe B.V.**

Moreover,  $\mu\text{CT}$  scans of the two microcarrier types allowed to run simulations mimicking the entrance of a particle of 0, 5, 10 and  $15\mu\text{m}$  diameter into the microcarriers (Figure 16). This particular simulation proved to be useful for the estimation of the total porosity of the scaffold, defined as the void volume of the microcarrier as a ratio of the total volume of the microcarrier, as this was detected by the infiltration of a particle of  $0\mu\text{m}$  diameter. On the other hand, this method allowed to estimate the average diameter of the interconnections between internal pores by determining the coefficient of the curves representing the relationship between the diameter of a particle and the accessible void volume occupied from that particle in the microcarriers. Assuming the average pore interconnection diameter

as equal to that of a particle able to access 50% of the void volume of a microcarrier, I was able to determine that Cellnest™-MCs present a significantly higher porosity ( $73\pm4\%$ ,  $n=7$ ,  $p<0.0001$ ) comparing to Cultispher®-G ( $52\pm6\%$ ,  $n=6$ ) and a significantly larger diameter of internal pore interconnections ( $20\pm3\mu\text{m}$ ,  $n=6$  vs  $8\pm1\mu\text{m}$ ,  $n=7$ ,  $p<0.001$ ).

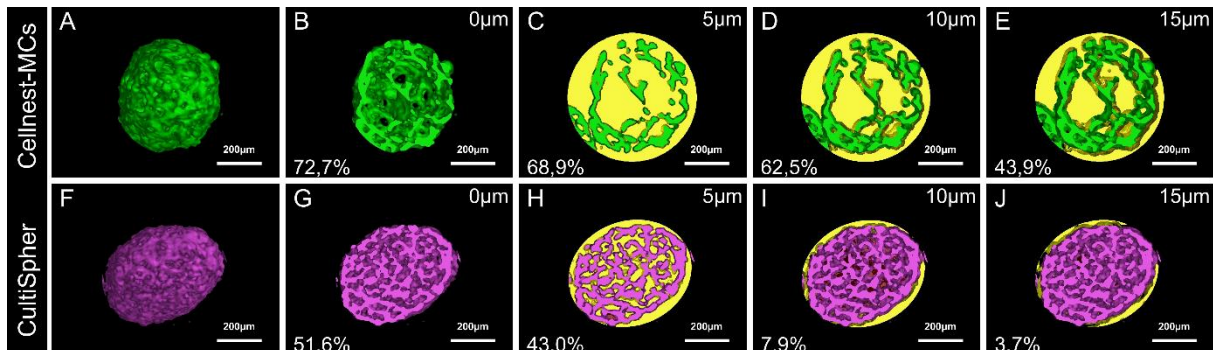


Figure 16: Computer simulation on  $\mu\text{CT}$  scan showing the void volume accessible by a particle of 0, 5, 10 and  $15\mu\text{m}$ . The larger diameter of the interconnection between pores gives Cellnest™-MCs a significantly higher accessible volume comparing to Cultispher®-G.

Since the manufactured microcarriers are not stable in water-based solutions such as culture medium, we optimized three distinct cross-linking strategies, two of whom (HMDIC and EDC) were chemical strategies and one (DHT) physical, to stabilize the material. Furthermore, we investigated the effect of the different cross-linking strategies on the vitality and proliferation of hBMSCs and of C2C12, a mouse myoblast cell line often used in research concerning signaling during osteogenic differentiation.

As shown in Figure 17, the employed crosslinking strategies did not lead to significant differences in the morphology of the microcarriers or in the diameter of the external pores.

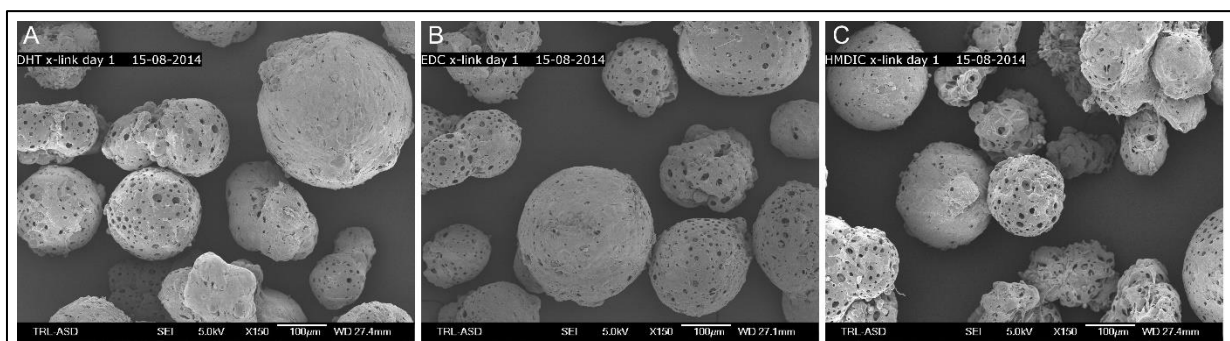


Figure 17: Cellnest™-MCs treated with different crosslinking strategies maintain similar external pore dimension. **A)** DHT **B)** EDC **C)** HMDIC. Images acquired at FUJIFilm Manufacturing Europe B.V.



Once established three possible crosslinking strategies for the microcarriers, we then investigated whether the different crosslinking methods had an influence on cell attachment, vitality and proliferation (Figure 18).

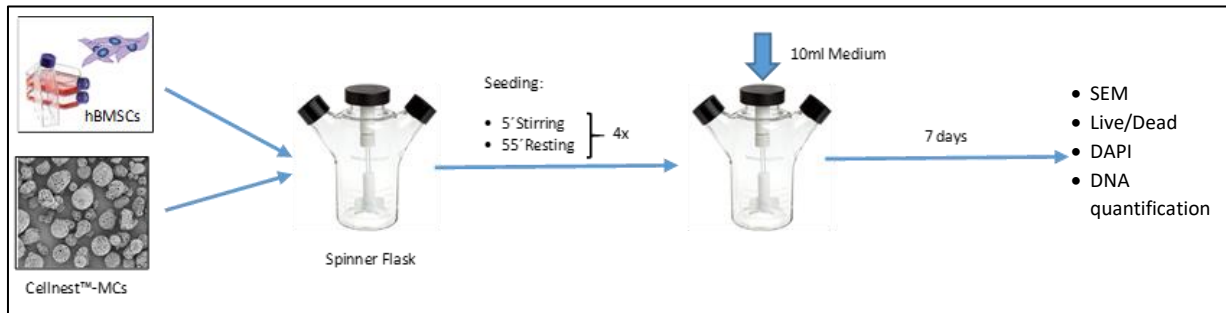


Figure 18: Schematic representation of the experiment.

Live and dead and DAPI staining of C2C12 cells and hBMSCs cultured on the different microcarrier types showed that both cell types attached better on HDMIC- and DHT-crosslinked Cellnest™-MCs comparing to EDC-crosslinked microcarriers, with no significant difference when comparing to CultiSpher®-G (n=3). However, while cells cultured on CultiSpher®-G reached confluence on the surface of the microcarrier already at day 4, cells cultured on Cellnest™-MCs continued growing and expanded into the microcarrier, as shown in Figure 19. In particular, a higher cell vitality and cell number can be detected at Day 7 for both C2C12 and hBMSCs cultured on DHT-crosslinked microcarriers compared to HMDIC- and EDC-crosslinked microcarriers and to cells cultured on CultiSpher®-G. Moreover, while cells cultured on Cellnest™-MCs appear to have a round morphology, it is possible to appreciate significant cell stretching on the surface of CultiSpher®-G (Figure 19A, E, I, M), which may potentially influence cell differentiation at later time points.

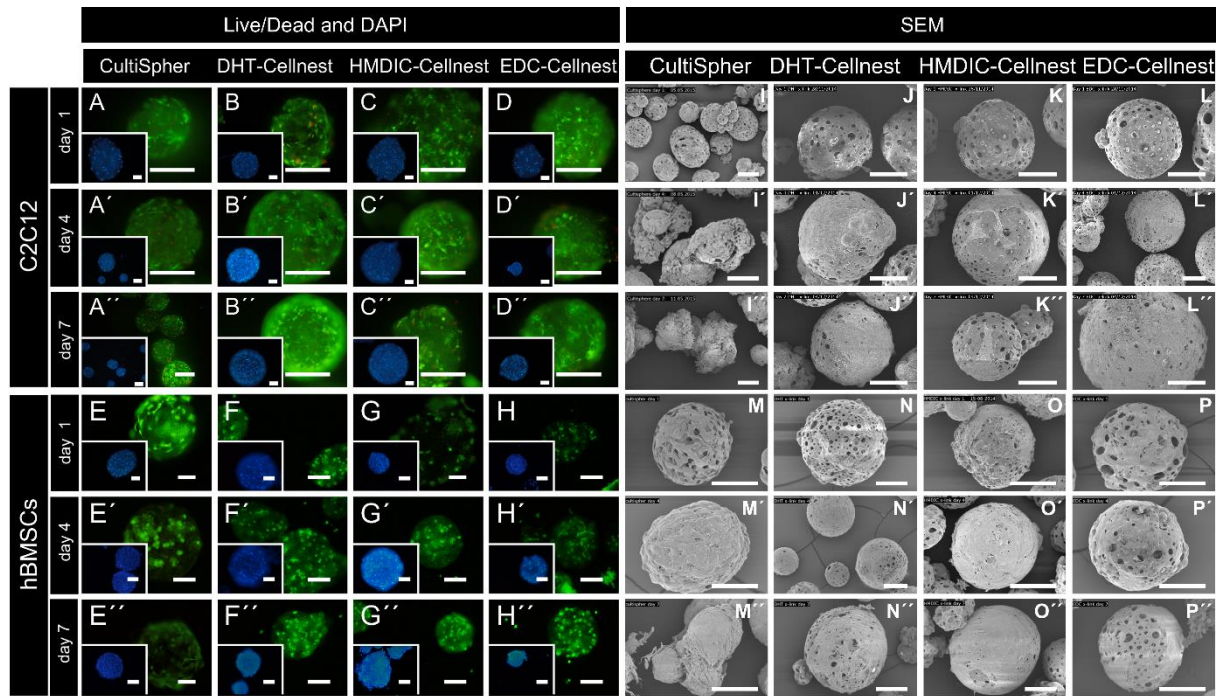
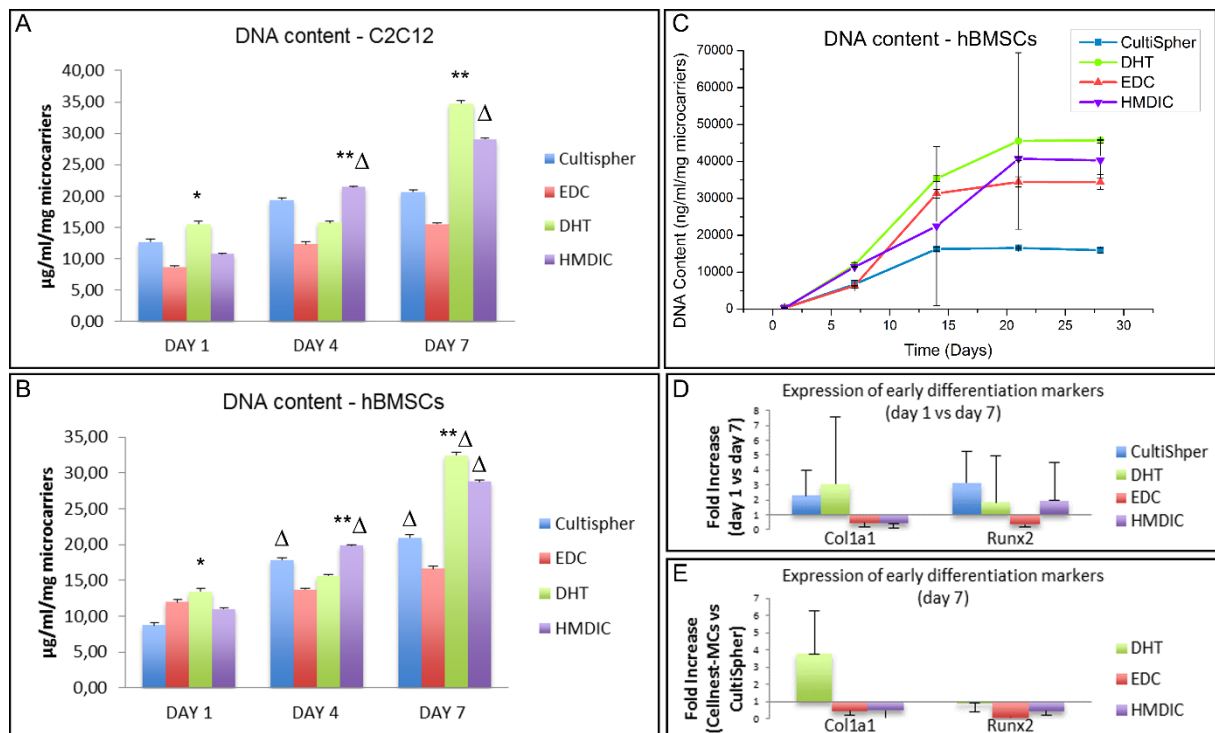


Figure 19: Live-dead, SEM and DAPI (Insert) of C2C12 and MSCs on CultiSpher®-G and on DHT-, HMDIC- and EDC-crosslinked Cellnest™-MCs. **Scalebar:** 100µm. **Insert scalebar:** 200µm. SEM images acquired at FUJIFilm Manufacturing Europe B.V.

In order to investigate the effect of the different crosslinking strategies on cell proliferation, we then cultured C2C12 cells or hBMSCs on the different microcarriers and quantified the DNA content at 1, 4 and 7 days after seeding in order to use this parameter as a predictor of cell number. Pico Green quantification of DNA content confirmed that although cells attached significantly better to DHT-crosslinked Cellnest-MCs (C2C12:  $15.6 \pm 0.5 \mu\text{g/ml/mg}$ ,  $n=3$ ,  $p<0.05$ ; hBMSCs:  $13.5 \pm 0.4 \mu\text{g/ml/mg}$ ,  $n=3$ ,  $p<0.05$ ) comparing to the other microcarriers (C2C12: CultiSpher-G  $12.7 \pm 0.5 \mu\text{g/ml/mg}$ , EDC  $8.7 \pm 0.2 \mu\text{g/ml/mg}$ , HMDIC  $10.77 \pm 0.03 \mu\text{g/ml/mg}$ ; hBMSCs: CultiSpher-G  $8.7 \pm 0.3 \mu\text{g/ml/mg}$ , EDC  $11.9 \pm 0.1 \mu\text{g/ml/mg}$ , HMDIC  $11.0 \pm 0.1 \mu\text{g/ml/mg}$ ), as demonstrated by DNA quantification at day 1, C2C12 cells cultured on HMDIC-crosslinked microcarriers presented a significantly higher growth kinetics (HDMIC:  $1.43 \pm 0.04$  PDs) when compared with EDC-crosslinked microcarriers (EDC:  $0.8 \pm 0.1$  PDs) and CultiSpher-G ( $0.7 \pm 0.2$  PDs) ( $n=3$ ,  $p<0.01$ ), which led to a significantly lower cell proliferation when compared to DHT- ( $1.2 \pm 0.1$  PDs,  $p<0.01$ ) and HMDIC-crosslinked Cellnest™-MCs ( $p<0.01$ ) (Figure 20A, B).

On the other hand, no significant difference in the overall PDs at day 7 was instead found between hBMSCs cultured on DHT- ( $1.3 \pm 0.1$  PDs) or HDMIC- ( $1.39 \pm 0.06$  PDs) crosslinked Cellnest™-MCs and CultiSpher® ( $1.3 \pm 0.2$  PDs). However, due to the higher cell attachment during cell seeding, DHT-crosslinked Cellnest-MCs yielded a significantly higher cell number for both C2C12 and hBMSC compared to HMDIC- and EDC-crosslinked Cellnest™-MCs and CultiSpher®-G ( $n=3$ ,  $p<0.001$ ) (Figure

20A, B). Although these results were highly suggestive of the role of crosslinking and surface properties in determining the yield of a cell culture, we performed further experiments to investigate the influence of a higher scaffold porosity and the consequent capability to support cell ingrowth, as presented by Cellnest™-MCs compared to CultiSpher®-G, on cell proliferation. In this setup, hBMSCs were expanded for 28 days in spinner flasks on CultiSpher®-G or on DHT-, EDC- or HMDIC-crosslinked Cellnest™-MCs, and DNA quantification was performed on samples taken from each flask at day 1, 7, 14, 21 and 28. Notably, while hBMSCs cultured on Cellnest™-MCs reached the growth plateau between day 21 and 28, cells cultured on CultiSpher®-G reached the plateau between day 7 and 14, supporting the idea that, once confluence is reached on the microcarrier's surface, the small diameter of the external pores of CultiSpher®-G does not allow ingrowth of the cells in the microcarrier. DNA quantification at day 28 shows that hBMSCs cultured on CultiSpher®-G underwent approximately 6 PDs before reaching the expansion plateau between day 7 and 14, while DHT-crosslinked Cellnest™-MCs reached the plateau between day 14 and 21 – undergoing approximately 8 PDs. EDC- and HMDIC-crosslinked Cellnest™-MCs on the other hand yielded lower PDs, reaching the plateau between day 7 to 14 and day 21 to 28 respectively (Figure 20C).



**Figure 20: Left: DNA quantification of A) C2C12 and B) hBMSCs cultured for 7 days on CultiSpher® and DHT-, EDC- or HMDIC-crosslinked Cellnest™-MCs. Right, Upper Panel: C) DNA quantification of hBMSCs cultured for 28 days on CultiSpher® and DHT-, EDC- or HMDIC-crosslinked Cellnest™-MCs. Right, Lower Panel) RealTime-PCR analysis of relative fold increase in Col1a1 and Runx2 expression in hBMSCs D) comparing day 1 and day 7 of culture or E) comparing DHT-, EDC- or HMDIC-crosslinked Cellnest™-MCs with CultiSpher® at day 7. DNA quantification performed at FUJIFilm Manufacturing Europe B.V.**

Since different crosslinking methods can impact the surface properties of the employed scaffolds and alter the differentiation potential of hBMSCs, we then investigated whether microcarriers crosslinked with different methods could differentially influence hBMSCs differentiation towards the osteo-chondro lineages. RT-Real Time – PCR analysis of two early differentiation markers of the osteo-chondro lineages, respectively collagen type 1 (Col1a1) and the key differentiation factor Runx2, revealed no significant upregulation of the differentiation markers after 7 days of expansion when compared to day 1 (n=3) (Figure 20D). Similarly, no significant difference could be detected between DHT-, HMDIC- and EDC-crosslinked Cellnest™-MCs and CultiSpher®-G at day 7 (n=3) (Figure 20E).

Because of their greater potential to support hBMSCs expansion without pre-differentiation into the osteo-chondro lineage during the expansion phase, DHT-crosslinked Cellnest™-MCs were chosen as best candidate for a cell-based therapy consisting of a cell-scaffold mixed formulation and were employed for all following experiments.

#### 4.4 Investigation of strategies for hBMSCs differentiation and mineralization of the microcarriers

In order to better investigate the potential of DHT-crosslinked Cellnest™-MCs for the regeneration of bone defects, I therefore explored the possibility for hBMSCs to differentiate on the microcarriers and deposit mineralized matrix. Interestingly, after 28 days of differentiation under dynamic conditions, RT-Real Time PCR analysis of gene expression did not show any significant upregulation of the early osteogenic differentiation marker Runx2 or of the late differentiation marker Osterix (OSX) comparing with day 1 (n=3) (Figure 21). Moreover, no significant difference could be detected between differentiated and undifferentiated cells.

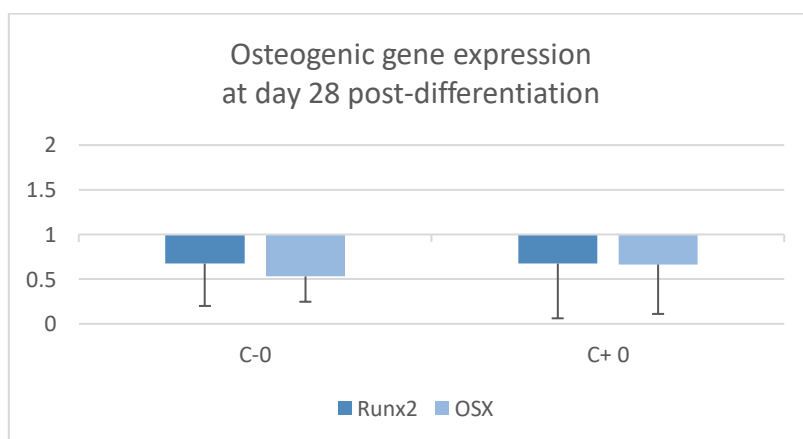
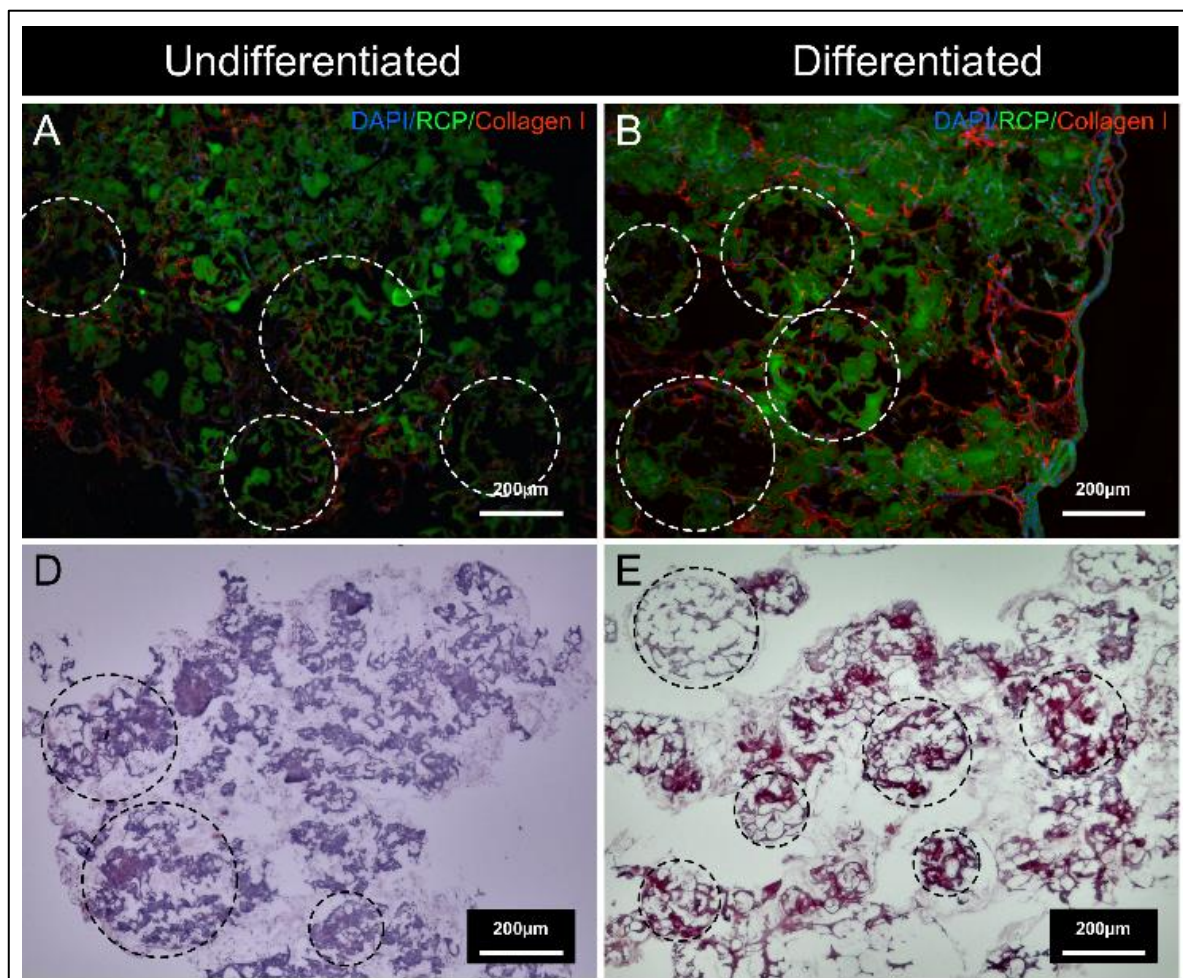


Figure 21: qPCR of osteogenic differentiation markers expressed by hBMSCs on Cellnest™-MCs

On the contrary, immunofluorescence staining of collagen type I shows intense deposition of organic matrix outside and inside the microcarriers, which is nonetheless still detectable also in undifferentiated samples in lower amounts. Moreover, Alizarin Red S staining of calcium phosphate deposits shows intense deposition of mineralized matrix on the deposited collagen in differentiated samples, while no mineralized material can be detected in undifferentiated samples (Figure 22).

Most Interestingly, the deposition of big amounts of extracellular matrix can be employed to assemble large amounts of microbeads in a solid construct that may be implanted after surgical exposure of the damaged area rather than injected. A mixed formulation between assembled microcarriers and monodispersed microcarriers may result in a more stable product that can still be molded to fit the defect shape and size.



*Figure 22: hBMSCs differentiate on the microcarriers and produce mineralized matrix. A, C): Immunofluorescence staining of collagen I. Collagen I (Red), DAPI (Blue), Scaffold (Green). D, E): Alizarin Red staining of mineralized matrix and counterstaining with Hematoxylin. Dashed circles: Remnants of the beads detectable in the samples.*

To test the possibility of assembling several microcarriers in a solid construct, I cultured hBMSCs-seeded microcarriers in a spinner flask at low speed in order to allow aggregation of microcarriers in clusters, and I later seeded these clusters in a perfusion bioreactor described by Kleinhans et al.<sup>228</sup>. After perfusing the microcarriers packed in the bioreactor for 14 days with either MSCGM-CD 2% FCS or osteogenic differentiation medium, I retrieved the microcarriers and embedded them in paraffin for immunofluorescent staining. In both conditions, the microcarriers assembled into solid scaffolds that could not be disrupted when compressed and that retained an elastic consistence (n=3). Scaffolds perfused with osteogenic medium in particular assumed a compact form, and could not be disrupted even when compressed for more than 90% of the original height (data not shown). After 14 days of culturing, cells were vimentin<sup>+</sup> in both conditions, but while hBMSCs cultured in MSCGM-CD showed active production of collagen type I, expression of OPN and of Runx2, cells cultured in osteogenic medium showed reduced expression of Runx2 and OPN, and extracellular deposition of collagen type I (Figure 23).

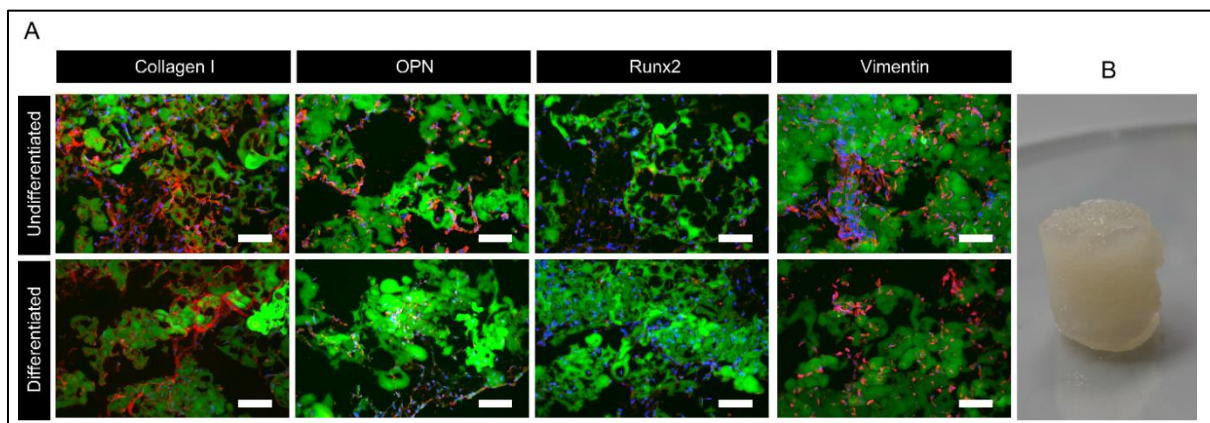


*Figure 23: hBMSCs cultured under perfusion **A)** differentiate towards the osteogenic lineage and **B)** assemble in solid scaffolds. **Scalebar:** 100 $\mu$ m*

Although extensive deposition of extracellular matrix was enough to bind different microcarriers together to form a solid construct, the deposited material was still far from being compact enough to be compared to the native bone matrix. For this reason, I explored the possibility of promoting cell differentiation and improving mineral deposition by co-culturing hBMSCs with composite microbeads composed of the Cellnest<sup>™</sup> peptide and hydroxyapatite in a 60/40 w/w ratio (Figure 24).

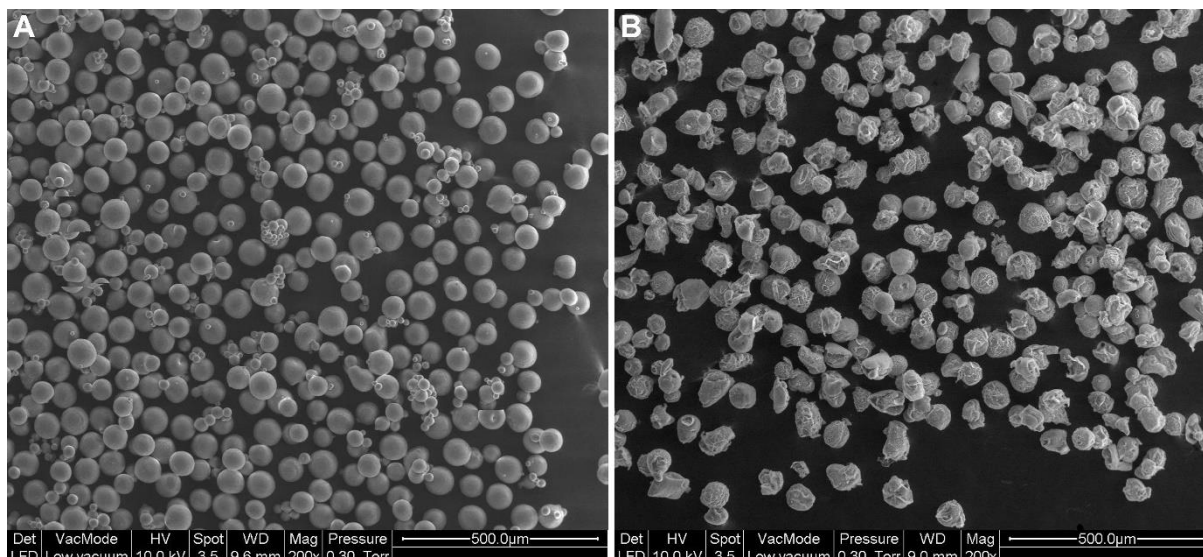
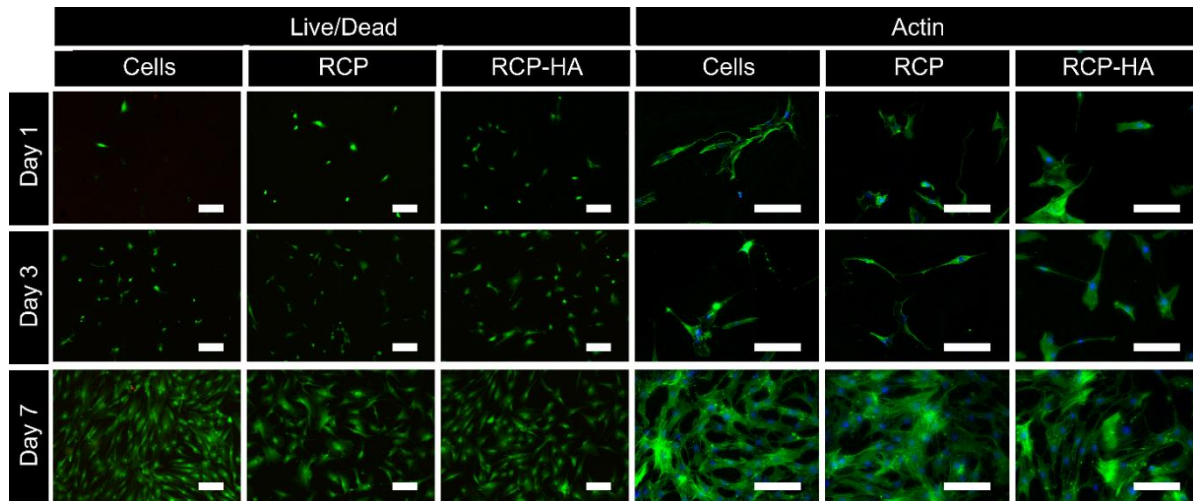


Figure 24: SEM images of **A)** RCP and **B)** RCP-HA beads. Images taken by Tatiana Patricio, ISTE-CNR.

In order to exclude toxic effects of the microbeads on hBMSCs, I cultured the cells in a proliferation medium composed of DMEM low glucose 10% FCS on collagen-coated glass slides and incubated them with either Cellnest™ peptide-hydroxyapatite composite microbeads (RCP-HA) or with microbeads composed of Cellnest™ alone (RCP) with comparable dimension produced in collaboration with ISTE-CNR. Live/Dead staining of the cells cultured for 1, 3 and 7 days with the microbeads revealed in both cases no difference in cell vitality when comparing to cells cultured without the microbeads (n=3). Similarly, GFP-phalloidin staining of the actin filaments after cell permeabilization showed no significant alterations in cell morphology when comparing cells cultured with the two microbead types and cell alone (n=3) (Figure 25). These results suggest that RCP and RCP-HA are not toxic for hBMSCs and that their use for promoting cell differentiation can be safely explored.

For this reason, I established a mineralization model by embedding hBMSCs and RCP or RCP-HA in a rat tail collagen I hydrogel and culturing the hydrogels in either osteogenic medium or in a proliferation medium composed by DMEM low glucose 10% FCS. Similarly to what was reported for the 2D conditions, incubation of hBMSCs with RCP or RCP-HA in 3D conditions did not lead to alterations in cell vitality over the course of 28 days when compared to cells alone, although a gradual increase in the number of dead cells could be detected in all cases concomitant with a progressive shrinking and contraction of the hydrogel upon deposition of collagen fibers in the extracellular matrix (n=3) (Figure 25).



*Figure 25: BMSCs incubated for 1, 3 or 7 days with Cellnest™-microbeads (RCP) or Cellnest™-hydroxyapatite composite microbeads (RCP-HA) do not present alterations in cell vitality and morphology when compared to cell alone.*

Interestingly, while Alizarin Red S staining did not detect deposition of mineralized material at any time point in samples cultured in proliferation medium and a strong mineral deposition for hBMSCs alone cultured in osteogenic medium starting from day 21-28, RCP and RCP-HA samples presented intermediate mineralization. More specifically, it is possible to observe in RCP-HA at day 14-21 a more intense staining surrounding the microcarriers but no mineralization in the rest of the hydrogel. Conversely, no mineral deposition can be detected in presence of RCP microbeads by day 28 (n=3) (Figure 26).



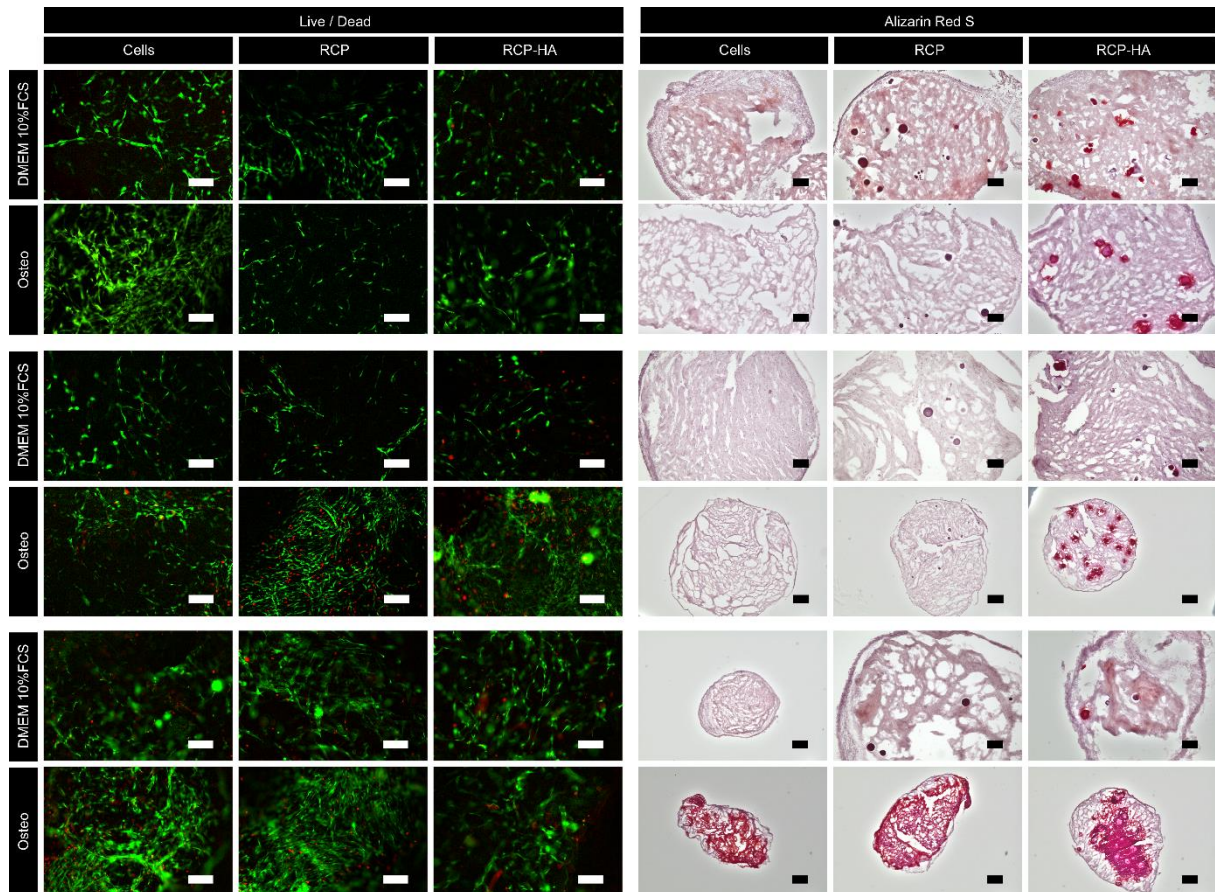


Figure 26: RCP and RCPHA beads do not have an effect on cell vitality (**left panel**) but may hinder mineralization in 3D (**right panel**). **Scalebar Live/Dead: 50µm. Scalebar Alizarin Red: 100µm.** Alizarin Red S Staining performed by Christine Baer.

#### 4.5 Establishment of a Bone Marrow Niche model

After establishing a bone-like stromal support using hBMSCs and the DHT-crosslinked Cellnest™-MCs, I investigated the possibility to demonstrate the functionality of the developed bone substitute through the establishment of a bone marrow niche model and the identification of a key component of the niche (Figure 27).

CD34<sup>+</sup> cells extracted from the model were seeded in a Methylcellulose Colony Forming Cell assay allowing the identification of the different hematopoietic progenitors contained in the original sample. Alternatively, RNA was isolated from both CD34<sup>+</sup> and CD34<sup>-</sup> fractions or whole scaffold, and co-culture constructs were processed for histological or SEM analysis.

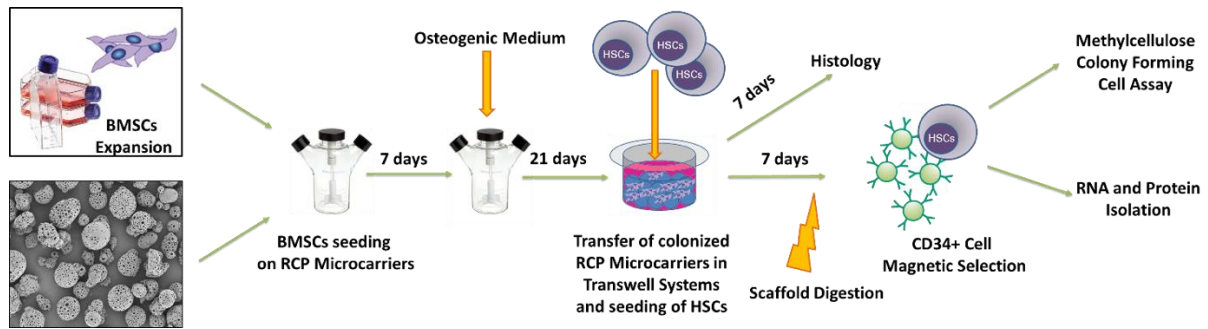
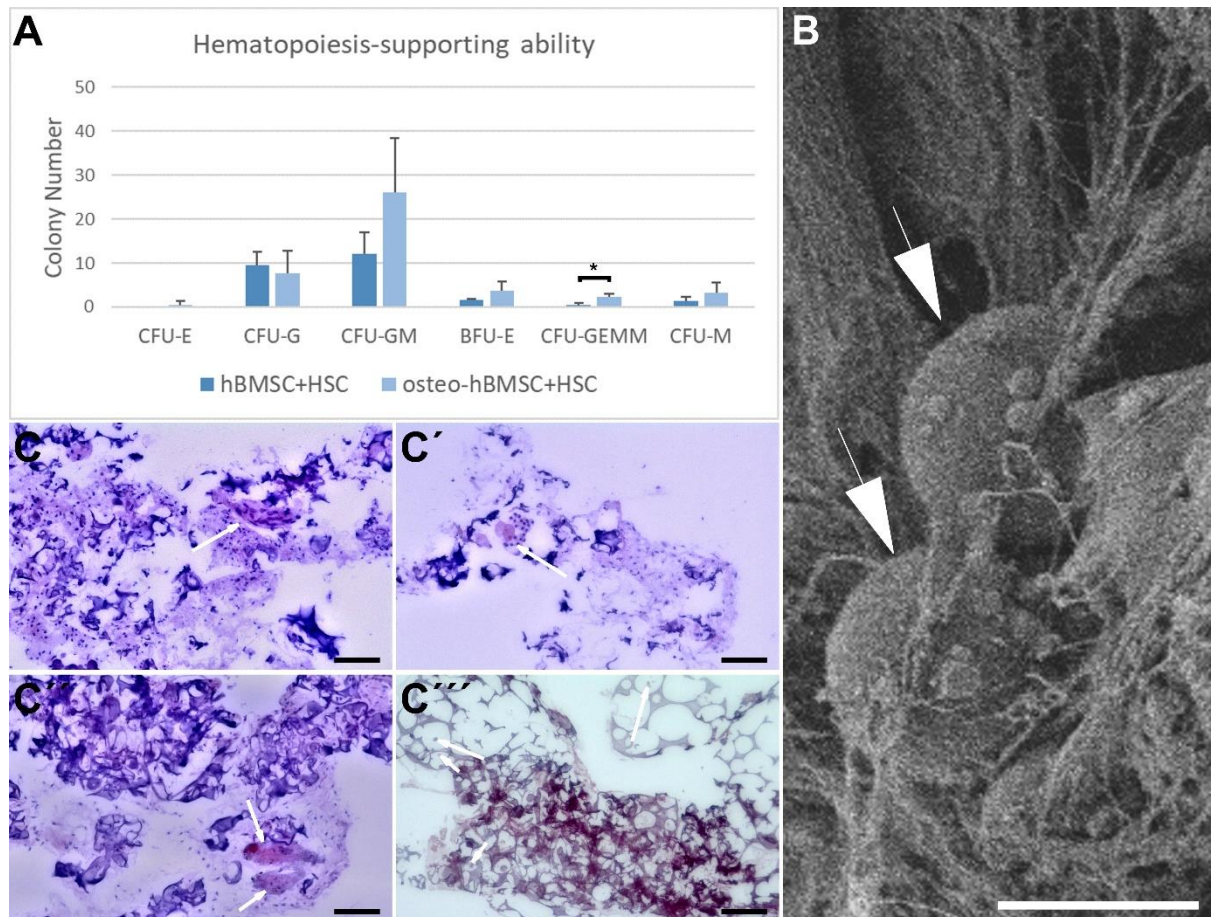


Figure 27: Schematic representation of the workflow for the establishment of the bone marrow niche model. hBMSCs were expanded for 7 days on DHT-crosslinked Cellnest™-MCs and differentiated for 21 days until the stage of osteo-progenitor cells in osteogenic medium. At day 21 the colonized MCs were transferred to transwell inserts and co-cultured with HSCs for 7 days before scaffold lysis, CD34-magnetic sorting and analysis.

SEM analysis of the hole construct showed a thick layer of extracellular matrix engulfing the porous microcarriers, confirming what previously observed for the reconstruction of a bone-like matrix, and two morphologically distinct cell populations, namely a flatter and more spread population, most likely hBMSCs, and a more roundish population, most likely cells of the hematopoietic lineage (n=3) (Figure 28B). This result was later confirmed by the detection, after hematoxylin-eosin staining of resin-embedded constructs (Figure 28C), of different populations of small, non-adherent cells, often characterized by a round morphology and gathered in clusters, surrounded by a more morphologically heterogeneous population of hBMSCs.

Distinction between hematopoietic cells and eventual contaminant stromal cells can be easily performed in this assay, since hematopoietic cells retain a rounded morphology and typically cluster in colonies, while stromal cells appear to migrate to the bottom of the culture plate where they elongate and take contact with other stromal cells. Quantification of the colonies originated by hematopoietic cells isolated from co-cultures between HSCs and undifferentiated (hBMSC) or osteogenically differentiated (osteo-hBMSCs) cells showed no significant difference in the overall number of colonies supported by hBMSC ( $25 \pm 6$  colonies/well, n=3) comparing to osteo-hBMSCs ( $42 \pm 17$  colonies/well, n=3) despite the large effect size (d=1.3) (Figure 28A). However, when analyzing the single progenitor cells supported by the two cell types, it is possible to notice a trend suggesting that osteo-hBMSCs support the maintenance or growth of a larger number of early hematopoietic progenitors comparing to undifferentiated hBMSCs. This results in a significant increase in the number of CFU-GEMM (colony forming unit granulocyte, erythrocyte, monocyte, megakaryocyte) ( $2.2 \pm 0.8$  colonies/well, n=3, p<0.05) comparing to hBMSCs ( $0.5 \pm 0.5$  colonies/well, n=3), and an overall non-significant difference in the number of CFU-GM (colony forming unit granulocyte monocyte) despite the large effect size (d=1.5). As far as more differentiated progenitors are concerned, no significant

difference could be noted for CFU-G (colony forming unit- granulocyte), BFU-E (burst forming unit erythrocytes) despite the large effect size ( $d=1.4$ ) and CFU-M (colony forming unit macrophages).



**Figure 28: hMSCs support HSCs growth without growth factors in the Bone Marrow niche model. A)** Number of colonies counted in methylcellulose assay starting from progenitor HSCs isolated from bone marrow niche models comparing co-cultures between undifferentiated (hBMSCs) or osteogenically differentiated (osteo-hBMSCs) cells and HSCs. **B)** SEM of the constructs after 7 days of co-culture. Cells of the hematopoietic lineage (arrows) can be detected behind the layer of deposited ECM deposited on the microcarriers. **Scalebar: 10 $\mu$ m** **C)** Hematoxylin eosin staining of the constructs retrieved after 7 days of co-culture. Cells indicated by the arrows represent cells of the hematopoietic lineage. **Scalebar: 100 $\mu$ m**

In order to investigate the effect of HSCs-hBMSCs co-culturing on the model's maintenance, I then performed a RT-Real Time- PCR analysis of the expression of key osteogenic differentiation markers and compared them with hBMSCs monocultures in the model. Interestingly, several of the differentiation markers presented a >2-fold increase (FI) during co-culturing of HSCs with undifferentiated hBMSCs (ALP: 3.27 FI; col1a1: 2.88 FI; BMP2: 4.74 FI; Runx2: 4.02 FI) or with osteogenically differentiated hBMSCs (ALP: 2.6 FI; col1a1: 2.4 FI;) comparing hBMSCs or osteo-hBMSCs monocultures, but although effect size ranged from middle to large, only Osteopontin (OPN) resulted

to be significantly upregulated during co-cultures of osteo-hBMSCs and HSCs ( $p < 0.05$ ,  $n = 3$ ) (Figure 29B).

OPN was highly expressed in both co-cultures between undifferentiated and osteogenically differentiated hBMSCs with HSCs, respectively  $407.2$  FI and  $98 \pm 11$  FI ( $n = 3$ ,  $p < 0.05$ ). In order to confirm this result, I then performed OPN immunofluorescent stainings on sections of the resin-embedded samples. Interestingly, while low expression of OPN could be detected mainly intracellularly for osteogenically differentiated hBMSCs, expression of OPN could be detected also and in higher levels in undifferentiated hBMSCs after co-culturing with HSCs. Surprisingly, the expression of OPN was not only intracellular in co-cultures between osteo-hBMSCs and HSCs, but also a prominent, diffuse deposition of OPN on the scaffold could be detected, supporting the idea that OPN plays an important role in the bone marrow niche homeostasis (Figure 29A).

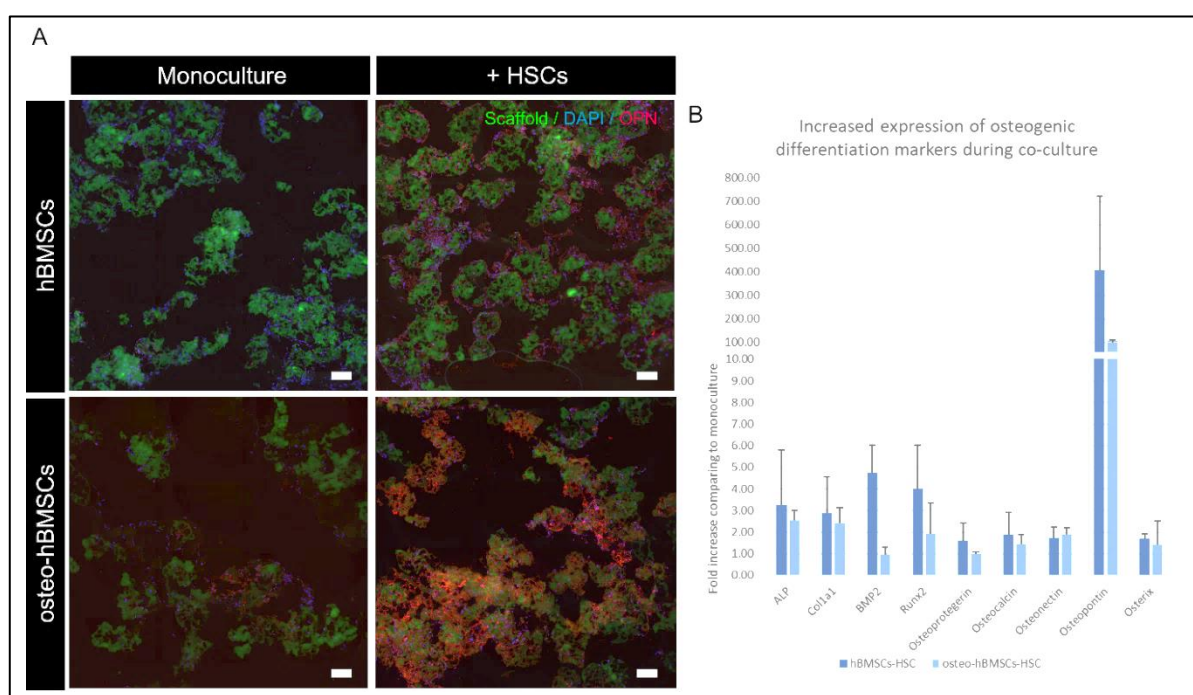


Figure 29: **A)** OPN is expressed in hBMSCs-HSCs co-cultures and deposited on the extracellular matrix just in co-cultures between differentiated hBMSC and HSCs. **Red:** OPN; **Blue:** DAPI; **Green:** Scaffold. **Scalebar:**  $100\mu\text{m}$ . **B)** RT-Real Time PCR of osteogenic markers expressed by undifferentiated (hBMSCs) or osteogenically differentiated (osteo-hBMSCs) cells in co-culture with HSCs. Values are expressed as fold increase comparing to monocultures.

However, further *in silico* analysis on the designed OPN primers employed for the RT-Real Time PCR analysis revealed that the employed primer couple specifically recognized a particular splice variant of OPN, the isoform OPNb. Therefore, I investigated whether the different behavior of OPN, as detected by immunofluorescence staining, could be reconducted to a cell-contact-induced splicing of the OPN's mRNA resulting in the production of different OPN isoforms. To do this, I performed a PCR using primers flanking a differentially spliced region on the mRNA and run them on an agarose gel in order

to distinguish the different PCR products based on their molecular weight, which all the five OPN isoforms resulting in bands with different molecular weights with >50 cycles and optimal detection cycles equal to 20 (Figure 30).

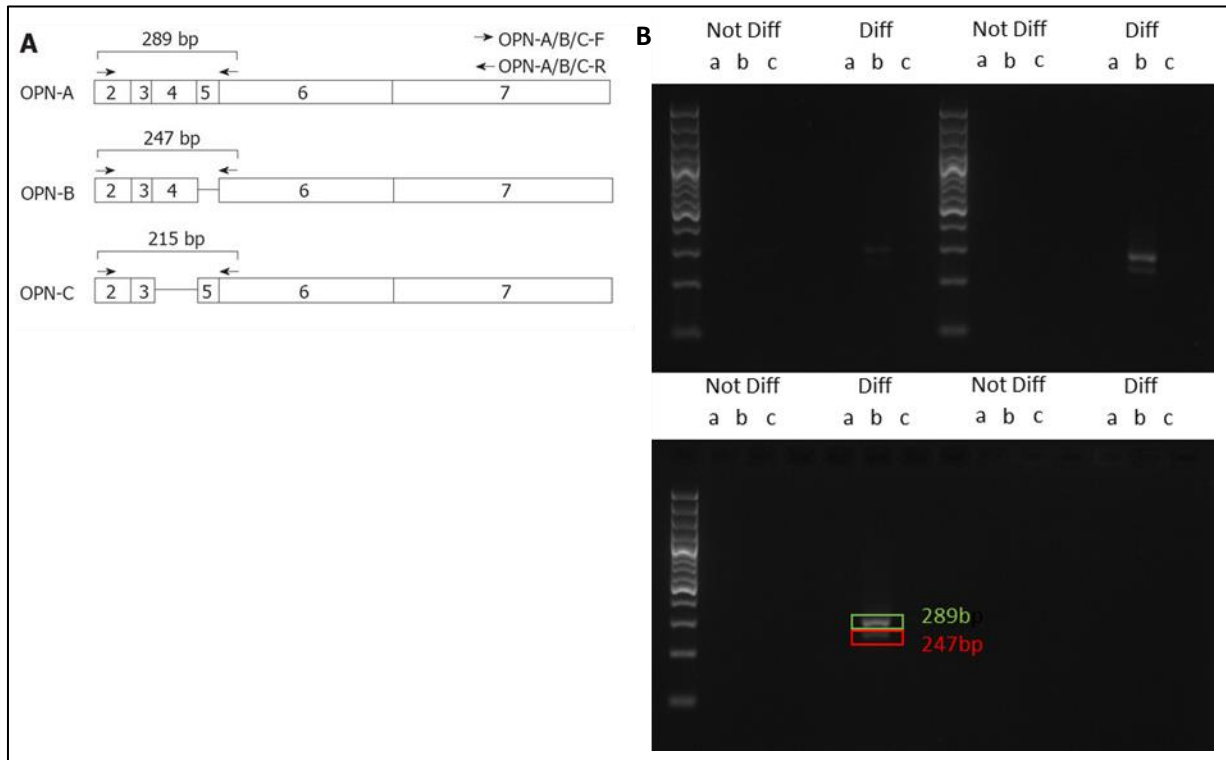


Figure 30: **A)** Schematic of the primers, image adapted from Phillips et al.<sup>231</sup>. **B)** OPNa and OPNb are produced after osteoMSCs-HSCs co-culture, gel performed by Anika Pritzl. **a:** hBMSCs monoculture; **b:** co-culture, CD34- fraction (hBMSCs); **c:** co-culture, CD34+ fraction (HSCs).

As already evidenced by histological staining, PCR performed with a limited cycle number of 20 could detect two different isoforms of OPN (n=3), marked by corresponding bands of 289bp and 247bp, being produced exclusively by differentiated hBMSCs upon co-culture with HSCs, while no to low expression could be detected in undifferentiated hBMSCs upon co-culture with HSCs or differentiated hBMSCs alone. After isolation and sequencing of the 289bp and 247bp bands (Figure 30B), the two isoforms were confirmed to be OPNa (289bp) and OPNb (247bp).

In order to better investigate the effect of Osteopontin in this *in vitro* bone marrow niche model, I incubated the hBMSCs-HSCs co-cultures with an anti-OPN antibody meant to inhibit the contact between OPN and other signaling molecules on the HSCs' surface. Counting of the colonies derived from hematopoietic progenitors at the end of the co-culture period could not demonstrate any significant effect of OPN inhibition with two different anti-OPN antibody concentrations (0.25µg/ml or 2.5µg/ml) on the total number of colonies supported by hBMSCs or osteo-hBMSCs comparing to

negative controls, nor could demonstrate any significant effect when taking in consideration the single progenitor types (n=3) (Figure 31).

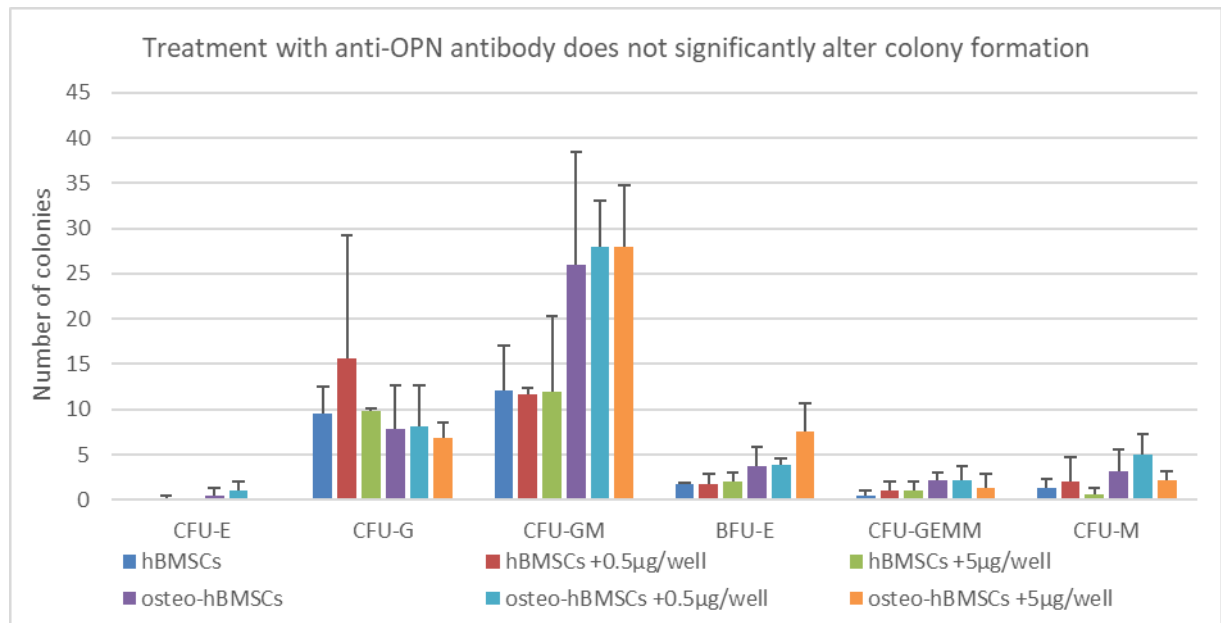


Figure 31: Colony counting after methylcellulose assay. Treatment of hBMSCs-HSCs or osteo-hBMSCs-HSCs co-cultures with an anti-OPN antibody does not affect colony formation.

#### 4.6 Recombinant OPNa and OPNb are differently produced and deposited

As no antibodies are in fact commercially available or can be easily developed to detect and identify different Osteopontin variants *in vivo* or in complex tissues, making it impossible to further investigate the role of OPNa and OPNb in our samples, we performed further characterization of the two isoforms starting from recombinant proteins.

For this aim, we transfected three different cell lines from different tissues, namely HEK293 (kidney) – CaCo2 (intestine) and hFOB1.19 (human fetal pre-osteoblast) with two plasmids for the expression of a fusion protein between the OPNa or OPNb isoforms and a FLAG-tag used to detect the proteins (pDest490-OPN-a and pDest490-OPN-b respectively<sup>232</sup>). All the transfection experiments were performed with different cell lines, in order to exclude a tissue-specific expression, splice or post-translational modification of the two isoforms and have a better predictor of the situation in the established bone marrow model.

Detection of OPNa and OPNb with a AlexaFluor 488-conjugated anti-FLAG antibody allowed to confirm the expression of the two isoforms in all the cell lines (Figure 32), while direct detection of the endogenous OPN could be detected only at low levels with an OPN-directed antibody.

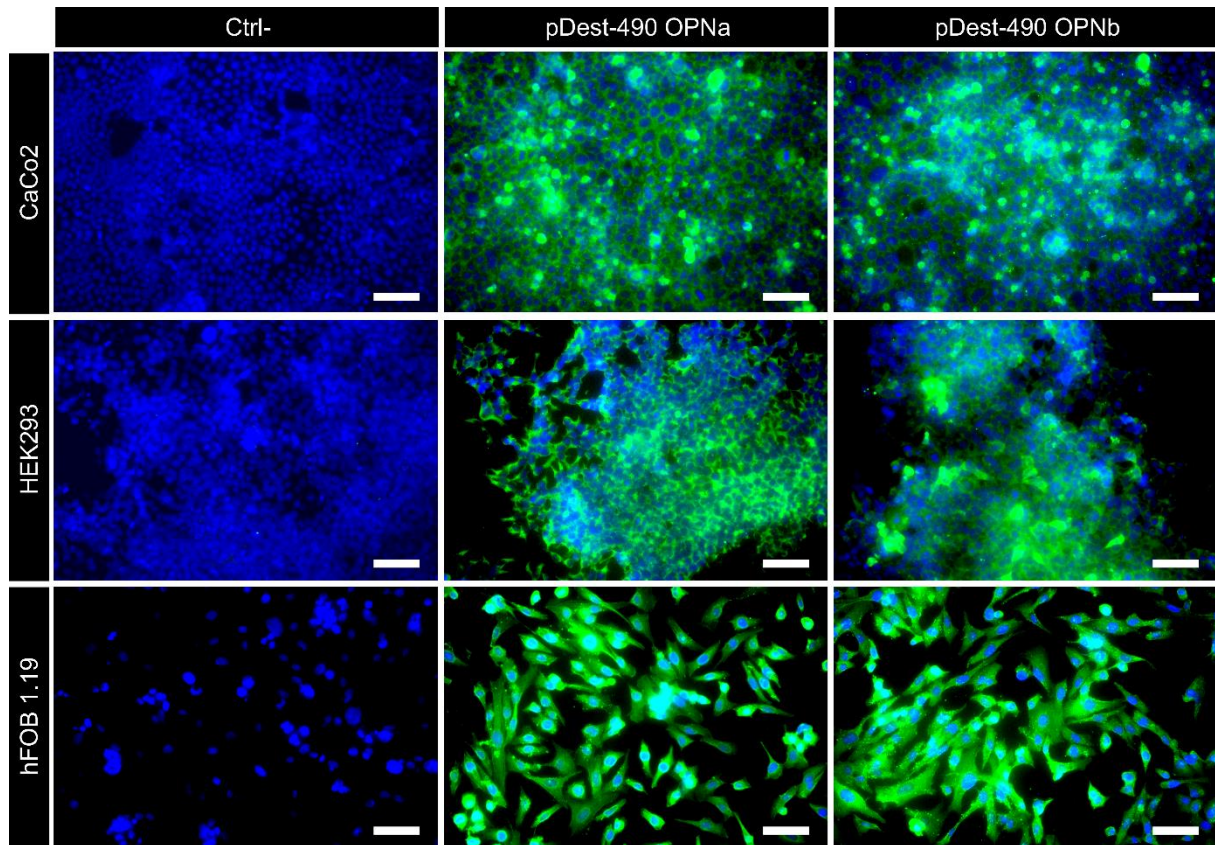


Figure 32: Recombinant OPNa and OPNb production in hFOB1.10, Caco2, HEK293. **Scalebar:** 100 $\mu$ m.  
Experiment Performed by Anika Pritzl.

In order to investigate the expression pattern of the two isoforms, we collected the supernatant of hFOB1.19, CaCo2 or HEK293 transfected with either pDest490-OPN-a or pDest490-OPN-b and we concentrated it in order to run it on a SDS-PAGE gel together with the cell lysate. Surprisingly, detection of the two isoforms with FLAG-directed antibodies in the Western Blot allowed to determine that while OPNa localizes exclusively in the cell lysate and extracellular matrix fraction, OPNb can be detected both in the cell lysate and in the supernatant (n=3) (Figure 33).

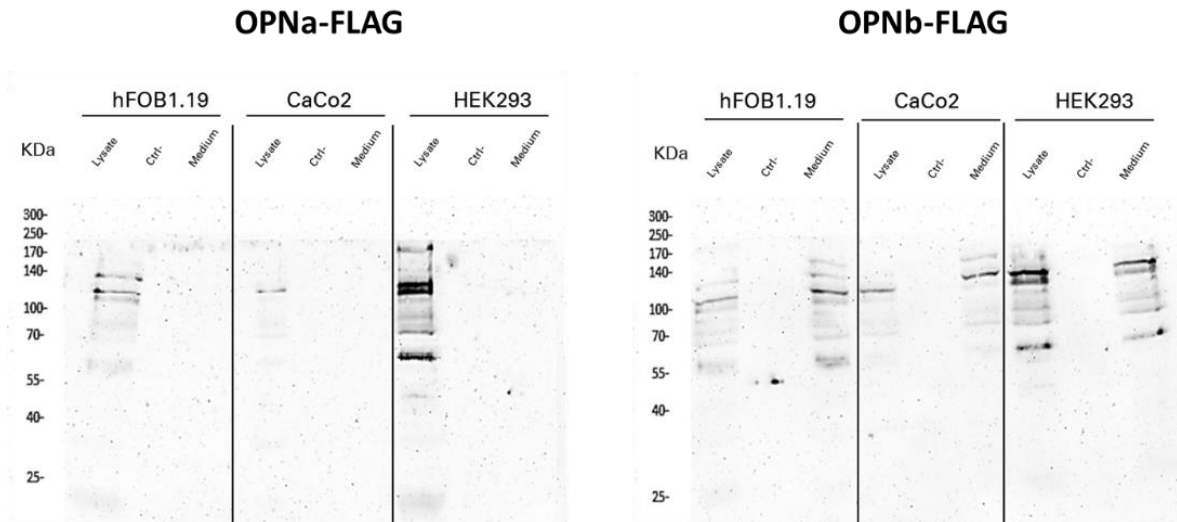


Figure 33: Recombinant OPNa and OPNb present different expression and deposition patterns. While OPNa (**left**) can be detected just in the lysate fraction of transfected cells, OPNb (**right**) can be also detected in the medium fraction of transfected cells.

In order to investigate the role of OPNa and OPNb on HSCs proliferation and differentiation, we modified the OPNa-FLAG- and OPNb-FLAG- expression plasmids to produce 6-histidine-tagged proteins in hFOB 1.19 that were incubated with a full length commercially available OPN version (OPN-FL) as a control with HSCs in a TPO, FLT3L, SCF and IL-3 supplemented medium for 16 hours and subsequently plated in a methylcellulose assay. Counting of the colonies after 14 days of incubation did not reveal any significant difference in the number of colonies formed in the methylcellulose assay between negative controls and cells treated with the different OPN isoforms (n=3) (Figure 34). Of note, no significant difference could be noted between the commercially available version of OPN and the recombinant proteins produced in-house. Interestingly, while methylcellulose assays run after extraction of HSCs from the previously reported bone marrow niche model showed the presence of all six the colony-forming progenitor HSCs, HSCs cultured in the methylcellulose assay without prior contact with hBMSCs or osteo-hBMSCs give only rise to colonies derived from early progenitors such as CFU-GEMM, CFU-GM and CFU-M.



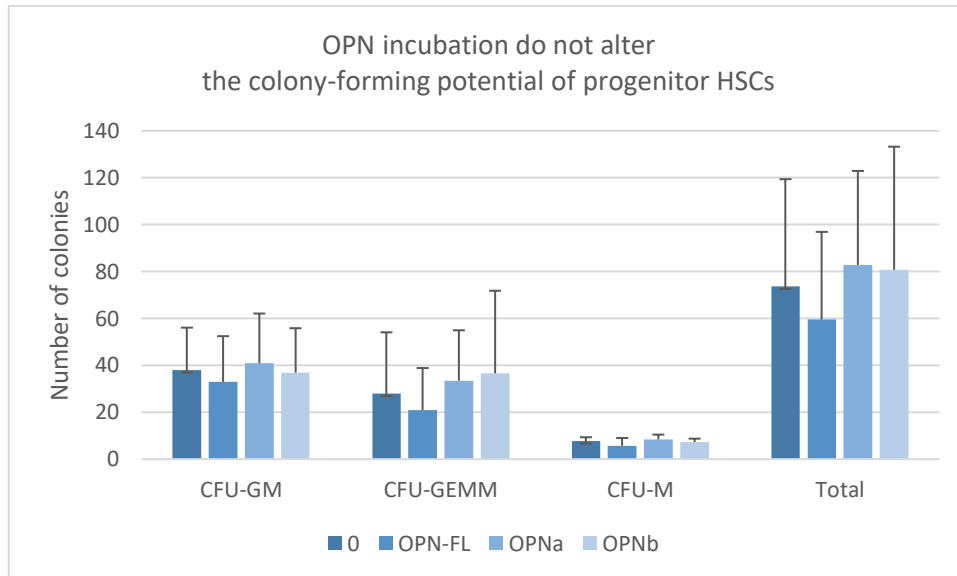


Figure 34: Methylcellulose assay after 16h incubation of OPN-FL, OPNa or OPNb with CD34<sup>+</sup> HSCs.

#### 4.7 Possible applications of a bone marrow niche model: the case of multiple myeloma

Since primary myeloma cells are difficult to maintain *in vitro* for long-term studies, requiring several different cytokines and surviving only for a limited time, I investigated in collaboration with the Prof. Franziska Jundt from the Hematology department of the University Hospital Würzburg the possibility to employ the previously established bone marrow niche model for the culturing of a multiple myeloma cell line. Differential detection of INA-6 and hBMSCs shows a gradual proliferation of multiple myeloma cells in the co-culture during the course of 7 days, concomitant with a gradual decrease in the number of hBMSCs, possibly induced by the multiple myeloma cells. In contrast, INA-6 cells undergo abrupt apoptosis when in absence of IL-6 and hBMSCs for more than 48h (n=2) (Figure 35).

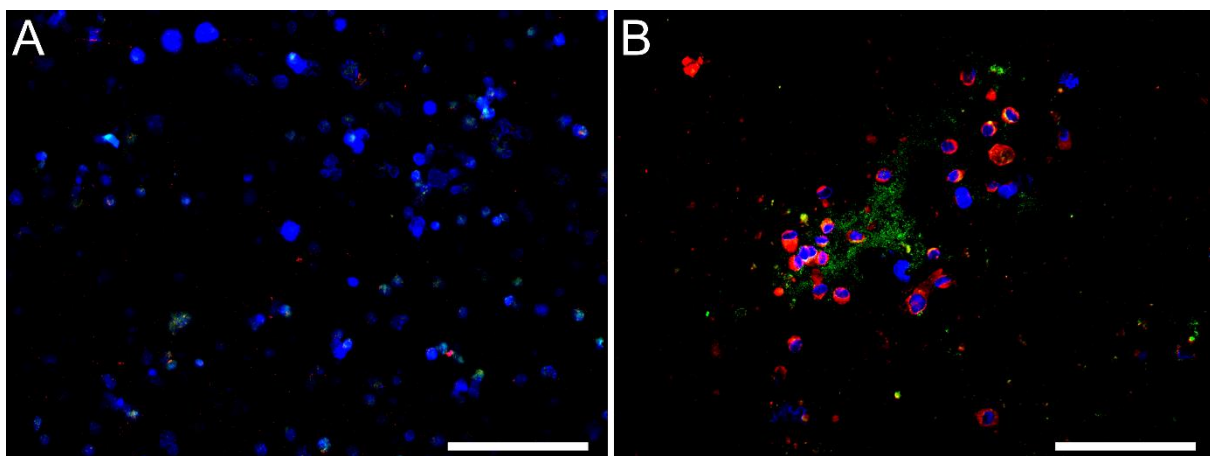


Figure 35: INA-6 survive in the bone marrow niche model. **A)** INA-6 cells undergo apoptosis after 48h of IL-6 starvation. **B)** INA-6 survive and proliferate despite no IL-6 supplementation when in co-culture with osteo-hBMSCs. **Red:** INA-6 cells; **Blue:** DAPI; **Green:** Scaffold remnants. **Scalebar:** 100 $\mu$ m. Experiments performed in collaboration with Tanja Schneider.

## DISCUSSION

Tissue Engineering and Regenerative Medicine is a multidisciplinary field of study focusing on the development of artificial organs or tissues. It represents a promising alternative for the treatment of several orthopedic diseases by avoiding the pitfalls of the available therapeutic options. Common problems of allogeneic and autologous bone transplantation are in fact tissue availability and immunological issues. On the other hand, artificial implants and prosthesis, often present poor mechanical matching with the hosting site and lack of important biological functions.

Primary aim of this work is the development of a cell-scaffold combined therapy for the treatment of critical size bone defects to be tested *in vivo*.

In order to standardize the conditions needed for the establishment of the cell therapy, I isolated human bone marrow-derived mesenchymal stromal cells (hBMSCs) from 15 osteoarthritis patients undergoing hip replacement surgery following the protocol as reported by Nöth et al.<sup>235</sup>. Since during the isolation step it is possible that macrophages, alongside hBMSCs, attach to the culturing surface<sup>236</sup>, further passaging of the cells is performed before hBMSCs characterization to detach eventual contaminant macrophages and select hBMSCs through cell-specific culturing medium. Although characterization of the surface antigen expression revealed expression of a panel of markers conform to the indications of the Society for Cellular Therapy (Figure 8), significant variations could be observed between different donors in the percentage of cells expressing a particular marker. This can be due to inter-donor differences in the original ratio between cell populations in the bone marrow, often determined to the health conditions of the donor; or to the isolation method, in that slightly higher agitation times during extraction of the cells from the spongy bone or prolonged contact with hematopoietic cells may lead to differences in the differentiation or proliferation potential<sup>236</sup>.

In fact, similar differences can be observed in the differentiation potential of different donors as detected by histological staining (Figure 9) and RT-Real Time PCR (Figure 10). Moreover, an important difference can be seen between the osteogenic and chondrogenic potential and the adipogenic potential (Figure 9). While all donors could efficiently differentiate into the osteogenic and chondrogenic lineages with various degree of efficiency, only 50-80% of the cells could differentiate towards the adipogenic lineage in most of the donors. This difference can be confirmed by several reports pointing out that cells isolated from different tissues present an environmental niche memory and differentiate better in the lineage characteristic of the tissue of origin<sup>33,34,237</sup>. It is therefore intuitive that hBMSCs differentiate better towards the chondrogenic and ultimately osteogenic lineages. However, when observing the expression of osteogenic differentiation markers by hBMSCs cultured in osteogenic differentiation medium compared to cells cultured in MSCGM-CD 2%FCS after 28 days (Figure 10), it is possible to evidence an important discrepancy with the histological data, in that no

significant upregulation of either early or late differentiation markers can be detected. This phenomenon can be observed despite the evident production of mineral deposit on cells cultured in osteogenically differentiation medium, which are otherwise absent in the MSCGM-CD 2%FCS -treated negative controls. This result therefore suggests that hBMSCs cultured in MSCGM-CD 2%FCS are not able to deposit calcium phosphate crystals due to the absence of a phosphate source in the medium, but that other growth factors or chemicals may be present in the medium and may be stimulating cell differentiation over time. An example for this is ascorbate, which is commonly used in several proliferation media and which also play an important role as a co-factor for collagen production and hBMSCs differentiation<sup>64</sup>. Moreover, MSCs isolated from different sources present a partial pre-commitment toward the tissue of origin, and it is therefore possible that hBMSCs pre-commitment toward the osteogenic lineage limits the observation of significant differences when treated with the two media<sup>33,34,237</sup>. Although osteogenic differentiation of hBMSCs is clearly evidenced by deposition of mineral phase, a finer characterization of cell differentiation is unfortunately impossible or difficult, since other histological staining such as hematoxylin eosin staining of cell nuclei and cytoplasm cannot be easily performed in parallel to the Alizarin Red staining of the mineral matrix, and since the positively charged hydroxyapatite deposited by differentiated hBMSCs easily sequester the negatively charged nucleic acids<sup>238</sup>, making DNA-based cell quantification difficult.

The establishment of a cell-based therapy for bone regeneration of critical size defects requires a careful consideration of several aspects concerning the characterization, feasibility and efficacy of the cell product to be administered. Although the choice of the appropriate cell type to be delivered will intuitively bring the major contribution to the success of the therapy, the regeneration of critical size defects requires an important amount of cell biomass to be produced, and safety- and legal requirement-driven optimization of the cell therapy products suggests that the isolation and expansion of cells from a donor should be subject to extensive characterization to ensure the maintenance of their cellular identity and exclude their tumorigenicity. Moreover, GMP-compliant treatment and expansion of the cells is required in order to ensure the safety of the cellular product and exclude possible contaminations, being them either of bacterial, viral or animal origin. For this reason, I explored the possibility to develop a GMP-compliant medium for the expansion of hBMSCs and their differentiation towards the osteogenic lineage.

The success of the use of a fibrin-rich gel derived from platelet-rich plasma<sup>239</sup> as a hydrogel for orthopedic surgery led me to the idea that platelet-derived lysate (PDL) could constitute a possible GMP-compliant, although non-chemically defined alternative to FCS for hBMSCs expansion. Therefore, I established a protocol for the production of PDL starting from the protocol published by Schallmoser et al.<sup>59</sup>. hBMSCs cultured in DMEM-F12 +5% PDL proliferated significantly better comparing to DMEM-F12 10% FCS, yielding 17±5 population doublings more, although they yielded 8±2 population

doublings less comparing to MSCGM-CD 2% FCS over the course of 60 days (Figure 13). These results are in agreement to what was published by Parsons et al.<sup>61</sup>, that showed that hBMSCs cultured in medium supplemented with 5% PDL yield 1 population doubling more comparing to cells cultured in medium supplemented with 10% FCS already in the first 5 days. Moreover, while cells cultured in MSCGM-CD 2% FCS reached confluence and started growing in layers or clusters, cells cultured in DMEM-F12 5% PDL underwent cell-cell contact inhibition upon reaching confluence and presented a nicely ordered cell monolayer (Figure 12B). This is in accordance to Ben Azouna et al.<sup>240</sup>, who reported that the layer of MSCs cultured in PDL-supplemented medium appears with many spaces between the cells in comparison with standard medium, in which one layer of very confluent MSCs can be observed.

hBMSCs of 5 different donors differentiated in osteogenic medium supplemented with PDL showed deposition of a significantly thicker layer of mineral material comparing to cells cultured in FCS-supplemented osteogenic medium (Figure 14). Moreover, deposition of mineral material could be detected already between day 7 and 14, while it could be detected only after day 14-21 in cells cultured in standard osteogenic medium. These results are in accordance to what reported in literature<sup>61,241</sup>, showing that supplementation of PDL to osteogenic medium can improve hBMSCs differentiation towards the osteogenic lineage. However, differentiation of hBMSCs in a rat tail collagen I gel showed only small differences between FCS- and PDL-supplemented osteogenic media in the mineral deposition capability (Figure 14), in agreement with what was reported by Castren<sup>60</sup>. The difference between the 2D and 3D conditions may be due to the spontaneous deposition of calcium phosphate in 2D conditions when in contact to some factors contained in the PDL, while elongation of hydroxyapatite crystals on the collagen fibers requires a more precise dynamic which is not influenced by PDL. Despite the small advantage conferred by PDL regarding mineralization on 3D supports, its use as a GMP-compliant substitute for FCS remains promising for clinical applications.

The microcarrier technology (MCs) constitutes a strategy for the expansion of adherent cell types under 3D conditions based on the culturing of the cells on small substrates in dynamic conditions. The choice of the scaffold dimension and architecture, the total porosity of the microcarriers and the surface properties of the material play a major role in determining the final yield of a culture, and several microcarriers are nowadays commercially available<sup>88</sup>. Since effective strategies for regeneration of critical-size bone defect often require the combined delivery of scaffold and cells, the microcarrier technology was chosen as the best approach for this study.

In this work I developed, in collaboration with FUJIFilm Manufacturing Europe B.V., a strategy for the manufacturing and crosslinking of a macroporous microcarrier based on a recombinant collagen I-based peptide (Cellnest™)<sup>234</sup>. This microcarrier holds the potential to provide a method for the scalable expansion of hBMSCs for their use for a cell-scaffold combined therapy for bone regeneration. The

developed microcarriers (Cellnest™-MCs) are characterized by high pore dimension, porosity and pore interconnection diameters when comparing to other commercially available equivalents (such as CultiSpher®-G)<sup>242</sup> (Figure 15). The effect of interconnectivity of ceramic scaffolds on osteoblasts growth has been investigated by Lu et al.<sup>243</sup>, who showed that interconnections of 20µm between internal pores are enough for cell penetration into the scaffold *in vivo*. However, bone ingrowth has been shown to occur only in pores between 50-100µm in ceramic scaffolds with total porosity higher than 50-60%<sup>243</sup>. In this regard, ECM-inspired materials such as Cellnest™ present several advantages over ceramic materials, holding a much higher biodegradation rate *in vivo*. This feature would in fact allow bone ingrowth into the material despite the reduce pore dimension, leading to bone formation. Such a phenomenon has been shown by Chen et al.<sup>63</sup>, who demonstrated ectopic bone formation in human adipose MSCs-laden CultiSpher® in a mouse model despite CultiSpher®'s pore dimension results to be significantly lower than Cellnest™-MCs. The possibility to digest Cellnest™ with papain or trypsin leaves therefore open the possibility for Cellnest™-MCs to be remodelled by tissue metalloproteases upon implantation.

Since Cellnest™-MCs are not stable in water-based solution, we therefore developed three crosslinking strategies. DHT-crosslinked Cellnest™-MCs appeared to support better cell adhesion, higher cell yield and cell vitality over 7 days for both C2C12 and hBMSCs comparing to CultiSpher® and HMDIC- or EDC-crosslinked Cellnest™-MCs (Figure 19, Figure 20A, B). These results may reflect differences in surface properties depending on the crosslinking strategy employed<sup>244</sup>, that may differently affect the cell expansion kinetic by delaying cell proliferation or migration into the bead core. To test this hypothesis, we therefore cultured hBMSCs on the different microcarriers over 28 days. DNA quantification showed that hBMSC enter the log phase after approximatively 7 days on both microcarrier types, but while they enter a plateau on CultiSpher® by day 14, possibly after reaching confluence on the microcarrier's surface, they enter plateau only by day 21 on DHT-crosslinked Cellnest™-MCs after yielding up to 2 population doublings more (Figure 20C). These results are in contrast with a previous report of Drexler et al.<sup>245</sup>, which pointed out that fibroblasts seeded on DHT-crosslinked electrospun collagen fibers presented decrease cellular metabolism comparing to when cultured on EDC-crosslinked fibers, and that DHT-crosslinking may reduce the wettability of materials and lead to lower cell attachment and proliferation. In this regards, it is possible that differences in the geometry, material type, concentration of the chemical crosslinker<sup>244</sup>, timing of the crosslinking and cell type employed<sup>246</sup> may account for the discrepancies with Dexler's study. Moreover, the progressive deposition of extracellular matrix by hBMSCs on the microcarriers makes it more difficult to precisely estimate the exact cell number on the microcarriers, since normalization of the DNA content, employed as a quantification method for determining the cell number, is performed on the base of the dry weight of the microcarriers. Although not optimal, DNA quantification has been chosen as quantification method

for the estimation of the cell number for being the only method not significantly influenced by the autofluorescence of the Cellnest™ material, that would otherwise affect the outcome of the measurements.

The development of a cell therapy for bone regeneration requires an exact control of the differentiation state of the cells to be transplanted. For this reason, since it has been reported that scaffold stiffness<sup>79,80</sup>, porosity<sup>247</sup> and permeability<sup>248</sup> can significantly influence hBMSCs differentiation, we investigated whether culturing of hBMSCs on different microcarriers could lead to osteogenic pre-commitment. Although stretching of hBMSCs and C2C12 could be observed on the surface of CultiSpher® (Figure 19A, E), no significant increase in the expression of col1a1 or Runx2 could be observed over the course of 7 days between DHT-, HMDIC- or EDC-crosslinked Cellnest™-MCs comparing to CultiSpher® (Figure 20D, E). This may be due to the fact that stretched hBMSCs may differentiate towards the myoblastic lineage<sup>249</sup>, or that eventual later differences in differentiation may be noted at later time point. In order to investigate the possibility to use DHT-crosslinked Cellnest™-MCs for bone regeneration, I therefore cultured hBMSCs on the microcarriers in osteogenic differentiation medium for 28 days. At the end of 28 days, extensive collagen type I deposition could be detected on Cellnest™-MCs (Figure 22A, B), with progressive mineral deposition (Figure 22D, E). These results show that hBMSCs can be expanded on Cellnest™-MCs without significantly altering their differentiation state and maintaining their differentiation potential, suggesting their suitability for further *in vitro* or *in vivo* applications not limited to bone regeneration.

Although porous microcarriers may constitute a promising injectable, non-invasive cell therapy solution for bone regeneration, their stability in the post-implantation phase remains poor. In order to improve stability and handling of the implant, I assembled the Cellnest™-MCs into solid scaffolds in a perfusion bioreactor. After 14 days of perfusion, I was able to assemble the microcarriers into a solid scaffold that would not be disrupted upon compression (Figure 23B). Histological analysis of the construct reported that cells cultured in the perfusion bioreactor differentiated and assembled the microcarriers by producing extensive extracellular matrix (Figure 23A), as previously reported by Chen et al.<sup>63</sup>. Moreover, MTT analysis of cell vitality allowed to demonstrate a much higher cell vitality and more uniform cell distribution when comparing to cells directly seeded into the scaffold by alternated flow in the perfusion bioreactor setup<sup>228</sup>. This result demonstrates the feasibility of utilizing Cellnest™-MCs-based solid scaffolds for implantation purposes.

However, since scaffold stiffness and mechanical properties were still far from the physiological values of lamellar or trabecular bone, we explored further options to improve hBMSCs differentiation and mineral deposition. To do this, we cultured hBMSCs in 2D and in a rat tail collagen I gel in contact with Cellnest™-based microparticles or Cellnest™-hydroxyapatite composite microparticles (Figure 24) and

tested the influence of these two particle types on cell vitality and mineralization. Although no difference in vitality and cell morphology could be noted between hBMSCs cultured in osteogenic or proliferation medium both in 2D and 3D conditions and between hBMSCs cultured in contact with Cellnest™ or Cellnest™-hydroxyapatite and hBMSCs alone (Figure 25, Figure 26), a gradual increase in cell mortality could be noted in all cases when cells were cultured in the rat tail collagen I gels (Figure 26, left panel). This could be due to shrinking of the hydrogels during culturing and matrix remodelling, reducing the dimension of the hydrogel pores overtime<sup>250</sup> and *de facto* limiting access of medium and nutrients to the inside of the hydrogel. Moreover, although a strong deposition of calcium phosphate by osteogenically differentiated hBMSCs could be detected in 3D conditions, mineral deposition appeared to be partially inhibited when Cellnest™-based microparticles or Cellnest™-hydroxyapatite composite microparticles were added to the hydrogel (Figure 26, right panel). This can be due to the fact that Cellnest™ sequesters the mineral ions from the hydrogels as already shown by Hennessy et al.<sup>251</sup>. In their experiments, they showed that RGD sequences, abundant in the Cellnest™ peptide, coated to hydroxyapatite implants significantly inhibited total bone formation as well as the amount of new bone directly contacting the implant perimeter *in vivo*. On the other hand, while it is possible to detect a mineralized area surrounding Cellnest™-hydroxyapatite composite microparticles into the hydrogel probably due to a release of calcium phosphate particles, the higher local concentration of phosphate may result in a delayed osteogenic differentiation of hBMSCs, as previously shown by Ma et al.<sup>252</sup>.

Although the employed strategies did not significantly improve the stability, stiffness and hardness of the scaffold to a degree comparable to the lamellar bone, a thorough observation of the overall architecture of the Cellnest™-MCs-based scaffold assembled in the perfusion bioreactor allowed to evidence a great similarity with the architecture of the trabecular bone. Since the trabecular bone naturally hosts the bone marrow and hBMSCs have been shown to play an important role in the maintenance of the bone marrow niche<sup>38</sup>, I therefore investigated the possibility of demonstrating the functionality of the previously developed artificial bone substitute by establishing a simplified bone marrow niche model (Figure 27).

Since osteo-progenitor cells have been shown to be particularly important in HSC maintenance<sup>36</sup>, I established a bone marrow niche model by co-culturing osteogenically differentiated hBMSCs and HSCs in DHT-crosslinked Cellnest™-MCs for 7 days without the addition of any other growth factor. This was particularly important for the establishment of a relevant model, since HSCs are normally maintained *in vitro* using a combination of several growth factors and cytokines, and have reported to rapidly die in their absence<sup>115</sup>. This kind of model provides significant advantages comparing to other reported models<sup>253</sup>, in that the higher cell-scaffold ratio allows to extract and analyse nucleic acids with higher efficiency while maintaining the possibility to analyse the cells with a wider range of techniques (Figure 28B, C). Since multi-color marking of hematopoietic cells is necessary for the correct

identification of the different hematopoietic cell types present in the model but it is made not practicable due to the high autofluorescence of the Cellnest™ material in a wide range of wavelengths, identification of hematopoietic progenitors maintained in the model despite the lack of externally supplemented cytokines was performed through methylcellulose assay. Methylcellulose assays revealed that both hBMSCs and osteogenic differentiated hBMSCs (osteo-hBMSCs) were able to maintain HSCs progenitors in culture inside the model, with no significant alteration into the overall number of colonies (Figure 28A). However, as already reported by Raaijmakers et al.<sup>120</sup>, osteo-hBMSCs promoted a significantly higher number of early progenitors comparing to undifferentiated cells, suggesting a role for osteo-progenitors in the maintenance of HSC stemness (Figure 28A). RT-Real Time PCR analysis in hBMSCs and osteo-hBMSCs revealed no significant upregulation of osteogenic markers when comparing to cells in monoculture, but revealed a significant increase in osteopontin in osteo-hBMSCs co-cultured with HSCs when compared to osteo-hBMSCs in monocultures (Figure 29B). This result could later be confirmed by histological analysis, that showed intense production of osteopontin when osteo-hBMSCs or undifferentiated hBMSCs are in co-culture with HSCs (Figure 29A). This result appeared to be particularly interesting, since osteopontin has been reported to play an important role in maintaining HSCs stemness and in regulating the HSC pool<sup>163,164</sup>. Although the expression of osteopontin in co-cultures between osteo-hBMSCs and HSCs has already been shown by Raaijmakers et al. in an *in vitro* model<sup>120</sup>, this is the first observation pointing out that expression of osteopontin is triggered by the contact between these two cell types similar to what reported for CCN1<sup>254</sup> after contact of MSCs with multiple myeloma cells. Moreover, a significant difference in the expression pattern was observable in the histological analysis. In fact, osteopontin produced by osteo-hBMSCs in monoculture, as reported in literature<sup>200</sup>, and in lower amount by hBMSCs in co-culture with HSCs could be detected only intracellularly, while in co-cultures between osteo-hBMSCs and HSCs osteopontin could be detected as extensively produced and deposited on the extracellular matrix (Figure 29A). Further *in silico* analysis run to investigate this phenomenon led to the discovery that the primers designed to target the osteopontin mRNAs could in fact just recognise a particular splice variant of osteopontin, the isoform OPNb. Using a new primer pair reported by Phillips et al.<sup>231</sup> and designed to flank and recognise a differentially spliced region on osteopontin mRNAs (Figure 30A), I was able to identify two different OPN splice variants produced exclusively by osteo-hBMSCs when in co-culture with HSCs (Figure 30B). After sequencing, the two isoforms were confirmed to be OPNa and OPNb.

The identification of these two isoforms demonstrates the power of such a simplified *in vitro* model comparing to the widely used murine *in vivo* models which are so far employed for the research on the physiology of the bone marrow niche. Most of the research and discoveries made on *in vivo* models are in fact largely dependent on immune-assays and antibodies targeting known molecules, which



cannot efficiently recognise highly variable molecules such as OPN and CD44, whose isoforms are still orphan of recognising antibodies<sup>255</sup>. Similarly, genotyping and proteome analysis are just possible on highly abundant cells, which are either easy to identify or to isolate, and a specific analysis of osteo-progenitor cells in contact with HSCs is so far not totally feasible. To demonstrate this concept, I therefore incubated the established bone marrow niche models with an anti-OPN directed antibody. This antibody is nonetheless unspecific, recognising a small, non-variable part of the protein. Incubation of the bone marrow models with the anti-OPN antibody did not lead to any significant alteration in the number of colonies originated by HSC progenitors in the model (Figure 31), suggesting that either binding of HSCs to osteopontin may be performed through CD44 expressed on the HSCs' surface, this bond being therefore not influenced by the antibody recognition of OPN and being allowed by the relative flexibility of osteopontin<sup>199</sup>; or that OPN inhibition through anti-OPN antibody may impair the splicing of OPN by thrombin<sup>256</sup> and therefore block the interactions between OPN and the  $\alpha_9\beta_1$  and  $\alpha_4\beta_1$  integrin on the HSCs' surface. Moreover, lack of binding between OPN and HSCs may influence HSC retention into the bone marrow niche under dynamic conditions *in vivo*, but may play a less important role under static conditions where HSCs can remain in contact with the osteo-progenitor cells.

To better study the behaviour of the two OPN variants *in vitro*, we therefore transfected three cell lines derived from three different tissues, HEK293 from kidney - CaCo2 from intestine - hFOB 1.19 foetal pre-osteoblasts, with a construct for the expression of either OPNa or OPNb, as reported by Takafuji et al.<sup>232</sup>. When analysing through western blot the two isoforms as produced by all three cell lines, it was possible to detect OPNa only in the cell lysate fraction, while OPNb could be reported also as secreted protein in the medium (Figure 33). This result is particularly interesting, since OPN has always been reported as a secreted protein<sup>186</sup>, and it is possible that the detection limits related to the poor availability of antibodies able to distinguish between different osteopontin isoforms have led to a wrong interpretation of the results so far. Moreover, this behaviour could be well explained by observing the structure of the two isoforms<sup>231</sup>. OPNb lacks in fact the exon 5 (Figure 6, Figure 30A), disrupting an area flanking a calcium-binding domain, while OPNa constitutes the full-length form of the protein. For this reason, it could be that OPNa, not detected into the medium, is in fact bound to the extracellular matrix or to the matrix of the plate, while OPNb, lacking the matrix-binding domain, remains in suspension. Differences in the secretion of the two isoforms can be reasonably excluded, since the expression vector and the secretion sequence of the two isoforms remain unaffected by eventual additional exon skipping.

In order to investigate the behaviour of the two OPN isoforms, we produced the 6-histidine-tagged recombinant OPNa and OPNb. Counting of the colonies emerging from hematopoietic progenitors incubated with the two isoforms or with a commercially available full-length version of OPN,

corresponding to OPNa according to the method published by Guidi et al.<sup>223</sup>, revealed no significant differences between the two isoforms (Figure 34) despite what previously reported by Stier et al.<sup>163</sup>. Similarly, no significant difference was detected between the two isoforms and the recombinant full-length version of the protein, partially excluding that lack of effects of the two isoforms may be due to defects or low quality of the in-house produced isoforms. Most interestingly, no significant difference was detected between the samples treated with the three version of OPN and the HSCs alone, confirming what reported by Guidi et al.<sup>223</sup>. This can be due to the fact that the isolated proteins have not been digested with thrombin, possibly exposing an additional ligand site of the protein to HSCs. This hypothesis would confirm the results from the inhibition of OPN with anti-OPN in the culture, showing that the produced OPN has to be made active by other cell types such as megakaryocytes in the bone marrow. Alternatively, this can be due to the fact that the binding of one of the isoforms of OPN to the bone matrix may be necessary for osteopontin to exert an effect on HSCs maintenance and quiescence.

Taken together, these results point out the importance of this simplified model as a way of investigating new molecules involved into the signalling of the bone marrow niche without the pitfalls of more complex models.

Moreover, this model is characterized by a large flexibility in its application, allowing to introduce different cell types and investigate the role of different signalling molecules in the homeostasis of the niche microenvironment. In order to investigate the possibility to use this bone marrow niche model to investigate a pathological situation, we established a co-culture between osteo-hBMSCs and a IL-6-dependent multiple myeloma cell line (INA6) in this model. The co-culture was performed without the supplementation of IL-6, so that the survival of the INA6 cells had to be granted by the osteo-hBMSCs alone. In agreement to what reported by Arnulf et al.<sup>177</sup>, the myeloma cells adapted to this model and proliferated inside the Cellnest™-MCs even in absence of IL-6, while monoculture of INA6 cells rapidly underwent apoptosis in the first 48 hours (Figure 35). Further experiments will have then to be performed to investigate whether the osteo-hBMSCs have been modified by the INA6 cells and how the different signaling axes are influenced by the co-culture; moreover, osteopontin has been shown to play an important role in multiple myeloma development, mediating the attachment of the malignant cells to the matrix and supporting their survival and bone marrow invasion<sup>257</sup>. Further experiments may be addressed to the investigation of the role of OPN in this model, and on how maintenance and proliferation of the INA6 cells change when introduced in a previously established osteo-hBMSCs-HSCs co-culture.

## 5 CONCLUSION

Critical size bone defects constitute nowadays an unresolved problem in the clinical scenario, where the golden standards do not live up to the expectations and do not match the physical and biological characteristics of the host tissue. In this context, Tissue Engineering approaches promise more effective ways to restore and regenerate the original functions without suffering the same pitfalls.

In this work, I developed a cell-scaffold mixed formulation for a putative cell-based therapy of critical size defects, demonstrating the possibility to use extracellular matrix-inspired macroporous microcarrier for the expansion and osteogenic differentiation of human bone marrow-derived mesenchymal stromal cells under GMP-compliant conditions.

Moreover, I demonstrated the functionality of the developed bone substitute as a hematopoietic pseudo-organ able to support the maintenance of bone marrow-derived hematopoietic stem cells in absence of externally supplemented cytokines.

Furthermore, the establishment of such a bone marrow niche model allowed me to investigate critical signaling pathways involved in the maintenance of the niche microenvironment and in the regulation of the hematopoietic process. This model brought in fact to the discovery of two different osteopontin splice variants being expressed by osteogenically differentiated bone marrow-derived mesenchymal stromal cells after co-culture with hematopoietic stem cells, demonstrating how a simplified *in vitro* model has a greater potential when compared to the classical *in vivo* models to investigate new or highly variable signaling molecules which still remain orphan of efficient detection methods in complex models.

Finally, I demonstrated the possibility to apply this bone marrow niche model to the study of other hematological malignancies, by maintaining an interleukin-6 dependent multiple myeloma cell line in the model without addition of interleukin-6 or any other cytokine.

This work opens the way for a further development of the injectable cell-based therapy as a cure for critical size bone defects in combination with other cell types of the endothelial lineage. Further studies will have to be conducted to prove the functionality of this mixed formulation in small and big animal models. Moreover, the established bone marrow niche model opens the possibility for the investigation of cell-cell signaling in a more cell-specific way, and further miniaturization of the system will allow to investigate the influence of flow and shear stress and the presence of other niche-specific cell types on the niche and model homeostasis. Finally, the specific formulation of the scaffold peptide and its known biochemical properties will allow the covalent linking of signaling molecules to the scaffold and an unprecedented study of matrix-bound proteins on the niche equilibrium.

## 6 BIBLIOGRAPHY

- 1 Kneser, U., Schaefer, D. J., Polykandriotis, E. & Horch, R. E. Tissue engineering of bone: the reconstructive surgeon's point of view. *Journal of cellular and molecular medicine* **10**, 7-19 (2006).
- 2 Laurencin, C., Khan, Y. & El-Amin, S. F. Bone graft substitutes. *Expert review of medical devices* **3**, 49-57, doi:10.1586/17434440.3.1.49 (2006).
- 3 Sarkar, S. K. & Lee, B. T. Hard tissue regeneration using bone substitutes: an update on innovations in materials. *Korean J Intern Med* **30**, 279-293, doi:10.3904/kjim.2015.30.3.279 (2015).
- 4 Kock, L., van Donkelaar, C. C. & Ito, K. Tissue engineering of functional articular cartilage: the current status. *Cell and tissue research* **347**, 613-627, doi:10.1007/s00441-011-1243-1 (2012).
- 5 Rho, J. Y., Kuhn-Spearing, L. & Zioupos, P. Mechanical properties and the hierarchical structure of bone. *Med Eng Phys* **20**, 92-102 (1998).
- 6 Fratzl, P., Gupta, H. S., Paschalis, E. P. & Roschger, P. Structure and mechanical quality of the collagen–mineral nano-composite in bone. *J. Mater. Chem.* **14**, 2115-2123, doi:10.1039/b402005g (2004).
- 7 Taylor, D., Hazenberg, J. G. & Lee, T. C. Living with cracks: damage and repair in human bone. *Nat Mater* **6**, 263-268, doi:10.1038/nmat1866 (2007).
- 8 Studyblue. *BIO - The Skeletal System*, <<https://www.studyblue.com/notes/note/n/bio-the-skeletal-system/deck/10150846>> (2017).
- 9 Sikes, C. S. & Wheeler, A. P. Regulators of Biomineralization. *American Chemical Society*, 620-626 (1988).
- 10 Fisher, L. W. *et al.* Proteoglycans of developing bone. *J Biol Chem* **258**, 6588-6594 (1983).
- 11 Glimcher, M. J. Molecular biology of mineralized tissues with particular reference to bone. *Rev. Med. Phys.* **31**, 359 (1959).
- 12 Heinegard, D. & Sommarin, Y. Structure and biology of cartilage and bone matrix noncollagenous macromolecules. *FASEB J* **3**, 2042-2051 (1987).
- 13 Boskey, A. L. Mineral-Matrix Interactions in Bone and Cartilage. *Clinical Orthopaedics and Related Research* **281**, doi:10.2142/biophys.20.259 (1992).
- 14 Silver, F. H. & Landis, W. J. Deposition of apatite in mineralizing vertebrate extracellular matrices: A model of possible nucleation sites on type I collagen. *Connect Tissue Res* **52**, 242-254, doi:10.3109/03008207.2010.551567 (2011).
- 15 Lees, S. & Probst, K. The locus of mineral crystallites in bone. *Connect Tissue Res* **18**, 41-54 (1988).
- 16 Nair, A. K., Gautieri, A., Chang, S.-W. & Buehler, M. J. Molecular mechanics of mineralized collagen fibrils in bone. *Nature Communications* **4**, 1724, doi:10.1038/ncomms2720 (2013).
- 17 Kanczler, J. M. & Oreffo, R. O. Osteogenesis and angiogenesis: the potential for engineering bone. *Eur Cell Mater* **15**, 100-114 (2008).
- 18 Marieb, E. N. & Hoehn, K. N. *Human Anatomy and Physiology with Interactive Physiology* (Pearson, 2010).
- 19 Germain, S., Monnot, C., Muller, L. & Eichmann, A. Hypoxia-driven angiogenesis: role of tip cells and extracellular matrix scaffolding. *Curr Opin Hematol* **17**, 245-251, doi:10.1097/MOH.0b013e32833865b9 (2010).
- 20 McCoy, R. J. & O'Brien, F. J. Influence of shear stress in perfusion bioreactor cultures for the development of three-dimensional bone tissue constructs: a review. *Tissue Eng Part B Rev* **16**, 587-601, doi:10.1089/ten.TEB.2010.0370 (2010).
- 21 Bullens, P. H., Schreuder, H. W., de Waal Malefijt, M. C., Verdonschot, N. & Buma, P. The presence of periosteum is essential for the healing of large diaphyseal segmental bone defects reconstructed with trabecular metal: a study in the femur of goats. *J Biomed Mater Res B Appl Biomater* **92**, 24-31, doi:10.1002/jbm.b.31485 (2010).
- 22 Simpson, A. H. The blood supply of the periosteum. *J Anat* **140 ( Pt 4)**, 697-704 (1985).

- 23 Soltan, M., Smiler, D. & Soltan, C. The inverted periosteal flap: a source of stem cells enhancing bone regeneration. *Implant Dent* **18**, 373-379, doi:10.1097/ID.0b013e3181b9d7df (2009).
- 24 Stevenson, S. Biology of bone grafts. *Orthop Clin North Am* **30**, 543-552 (1999).
- 25 Li, C. Y. *et al.* Comparative analysis of human mesenchymal stem cells from bone marrow and adipose tissue under xeno-free conditions for cell therapy. *Stem Cell Res Ther* **6**, 55, doi:10.1186/s13287-015-0066-5 (2015).
- 26 Secunda, R. *et al.* Isolation, expansion and characterisation of mesenchymal stem cells from human bone marrow, adipose tissue, umbilical cord blood and matrix: a comparative study. *Cytotechnology* **67**, 793-807, doi:10.1007/s10616-014-9718-z (2015).
- 27 Uezumi, A. *et al.* Functional heterogeneity of side population cells in skeletal muscle. *Biochem Biophys Res Commun* **341**, 864-873, doi:10.1016/j.bbrc.2006.01.037 (2006).
- 28 Laino, G. *et al.* An approachable human adult stem cell source for hard-tissue engineering. *J Cell Physiol* **206**, 693-701, doi:10.1002/jcp.20526 (2006).
- 29 Santhagunam, A., Dos Santos, F., Madeira, C., Salgueiro, J. B. & Cabral, J. M. Isolation and ex vivo expansion of synovial mesenchymal stromal cells for cartilage repair. *Cytotherapy* **16**, 440-453, doi:10.1016/j.jcyt.2013.10.010 (2014).
- 30 Frausin, S. *et al.* Wharton's jelly derived mesenchymal stromal cells: Biological properties, induction of neuronal phenotype and current applications in neurodegeneration research. *Acta Histochem* **117**, 329-338, doi:10.1016/j.acthis.2015.02.005 (2015).
- 31 Al-Nbaheen, M. *et al.* Human stromal (mesenchymal) stem cells from bone marrow, adipose tissue and skin exhibit differences in molecular phenotype and differentiation potential. *Stem Cell Rev* **9**, 32-43, doi:10.1007/s12015-012-9365-8 (2013).
- 32 Dominici, M. *et al.* Minimal criteria for defining multipotent mesenchymal stromal cells. The International Society for Cellular Therapy position statement. *Cytotherapy* **8**, 315-317, doi:10.1080/14653240600855905 (2006).
- 33 Ragni, E. *et al.* Differential microRNA signature of human mesenchymal stem cells from different sources reveals an "environmental-niche memory" for bone marrow stem cells. *Experimental cell research* **319**, 1562-1574, doi:10.1016/j.yexcr.2013.04.002 (2013).
- 34 Heo, J. S., Choi, Y., Kim, H. S. & Kim, H. O. Comparison of molecular profiles of human mesenchymal stem cells derived from bone marrow, umbilical cord blood, placenta and adipose tissue. *Int J Mol Med* **37**, 115-125, doi:10.3892/ijmm.2015.2413 (2016).
- 35 Hass, R., Kasper, C., Bohm, S. & Jacobs, R. Different populations and sources of human mesenchymal stem cells (MSC): A comparison of adult and neonatal tissue-derived MSC. *Cell Commun Signal* **9**, 12, doi:10.1186/1478-811X-9-12 (2011).
- 36 Sacchetti, B. *et al.* Self-renewing osteoprogenitors in bone marrow sinusoids can organize a hematopoietic microenvironment. *Cell* **131**, 324-336, doi:10.1016/j.cell.2007.08.025 (2007).
- 37 Sugiyama, T., Kohara, H., Noda, M. & Nagasawa, T. Maintenance of the hematopoietic stem cell pool by CXCL12-CXCR4 chemokine signaling in bone marrow stromal cell niches. *Immunity* **25**, 977-988, doi:10.1016/j.immuni.2006.10.016 (2006).
- 38 Mendez-Ferrer, S. *et al.* Mesenchymal and haematopoietic stem cells form a unique bone marrow niche. *Nature* **466**, 829-834, doi:10.1038/nature09262 (2010).
- 39 Ding, L., Saunders, T. L., Enikolopov, G. & Morrison, S. J. Endothelial and perivascular cells maintain haematopoietic stem cells. *Nature* **481**, 457-462, doi:10.1038/nature10783 (2012).
- 40 Greenbaum, A. *et al.* CXCL12 in early mesenchymal progenitors is required for haematopoietic stem-cell maintenance. *Nature* **495**, 227-230, doi:10.1038/nature11926 (2013).
- 41 Park, D. *et al.* Endogenous bone marrow MSCs are dynamic, fate-restricted participants in bone maintenance and regeneration. *Cell Stem Cell* **10**, 259-272, doi:10.1016/j.stem.2012.02.003 (2012).
- 42 Omatsu, Y. *et al.* The essential functions of adipo-osteogenic progenitors as the hematopoietic stem and progenitor cell niche. *Immunity* **33**, 387-399, doi:10.1016/j.immuni.2010.08.017 (2010).

- 43 Kusumbe, A. P., Ramasamy, S. K. & Adams, R. H. Coupling of angiogenesis and osteogenesis by a specific vessel subtype in bone. *Nature* **507**, 323-328, doi:10.1038/nature13145 (2014).
- 44 Kunisaki, Y. *et al.* Arteriolar niches maintain haematopoietic stem cell quiescence. *Nature* **502**, 637-643, doi:10.1038/nature12612 (2013).
- 45 Ono, N. *et al.* Vasculature-associated cells expressing nestin in developing bones encompass early cells in the osteoblast and endothelial lineage. *Dev Cell* **29**, 330-339, doi:10.1016/j.devcel.2014.03.014 (2014).
- 46 Chan, C. K. *et al.* Endochondral ossification is required for haematopoietic stem-cell niche formation. *Nature* **457**, 490-494, doi:10.1038/nature07547 (2009).
- 47 Nakamura, Y. *et al.* Isolation and characterization of endosteal niche cell populations that regulate hematopoietic stem cells. *Blood* **116**, 1422-1432, doi:10.1182/blood-2009-08-239194 (2010).
- 48 Rastogi, S. *et al.* Intralesional autologous mesenchymal stem cells in management of osteonecrosis of femur: a preliminary study. *Musculoskeletal surgery* **97**, 223-228, doi:10.1007/s12306-013-0273-0 (2013).
- 49 Fuerst, G. *et al.* Are culture-expanded autogenous bone cells a clinically reliable option for sinus grafting? *Clinical oral implants research* **20**, 135-139, doi:10.1111/j.1600-0501.2008.01624.x (2009).
- 50 Rickert, D. *et al.* Maxillary sinus floor elevation with bovine bone mineral combined with either autogenous bone or autogenous stem cells: a prospective randomized clinical trial. *Clinical oral implants research* **22**, 251-258, doi:10.1111/j.1600-0501.2010.01981.x. (2011).
- 51 Shayesteh, Y. *et al.* Sinus augmentation using human mesenchymal stem cells loaded into a beta-tricalcium phosphate/hydroxyapatite scaffold. *Oral Surg Oral Med Oral Pathol Oral Radiol Endod* **106**, 203-209, doi:10.1016/j.tripleo.2007.12.001. (2008).
- 52 Ueda, M., Yamada, Y., Kagami, H. & Hibi, H. Injectable bone applied for ridge augmentation and dental implant placement: human progress study. *Implant Dent* **17**, 82-90, doi:10.1097/ID.0b013e31815cd591 (2008).
- 53 Sensebe, L., Krampera, M., Schrezenmeier, H., Bourin, P. & Giordano, R. Mesenchymal stem cells for clinical application. *Vox sanguinis* **98**, 93-107, doi:10.1111/j.1423-0410.2009.01227.x (2010).
- 54 Centeno, C. J. *et al.* A multi-center analysis of adverse events among two thousand, three hundred and seventy two adult patients undergoing adult autologous stem cell therapy for orthopaedic conditions. *Int Orthop* **40**, 1755-1765, doi:10.1007/s00264-016-3162-y (2016).
- 55 English, K. Mechanisms of mesenchymal stromal cell immunomodulation. *Immunology and cell biology* **91**, 19-26, doi:10.1038/icb.2012.56 (2013).
- 56 Jo, C. H. *et al.* Intra-articular injection of mesenchymal stem cells for the treatment of osteoarthritis of the knee: a proof-of-concept clinical trial. *Stem Cells* **32**, 1254-1266, doi:10.1002/stem.1634 (2014).
- 57 Zhao, K. *et al.* Immunomodulation effects of mesenchymal stromal cells on acute graft-versus-host disease after hematopoietic stem cell transplantation. *Biol Blood Marrow Transplant* **21**, 97-104, doi:10.1016/j.bbmt.2014.09.030 (2015).
- 58 van der Garde, M. *et al.* Direct Comparison of Wharton's Jelly and Bone Marrow-Derived Mesenchymal Stromal Cells to Enhance Engraftment of Cord Blood CD34(+) Transplants. *Stem Cells Dev* **24**, 2649-2659, doi:10.1089/scd.2015.0138 (2015).
- 59 Schallmoser, K. *et al.* Human platelet lysate can replace fetal bovine serum for clinical-scale expansion of functional mesenchymal stromal cells. *Transfusion* **47**, 1436-1446, doi:10.1111/j.1537-2995.2007.01220.x (2007).
- 60 Castren, E. *et al.* Osteogenic differentiation of mesenchymal stromal cells in two-dimensional and three-dimensional cultures without animal serum. *Stem Cell Res Ther* **6**, 167, doi:10.1186/s13287-015-0162-6 (2015).
- 61 Parsons, P. *et al.* Platelet-Rich Concentrate Supports Human Mesenchymal Stem Cell Proliferation, Bone Morphogenetic Protein-2 Messenger RNA Expression, Alkaline

- Phosphatase Activity, and Bone Formation In Vitro: A Mode of Action to Enhance Bone Repair. *Journal of Orthopaedic Trauma* **22**, 595, doi:10.1097/bot.0b013e318188dbb7 (2008).
- 62 Valenti, M. T., Dalle Carbonare, L. & Mottes, M. Osteogenic Differentiation in Healthy and Pathological Conditions. *Int J Mol Sci* **18**, doi:10.3390/ijms18010041 (2016).
- 63 Chen, M., Zhou, M., Ye, Z., Zhou, Y. & Tan, W. S. Ectopic osteogenesis of macroscopic tissue constructs assembled from human mesenchymal stem cell-laden microcarriers through in vitro perfusion culture. *PLoS One* **9**, e109214, doi:10.1371/journal.pone.0109214 (2014).
- 64 Tsai, K. S. *et al.* Type I collagen promotes proliferation and osteogenesis of human mesenchymal stem cells via activation of ERK and Akt pathways. *Journal of biomedical materials research. Part A* **94**, 673-682, doi:10.1002/jbm.a.32693 (2010).
- 65 Joshi, M. K. *et al.* Three-dimensional cellulose sponge: Fabrication, characterization, biomimetic mineralization, and in vitro cell infiltration. *Carbohydrate polymers* **136**, 154-162, doi:10.1016/j.carbpol.2015.09.018 (2016).
- 66 Phadke, A. *et al.* Effect of scaffold microarchitecture on osteogenic differentiation of human mesenchymal stem cells. *Eur Cell Mater* **25**, 114-128; discussion 128-119 (2013).
- 67 Gariboldi, M. I. & Best, S. M. Effect of Ceramic Scaffold Architectural Parameters on Biological Response. *Frontiers in bioengineering and biotechnology* **3**, 151, doi:10.3389/fbioe.2015.00151 (2015).
- 68 Kasten, P. *et al.* Influence of platelet-rich plasma on osteogenic differentiation of mesenchymal stem cells and ectopic bone formation in calcium phosphate ceramics. *Cells, tissues, organs* **183**, 68-79, doi:10.1159/000095511 (2006).
- 69 Okuda, T. *et al.* The slow resorption with replacement by bone of a hydrothermally synthesized pure calcium-deficient hydroxyapatite. *Biomaterials* **29**, 2719-2728, doi:10.1016/j.biomaterials.2008.03.028 (2008).
- 70 Wang, C., Lin, K., Chang, J. & Sun, J. The stimulation of osteogenic differentiation of mesenchymal stem cells and vascular endothelial growth factor secretion of endothelial cells by beta-CaSiO<sub>3</sub>/beta-Ca<sub>3</sub>(PO<sub>4</sub>)<sub>2</sub> scaffolds. *Journal of biomedical materials research. Part A* **102**, 2096-2104, doi:10.1002/jbm.a.34880 (2014).
- 71 Lei, B. *et al.* Surface nanoscale patterning of bioactive glass to support cellular growth and differentiation. *Journal of biomedical materials research. Part A* **94**, 1091-1099, doi:10.1002/jbm.a.32776 (2010).
- 72 Habibovic, P. *et al.* Relevance of osteoinductive biomaterials in critical-sized orthotopic defect. *Journal of orthopaedic research : official publication of the Orthopaedic Research Society* **24**, 867-876, doi:10.1002/jor.20115 (2006).
- 73 Lee, J. H. *et al.* Biointerface control of electrospun fiber scaffolds for bone regeneration: engineered protein link to mineralized surface. *Acta biomaterialia* **10**, 2750-2761, doi:10.1016/j.actbio.2014.01.021 (2014).
- 74 Duan, B. & Wang, M. Customized Ca-P/PHBV nanocomposite scaffolds for bone tissue engineering: design, fabrication, surface modification and sustained release of growth factor. *J R Soc Interface* **7 Suppl 5**, S615-629, doi:10.1098/rsif.2010.0127.focus (2010).
- 75 Ajiboye, R. M., Hamamoto, J. T., Eckardt, M. A. & Wang, J. C. Clinical and radiographic outcomes of concentrated bone marrow aspirate with allograft and demineralized bone matrix for posterolateral and interbody lumbar fusion in elderly patients. *Eur Spine J* **24**, 2567-2572, doi:10.1007/s00586-015-4117-5 (2015).
- 76 Soicher, M. A. *et al.* Remineralized bone matrix as a scaffold for bone tissue engineering. *Journal of biomedical materials research. Part A* **102**, 4480-4490, doi:10.1002/jbm.a.35118 (2014).
- 77 Sen, B. *et al.* Mechanical strain inhibits adipogenesis in mesenchymal stem cells by stimulating a durable beta-catenin signal. *Endocrinology* **149**, 6065-6075, doi:10.1210/en.2008-0687 (2008).
- 78 Engler, A. J., Sen, S., Sweeney, H. L. & Discher, D. E. Matrix elasticity directs stem cell lineage specification. *Cell* **126**, 677-689, doi:10.1016/j.cell.2006.06.044 (2006).

- 79 McBeath, R., Pirone, D. M., Nelson, C. M., Bhadriraju, K. & Chen, C. S. Cell shape, cytoskeletal tension, and RhoA regulate stem cell lineage commitment. *Dev Cell* **6**, 483-495 (2004).
- 80 Kelly, D. J. & Jacobs, C. R. The role of mechanical signals in regulating chondrogenesis and osteogenesis of mesenchymal stem cells. *Birth Defects Res C Embryo Today* **90**, 75-85, doi:10.1002/bdrc.20173 (2010).
- 81 Sathy, B. N. *et al.* Bone Tissue Engineering with Multilayered Scaffolds-Part I: An Approach for Vascularizing Engineered Constructs In Vivo. *Tissue Eng Part A* **21**, 2480-2494, doi:10.1089/ten.TEA.2015.0098 (2015).
- 82 Rucker, C., Kirch, H., Pullig, O. & Walles, H. Strategies and First Advances in the Development of Prevascularized Bone Implants. *Curr Mol Biol Rep* **2**, 149-157, doi:10.1007/s40610-016-0046-2 (2016).
- 83 Confalonieri, D., La Marca, M., van Dongen, E., Walles, H. & Ehlicke, F. A Novel Injectable Recombinant Collagen I Peptide - based Macroporous Microcarrier Allows Superior Expansion of C2C12 and Human Bone Marrow - derived Mesenchymal Stromal Cells and Supports Deposition of Mineralized Matrix. *Tissue Eng Part A*, doi:10.1089/ten.TEA.2016.0436 (2017).
- 84 Rodrigues, M. E., Costa, A. R., Henriques, M., Azeredo, J. & Oliveira, R. Evaluation of solid and porous microcarriers for cell growth and production of recombinant proteins. *Methods Mol Biol* **1104**, 137-147, doi:10.1007/978-1-62703-733-4\_10 (2014).
- 85 Fitzgerald, K. A., Malhotra, M., Curtin, C. M., Brien, F. J. O. & O'Driscoll, C. M. Life in 3D is never flat: 3D models to optimise drug delivery. *Journal of Controlled Release* **215**, 39-54, doi:10.1016/j.jconrel.2015.07.020 (2015).
- 86 Akhmanova, M., Osidak, E., Domogatsky, S., Rodin, S. & Domogatskaya, A. Physical, Spatial, and Molecular Aspects of Extracellular Matrix of In Vivo Niches and Artificial Scaffolds Relevant to Stem Cells Research. *Stem Cells Int* **2015**, 167025, doi:10.1155/2015/167025 (2015).
- 87 van Wezel, A. L. Growth of cell-strains and primary cells on micro-carriers in homogeneous culture. *Nature* **216**, 64-65 (1967).
- 88 Tan, K. Y., Reuveny, S. & Oh, S. K. W. Recent advances in serum-free microcarrier expansion of mesenchymal stromal cells: Parameters to be optimized. *Biochemical and Biophysical Research Communications* **473**, 769-773, doi:10.1016/j.bbrc.2015.09.078 (2016).
- 89 de Soure, A. M., Fernandes-Platzgummer, A., da Silva, C. L. & Cabral, J. M. Scalable microcarrier-based manufacturing of mesenchymal stem/stromal cells. *J Biotechnol* **236**, 88-109, doi:10.1016/j.jbiotec.2016.08.007 (2016).
- 90 Schop, D. *et al.* Expansion of human mesenchymal stromal cells on microcarriers: growth and metabolism. *J Tissue Eng Regen Med* **4**, 131-140, doi:10.1002/term.224 (2010).
- 91 Carmelo, J. G., Fernandes-Platzgummer, A., Diogo, M. M., da Silva, C. L. & Cabral, J. M. A xeno-free microcarrier-based stirred culture system for the scalable expansion of human mesenchymal stem/stromal cells isolated from bone marrow and adipose tissue. *Biotechnol J* **10**, 1235-1247, doi:10.1002/biot.201400586 (2015).
- 92 Malda, J. & Frondoza, C. G. Microcarriers in the engineering of cartilage and bone. *Trends Biotechnol* **24**, 299-304, doi:10.1016/j.tibtech.2006.04.009 (2006).
- 93 Davidenko, N. *et al.* Control of crosslinking for tailoring collagen-based scaffolds stability and mechanics. *Acta biomaterialia* **25**, 131-142, doi:10.1016/j.actbio.2015.07.034 (2015).
- 94 Jin, G. Z., Park, J. H., Seo, S. J. & Kim, H. W. Dynamic cell culture on porous biopolymer microcarriers in a spinner flask for bone tissue engineering: a feasibility study. *Biotechnol Lett* **36**, 1539-1548, doi:10.1007/s10529-014-1513-6 (2014).
- 95 Sankaran, V. G. & Weiss, M. J. Anemia: progress in molecular mechanisms and therapies. *Nat Med* **21**, 221-230, doi:10.1038/nm.3814 (2015).
- 96 Dobzhansky, T. Nothing in Biology Makes Sense except in the Light of Evolution. *The American Biology Teacher* **35**, 125-129, doi:10.2307/4444260 (1973).
- 97 MacLean, A. L., Lo Celso, C. & Stumpf, M. P. Concise Review: Stem Cell Population Biology: Insights from Hematopoiesis. *Stem Cells* **35**, 80-88, doi:10.1002/stem.2508 (2017).



- 98 Vunjak-Novakovic, G. *et al.* Challenges in cardiac tissue engineering. *Tissue Eng Part B Rev* **16**, 169-187, doi:10.1089/ten.TEB.2009.0352 (2010).
- 99 Schofield, R. The relationship between the spleen colony-forming cell and the haemopoietic stem cell. *Blood cells* (1978).
- 100 Morrison, S. J. & Spradling, A. C. Stem cells and niches: mechanisms that promote stem cell maintenance throughout life. *Cell* **132**, 598-611, doi:10.1016/j.cell.2008.01.038 (2008).
- 101 Risau, W. Embryonic angiogenesis factors. *Pharmacol Ther* **51**, 371-376 (1991).
- 102 Choi, K., Kennedy, M., Kazarov, A., Papadimitriou, J. C. & Keller, G. A common precursor for hematopoietic and endothelial cells. *Development* **125**, 725-732 (1998).
- 103 Khan, J. A. *et al.* Fetal liver hematopoietic stem cell niches associate with portal vessels. *Science* **351**, 176-180, doi:10.1126/science.aad0084 (2016).
- 104 Kiel, M. J. *et al.* SLAM family receptors distinguish hematopoietic stem and progenitor cells and reveal endothelial niches for stem cells. *Cell* **121**, 1109-1121, doi:10.1016/j.cell.2005.05.026 (2005).
- 105 Trueta, J. & Harrison, M. H. The normal vascular anatomy of the femoral head in adult man. *J Bone Joint Surg Br* **35-B**, 442-461 (1953).
- 106 Ding, L. & Morrison, S. J. Haematopoietic stem cells and early lymphoid progenitors occupy distinct bone marrow niches. *Nature* **495**, 231-235, doi:10.1038/nature11885 (2013).
- 107 Munka, V. & Gregor, A. Lymphatics and bone marrow. *Folia Morphol (Praha)* **13**, 404-412 (1965).
- 108 Kiel, M. J., Radice, G. L. & Morrison, S. J. Lack of evidence that hematopoietic stem cells depend on N-cadherin-mediated adhesion to osteoblasts for their maintenance. *Cell Stem Cell* **1**, 204-217, doi:10.1016/j.stem.2007.06.001 (2007).
- 109 Bruns, I. *et al.* Megakaryocytes regulate hematopoietic stem cell quiescence through CXCL4 secretion. *Nat Med* **20**, 1315-1320, doi:10.1038/nm.3707 (2014).
- 110 Itkin, T. *et al.* Distinct bone marrow blood vessels differentially regulate haematopoiesis. *Nature* **532**, 323-328, doi:10.1038/nature17624 (2016).
- 111 Spencer, J. A. *et al.* Direct measurement of local oxygen concentration in the bone marrow of live animals. *Nature* **508**, 269-273, doi:10.1038/nature13034 (2014).
- 112 Ito, K. *et al.* Reactive oxygen species act through p38 MAPK to limit the lifespan of hematopoietic stem cells. *Nat Med* **12**, 446-451, doi:10.1038/nm1388 (2006).
- 113 Tesio, M. *et al.* Enhanced c-Met activity promotes G-CSF-induced mobilization of hematopoietic progenitor cells via ROS signaling. *Blood* **117**, 419-428, doi:10.1182/blood-2009-06-230359 (2011).
- 114 Li, W., Johnson, S. A., Shelley, W. C. & Yoder, M. C. Hematopoietic stem cell repopulating ability can be maintained in vitro by some primary endothelial cells. *Exp Hematol* **32**, 1226-1237, doi:10.1016/j.exphem.2004.09.001 (2004).
- 115 Butler, J. M. *et al.* Endothelial cells are essential for the self-renewal and repopulation of Notch-dependent hematopoietic stem cells. *Cell Stem Cell* **6**, 251-264, doi:10.1016/j.stem.2010.02.001 (2010).
- 116 Winkler, I. G. *et al.* Vascular niche E-selectin regulates hematopoietic stem cell dormancy, self renewal and chemoresistance. *Nat Med* **18**, 1651-1657, doi:10.1038/nm.2969 (2012).
- 117 Hooper, A. T. *et al.* Engraftment and reconstitution of hematopoiesis is dependent on VEGFR2-mediated regeneration of sinusoidal endothelial cells. *Cell Stem Cell* **4**, 263-274, doi:10.1016/j.stem.2009.01.006 (2009).
- 118 Kuznetsov, S. A. *et al.* The interplay of osteogenesis and hematopoiesis: expression of a constitutively active PTH/PTHrP receptor in osteogenic cells perturbs the establishment of hematopoiesis in bone and of skeletal stem cells in the bone marrow. *J Cell Biol* **167**, 1113-1122, doi:10.1083/jcb.200408079 (2004).
- 119 Taichman, R. S. & Emerson, S. G. Human Osteoblasts Support Hematopoiesis through the Production of Granulocyte-Colony-Stimulating Factor. *Journal of Experimental Medicine* **179**, 1677-1682, doi:DOI 10.1084/jem.179.5.1677 (1994).

- 120 Raaijmakers, M. H. *et al.* Bone progenitor dysfunction induces myelodysplasia and secondary  
leukaemia. *Nature* **464**, 852-857, doi:10.1038/nature08851 (2010).
- 121 Visnjic, D. *et al.* Hematopoiesis is severely altered in mice with an induced osteoblast  
deficiency. *Blood* **103**, 3258-3264, doi:10.1182/blood-2003-11-4011 (2004).
- 122 Lymperi, S. *et al.* Strontium can increase some osteoblasts without increasing hematopoietic  
stem cells. *Blood* **111**, 1173-1181, doi:10.1182/blood-2007-03-082800 (2008).
- 123 Zhao, M. *et al.* Megakaryocytes maintain homeostatic quiescence and promote post-injury  
regeneration of hematopoietic stem cells. *Nat Med* **20**, 1321-1326, doi:10.1038/nm.3706  
(2014).
- 124 de Graaf, C. A. *et al.* Regulation of hematopoietic stem cells by their mature progeny. *Proc  
Natl Acad Sci U S A* **107**, 21689-21694, doi:10.1073/pnas.1016166108 (2010).
- 125 Lemieux, J. M., Horowitz, M. C. & Kacena, M. A. Involvement of integrins alpha(3)beta(1) and  
alpha(5)beta(1) and glycoprotein IIb in megakaryocyte-induced osteoblast proliferation. *J Cell  
Biochem* **109**, 927-932, doi:10.1002/jcb.22468 (2010).
- 126 Winter, O. *et al.* Megakaryocytes constitute a functional component of a plasma cell niche in  
the bone marrow. *Blood* **116**, 1867-1875, doi:10.1182/blood-2009-12-259457 (2010).
- 127 Chow, A. *et al.* CD169(+) macrophages provide a niche promoting erythropoiesis under  
homeostasis and stress. *Nat Med* **19**, 429-436, doi:10.1038/nm.3057 (2013).
- 128 Yamazaki, S. *et al.* Nonmyelinating Schwann cells maintain hematopoietic stem cell  
hibernation in the bone marrow niche. *Cell* **147**, 1146-1158, doi:10.1016/j.cell.2011.09.053  
(2011).
- 129 Wolkenhauer, O., Shibata, D. K. & Mesarovic, M. D. A stem cell niche dominance theorem.  
*BMC Syst Biol* **5**, 4, doi:10.1186/1752-0509-5-4 (2011).
- 130 Wilson, A. *et al.* Hematopoietic stem cells reversibly switch from dormancy to self-renewal  
during homeostasis and repair. *Cell* **135**, 1118-1129, doi:10.1016/j.cell.2008.10.048 (2008).
- 131 Heissig, B. *et al.* Recruitment of stem and progenitor cells from the bone marrow niche  
requires MMP-9 mediated release of kit-ligand. *Cell* **109**, 625-637 (2002).
- 132 Yamashita, Y. M., Jones, D. L. & Fuller, M. T. Orientation of asymmetric stem cell division by  
the APC tumor suppressor and centrosome. *Science* **301**, 1547-1550,  
doi:10.1126/science.1087795 (2003).
- 133 Nie, Y., Han, Y. C. & Zou, Y. R. CXCR4 is required for the quiescence of primitive  
hematopoietic cells. *J Exp Med* **205**, 777-783, doi:10.1084/jem.20072513 (2008).
- 134 Zhang, Y. *et al.* CXCR4/CXCL12 axis counteracts hematopoietic stem cell exhaustion through  
selective protection against oxidative stress. *Scientific Reports* **6**, 37827,  
doi:10.1038/srep37827 (2016).
- 135 Staal, F. J. T., Luis, T. C. & Tiemessen, M. M. WNT signalling in the immune system: WNT is  
spreading its wings. *Nature Reviews Immunology* **8**, 581-593, doi:10.1038/nri2360 (2008).
- 136 Sugimura, R. *et al.* Noncanonical Wnt signaling maintains hematopoietic stem cells in the  
niche. *Cell* **150**, 351-365, doi:10.1016/j.cell.2012.05.041 (2012).
- 137 Arai, F. *et al.* Tie2/angiopoietin-1 signaling regulates hematopoietic stem cell quiescence in  
the bone marrow niche. *Cell* **118**, 149-161, doi:10.1016/j.cell.2004.07.004 (2004).
- 138 Sansilvestri, P. *et al.* Early CD34 high cells can be separated into KIThigh cells in which  
transforming growth factor-beta (TGF-beta) downmodulates c-kit and KIT low cells in which  
anti-TGF-beta upmodulates c-kit. *Blood* **86**, 1729-1735 (1995).
- 139 Larsson, J., Blank, U., Klintman, J., Magnusson, M. & Karlsson, S. Quiescence of  
hematopoietic stem cells and maintenance of the stem cell pool is not dependent on TGF-  
beta signaling in vivo. *Exp Hematol* **33**, 592-596, doi:10.1016/j.exphem.2005.02.003 (2005).
- 140 Thomas, J., Liu, F. & Link, D. C. Mechanisms of mobilization of hematopoietic progenitors  
with granulocyte colony-stimulating factor. *Curr Opin Hematol* **9**, 183-189 (2002).
- 141 Trowbridge, J. J., Scott, M. P. & Bhatia, M. Hedgehog modulates cell cycle regulators in stem  
cells to control hematopoietic regeneration. *Proc Natl Acad Sci U S A* **103**, 14134-14139,  
doi:10.1073/pnas.0604568103 (2006).

- 142 Himburg, H. A. *et al.* Pleiotrophin regulates the retention and self-renewal of hematopoietic stem cells in the bone marrow vascular niche. *Cell Rep* **2**, 964-975, doi:10.1016/j.celrep.2012.09.002 (2012).
- 143 Doan, P. L. *et al.* Tie2(+) bone marrow endothelial cells regulate hematopoietic stem cell regeneration following radiation injury. *Stem Cells* **31**, 327-337, doi:10.1002/stem.1275 (2013).
- 144 Goncalves, K. A. *et al.* Angiogenin Promotes Hematopoietic Regeneration by Dichotomously Regulating Quiescence of Stem and Progenitor Cells. *Cell* **166**, 894-906, doi:10.1016/j.cell.2016.06.042 (2016).
- 145 Cho, S. W. *et al.* Osteal macrophages support physiologic skeletal remodeling and anabolic actions of parathyroid hormone in bone. *Proc Natl Acad Sci U S A* **111**, 1545-1550, doi:10.1073/pnas.1315153111 (2014).
- 146 Itkin, T. *et al.* FGF-2 expands murine hematopoietic stem and progenitor cells via proliferation of stromal cells, c-Kit activation, and CXCL12 down-regulation. *Blood* **120**, 1843-1855, doi:10.1182/blood-2011-11-394692 (2012).
- 147 De Smet, F. *et al.* Fibroblast growth factor signaling affects vascular outgrowth and is required for the maintenance of blood vessel integrity. *Chem Biol* **21**, 1310-1317, doi:10.1016/j.chembiol.2014.07.018 (2014).
- 148 Nagai, Y. *et al.* Toll-like receptors on hematopoietic progenitor cells stimulate innate immune system replenishment. *Immunity* **24**, 801-812, doi:10.1016/j.immuni.2006.04.008 (2006).
- 149 Andonegui, G. *et al.* Mice that exclusively express TLR4 on endothelial cells can efficiently clear a lethal systemic Gram-negative bacterial infection. *Journal of Clinical Investigation* **119**, 1921-1930, doi:10.1172/Jci36411 (2009).
- 150 Mendez-Ferrer, S., Lucas, D., Battista, M. & Frenette, P. S. Haematopoietic stem cell release is regulated by circadian oscillations. *Nature* **452**, 442-447, doi:10.1038/nature06685 (2008).
- 151 Boettcher, S. *et al.* Endothelial cells translate pathogen signals into G-CSF-driven emergency granulopoiesis. *Blood* **124**, 1393-1403, doi:10.1182/blood-2014-04-570762 (2014).
- 152 Rutkowski, M. R. *et al.* Microbially Driven TLR5-Dependent Signaling Governs Distal Malignant Progression through Tumor-Promoting Inflammation. *Cancer Cell* **27**, 27-40, doi:10.1016/j.ccell.2014.11.009 (2015).
- 153 Poulos, M. G. *et al.* Endothelial Jagged-1 Is Necessary for Homeostatic and Regenerative Hematopoiesis. *Cell Reports* **4**, 1022-1034, doi:10.1016/j.celrep.2013.07.048 (2013).
- 154 Papayannopoulou, T., Priestley, G. V., Nakamoto, B., Zafiroopoulos, V. & Scott, L. M. Molecular pathways in bone marrow homing: dominant role of alpha(4)beta(1) over beta(2)-integrins and selectins. *Blood* **98**, 2403-2411 (2001).
- 155 Sipkins, D. A. *et al.* In vivo imaging of specialized bone marrow endothelial microdomains for tumour engraftment. *Nature* **435**, 969-973, doi:10.1038/nature03703 (2005).
- 156 Hur, J. *et al.* CD82/KAI1 Maintains the Dormancy of Long-Term Hematopoietic Stem Cells through Interaction with DARC-Expressing Macrophages. *Cell Stem Cell* **18**, 508-521, doi:10.1016/j.stem.2016.01.013 (2016).
- 157 Kubota, Y., Takubo, K. & Suda, T. Bone marrow long label-retaining cells reside in the sinusoidal hypoxic niche. *Biochem Biophys Res Commun* **366**, 335-339, doi:10.1016/j.bbrc.2007.11.086 (2008).
- 158 Adams, G. B. *et al.* Stem cell engraftment at the endosteal niche is specified by the calcium-sensing receptor. *Nature* **439**, 599-603, doi:10.1038/nature04247 (2006).
- 159 Saez, B. *et al.* Inhibiting stromal cell heparan sulfate synthesis improves stem cell mobilization and enables engraftment without cytotoxic conditioning. *Blood* **124**, 2937-2947, doi:10.1182/blood-2014-08-593426 (2014).
- 160 Reinholt, F. P., Hulthén, K., Oldberg, A. & Heinegård, D. Osteopontin--a possible anchor of osteoclasts to bone. *Proc Natl Acad Sci U S A* **87**, 4473-4475 (1990).
- 161 Thoren, L. A. *et al.* Kit regulates maintenance of quiescent hematopoietic stem cells. *J Immunol* **180**, 2045-2053 (2008).

- 162 Bersenev, A., Wu, C., Balcerek, J. & Tong, W. Lnk controls mouse hematopoietic stem cell self-renewal and quiescence through direct interactions with JAK2. *J Clin Invest* **118**, 2832-2844, doi:10.1172/JCI35808 (2008).
- 163 Stier, S. *et al.* Osteopontin is a hematopoietic stem cell niche component that negatively regulates stem cell pool size. *J Exp Med* **201**, 1781-1791, doi:10.1084/jem.20041992 (2005).
- 164 Nilsson, S. K. *et al.* Osteopontin, a key component of the hematopoietic stem cell niche and regulator of primitive hematopoietic progenitor cells. *Blood* **106**, 1232-1239, doi:10.1182/blood-2004-11-4422 (2005).
- 165 Colmone, A. *et al.* Leukemic cells create bone marrow niches that disrupt the behavior of normal hematopoietic progenitor cells. *Science* **322**, 1861-1865, doi:10.1126/science.1164390 (2008).
- 166 Schepers, K. *et al.* Myeloproliferative neoplasia remodels the endosteal bone marrow niche into a self-reinforcing leukemic niche. *Cell Stem Cell* **13**, 285-299, doi:10.1016/j.stem.2013.06.009 (2013).
- 167 Uy, G. L. *et al.* Targeting bone marrow lymphoid niches in acute lymphoblastic leukemia. *Leuk Res* **39**, 1437-1442, doi:10.1016/j.leukres.2015.09.020 (2015).
- 168 Collins, R. J. *et al.* Spontaneous programmed death (apoptosis) of B-chronic lymphocytic leukaemia cells following their culture in vitro. *British Journal of Haematology* **71**, 343-350, doi:10.1111/j.1365-2141.1989.tb04290.x (2008).
- 169 Abe-Suzuki, S. *et al.* CXCL12+ stromal cells as bone marrow niche for CD34+ hematopoietic cells and their association with disease progression in myelodysplastic syndromes. *Lab Invest* **94**, 1212-1223, doi:10.1038/labinvest.2014.110 (2014).
- 170 Zhang, B. *et al.* Altered microenvironmental regulation of leukemic and normal stem cells in chronic myelogenous leukemia. *Cancer Cell* **21**, 577-592, doi:10.1016/j.ccr.2012.02.018 (2012).
- 171 Boyerinas, B. *et al.* Adhesion to osteopontin in the bone marrow niche regulates lymphoblastic leukemia cell dormancy. *Blood* **121**, 4821-4831, doi:10.1182/blood-2012-12-475483 (2013).
- 172 Brachtl, G. *et al.* Differential bone marrow homing capacity of VLA-4 and CD38 high expressing chronic lymphocytic leukemia cells. *PLoS One* **6**, e23758, doi:10.1371/journal.pone.0023758 (2011).
- 173 Zhang, S. *et al.* Targeting chronic lymphocytic leukemia cells with a humanized monoclonal antibody specific for CD44. *Proc Natl Acad Sci U S A* **110**, 6127-6132, doi:10.1073/pnas.1221841110 (2013).
- 174 Chagraoui, H. *et al.* Prominent role of TGF-beta 1 in thrombopoietin-induced myelofibrosis in mice. *Blood* **100**, 3495-3503, doi:10.1182/blood-2002-04-1133 (2002).
- 175 Malaponte, G. *et al.* Tumor microenvironment in diffuse large B-cell lymphoma: Matrixmetalloproteinases activation is mediated by osteopontin overexpression. *Biochim Biophys Acta* **1863**, 483-489, doi:10.1016/j.bbamcr.2015.09.018 (2016).
- 176 Pamuk, G. E., Uyanik, M. S., Pamuk, O. N., Maden, M. & Tapan, U. Decreased dickkopf-1 levels in chronic lymphocytic leukemia and increased osteopontin levels in non-Hodgkin's lymphoma at initial diagnosis: Could they be playing roles in pathogenesis? *Hematology* **20**, 267-271, doi:10.1179/1607845414Y.0000000205 (2015).
- 177 Arnulf, B. *et al.* Phenotypic and functional characterization of bone marrow mesenchymal stem cells derived from patients with multiple myeloma. *Leukemia* **21**, 158-163, doi:10.1038/sj.leu.2404466 (2007).
- 178 Chen, Z., Orlowski, R. Z., Wang, M., Kwak, L. & McCarty, N. Osteoblastic niche supports the growth of quiescent multiple myeloma cells. *Blood* **123**, 2204-2208, doi:10.1182/blood-2013-07-517136 (2014).
- 179 Sethi, N., Dai, X., Winter, C. G. & Kang, Y. Tumor-derived JAGGED1 promotes osteolytic bone metastasis of breast cancer by engaging notch signaling in bone cells. *Cancer Cell* **19**, 192-205, doi:10.1016/j.ccr.2010.12.022 (2011).

- 180 Shiozawa, Y. *et al.* Human prostate cancer metastases target the hematopoietic stem cell niche to establish footholds in mouse bone marrow. *J Clin Invest* **121**, 1298-1312, doi:10.1172/JCI43414 (2011).
- 181 O'Donnell, R. K. *et al.* VEGF-A/VEGFR Inhibition Restores Hematopoietic Homeostasis in the Bone Marrow and Attenuates Tumor Growth. *Cancer Res* **76**, 517-524, doi:10.1158/0008-5472.CAN-14-3023 (2016).
- 182 Wu, W. C. *et al.* Circulating hematopoietic stem and progenitor cells are myeloid-biased in cancer patients. *Proc Natl Acad Sci U S A* **111**, 4221-4226, doi:10.1073/pnas.1320753111 (2014).
- 183 Thoms, J. W. *et al.* Plasma osteopontin as a biomarker of prostate cancer aggression: relationship to risk category and treatment response. *Brit J Cancer* **107**, 840-846, doi:10.1038/bjc.2012.345 (2012).
- 184 Fremder, E. *et al.* Tumor-derived microparticles induce bone marrow-derived cell mobilization and tumor homing: a process regulated by osteopontin. *Int J Cancer* **135**, 270-281, doi:10.1002/ijc.28678 (2014).
- 185 Lund, S. A. *et al.* Osteopontin mediates macrophage chemotaxis via alpha4 and alpha9 integrins and survival via the alpha4 integrin. *J Cell Biochem* **114**, 1194-1202, doi:10.1002/jcb.24462 (2013).
- 186 Prince, C. W. *et al.* Isolation, characterization, and biosynthesis of a phosphorylated glycoprotein from rat bone. *J Biol Chem* **262**, 2900-2907 (1987).
- 187 Oldberg, A., Franzen, A. & Heinegard, D. Cloning and sequence analysis of rat bone sialoprotein (osteopontin) cDNA reveals an Arg-Gly-Asp cell-binding sequence. *Proc Natl Acad Sci U S A* **83**, 8819-8823 (1986).
- 188 Giachelli, C. M., Lombardi, D., Johnson, R. J., Murry, C. E. & Almeida, M. Evidence for a role of osteopontin in macrophage infiltration in response to pathological stimuli in vivo. *Am J Pathol* **152**, 353-358 (1998).
- 189 Young, M. F. *et al.* cDNA cloning, mRNA distribution and heterogeneity, chromosomal location, and RFLP analysis of human osteopontin (OPN). *Genomics* **7**, 491-502 (1990).
- 190 Sodek, J., Ganss, B. & McKee. Osteopontin. *Critical reviews in oral biology and medicine : an official publication of the American Association of Oral Biologists* **11**, 279-303 (2000).
- 191 Agnihotri, R. *et al.* Osteopontin, a novel substrate for matrix metalloproteinase-3 (stromelysin-1) and matrix metalloproteinase-7 (matrilysin). *J Biol Chem* **276**, 28261-28267, doi:10.1074/jbc.M103608200 (2001).
- 192 Kazaneki, C. C., Uzwiak, D. J. & Denhardt, D. T. Control of osteopontin signaling and function by post-translational phosphorylation and protein folding. *Journal of Cellular Biochemistry* **102**, 912-924, doi:10.1002/jcb.21558 (2007).
- 193 Christensen, B., Petersen, T. E. & Sorensen, E. S. Post-translational modification and proteolytic processing of urinary osteopontin. *Biochem J* **411**, 53-61, doi:10.1042/BJ20071021 (2008).
- 194 Singh, K., DeVouge, M. W. & Mukherjee, B. B. Physiological properties and differential glycosylation of phosphorylated and nonphosphorylated forms of osteopontin secreted by normal rat kidney cells. *J Biol Chem* **265**, 18696-18701 (1990).
- 195 Nagata. Sulphation of secreted phosphoprotein I (SPPI, osteopontin) is associated with mineralized tissue formation. *Biochem Biophys Res Commun* (1989).
- 196 Sorensen, E. S., Hojrup, P. & Petersen, T. E. Posttranslational modifications of bovine osteopontin: identification of twenty-eight phosphorylation and three O-glycosylation sites. *Protein Sci* **4**, 2040-2049, doi:10.1002/pro.5560041009 (1995).
- 197 Beninati, S. *et al.* Osteopontin: its transglutaminase-catalyzed posttranslational modifications and cross-linking to fibronectin. *J Biochem* **115**, 675-682 (1994).
- 198 Kaartinen, M. T., Pirhonen, A., Linnala-Kankkunen, A. & Maenpaa, P. H. Cross-linking of osteopontin by tissue transglutaminase increases its collagen binding properties. *J Biol Chem* **274**, 1729-1735 (1999).

- 199 Gericke, A. *et al.* Importance of phosphorylation for osteopontin regulation of  
biomineralization. *Calcif Tissue Int* **77**, 45-54, doi:10.1007/s00223-004-1288-1 (2005).
- 200 Zohar, R., Cheifetz, S., McCulloch, C. A. G. & Sodek, J. Analysis of intracellular osteopontin as  
a marker of osteoblastic cell differentiation and mesenchymal cell migration. *Eur J Oral Sci*  
**106**, 401-407 (1998).
- 201 McKee, M. D. & Nanci, A. Postembedding colloidal-gold immunocytochemistry of  
noncollagenous extracellular matrix proteins in mineralized tissues. *Microsc Res Tech* **31**, 44-  
62, doi:10.1002/jemt.1070310105 (1995).
- 202 Dodds, R. A. *et al.* Human osteoclasts, not osteoblasts, deposit osteopontin onto resorption  
surfaces: an in vitro and ex vivo study of remodeling bone. *J Bone Miner Res* **10**, 1666-1680,  
doi:10.1002/jbmr.5650101109 (1995).
- 203 Keykhosravani, M. *et al.* Comprehensive identification of post-translational modifications of  
rat bone osteopontin by mass spectrometry. *Biochemistry* **44**, 6990-7003,  
doi:10.1021/bi050109p (2005).
- 204 Giachelli, C. M., Liaw, L., Murry, C. E., Schwartz, S. M. & Almeida, M. Osteopontin expression  
in cardiovascular diseases. *Ann N Y Acad Sci* **760**, 109-126 (1995).
- 205 Bautista, D. S. *et al.* Quantification of osteopontin in human plasma with an ELISA: basal  
levels in pre- and postmenopausal women. *Clin Biochem* **29**, 231-239 (1996).
- 206 Wai, P. Y. & Kuo, P. C. The role of Osteopontin in tumor metastasis. *J Surg Res* **121**, 228-241,  
doi:10.1016/j.jss.2004.03.028 (2004).
- 207 Giachelli, C. M. *et al.* Osteopontin is elevated during neointima formation in rat arteries and  
is a novel component of human atherosclerotic plaques. *J Clin Invest* **92**, 1686-1696,  
doi:10.1172/JCI116755 (1993).
- 208 Panda, D. *et al.* Potential roles of osteopontin and  $\alpha V\beta 3$  integrin in the development of  
coronary artery restenosis after angioplasty. *Proc Natl Acad Sci USA* **94**, 9308-9313. (1997).
- 209 Krishnamurthy, P., Peterson, J. T., Subramanian, V., Singh, M. & Singh, K. Inhibition of matrix  
metalloproteinases improves left ventricular function in mice lacking osteopontin after  
myocardial infarction. *Mol Cell Biochem* **322**, 53-62, doi:10.1007/s11010-008-9939-6 (2009).
- 210 McKee, M. D., Nanci, A. & Khan, S. R. Ultrastructural immunodetection of osteopontin and  
osteocalcin as major matrix components of renal calculi. *J Bone Miner Res* **10**, 1913-1929,  
doi:10.1002/jbmr.5650101211 (1995).
- 211 Chambers, A. F. *et al.* Osteopontin expression in lung cancer. *Lung Cancer* **15**, 311-323  
(1996).
- 212 Boskey, A. L. *et al.* Osteopontin-hydroxyapatite interactions in vitro: inhibition of  
hydroxyapatite formation and growth in a gelatin-gel. *Bone Miner* **22**, 147-159 (1993).
- 213 Steitz, S. A. *et al.* Osteopontin Inhibits Mineral Deposition and Promotes Regression of  
Ectopic Calcification. *The American Journal of Pathology* **161**, 2035-2046, doi:10.1016/s0002-  
9440(10)64482-3 (2002).
- 214 Goldberg, H. A., Warner, K. J., Li, M. C. & Hunter, G. K. Binding of bone sialoprotein,  
osteopontin and synthetic polypeptides to hydroxyapatite. *Connect Tissue Res* **42**, 25-37  
(2001).
- 215 McKee, M. D. & Nanci, A. Secretion of osteopontin by macrophages and its accumulation at  
tissue surfaces during wound healing in mineralized tissues: A potential requirement for  
macrophage adhesion and phagocytosis. *Anat Record* **245**, 394-409, doi:Doi  
10.1002/(Sici)1097-0185(199606)245:2<394::Aid-Ar19>3.0.Co;2-K (1996).
- 216 Ross, F. P. *et al.* Interactions between the Bone-Matrix Proteins Osteopontin and Bone  
Sialoprotein and the Osteoclast Integrin Alpha-V-Beta-3 Potentiate Bone-Resorption. *Journal*  
*of Biological Chemistry* **268**, 9901-9907 (1993).
- 217 Liaw, L. *et al.* The adhesive and migratory effects of osteopontin are mediated via distinct cell  
surface integrins. Role of alpha v beta 3 in smooth muscle cell migration to osteopontin in  
vitro. *J Clin Invest* **95**, 713-724, doi:10.1172/JCI117718 (1995).

- 218 Nishimichi, N. *et al.* Osteopontin undergoes polymerization in vivo and gains chemotactic activity for neutrophils mediated by integrin alpha9beta1. *J Biol Chem* **286**, 11170-11178, doi:10.1074/jbc.M110.189258 (2011).
- 219 Denda, S., Reichardt, L. F. & Muller, U. Identification of osteopontin as a novel ligand for the integrin alpha8 beta1 and potential roles for this integrin-ligand interaction in kidney morphogenesis. *Mol Biol Cell* **9**, 1425-1435 (1998).
- 220 Zhang, X. F., Liu, S., Zhou, Y. J., Zhu, G. F. & Foda, H. D. Osteopontin protects against hyperoxia-induced lung injury by inhibiting nitric oxide synthases. *Chin Med J (Engl)* **123**, 929-935 (2010).
- 221 Weber, G. F., Ashkar, S., Glimcher, M. J. & Cantor, H. Receptor-ligand interaction between CD44 and osteopontin (Eta-1). *Science* **271**, 509-512, doi:DOI 10.1126/science.271.5248.509 (1996).
- 222 Crawford, H. C., Matrisian, L. M. & Liaw, L. Distinct roles of osteopontin in host defense activity and tumor survival during squamous cell carcinoma progression in vivo. *Cancer Res* **58**, 5206-5215 (1998).
- 223 Guidi, N. *et al.* Osteopontin attenuates aging-associated phenotypes of hematopoietic stem cells. *The EMBO Journal*, doi:10.15252/embj.201694969 (2017).
- 224 Qiagen. *RNeasy Mini Handbook*, <<https://www.qiagen.com/us/resources/resourcedetail?id=14e7cf6e-521a-4cf7-8cbc-bf9f6fa33e24&lang=en>> (2017).
- 225 Percell\_Biolytica\_AB. [http://www.percell.se/inst\\_g.pdf](http://www.percell.se/inst_g.pdf).
- 226 Sigma-Aldrich. *Cellstain double staining kit*, <<http://www.sigmaaldrich.com/content/dam/sigma-aldrich/docs/Sigma/Datasheet/10/04511dat.pdf>> (2014).
- 227 invitrogen. *Quant-iT PicoGreen dsDNA Reagent and Kits*, <<https://tools.thermofisher.com/content/sfs/manuals/mp07581.pdf>> (2008).
- 228 Kleinhans, C. *et al.* A perfusion bioreactor system efficiently generates cell-loaded bone substitute materials for addressing critical size bone defects. *Biotechnol J* **10**, 1727-1738, doi:10.1002/biot.201400813 (2015).
- 229 Molecular\_Probes. *LIVE/DEAD Viability/Cytotoxicity Kit \*for mammalian cells\**, <<https://tools.thermofisher.com/content/sfs/manuals/mp03224.pdf>> (2005).
- 230 Miltenyi\_Biotec. *CD34 MicroBead Kit UltraPure*, (2014).
- 231 Phillips, R. J., Helbig, K. J., Van der Hoek, K. H., Seth, D. & Beard, M. R. Osteopontin increases hepatocellular carcinoma cell growth in a CD44 dependant manner. *World J Gastroenterol* **18**, 3389-3399, doi:10.3748/wjg.v18.i26.3389 (2012).
- 232 Takafuji, V., Forgues, M., Unsworth, E., Goldsmith, P. & Wang, X. W. An osteopontin fragment is essential for tumor cell invasion in hepatocellular carcinoma. *Oncogene* **26**, 6361-6371, doi:10.1038/sj.onc.1210463 (2007).
- 233 Roche. *FuGENE HD Transfection Reagent*, <[https://roche-biochem.jp/pdf/prima/transfection/fugenehd\\_appnote4.pdf](https://roche-biochem.jp/pdf/prima/transfection/fugenehd_appnote4.pdf)> (2006).
- 234 Tuin, A., Kluijtmans, S. G., Bouwstra, J. B., Harmsen, M. C. & Van Luyn, M. J. Recombinant gelatin microspheres: novel formulations for tissue repair? *Tissue Eng Part A* **16**, 1811-1821, doi:10.1089/ten.TEA.2009.0592 (2010).
- 235 Nöth, U. *et al.* Chondrogenic differentiation of human mesenchymal stem cells in collagen type I hydrogels. *Journal of Biomedical Materials Research Part A* **83A**, 626-635, doi:10.1002/jbm.a.31254 (2007).
- 236 Harichandan, A. & Buhring, H. J. Prospective isolation of human MSC. *Best Pract Res Clin Haematol* **24**, 25-36, doi:10.1016/j.beha.2011.01.001 (2011).
- 237 Jeon, Y. J., Kim, J., Cho, J. H., Chung, H. M. & Chae, J. I. Comparative Analysis of Human Mesenchymal Stem Cells Derived From Bone Marrow, Placenta, and Adipose Tissue as Sources of Cell Therapy. *J Cell Biochem* **117**, 1112-1125, doi:10.1002/jcb.25395 (2016).

- 238 Brundin, M., Figdor, D., Sundqvist, G. & Sjogren, U. DNA binding to hydroxyapatite: a potential mechanism for preservation of microbial DNA. *J Endod* **39**, 211-216, doi:10.1016/j.joen.2012.09.013 (2013).
- 239 Malhotra, A., Pelletier, M., Oliver, R., Christou, C. & Walsh, W. R. Platelet-rich plasma and bone defect healing. *Tissue Eng Part A* **20**, 2614-2633, doi:10.1089/ten.TEA.2013.0737 (2014).
- 240 Ben Azouna, N. *et al.* Phenotypical and functional characteristics of mesenchymal stem cells from bone marrow: comparison of culture using different media supplemented with human platelet lysate or fetal bovine serum. *Stem Cell Res Ther* **3**, 6, doi:10.1186/scrt97 (2012).
- 241 Santo, V. E. *et al.* Enhancement of osteogenic differentiation of human adipose derived stem cells by the controlled release of platelet lysates from hybrid scaffolds produced by supercritical fluid foaming. *Journal of controlled release : official journal of the Controlled Release Society* **162**, 19-27, doi:10.1016/j.jconrel.2012.06.001 (2012).
- 242 Tebb, T. A. *et al.* Development of porous collagen beads for chondrocyte culture. *Cytotechnology* **52**, 99-106, doi:10.1007/s10616-006-9034-3 (2006).
- 243 Lu, J. X. *et al.* Role of interconnections in porous bioceramics on bone recolonization in vitro and in vivo. *J Mater Sci Mater Med* **10**, 111-120 (1999).
- 244 Mirzadeh, H., Shokrolahi, F. & Daliri, M. Effect of silicon rubber crosslink density on fibroblast cell behavior in vitro. *J Biomed Mater Res A* **67**, 727-732, doi:10.1002/jbm.a.10107 (2003).
- 245 Drexler, J. W. & Powell, H. M. Dehydrothermal crosslinking of electrospun collagen. *Tissue Eng Part C Methods* **17**, 9-17, doi:10.1089/ten.TEC.2009.0754 (2011).
- 246 Pieper, J. S., Oosterhof, A., Dijkstra, P. J., Veerkamp, J. H. & van Kuppevelt, T. H. Preparation and characterization of porous crosslinked collagenous matrices containing bioavailable chondroitin sulphate. *Biomaterials* **20**, 847-858 (1999).
- 247 Perez, R. A. & Mestres, G. Role of pore size and morphology in musculo-skeletal tissue regeneration. *Mater Sci Eng C Mater Biol Appl* **61**, 922-939, doi:10.1016/j.msec.2015.12.087 (2016).
- 248 Kempainen, J. M. & Hollister, S. J. Differential effects of designed scaffold permeability on chondrogenesis by chondrocytes and bone marrow stromal cells. *Biomaterials* **31**, 279-287, doi:10.1016/j.biomaterials.2009.09.041 (2010).
- 249 Rothdiener, M. *et al.* Stretching human mesenchymal stromal cells on stiffness-customized collagen type I generates a smooth muscle marker profile without growth factor addition. *Sci Rep* **6**, 35840, doi:10.1038/srep35840 (2016).
- 250 Walters, B. D. & Stegemann, J. P. Strategies for directing the structure and function of three-dimensional collagen biomaterials across length scales. *Acta biomaterialia* **10**, 1488-1501, doi:10.1016/j.actbio.2013.08.038 (2014).
- 251 Hennessy, K. M. *et al.* The effect of RGD peptides on osseointegration of hydroxyapatite biomaterials. *Biomaterials* **29**, 3075-3083, doi:10.1016/j.biomaterials.2008.04.014 (2008).
- 252 Ma, S. *et al.* Effects of Dissolved Calcium and Phosphorous on Osteoblast Responses. *Journal of Oral Implantology* **31**, 61-67, doi:10.1563/0-742.1 (2005).
- 253 Lai, W. Y. *et al.* Reconstitution of bone-like matrix in osteogenically differentiated mesenchymal stem cell–collagen constructs: A three-dimensional in vitro model to study hematopoietic stem cell niche. *Journal of Tissue Engineering* **4**, doi:10.1177/2041731413508668 (2013).
- 254 Dotterweich, J. *et al.* Mesenchymal stem cell contact promotes CCN1 splicing and transcription in myeloma cells. *Cell Commun Signal* **12**, 36, doi:10.1186/1478-811X-12-36 (2014).
- 255 Kon, S. *et al.* Mapping of functional epitopes of osteopontin by monoclonal antibodies raised against defined internal sequences. *Journal of Cellular Biochemistry* **84**, 420-432, doi:10.1002/jcb.10039 (2002).
- 256 Grassinger, J. *et al.* Thrombin-cleaved osteopontin regulates hemopoietic stem and progenitor cell functions through interactions with alpha9beta1 and alpha4beta1 integrins. *Blood* **114**, 49-59, doi:10.1182/blood-2009-01-197988 (2009).



- 257 Caers, J. *et al.* The involvement of osteopontin and its receptors in multiple myeloma cell survival, migration and invasion in the murine 5T33MM model. *Br J Haematol* **132**, 469-477, doi:10.1111/j.1365-2141.2005.05886.x (2006).

## 7 APPENDIX



## 1. Materials

- Protective Goggles
- Volumetric Flask (1L) with Plug
- Magnetic Stirring Bar, Magnetic Stirring Bar Retriever
- Scale Pan
- Spatula
- Powder Funnel
- Sterile Petri Dishes
- 2 Sterile 500 mL Bottles

## 2. Equipment

- Safety Cabinet
- pH- Meter
- Magnetic Stirrer
- Scales

## 3. Solutions

- Ultrapure Water (Ger., „Reinstwasser“)
- NaOH 1 M
- HCl 1 M

## 4. Chemicals

- 10 g Casein Tryptone (Roth, order number 8952.4 )
- 5 g Yeast Extract (Roth, order number 2363.2)
- 10 g NaCl
- 7,5 g Agar (Roth, order number 5210.2)

## 5. Protocol

- Fill 500 mL ultrapure water into volumetric flask, add magnetic stirring bar and place the flask onto the magnetic stirrer.
- Add weighed chemicals one by one to the flask via powder funnel. Let it stir until all chemicals are dissolved.
- Set pH-value to 7,5
- Fill up to 1L with ultrapure water
- Split the resulting LB-medium into two 500mL bottles
- Add 3,75 g agar to each bottle (dissolves while being autoclaved)
- Autoclave the bottles immediately (please arrange this with Moni beforehand)
- Let LB medium with agar cool off to about 80 °C. NOTE: It needs to remain liquid and without lumps for the next steps!
- If agar plates should contain antibiotic, add 500 µL antibiotic per 500 mL agar under the safety cabinet
- Fill petri dishes with LB agar under the safety cabinet
- Place lit onto dish (tilted) and let agar dry
- Package petri dishes sterile
- Label petri dishes with „LB-Agar“ / (antibiotic) / date / your name abbreviation



**1. Materialien**

- Färbeküvetten
- Trägerkorb
- Metallhenkel
- Trichter
- Faltenfilter
- Deckgläser
- Pinzette

**2. Geräte**

- Abzug
- Wärmeschrank (60°C)

**3. Lösungen**

- VE-Wasser

**4. Chemikalien**

- Aluminiumsulfat
- Alcianblau 8GX (Sigma, A3157-10G)
- Essigsäure 100%
- EtOH (96%, 70%, 50%)
- 2-Propanol = Isopropanol
- Kernechtrot (Merck, 1.15939.0025)
- Xylol

**5. Durchführung**

Herstellung der Lösungen:

- Kernechtrot: 5 g Aluminiumsulfat in 100 ml VE-Wasser lösen, erhitzen bis zum Kochen, 0,1 g Kernechtrot zugeben und nach dem Abkühlen filtrieren.
- 1% Alcianblau: 1 g Alcianblau 8GX in 100 ml VE-Wasser lösen
- 3% Essigsäure: 3 ml 100% Essigsäure mit 97 ml VE-Wasser verdünnen

Ablauf der Alcianblau-Färbung:

- Paraffinschnitte in Trägerkorb mit Metallhenkel einordnen und für 1 h in den Wärmeschrank stellen (Paraffin muss vollständig geschmolzen sein!)
  - direkt in Xylol I überführen
- Beachten: Ab hier darf der Schnitt nicht mehr trockenfallen!

Zeitablauf [min]	Lösung	Ziel/Bemerkung
10	Xylol I	absteigende Reihe: Entparaffinieren, Rehydrieren
10	Xylol II	
3 x auf- und abtauchen	96% EtOH I	
3 x auf- und abtauchen	96% EtOH II	
3 x auf- und abtauchen	70% EtOH	
3 x auf- und abtauchen	50% EtOH	
	VE-Wasser	Schwenken, bis keine Turbulenzen mehr
3	3 % Essigsäure	

Zeitablauf [min]	Lösung	Ziel/Bemerkung
30	1% Alcianblau 8GX	Anfärben der negativ geladenen sulfatierten Proteoglykane
	VE-Wasser	spülen
5	Kernechtrot	Anfärben der Zellkerne
	VE-Wasser	spülen
2x kurz eintauchen	70% EtOH	Differenzieren
2	96% EtOH	aufsteigende Reihe: Entwässern
5	2-Propanol I	
5	2-Propanol II	
5	Xylol I	
5	Xylol II	

**Beachten: Alle Lösungen werden bei Bedarf, wenn z.B. starke Verunreinigungen erkennbar sind, in die halogenfreien organischen Lösemittelabfälle entsorgt!**

**Falls nach dem Entparaffinieren die Objektträger weiße Ablagerungen haben, dann die Alkoholreihe wieder bis ins Xylol zurückgehen und alle Alkohole und Xylol erneuern. Danach nochmals 10 min in Xylol bleiben und dann nochmal die absteigende Alkoholreihe wiederholen.**

- Objektträger mit Hilfe einer Pinzette aus dem Xylol entnehmen
- mit Entellan und einem Deckglas luftblasenfrei eindecken
- über Nacht unter dem Abzug trocknen lassen, dabei darauf achten, dass die Objektträger waagrecht positioniert werden, um ein Verrutschen der Deckgläser zu verhindern.

### 6. Ergebnis

- Die Zellkerne sind rot, die Extrazellulärmatrix des Knorpelgewebes (negativ geladene sulfatierte Proteoglykane) blau angefärbt.

## 1. Materials

- Coverslides
- Pasteur pipette
- Pipetter
- 15ml centrifuge tubes

## 2. Equipment

- Chemical Hood

## 3. Chemicals and solutions

- PBS<sup>-</sup>
- Deionized Water (dH<sub>2</sub>O)
- Methanol
- Alizarin Red S (Sigma, A5533-25G)
- 25% Ammonia (NaOH) (Roth, Order N.5460.1)
- Aquatex mounting glue or Entellan
- NaOH 25%
- HCl 1M

## 4. Protocol

Preparation of the staining solution:

**Stock solution:** Solve 0,25g Alizarin Red S in 25ml dH<sub>2</sub>O

**Working solution:** Set the pH of the solution to 4.1-4.3 with NaOH or HCl.

Expiration of Alizarin Red S staining:

**Attention: All solutions must be discarded in the organic waste**

Time (min)	Solution	Process/ Marking
Wash 1x	PBS <sup>-</sup>	
10	Methanol (Ice cold)	Fixation
Wash 1x	dH <sub>2</sub> O	
2	Alizarin Red S	Staining of the Calcium-hydrogen phosphate
Wash 3x	dH <sub>2</sub> O	

- Transfer glass slides in dH<sub>2</sub>O
- Add Aquatex glue or Entellan and cover with coverslide ( Pay attention not to include air bubbles)
- Let it dry under the chemical hood, making sure that the glass slides are in the horizontal position in order to prevent slipping of the coverslides

## 5. Annotations

- Calcium hydrogen phosphate is stained in Red (Osteogenic Differentiation)
- The pH of the staining solution is critical for the staining. Higher pH will give purple stainings instead of bright red
- Organic material may uptake the staining but will not stain bright red.

**1. Materialien      Achtung: immer Handschuhe verwenden, sauber arbeiten!**

- Styroporbehälter mit Eis
- Filterspitzen für RNA
- Kleine Reaktionsgefäße (0,2 ml)
- Ständer für RNA

**2. Geräte**

- Pipetten für RNA
- Thermocycler
- Tischzentrifuge
- Mini-Tubes Zentrifuge Vortex

**3. Lösungen/Reagenzien**

- RNA zur Transkription (0,5 – 1µg)
- RNase-freies Wasser
- iScript cDNA-Synthese-Kit (BioRad): enthält Reaktions-Mix, RNase-freies Wasser und reverse Transkriptase

**ACHTUNG**

- **Mit Handschuhen arbeiten, Reagenzien und Gebrauchsmaterial nicht ohne Handschuhe anfassen!!!**
- **Reverse Transkriptase erst kurz vor Gebrauch aus dem Kühlblock entnehmen!!!**
- **Eine Negativkontrolle (statt RNA nimmt man Wasser) mitmachen**

**4. Durchführung**

- Benötigte Reagenzien auf Eis auftauen lassen und auf Eis pipettieren
- **Am RNA Arbeitsplatz** die RNA mit RNase-freiem Wasser so verdünnen, dass **0,5 - 1 µg** (möglichst einheitlich für alle Proben) **in 15 µl** erreicht werden
- Zu den 15 µl je Probe **einen Mastermix aus je 4 µl „iScript Reaction Mix“ und je 1 µl „iScript reverse Transcriptase“ pipettieren** (Endvolumen je Probe 20 µl)

**Reverse Transkriptase erst kurz vor dem Pipettieren hinzugeben! Auf Eis arbeiten!**

-	<b>Übersicht:</b>		
-	<b>5x iScript Reaction Mix</b>	<b>4µl</b>	<b>im Mastermix</b>
-	<b>iScript Reverse Transcriptase</b>	<b>1µl</b>	<b>im Mastermix</b>
-	Nuclease-free water	xµl	
-	RNA template	xµl	
-	Total Volume	20 µl	

Gesamtansatz danach im Thermocycler wie folgt behandeln (Protokoll evtl. schon gespeichert):

5 min bei 25°C  
30 min bei 42°C  
5 min bei 85°C  
4°C (optional)

cDNA danach kurz abzentrifugieren und entweder weiter bearbeiten/verdünnen (siehe Protokoll qRT-PCR) oder (optional auch verdünnt) bei **- 20 °C** wegfrieren

**cDNA nach Möglichkeit nicht länger als 2 Wochen bei 20°C lagern!!! (Ansonsten: Kontrolle mit Housekeeping-Gen. Bei -80°C kann sie auch länger gelagert werden.)**

## 5. Bemerkungen

- Zu Beginn: Arbeitsfläche mit **RNase Exitus Plus** reinigen (kein Waschethanol verwenden, ist nicht RNase-frei)
- Beim Ansatz des Mastermixes werden bei bis zu 20 Proben **mindestens 1 Ansatz**, bei bis zu 30 Proben **mindestens 2 Ansätze**, usw. **dazugerechnet**.
- Allgemein ist eine **strenge Trennung** der beiden Arbeitsplätze für **RNA** und **DNA**, sowie von **Gebrauchsmaterial** (wie Filterspitzen, Reaktionsgefäße usw.) aber auch **Geräten** (wie Pipettierhilfe, Zentrifuge, Schüttler usw.) entscheidend für den Erfolg der PCR!!!
-



## 1. Materials

- 10 cm cell culture dish or crowns for static culture
- Sterile pipettes and Pasteur pipettes
- 1.5 ml reaction vessels
- Pipette tips
- Sterile cell scraper
- 96-well plate and possibly 12well

## 2. Equipment

- Safety Cabinet
- Pipetboy
- Eppendorf pipettes
- Rocking platform
- Eppendorf tubes
- Refrigerated Centrifuge
- If necessary, scalpel holder and scalpel
- TECAN Infinite M200 photometer, Program I-control
- rocking platform
- Tissue mixer
- Glass homogenizer

## 3. Chemicals and Solutions

- PBS<sup>-</sup> (Sigma, D8537-500ml)
- Lysis buffer (see SOP production of lysis buffer)
- BSA stock solution 2mg / ml (Sigma, P083410x1ml)
- Ultrapure water
- DC protein assay kit (Bio-Rad, 500-0112)

## 4. Protocol

### Lysis of cells in 2D culture

- Cultivate cells in 10 cm culture dishes
- Wash cells 2x with cold PBS<sup>-</sup>
- add lysis buffer: 1 mL per 100% confluence in 10 cm culture dish (eg 70% confluence → 700µL lysis buffer)
- Incubate for 30 min at 4 ° C on the rocking platform
- Scrape cells with cell scraper and transfer to an Eppendorf tube
- Centrifugate at 10.000xg 15 min at 4 ° C to pellet cell debris
- Transfer supernatant into a fresh Eppendorf tube and stored at -80 ° C

### Lysis of cells from static 3D culture

- wash membrane in the crown 2x with cold PBS<sup>-</sup>
- remove membrane, cut off cell-free edges
- Cover membrane in a 12well plate with lysis buffer (500 - 1000µL depending on cell count)
- Incubate for 30 min at 4 ° C on the rocking platform

Page 2 of 2

- Scrape cells off the membrane with a cell scraper
- transfer lysis buffer to an Eppendorf tube
- pellet cell- and matrix debris by centrifugation: 10.000xg 15 min at 4 ° C
- Transfer supernatant (=lysate) into a fresh Eppendorf tube and store at -80 ° C
- Membranes can be stained at the end of the cell harvest to control complete harvest.

#### **Lysis of tissue**

- Weigh tissue in Eppendorf tube
- Add 50- 100 µl lysis buffer per mg of tissue (see SOP production of lysis buffer)
- homogenize tissue homogenization (glas homogenizer, tissue-ruptor or tissue-lyser)
- Incubate for 30 min at 4 ° C on the rocking platform
- pellet cell- and matrix debris by centrifugation: 10.000xg 15 min at 4 ° C
- Transfer supernatant to perform protein concentration determination or store at -80 ° C

#### **Protein concentration determination using the DC Protein Assay**

- prepare BSA standards: Use the following pipetting scheme for a stock solution of 2 mg / mL

Standard	BSA Conc. µg/mL	Volume BSA/µl	Volume DI water /µl
1	1000	500 ( from stock solution)	500
2	800	80 (from 1)	20
3	600	60 (from 1)	40
4	400	40 (from 1)	60
5	200	20 (from 1)	80
6	100	10 (from 1)	90
7	50	50 (from 6)	50

- Pipet 5µl of the standards 1 to 7 (and ultrapure water as blank) in duplicates in a 96 well plate
- Pipet 5µl of each sample (and the lysis buffer as blank) in duplicates in the plate
- prepare the alkaline copper solution with reagent A and reagent S 50:1
- Add 25 µl / well of this copper solution
- Add 200 µl / well of Folinlösung (= reagent B)
- Incubate for 15 min at RT in the dark
- Measure the optical density at 750 nm (bandwidth 9 nm, 25 flashes)

#### **5. Notes**

- Perform cell lysis on ice or at 4 ° C, as proteinases and phosphatases are less active.
- Proteins can be diluted with ultrapure water or lysis buffer; it's not necessary to use RNase-free water or autoclaved Eppendorf tubes
- When determining the protein concentration of the lysate, the values measured must lie within the range of the measured BSA standards. If necessary, dilute the lysate.



**1. Materials**

- sterile glass pipettes
- sterile centrifuge tubes (15 ml)
- sterile reaction vessels
- 4 well Chamberslides Permanox
- 24 well plate

**2. Equipment**

- Biological safety cabinet/ tissue culture hood
- Pipetting aids
- Extraction unit
- centrifuge
- incubator (37°C, 5% CO<sub>2</sub>)
- water bath (37°C)

**3. Solutions**

- differentiation additives:
  - o 50 mg/ml Ascorbate-2-phosphate-solution (Sigma, Bestell Nr. A8960)
  - o 1 mM dexamethasone (1:10-dilution with 100 % EtOH of the 10 mM stocksolution) (Sigma, Bestell Nr. D4902-100mg)
  - o 1 M  $\beta$ -glycerophosphate (Glycerol 2-phosphate disodium salt hydrate, Sigma, Bestell Nr. G9422-10G)
  - o 500 mM IBMX (Applichem, Bestell Nr. A0695.0001)
  - o 100 mM Indomethacin (Sigma, Bestell Nr. I8280-5G)
  - o 100 mg/ml Pyruvate (Sigma, Bestell Nr. P5280-25G)
  - o 40 mg/ml L-Proline (Sigma, Bestell Nr. P8865) o 10 mg/ml Insulin (Sigma, Bestell Nr. I9278-5ML) o ITS (BD, Bestell Nr. 354350)
  - o 10  $\mu$ g/ml TGF- $\beta$ 3 (R&D Systems, Bestell Nr. 100-B-010)
- DMEM High Glucose (4,5 g/l)
- FCS (LONZA, Bestell Nr.DE14-801F, Lot: 8SB016 (Stand 12.06.2013))
- hMSC-culture medium: MSCGM-CD (LONZA, Bestell Nr. 00192125) + 2% FCS

**Differentiation media are to be prepared in quantities that can be used up in one week!**

Medium for osteogenic differentiation:

DMEM + 10% FCS	<b>100 ml</b>	<b>50 ml</b>	<b>10 ml</b>	<i>final concentration: 10% FCS</i>
Ascorbat-2-Phosphat	100 $\mu$ l	50 $\mu$ l	10 $\mu$ l	<i>50 <math>\mu</math>g/ml</i>
$\beta$ -Glycerophosphat	1 ml	500 $\mu$ l	100 $\mu$ l	<i>10 mM</i>

Erstellt

von:

Amrehn/Reboredo

Gültig ab:




Dexamethason	10 µl	5 µl	1 µl	100 nM
--------------	-------	------	------	--------

Medium for adipogenic differentiation:

DMEM + 10% FCS	100 ml	50 ml	10 ml	<i>final concentration:</i> 10% FCS
Dexamethason	100 µl	50 µl	10 µl	1 µM
IBMX	100 µl	50 µl	10 µl	500 µM
Insulin	100 µl	50 µl	10 µl	1 µg/ml
Indomethacin	100 µl	50 µl	10 µl	100 µM

Medium for chondrogenic differentiation:

DMEM HG	100 ml	50 ml	10 ml	<i>final concentration:</i> -
Ascorbat-2-Phosphat	100 µl	50 µl	10 µl	50 µg/ml
Dexamethason	10 µl	5 µl	1 µl	100 nM
Na-Pyruvate	100 µl	50 µl	10 µl	100 µg/ml
L-Proline	100 µl	50 µl	10 µl	40 µg/ml
ITS	100 µl	5 µl	1 µl	1 %
(TGF-β3  always add fresh to the medium! – see also below)	100 µl	50µl	10 µl	10 ng/ml



#### 4. Protocol

- Turn biological safety cabinet on
- Detach and count mesenchymal precursor cells (MSCs)

Osteogenic or adipogenic differentiation in 4 well Chamberslides Permanox or on glass slides in 24 well plate:

- Per assay 2 2 differentiation assays (Diff.) and 2 negative controls (NK) are cultivated

Diff	Diff	NK	NK
------	------	----	----

- Per chamber 100.000 cells, or per well 50.000 cells are seeded and at first each chamber is filled up with 900  $\mu$ l, or each well with 500  $\mu$ l of the stem cell medium and cultivated to a confluency of 70%.
- Note: For the negative control stem cell medium is continued to be used and for the differentiation assay the respective (osteogenic or adipogenic) differentiation medium.
- For **osteogenic differentiation** the MSCs are cultured for **28 days** with the culture medium
- For **adipogenic differentiation** the MSCs are cultured for **14 days** with the differentiation medium
- Changing the medium needs to be done thrice a week (Mon, Wed, Fri).

Chondrogenic differentiation in Differenzierung in pellet culture:

- Chondrogenic differentiation is done in a 24 well plate
- At least one differentiation assay and one negative control is needed
- Centrifuge 250.000 cells per assay in a 15ml centrifuge tube for 15 minutes at 1200/rpm
- Incubate overnight in in incubator
- Transfer into a 24 well plate (1 aggregate/well) the day after
- Carefully overlay aggregate with 300  $\mu$ l differentiation medium
- Note: for the negative control the chondrogenic differentiation medium is used without TGF- $\beta$ 3; for the differentiation assay the differentiation medium is used with TGF- $\beta$ 3.
- **TGF- $\beta$ 3 is always added afresh to the medium before medium is changed (1  $\mu$ l TGF- $\beta$ 3 /2ml chondrogenic medium)!** Medium should always be prepared for all differentiation assay (see remarks)
- For **chondrogenic differentiation** pellets are cultivated with the differentiation medium for **21 days**
- Medium should be changed twice a week (Mon, Fri).

#### 5. Remarks

- If not all of the TGF- $\beta$  of one aliquot is needed do NOT freeze again but store it in the fridge (at 4 °C) until medium is changed next.
- With chondrogenic differentiation the differentiation medium (not the stem cell medium) is used from the beginning.

## 1. Materials

- Polyethylene embedding moulds (Heraeus Kulzer)
- Embedding cassettes ([see annotations](#))

## 2. Equipment

- Desiccator
- Vacuum pump
- Heat sink

## 3. Solutions and chemicals ([see annotations](#))

- Technovit 9100 bundle (Heraeus Kulzer, order number 64715444), consisting of:
  - Basic solution, stabilized (1l)
  - PMMA-Powder (120g)
  - Hardener 1 (8 bags á 1g)
  - Hardener 2 (10 ml)
  - Polymerization regulator (5 ml)
- Paraformaldehyde, 4% solution
- Ethanol 96% (Roth, order number T171.4)
- Isopropyl alcohol (Roth, order number 6752.5)
- Xylenes (Sigma, order number. 1644)

## 4. Protocol

### - Sample fixation and dehydration:

- The sample is fixated in an embedding cassette with paraformaldehyde solution. ([see annotations](#))
- Dehydration can be done by hand or with the embedding station. If the embedding station is used, make sure the program stops in the second xylene beaker. There is also a preconfigured program, number 8, which uses the hereafter listed times.
- The dehydration process is broken down in the following table:

Step	Solution	Concentration	Time*
Fixation	PFA	4 %	2 h
Washing	ddH <sub>2</sub> O	-	2 h
Dehydration	Ethanol	70 %	2 h
	Ethanol	80 %	2 h
	Ethanol	96 %	2 h
	Isopropyl alcohol	abs.	min. 2 h
	Isopropyl alcohol	abs.	min. 2 h
	Xylene	abs.	min. 2 h
	Xylene	abs.	min. 2 h

\*: [see annotations](#)

times relate to processing at room temperature

### - Sample pre-infiltration and infiltration:

- **All following steps need to be done in a fume hood!**
- The sample in the embedding casket is now processed by hand according to the following table. All the solutions are already prepared in clearly labeled wide neck bottles. ([see annotations](#))

Step	Solution	Concentration	Time*
Pre-infiltration I	Xylene/Technovit basic solution	1:1	overnight
Pre-infiltration II	Technovit basic solution + Hardener 1	abs.	overnight
Pre-infiltration III	Technovit basic solution <sup>†</sup> + Hardener 1	abs.	overnight at 4°C
Infiltration	Technovit basic solution <sup>†</sup> + Hardener 1 + PMMA-Powder	abs.	overnight at 4°C

†: In these steps either the normal (stabilized) or the destabilized basic solution can be used. The destabilized solution can be used for samples which will be processed immunochemically ([see annotations](#)).

- **Sample embedding:**

- For embedding the polymerization solutions A and B are poured together at a volume ratio of  $A : B = 9 : 1$  and are thoroughly mixed. The resulting solution is quickly transferred to the prepared embedding moulds.
- Now, the samples are quickly inserted into the filled moulds and should be orientated for the polymerization.
- Thereafter, the moulds are filled up to near the brim with the mixed polymerization solution, transferred to a desiccator and degassed with vacuum for at least 5 minutes.
- When no more bubbles appear, the moulds are taken out of the desiccator, closed with the pertaining lid, placed in the heat sink and stored overnight on ice at 4°C to complete the polymerization.
- After completing the polymerization, the samples can easily be pressed out of the moulds.
- The samples can and should be stored at room temperature.

**5. Annotations**

- Although resin embedding is primarily used for hard samples like bone or ceramics, soft tissue can also be processed, for example to create ultra-thin sections for electron microscopy.
- All samples, size permitting, should be handled in embedding moulds from fixation through to infiltration. Bigger samples should be processed in 50 ml falcon tubes. If you have really big samples, please ask either Holger Kirch or Andrea Schwab for further instructions.
- When preparing big samples (one or more dimensions larger than 1 cm) it is suggested to change the PFA solution once or twice during fixation as it is used up while the reaction takes place.
- To calculate the approximate time for all steps from fixation to infiltration, the following rule can be applied: if the sample has no dimension larger than 5 mm, the diffusion speed is 1 mm/h. For bigger samples, the diffusion is slowed to 0.5 mm/h. Furthermore, the density, hardness and geometry need to be factored in, the stiffer/denser the material, the longer the diffusion takes. If you are unsure about the time your sample needs, please ask either Holger or Andrea.
- After fixation, the sample should be washed with ddH<sub>2</sub>O for the same duration it was fixated, to remove excess PFA from the sample. If the sample is bigger, the ddH<sub>2</sub>O can be changed once or twice during washing.
- All solutions should be ready to use in clearly labeled wide neck bottles. Should this not be the case, please contact Holger or Andrea.
- All steps up to infiltration can, in principle, be done with vacuum support, which speeds up the diffusion. If vacuum is used, please keep in mind the vapor pressure of the solutions you work with, so there are no spontaneous evaporation and bubbling. As a rule of thumb, the vacuum should not be lower than 200 mbar.
- When embedding the samples, the moulds need to be filled to the effect that as little air as possible is inside, but the lid should still be closeable without spilling any polymerization solution. Depending on the porosity of the sample, the degassing step should be done two or three times, to minimize the bubbling during polymerization.
- If the samples will be used for immunohistochemical analysis, the destabilized basic solution must be used in every step from pre-infiltration onwards. Every solution used in these steps is available in two variants, one normal and one destabilized. If any of these solutions are empty, contact Holger or Andrea.



## 1. Materials

- sterile graduated glass pipettes
- sterile Pasteur pipettes
- sterile centrifuge tubes, 50 ml
- sterile cryo tubes 1.8 ml
- Cold Protection Gloves, safety goggles, if needed: Dry-Ice Bath for the Transport

## 2. Equipment

- Aspiration Pump
- Freezer (-80 °C)
- Microscope
- Mr. Frosty (should be at room temperature, if not otherwise noted)
- Neubauer Cell Counter
- Automatic pipette (Pipet Boy)
- Eppendorf pipette (1000 µl) with corresponding sterile tips
- Biosafety cabinet
- Liquid Nitrogen Storage Tank (-180 °C)
- Water Bath (37 °C)
- Centrifuge

## 3. Chemicals

- DMSO (Dimethyl sulfoxide) (Sigma, Order Nr. D2438-50ML)
- 70% EtOH

## 4. Solutions

- PBS/EDTA
- 0.05% Trypsine/EDTA Working Solution
- Cell-Specific Culture Medium
- FCS

## 5. Protocol

### Freezing:

- Label the cryo tubes with the following: cell type, number of passage you are coming from (also see Remarks), number of cells/ml, your name abbreviation and date.
- Detach cells according to SOP ‚Passaging Cells‘ and count them.
- Adjust the cell density in solution to  $10^6$  cells per ml.
- Dispense 1 ml of the cell solution into each cryo tube.
- Add the same percentage of FCS to each cryo tube as there is in the cell-specific culture medium. (e.g. if the medium is DMEM + 10% FCS, add another 10%, thus 100 µl, to each cryo tube)
- Also add 10% DMSO (100 µl).
- Close the Cryo Tubes tightly, sort them into the Mr. Frosty and put it into the -80 °C-Freezer at once.
- After 24 hours waiting time the cryo tubes can be transferred into the Liquid Nitrogen Storage Tank. Use either the Mr. Frosty or a Dry-Ice Bath for the Transport.
- Record the location of the tubes in the respective worksheet available on the network drive under ‘Q:\Labor\_Antje\Übersichten\Cryotank\_Lagerplan’.

### Unfreezing:

- Warm up the cell-specific culture medium in the water bath to 37 °C.
- Prepare a 50 ml centrifuge tube with 9 ml of the warmed medium.
- Withdraw the cells from the freezer or the storage tank.
- **Swiftly** warm the cryo tube in the water bath until there is only a tiny amount of ice left in the tube.
- Transfer the cell suspension with the Eppendorf pipette into the prepared centrifuge tube.





- Centrifugate cell suspension: 1200 rpm, 5 min
- Seed cells in desired density into new flasks.
- Record the withdrawal of the tube in the respective worksheet available on the network drive under 'Q:\Labor\Übersichten\_und\_Vorlagen\Cryotank\_Lagerplan'.

## 6. Remarks

- DMSO as a frost protection agent prevents the forming of ice crystals during the freezing, which could destroy cell organelles and thus bring about apoptosis.
- DMSO is cytotoxic at room temperature, i.e. after adding it to the medium, one has to work as fast as possible to get the cells into the freezer, or the cells are likely to get damaged.
- Accordingly, the unfreezing and the following centrifugation should be effected as fast as possible to minimize cell damage. If the cells are hardy (e.g. fibroblasts) and/or more than one flask is going to be seeded, the washing step may be omitted.
- **Regarding the number of passage: as cells are passaged, the number of passage always goes up by one. Freezing of cells acts as an intermediate step, i.e. the continuous culture is interrupted. Thus, the number of passage doesn't go up until the cells are unfrozen and again in culture.**
- The cryo tubes should be handled cautiously, particularly when opening and closing them, to prevent contamination. This holds true especially after warming in the water bath.

### Special remarks for the freezing and unfreezing of Keratinocytes:

#### Freezing:

- All solutions and the Mr. Frosty must be precooled for at least 30 minutes at 4 °C (i.e. in the cold-storage room), to counter the cytotoxic effect of DMSO. The DMSO is **not** cooled, as its freezing point is 18 °C.
- Don't add FCS.
- Only 5% DMSO is added to the medium. Instead of adding a little DMSO to every cryo tube, the whole volume of DMSO is added to the cell suspension and mixed very well, thereafter the suspension is swiftly portioned into the cryo tubes.  
Example: 0.5 ml DMSO is added to 9.5 ml cell suspension.

#### Unfreezing:

- The cryo tube is warmed for approx. 3 minutes in the water bath.
- The cell suspension is added to 9 ml pre-warmed medium and then centrifugated.



### 1. Materials

- 24well-plate
- Sterile glass- and Pasteurpipettes
- Sterile pipette tips
- Centrifuge tubes

### 2. Equipment

- Safety cabinet
- Centrifuge
- Incubator 37°C, 5% CO<sub>2</sub>
- Water Bath (37°C)
- Pipet Boy
- Multistepper or multichannel pipette
- Aspiration Pump
- Eppendorf pipettes
- Neubauer counting chamber and cover glass

### 3. Solutions

- PBS/EDTA
- 0,05% Trypsin/EDTA-Solution
- FCS (LONZA, order number DE14-801F, Lot: 8SB016 (status 12.06.2013))
- Culture medium

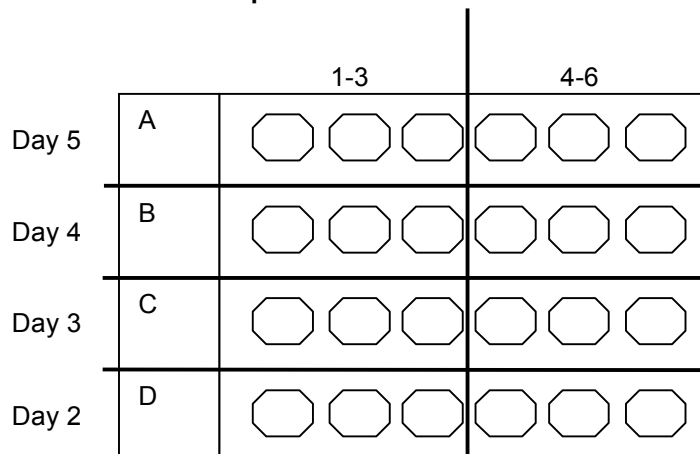
### 4. Protocol

#### Day 1

- Detachment of cells, determination of cell number
- Adjust pelleted cells with **adequate culture medium** to 1x10<sup>6</sup> cells/mL
- Dilute these 1:10 = 1x10<sup>6</sup> cells/10 mL (= 1x10<sup>5</sup> cells/mL; 200 µL = 2x10<sup>4</sup> cells; 50 µL = 5x10<sup>3</sup> cells)

#### Seeding of 24well-plate:

- 5x10<sup>3</sup> cells/50 µL culture medium
- Seed whole plate with cells (see figure; make at least one triplicate [1-3]; 2. Triplicate [4-6] optional)
- Add 2mL of **adequate culture medium** to each well



- Incubate 24h at 37°C, 5 % CO<sub>2</sub>



# TERM

Department Tissue Engineering & Regenerative Medicine

## Growth curve in 24well-plate

**Analysis: Proliferation**

Page 2 of 2

### **Day 2**

- Detach cells in row D (at least 3 wells; triplicate), determine cell number
  - For this purpose:
    - Aspirate medium
    - Rinse each well with 1 mL PBS/EDTA
    - Add 500  $\mu$ L Trypsin/EDTA to each well, incubate for 3 min in incubator
    - stop enzyme reaction by adding 100  $\mu$ L FCS, resuspend, transfer to centrifuge tube
    - Rinse each well with 500  $\mu$ L PBS/EDTA, transfer into centrifuge tube
    - Centrifuge
    - According to pellet size, add 10-100  $\mu$ L Buffer/Medium and Trypanblue and resuspend
    - Count cells (Neubauer counting chamber)

### **Day 3-5**

- See Day 2

## 1. Materials

- measuring cylinder
- 250mL glass bottle
- staining cuvettes
- carrying basket
- steel handle
- funnel
- folded filter
- coverslips
- tweezer

## 2. Equipment

- warming cabinet (60°C)
- fume hood

## 3. Chemicals and solutions

- VE-water
  - tap water
  - Xylene
  - Ethanol (absolut, 96%, 70%, 50%)
  - Hämatoxylin, sauer nach Mayer (Morphisto: order number: 10231)
- optional:
- HCl-alcohol
    - fill 100 ml 50% EtOH in a measuring cylinder
    - add 13,7 ml 1 M HCl by pipetting
    - fill up to 200 ml with 50% EtOH
    - transfer in a glass bottle and mix well
  - Eosin 1% wässrig (Morphisto, order number 10177)
  - 2-Propanol = Isopropanol
  - organic mounting medium Entellan (Merck, order number 1.079.600.500)

## 4. Protocol

- place paraffin sections in the carrying basket with steel handle and put in the warming cabinet for 1 h (paraffin has to be melted completely!)
  - transfer directly in Xylene I of Descending series
- note: From now on the sections shall not fall dry!**

Course of time (min)	Solution	Aim/notes
10	Xylene I	<b>Descending series: Deparaffining, rehydration</b>
10	Xylene II	
3 x dip in and out	EtoH 96%	
3 x dip in and out	EtoH 96%	
3 x dip in and out	EtoH 70%	
3 x dip in and out	EtoH 50%	
	VE-water	
6	Hämatoxylin sauer nach Mayer (Morphisto)	<b>Staining of cell nuclei</b>
	VE-water	<b>Flow weakly until no color is washed out any more</b>
<b>(Optional : if the staining to strong) 2x dip in briefly</b>	<b>HCl alcohol</b>	<b>Differentiate Haematoxylin</b>
<b>after HCl alcohol</b>	<b>VE-Wasser</b>	<b>Rinsing</b>
5	Tap water	<b>Blueing</b>
6	Eosin	<b>Staining</b>
	VE-water	<b>Flow weakly until no color is washed out any more</b>
2x dip in briefly	EtoH 70%	<b>Ascending series: Dehydration</b>
2	EtoH 96%	
5	Isopropanol I	
5	Isopropanol II	
5	Xylene I	
5	Xylene II	

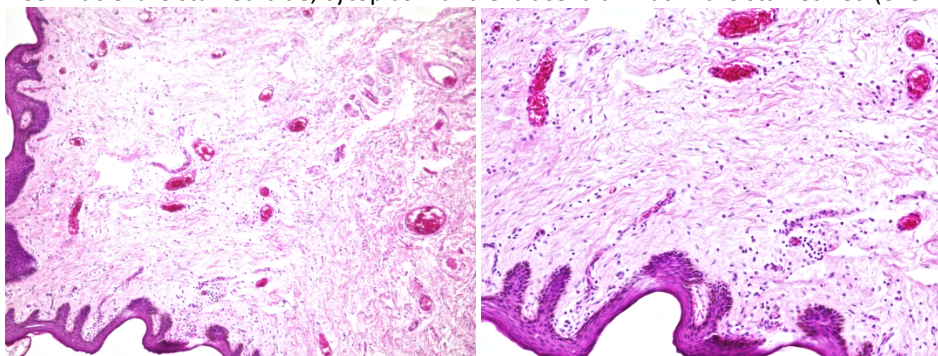
**Note:** If needed, e.g. if heavy contamination can be seen, all solutions will be discarded in the halogenfree organic solvent waste!

If slides show white deposits after deparaffinization, go back with alcohol series unto Xylene and renew all alcohols and Xylene. Then incubate again in Xylene for 10 min and repeat again the descending alcohol series.

- Remove slides out of Xylene with tweezers
- Embed with Entellan and a coverslip, avoid making air bubbles
- Dry over night in the fume hood. Place slides horizontally to avoid slipping of the coverslips.

## 5. Results

- Cell nuclei are stained blue, cytoplasm and extracellular matrix are stained red (overview staining).



10x

20x

## 1. Materialien

- Pipetten
- Wägeschälchen

## 2. Geräte

- Pipetboy
- Waage

## 3. Lösungen

### Für NP40-Puffer

- 50mM Tris base pH 8,0 (MW=121,14g/mol, Sigma, T6066-5KG)
- 150mM NaCl (MW=75,44g/mol, Roth HN00.3)
- 1% (v/v) NP40 (AppliChem 68412-54-4)

### Für RIPA-Puffer

- 50mM Tris base pH 7,5 (MW=121,14g/mol, Sigma, 4855.1)
- 150mM NaCl (MW=75,44g/mol, Roth HN00.3)
- 1mM EDTA (MW=372,24g/mol, Sigma 6381-92-6)
- 1% (v/v) Triton-X 100 (Roth, 3051.2)
- 1% (w/v) Na-Desoxycholat (Sigma, D6750-25G)
- 0,1% (w/v) SDS Pellets (MW=288,38 g/mol, Roth, CN30.3)

### Für modifizierten RIPA-Puffer

- 20mM Tris base pH 8,0 (MW=121,14g/mol, Sigma, T6066-5KG)
- 137mM NaCl (MW=75,44g/mol, Roth HN00.3)
- 10% (v/v) Glycerin (92,09g/mol, Roth, 3783.2)
- 2mM EDTA (MW=372,24g/mol, Sigma 6381-92-6)
- 1% (v/v) NP40 (AppliChem 68412-54-4)
- 0,5% (w/v) Na-Desoxycholat (Roth 3484.7)
- 0,1% (w/v) SDS (BioRad 161-0416)
- 50mM NaF (MW=41,99 g/mol Sigma S7920-100G)
- direkt vor der Verwendung zugeben: 1mM Na-Orthovanadat (Sigma S6508-10G)

## 4. Durchführung

- Sich für einen geeigneten Puffer entscheiden (siehe Anmerkungen)
- Viele Stocklösungen sind vorhanden, sonst herstellen
- Angesetzte Puffer bei 4°C lagern
- Vor der Verwendung Proteinase-Inhibitoren (Proteinase-Inhibitor Cocktail (04693159001 von Roche, 1 Tablette auf 10 ml Lösung) bzw. Na-Orthovanadat) zugeben. Puffer mit Inhibitor kann über wenige Wochen bei -20°C gelagert werden

## 5. Bemerkungen

- Cytoplasmatische Proteine mit einem milden Puffer (NP40-Lysepuffer) lysieren
- Transmembrane oder kernständige Proteine mit stärkerem Puffer (RIPA-Puffer) lysieren
- Phosphorylierte Proteine mit modifiziertem RIPA-puffer lysieren
- NP40 und Triton-X 100 mit abgeschnittener Pipettenspitze pipettieren, da beide sehr zähflüssig sind
- Stammlösungen werden wie folgt gelagert:
- bei RT in Labor „Vorbereitung“: Tris, NaCl, NaF
- bei 4°C im PCR-Labor: Proteinase-Inhibitor Cocktail Tabletten
- bei -20°C: Na-Orthovanadat (Raum 109 im Fach von Sarah und Gudrun)
- bei Herstellung von EDTA-Stocklösung beachten: EDTA löst sich erst bei pH =8.0, entsprechend einstellen

### 1. Materials

- Glass cuvettes with lid, wrapped in aluminum foil
- Cover slips
- Reaction vessels
- Humidity chamber
- Pipette tips

### 2. Equipment

- Heating cabinet (60°C)
- Eppendorf pipettes
- Shaker

### 3. Solutions

- Primary antibody
- Secondary antibody
- Normal serum for blocking
- Isotype control
- Wash Buffer PBS/ TBS + Tween-20 (0,5 %)
- Roticlear (equal to Xylene) and descending alcohol chain for deparaffinization resp. dehydrating
- Antigen unmasking buffers: according to primary antibody
- For the pre-treatment of Chamber slides or Cytospots: 0,2% Triton-X100 in PBS
- If necessary blocking solution: 1% FISH Skin (0,1g), 0,3% Triton-X 100 (30 µl), 1% BSA (0,1 g) in PBS (9970 µl)
- Antibody diluent (DCS Innovative Diagnostik-Systeme #ALI20R500)
- MOVIOL DABCO containing 0,1% DAPI or Fluoromount G

### 4. Protocol

Paraffin sections need to be deparaffinized and their antigens need to be unmasked according to primary antibody. If cells are going to be stained on Chamber slides or Cytospots, they need to be pre-treated with 0,2% Triton-X in PBS for 5 minutes. Frozen sections should be further treated according to fixation.

#### Pre-treatment of paraffinized sections:

- Label sections with your abbreviation and the name of the antibody you want to use
- Don't forget isotype control and optional native tissue section as a positive control!
- Poorly adherent sections should be stored at 38°C overnight before staining
- Place slides into slide rack and incubate for 1 h at 60°C (make sure that the paraffin is fully melted)
- Directly transfer into Roticlear I

**Note: From now on, sections must not dry!**

Time [min]	Solution	Aim/Note
10	Roticlear I	descending chain: deparaffinization, dehydration
10	Roticlear II	
Dip 3 times	Ethanol 96%	
Dip 3 times	Ethanol 70%	
Dip 3 times	Ethanol 50%	
	Demineralized Water ("VE")	Slew
		transfer into washing buffer

Antigen Retrieval (heat-induced):

- Unmasking of the sections with corresponding 1x buffer (100°C preheated with steamer) 20 min
- Directly transfer sections into Wash Buffer and circle them with fat pen

Antigen Retrieval (enzymatic):

- Circle sections with diamond pen
- Pipette enzyme solution onto sections, incubate (see corresponding data sheet)
- Transfer into Wash Buffer 5 min

Pre-treatment of Chamber slides and Cytospots

- 0,2% Triton-X 100 in PBS 5 min
- Wash in Wash Buffer 5 min

IF Staining

- Dilute 5% normal serum (same species like secondary antibody) in antibody diluent for blocking 20 min
- Primary antibody (e.g. mouse AB1 and/or rabbit AB1)  
Incubation conditions dependent on primary antibody
- Wash three times in Wash Buffer 5 min each
- Dilute secondary antibody conjugated with fluorochrome in antibody diluent  
(e.g. donkey anti-mouse-Cy5 and/or donkey anti-rabbit-Cy2)  
Incubation at room temperature (keep dark) 60 min
- Wash three times in Wash Buffer 5 min each

Example for double staining with both primary antibodies stemming of the same species:

- Dilute 5% normal serum (same species like secondary antibody) in antibody diluent for blocking 20 min
- Incubation with first primary antibody (e.g. mouse AB1)
- Wash three times in Wash Buffer 5 min each
- First secondary antibody with fluorochrome (e.g. donkey anti-mouse-Cy5)  
Incubation at room temperature (keep dark) 60 min
- Wash three times in Wash Buffer 5 min each
- **Dilute 5% normal serum (e.g. mouse) in antibody diluent for blocking 20 min**
- **Incubation with second primary antibody (mouse AB2)**
- **Wash three times in Wash Buffer 5 min each**
- **Incubation with second secondary antibody (e.g. donkey anti-mouse-Cy2)**  
**Incubation at room temperature (keep dark) 60 min**
- **Wash three times in Wash Buffer 5 min each**
  
- Mount samples with MOVIOL DABCO containing 0,1% DAPI, Fluoromount G + DAPI according to fluorochrome
- Let samples dry overnight, store in a dark place!

**5. Notes**

- Before first-time performance of multiple stainings: discuss procedure with Christa!





## 1. Materialien

- sterile Pasteurpipetten
- sterile Glaspipetten
- T150 Zellkulturflaschen
- 50ml-Zentrifugenröhrchen
- sterile Pinzette
- 10ml-Einmalpipetten
- Zellzählkammer

## 2. Geräte

- Sicherheitswerkbank
- Brutschrank (37°C, 5% CO<sub>2</sub>)
- Absaugeinrichtung
- Pipettierhilfe
- Wasserbad (37°C)
- Zentrifuge
- Mikroskop

## 3. Lösungen

- MSC-Kulturmedium:  
MSCGM-CD (LONZA, 00190632) + 2% FCS + 1% Antibiotikum
- 1x Lysis Puffer (NEB, 9803)
- PBS<sup>+</sup>
- Trypanblau (0,4%)

## 4. Durchführung

### Isolation:

- Spongiosa in 50ml-Zentrifugenröhrchen mit steriler Pinzette überführen (max. halb füllen)
- vorgewärmtes PBS<sup>+</sup> zugeben (ca. 20ml pro Durchgang zugeben)
- kräftig schütteln, um die Zellen aus der Spongiosa herauszuwaschen
- Überstand mit Einmalpipette aufnehmen und in ein neues Röhrchen überführen
- so lange wiederholen, bis die Spongiosa fast weiß ist
- gesammelte Zellsuspension für 5 min bei 300 xg zentrifugieren
- Überstand absaugen
- Zellen in ausreichend Medium gut resuspendieren (ca. 25 ml)
- Probe zum Zählen entnehmen (50 µl) und mit 1x Lysis Puffer 1:1 mischen
- Anschließend das Zell-Lysis Puffer Gemisch 1:1 mit Trypanblau mischen (→ Endkonzentration 1:4)
- Zellzahl- und Vitalitätsbestimmung durchführen
- 5 x 10<sup>5</sup> Zellen/T150-Zellkulturflasche aussäen

### Kultivierung:

- nach ca. 3-4 Tagen Überstand (mit Blutzellen) entfernen, adhärenente Zellen mit PBS<sup>+</sup> waschen
- Zugabe von 20 ml Kulturmedium
- Medienwechsel 2x pro Woche

## 5. Bemerkungen

- Alter und Geschlecht des Spenders sowie Tag der Aufarbeitung und Name des Durchführenden in der Biopsatentabelle (unter Q:\Labor\Biopsatentabelle) vermerken

Bei einer „guten“ MSC-Kultur ist die Konfluenz der Primärkultur nach ca. 10-14 Tagen zu erwarten.

### weitere Kultivierung:

Bei einer Aussaat von 4x10<sup>5</sup> Zellen pro T150-Zellkulturflasche in den weiteren Passagen ist nach ca. 7 Tagen mit Konfluenz zu rechnen. Bis Passage 5 verwendbar.

### 1. Materialien

- Rattenschwänze (8-10 Wochen alt/Geschlecht unspezifisch)
- Skalpellhalter mit Skalpellklingen
- sterile Glaspipetten
- sterile Pasteurpipetten
- sterile Zentrifugenröhrchen 15 ml
- Hackenpinzette
- Sterile Petrischalen 14 cm
- Klemmscheren
- 250 ml Glasflasche
- sterile Spinnerflask
- sterile Metallwanne
- 1l-Becherglas
- sterile Zentrifugenbecher
- sterile Magnetrührstäbchen

### 2. Geräte

- Sicherheitswerkbank
- Pipettierhilfe
- Zentrifuge
- Rührreaktor
- Magnetrührer
- Analysenwaage

### 3. Lösungen

- PBS<sup>-</sup>
- 70% EtOH
- sterile Essigsäure (0,1%)

### 4. Durchführung

- Sterile Metallwanne mit PBS<sup>-</sup> befüllen
- Rattenschwänze einlegen und auftauen lassen
- Rattenschwänze für 2 min in ein 1l-Becherglas mit 400 ml 70% EtOH einlegen
- Rattenschwänze einzeln mit einer Pinzette entnehmen, in eine Petrischale ablegen und die Schwanzhaut mit einem Skalpell der Länge nach mindestens zu zwei Drittel aufschneiden
- Schwanz am Ende der Schnittstelle mit einer Hackenpinzette festhalten, die Haut mit einer zweiten Hackenpinzette abziehen und entsorgen
- Die abgehäuteten Schwänze in eine zweite Metallwanne mit PBS<sup>-</sup> ablegen
- Die Schwänze mit einer Pinzette am Schwanzende halten und 2-3 cm vom Schwanzende entfernt mit einer Klemmschere abklemmen, drehen und die Sehnen herausziehen
- Die isolierten Sehnen vom Schwanzstück mit einem Skalpell abtrennen und in einer Petrischale mit PBS<sup>-</sup> Puffer sammeln, Das Schwanzstück verwerfen
- Den Vorgang wiederholen, bis die Sehnen aus dem ganzen Schwanz herausgezogen sind
- Isolierte Sehnenstücke dreimal mit PBS<sup>-</sup> Puffer spülen. Den Puffer mit einer Pipette vorsichtig absaugen und dabei die Sehnenstücke mit einer Pinzette zurückhalten, damit sie nicht mit abgesaugt werden.
- Die Fasern 1x mit 70% EtOH spülen, vorsichtig absaugen und erneut 70% EtOH zugeben
- 10 min inkubieren zum Zweck der Desinfektion
- Anschließend dreimal mit PBS<sup>-</sup> Puffer spülen
- 5 ml des letzten Spül-Puffers aus der Petrischale abnehmen und in ein Zentrifugenröhrchen pipettieren (für Steriltest)
- restliches PBS<sup>-</sup> absaugen
- die Fasern in der Petrischale wiegen

- 500 ml Essigsäure in Spinnerflask vorlegen
- Präparierte Fasern mit einer Pinzette in die Spinnerflask überführen
- Sterilen Rührkern zugeben und Flasche verschließen
- Rührreaktoraufsatz aufsetzen
- Im Kühlraum bei 4°C rühren lassen, bis makroskopisch keine Faserreste oder transparente Klumpen erkennbar sind. (2-3 Wochen)
- Kollagenlösung in die Zentrifugenbecher dekantieren
- 1h bei 4°C mit 17.700 xg zentrifugieren
- Kollagenlösung aus allen Zentrifugenröhrchen in einer Glasflasche sammeln und 20 min auf dem Magnetrührer rühren lassen, Flasche mehrmals vom Rührer nehmen und kräftig schütteln
- Probe für die Kollagengehaltsbestimmung entnehmen
- Ggf. fehlende Essigsäuremenge zum Kollagen zugeben
- 20 min auf dem Magnetrührer rühren lassen, Flasche mehrmals vom Rührer nehmen und kräftig schütteln
- in 50 ml Zentrifugenröhrchen aliquotieren (zwischen 5 und 10 ml Aliquots) und bei -20°C bis zum Gebrauch lagern

## 5. Bemerkungen

- Sobald ein Aliquot der Kollagenlösung aufgetaut ist, bei 4°C lagern, innerhalb von 10 Wochen aufbrauchen und nicht wieder einfrieren!

### 1. Materials

- Sterile Glass Pipettes
- Sterile Laboratory Bottle 250 mL

### 2. Equipment

- Safety Cabinet
- Eppendorf Pipettes 100/100 µL with Sterile Tips
- Pipet Boy

### 3. Solutions

- 232,5 mL 2x concentrated DMEM Medium
- 7,5 mL 3 M HEPES Solution
- 2,5 mL Chondroitin Sulfate Solution (5 mg/ml in PBS)
- 7,5 mL FCS (Fetal Calf Serum)

### 4. Protocol

- Add components for 250 mL of gel neutralization solution (Ger. „GNL“) to a 250 mL laboratory bottle and mix

### 5. Notes

- Store at 4°C
- Durability: 6 months



### 1. Materials

- sterile glass pipettes
- sterile pasteur pipettes

### 2. Equipment

- Safety Cabinet
- Incubator 37°C, 5% CO<sub>2</sub>
- Water bath (37°C)
- Pipet Boy
- Aspiration Device

### 3. Solutions

- Cell-specific culture medium with supplements and antibiotics (if needed)

### 4. Protocol

- Warm up cell-specific culture medium in water bath (37°C)
- Label culture flask: cell type, number of passage, date, your name abbreviation
- Turn on safety cabinet, let it run for 15min, clean working surface with EtOH 70% and wipe with disposable tissues
- Open sterile glass and Pasteur pipettes under safety cabinet
- Take medium bottle from water bath and pose under safety cabinet, place lid face-down when opening the bottle (the opening of the lit showing down)
- Open cell culture flask, place lid like-wise, aspirate medium with Pasteur pipette
- Add new medium (T25 = 2-3 ml, T75 = 6-9 ml, T150 = 18-20 ml)
- If drops of medium remain within the neck of the flask, aspirate them with Pasteur pipette
- Close cell culture flask and place in incubator

### 5. Note

- Attention: Lid and neck of the medium bottle must be kept clean and dry, especially after warm-up in the water bath, to avoid contamination!

### 1. Materialien

- Deckgläser
- Pasteurpipetten
- Pipettenspitzen
- 15ml-Zentrifugenröhrchen

### 2. Geräte

- Abzug

### 3. Lösungen

- Leitungswasser
- PBS<sup>-</sup>
- VE-Wasser

### 4. Chemikalien

- 99% Isopropanol = 2-Propanol
- Oilred O
- 4% Paraformaldehyd (PFA)
- 60% Isopropanol
- Hämatoxylin
- wässriges Eindeckmittel Aquatex

### 5. Durchführung

Herstellung der Färbelösung zum Anfärben der Lipidtröpfchen:

- Stammlösung: 0,5 g Oilred O in 100 ml 99%igem Isopropanol lösen
- Gebrauchslösung: 6 Teile der Stammlösung mit 4 Teilen VE-Wasser mischen, **24 h** stehen lassen und vor Gebrauch filtrieren

Ablauf der Ölrot-Färbung:

**Beachten: Alle Lösungen werden in die halogenfreien organischen Lösemittelabfälle entsorgt!**

Zeitablauf [min]	Lösung	Ziel/Bemerkung
1x spülen	PBS <sup>-</sup>	
10	4% PFA	Fixieren
1x waschen	VE-Wasser	
5	60% Isopropanol	
10	Färbelösung ( <i>vom Vortag!!!</i> )	Anfärben der Lipidtröpfchen
1x waschen	60% Isopropanol	
1x waschen	VE-Wasser	
30 sec	Hämatoxylin	Anfärben der Zellkerne
1	Leitungswasser	Bläuen

- Objektträger in VE-Wasser überführen
- mit Aquatex und einem Deckgläschen wässrig eindecken (luftblasenfrei!)
- über Nacht unter dem Abzug trocknen lassen, dabei darauf achten, dass die Objektträger waagrecht positioniert werden, um ein Verrutschen der Deckgläser zu verhindern.

### 6. Ergebnis

- Die Zellkerne sind blau, die Lipidtröpfchen rot angefärbt (adipogene Differenzierung).



## 1. Materials

- sterile glass pipettes
- sterile Pasteur pipettes
- Cell culture flasks
- Centrifuge tubes
- Neubauer cell counting chamber

## 2. Equipment

- Safety cabinet
- Incubator (37°C, 5% CO<sub>2</sub>)
- Water bath (37°C)
- Pipet boy
- Aspiration device
- Centrifuge
- Cell counter
- Microscope

## 3. Solutions

- Washing Buffer: PBS/EDTA Solution (see SOP)
- Detachment buffer: Trypsin/EDTA working solution (0.05 % in PBS/EDTA) (see SOP)
- Cell-specific culture medium with supplements and/or antibiotics, if needed
- FCS
- Trypan blue (0.4%)

## 4. Protocol

### General Remarks:

All cells that can easily be detached from the culturing surface (e.g. most of cell lines, primary fibroblasts) may be detached directly with trypsin solution without prior incubation in PBS/EDTA solution. **Reaction time of the enzyme should not exceed 5 minutes.**

**Cells that cannot easily be detached** (e.g. primary keratinocytes) **need to be incubated in PBS/EDTA solution for at least 10 min prior** to adding detachment buffer. After this incubation, cells should already partly show a globular shape and have loosened their attachment. If this is not the case, incubation in PBS/EDTA solution needs to be repeated.

Trypsin reaction time should never exceed 5min, as cell damage may occur!

- Control cell culture under the microscope for typical criteria (e.g. morphology, cell density, contamination)
- Warm up all needed washing and detachment buffers as well as cell-specific medium and FCS (37°C)
- Label new cell culture flask(s): cell type, number of passage, date, your name abbreviation
- Prepare safety cabinet for use
- Take washing and detachment buffer from water bath, wipe dry and disinfect
- Aspirate medium, add washing buffer (T25: 4 ml, T75: 10 ml, T175: 15 ml), rinse and aspirate
- Optional: add washing buffer (T25: 2 ml, T75: 5 ml, T175: 9 ml) and incubate in incubator for 10min
- Repeat last step, if necessary (if cells are not globular)
- Add detachment buffer (T25: 2 ml, T75: 5 ml, T175: 9 ml), incubate in incubator for max. 3-5 min
- Check cell detachment under microscope. If needed, gently tap the flask to enhance detachment
- Take FCS from water bath and pose under safety cabinet, place lid face-down when opening the bottle (the opening of the lid showing down)
- Stop enzyme reaction by adding > 10% of FCS (centrifuge FCS after thawing at 1200 rpm 5 min, transfer supernatant in sterile 50 ml centrifuge tube, discard pellet)
- Resuspend cells by gently pipetting them up and down, then transfer them to centrifuge tube

- Rinse cell culture flask with PBS/EDTA solution (T25: 4 ml, T75: 10 ml, T175: 15 ml) and transfer all to centrifuge tube
- Centrifuge cell suspension: 1200 rpm, 5 min
- Carefully aspirate supernatant and resuspend pellet in new medium
- Use small aliquot (min. 10  $\mu$ l, max. 50  $\mu$ l) for cell count
- Perform cell count
- Add medium to new cell culture flask(s)
- Seed cells in desired density into the new flasks (Total volume: T25: 2-3 ml, T75: 6-9 ml, T175: 18-20 ml)

**5. Note**

- Attention: Lid and neck of the medium bottle must be kept clean and dry, especially after warm-up in a water bath, to avoid contamination!
- When passaging cells, add one passage to passage number



## 1. Materials

- Glass slides (SuperFrost®)
- Glass cuvette

## 2. Equipment

- Fume hood

## 3. Solutions

- Deionized H<sub>2</sub>O (ddH<sub>2</sub>O)

## 4. Chemicals

- Wood glue (Ponal Express, orange cap, EAN 4015000071291)
- Poly-L-lysin solution 0,1% (Sigma P8920)

## 5. Protocol

### Preparation of Ponal solution

quantity	chemicals	end concentration	procedure
2 g	Wood glue (Ponal)	2%	Dissolve in 100 ml ddH <sub>2</sub> O
5 ml	Poly-L-Lysin	0,01%	Mix with 45 ml ddH <sub>2</sub> O

After dissolving both chemicals, the resulting solutions are poured together and mixed to create the working solution.

### Coating process

- Dip glass slides for 10 min at room temperature in Ponal working solution.
- Dry glass slides in racks overnight at room temperature.

## 6. Annotations

- 100 ml Ponal working solution is sufficient to coat up to 100 glass slides.
- Stability of Ponal working solution is limited to a few weeks.
- Coated slides can be stored up to 1 year at room temperature.

## 1. Materialien **Achtung: immer Handschuhe verwenden, sauber arbeiten!**

- Saubere Eppendorf-Caps ohne DNA-Verunreinigungen
- 96-Well-Platte (low profile), kann auch zurechtgeschnitten werden (Vorsicht! Nicht verunreinigen mit DNA! Handschuhe!)
- Klebefolie für die 96-Well-Platte (kann auch zugeschnitten werden, wenn nur ein Teil der Platte verwendet wird)
- Alternativ: 8-Well-Stripes mit durchsichtigem Deckel (**low profile!!!**)

## 2. Geräte

- CFX96 von Biorad
- Vortex
- Kleine Zentrifuge
- Pipetten + Filterspitzen

## 3. Chemikalien

- EvaGreen/SYBRGreen Supermix von BioRad (SsoFast EvaGreen Supermix, 172-5202)
- Primer (einmal Forward (F) und einmal Reverse (R)) **Produkt sollte kleiner als 200 bp sein.**
- sauberes Wasser (ohne DNA-Verunreinigungen)
- sauberer TE-Puffer oder Wasser zum Verdünnen der cDNA

## 4. Lösungen

- Primer-Verdünnungen (in Wasser): Stocklösung 100 pmol/μl -> 1:25 verdünnen -> für 0,4 pmol/μl muss man 2 μl je Probenansatz (Probe hat insges. 20 μl Volumen) einsetzen (Ziel: 400 nM Primer-Konzentration)
- cDNA: kann man, je nachdem, wie hoch die Expression ist, verdünnen (TE-Puffer oder Wasser) oder unverdünnt einsetzen

## 5. Durchführung

- Alle Chemikalien auftauen (werden bei -20°C gelagert) und alles auf Eis durchführen
- Der Supermix ist lichtempfindlich: Alufolie um das Cap oder anders vor Licht schützen! Supermix nur einmal auftauen, dann bei 4°C lagern.
- Alle Lösungen vor Verwendung vortexen und abzentrifugieren
- Mastermix ansetzen: pro Probe 10 μl BioRad-Mix, 2 μl F-Primer-Verdünnung, 2 μl R-Primer-Verdünnung, Wasser -> so viel Wasser, dass man zusammen mit der cDNA (1-5 μl) pro Probe insgesamt auf 20 μl kommt
- Für den Mastermix immer ein paar Proben mehr berechnen (sonst reicht er meistens bei der letzten Probe nicht)
- Mastermix vorlegen in der 96-Well-Platte (vorher Plan machen, was wo hin soll!)
- cDNA pipettieren (Duplikate!)
- negativ-Kontrollen (nur mit Wasser statt cDNA) pipettieren
- Folie aufkleben, Gerät über die Software öffnen -> Platte hineinstellen -> Gerät über die Software schließen, Lauf starten

## 6. Bemerkungen

- Plattenbelegungsplan muss vorher mit der Software erstellt werden, Protokoll muss ebenfalls vorher ausgewählt werden (Ansprechpartner: Sarah, Sylvia)
- Auswertung: Bei Verwendung mindestens eines Housekeeping-Genes auch über die Software möglich -> alle Proben müssen dort ausführlich beschriftet sein!
- Primer-Austesten: Gradienten-PCR mit Schmelzkurve und anschließende Agarose-Gelelektrophorese (Kontrolle, ob Doppelbanden vorhanden sind)
- Standardkurven: für jeden Primer sollte die Effizienz über eine Standardkurve ermittelt werden: hierzu das PCR-Produkt dieses Primers isolieren und die Verdünnungen 1:10<sup>3</sup>, 1:10<sup>4</sup>, 1:10<sup>5</sup>, 1:10<sup>6</sup>, 1:10<sup>7</sup>, 1:10<sup>8</sup> in Duplikaten für eine qRT-PCR einsetzen: Software kann aus der Steigung der Geraden die Effizienz berechnen. **Von Biorad wird cDNA für die Standardreihe empfohlen. Falls damit die Standardkurve zu schlecht wird, lieber PCR-Produkt einsetzen.**



### 1. Materialien

- Papiertücher
- Pipetten
- Insterile Pasteurpipetten
- 50 ml Zentrifugenröhrchen

### 2. Geräte

- Gelkammer
- Gießstand
- Gelgläser (pro Gel ein Glas mit sowie ohne Ohren)
- Spacer (pro Gel 2)
- Kamm
- Dummy (dicke Glasscheibe)
- Pipettierhilfe
- Heizblock

### 3. Lösungen

- 10x- SDS- Laufpuffer (1 Liter)  
250mM Tris base (MW=121,14g/mol Sigma T6066-5KG)  
1,9M Glycin (MW= 75,05g/mol Sigma 3908.3)  
1,5% SDS aus Pellets (MW=288,38g/mol Roth CN30.3)
- 5x SDS-reduzierender Probenpuffer (20 ml)  
1,5M Tris base (MW=121,14g/mol T6066-5KG) (pH=6,8)  
2% SDS aus Pellets (MW=288,38g/mol Roth CN30.3)  
10% Glycerin (MW=92,09g/mol Roth 3783.2)  
0,01% Bromphenolblau Na-Salz (MW=691,9g/mol Roth A512.1)  
5%  $\beta$ -Mercaptoethanol (MW=78,13g/mol Roth 4227.3)  
für nicht reduzierenden Puffer  $\beta$ - Mercaptoethanol weglassen
- Lower Tris (1 Liter)  
1,5M Tris base (MW=121,14g/mol Sigma T6066-5KG) (pH=8,8)  
0,4% SDS aus Pellets (288,38g/mol Roth CN30.3)
- Upper Tris (1 Liter)  
0,5M Tris base (MW=121,14g/mol Sigma T6066-5KG) (pH=6,8)  
0,4% SDS aus Pellets (MW=288,38g/mol Roth CN30.3)
- Acrylamid Rotipherese Gel30 (Roth 3029.1)
- APS (40%)  
4g Ammoniumperoxodisulfat (MW=228,20g/mol Roth, 9592.1) in 10 ml steriles Reinstwasser lösen  
1 ml Aliquots einfrieren bei -20°C
- TEMED (Roth, 2367.2)
- Proteinmarker  
Für Coomassie-Färbungen: unstained marker, Peqlab PeqGold Protein Marker,14,4-116kDa, 27-1010
- Glycerin (100%)
- 70% Ethanol
- Coomassie (Einfärber)  
250ml Essigsäure (Roth, 3737.1)  
1000ml Methanol (Sigma,34860-2.5L-R)  
1250ml Reinstwasser  
6,25g Brillant Blau R 250 (Roth, 3862.2)

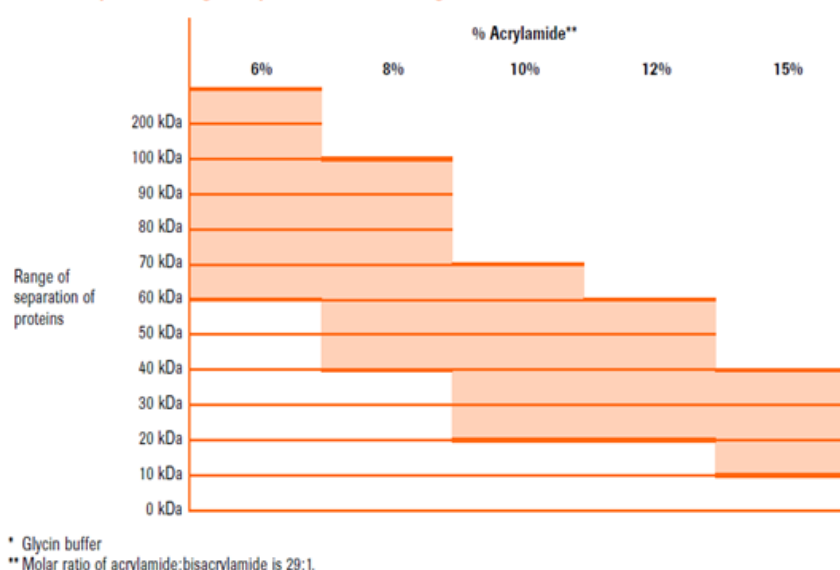
Filtrieren vor Gebrauch

- Entfärber  
10% 2-Propanol (200ml) (Sigma, 33539-2.5L-R)  
10% Essigsäure (200ml) (Roth, 3737.1)  
80% Reinswasser(1600ml)

#### 4. Durchführung

- Pro Gel 2 Glasscheiben sowie Spacer mit VE-Wasser spülen und mit 70% EtOH reinigen. Wird nur 1 Gel benötigt Dummy verwenden
- Zusammenbau der Gelapparatur:
  - Spacer zwischen den Gläsern positionieren.
  - Basisplatte mit den Füßen nach oben stellen, weiße Stifte aufdrehen.
  - Beide Gläser gleichzeitig in Plattenhalterung geben, dabei zeigt Glas mit Ohen nach hinten.
  - Flügelschrauben der Plattenhaltung festdrehen, dabei auf gerade Ausrichtung der Spacer achten.
  - Plattenhalterung entnehmen und Basisplatte umdrehen, Silikonstreifen zeigen jetzt nach oben.
  - Plattenhalterung einsetzen, weiße Stifte einschieben und in dieselbe Richtung nach unten drehen.
  - Dichtigkeit kann mit VE-Wasser überprüft werden
- 10 ml Trenngel ansetzen, ausreichend für 2 Gele. Prozentigkeit ist abhängig von Proteingröße.
- 4,95 ml Sammelgel ansetzen, ausreichend für 2 Gele

Separation ranges of proteins in denaturing SDS-PAGE\*



	Sammelgel(5%)	Trenngel (8%)	Trenngel(10%)	Trenngel(12%)
Upper Tris	1,25 ml	-----	-----	-----
Lower Tris	-----	2,5 ml	2,5 ml	2,5 ml
Acrylamid	0,5 ml	2,7 ml	3,3 ml	4 ml
Wasser	3,2 ml	3,1 ml	2,2 ml	1,5 ml
Glycerin	-----	2 ml	2 ml	2 ml
APS 40%	12 µl	14 µl	14 µl	14 µl
TEMED	12 µl	14 µl	14 µl	14 µl

- Reagenzien in dieser Reihenfolge pipettieren, vor Zugabe von APS und nach Zugabe von TEMED vortexen, zügig arbeiten
- Erst Trenngel ansetzen, während Trenngel auspolymerisiert Sammelgel ansetzen
- Trenngel mit Pasteurpipette aufnehmen und in den Zwischenraum der Gläser füllen, bis er zu 2/3 gefüllt ist
- Mit VE-Wasser auffüllen, damit Trenngel gerade Abschlusslinie bildet.
- Auspolymerisieren abwarten, ca. 10 Min
- VE-Wasser abnehmen, ggf. mit Hilfe von Filterpapier
- Sammelgel bis zu den Ohren einfüllen, zügig den Kamm gerade einschieben
- Auspolymerisieren abwarten, ca. 15 Min
- Plattenhalterung von Basisplatte nehmen und in Gelwann einhängen
- Gelwanne bis zur Fülllinie mit 1x SDS-Laufpuffer füllen, auch Zwischenraum zwischen den Gelen füllen
- Kamm entfernen
- Pro Geltasche können 20 µl, max. 30 µl Probe eingesetzt werden
- Probe mit 5x Ladepuffer versetzen, so dass Ladepuffer mit Probe auf 1x Ladepuffer verdünnt wird
- Proben aufkochen, 5 Min bei 95°C (Heizblock) und abzentrifugieren
- Taschen beladen, pro Gel eine Lane mit 5 µl Marker befüllen
- Deckel aufsetzen und an Stromquelle anschließen
- 1 Gel wird bei 25 mA für 1 Stunde laufen gelassen, Volt und Wattzahl maximal stellen (400 V, 50 Watt). Bei 2 Gelen in der Gelkammer entsprechen 50 mA
- Gel stoppen, wenn die Lämmli-Bande auf Höhe des unteren roten Dichtungsgummi ist
- Gel in Glasschale mit Deckel überführen, mit Coomassie-Färbelösung überschichten
- Inkubation für mind. 1 Std. auf Wippschüttler
- Coomassie in die Flasche „gebrauchtes Coomassie“ umfüllen
- Gel in Entfärber-Lösung entfärben, bei gewünschter Sichtbarkeit der Banden Gel dokumentieren

## 1. Materialien

- Papiertücher
- Pipetten
- Insterile Pasteurpipetten
- 50 ml Zentrifugenröhrchen
- Handschuhe
- 1,5mL Reaktionsgefäße
- Whatman-Paper
- Blotting Membran (Nitrocellulose, Porengröße 0,2  $\mu$ m, Whatman, VWR 732-4016)
- Schale
- Frischhaltefolie

## 2. Geräte

- Gelkammer
- Gießstand
- Gelgläser (pro Gel ein Glas mit sowie ohne Ohren)
- Spacer (pro Gel 2)
- Kamm
- Dummy (dicke Glasscheibe)
- Pipettierhilfe
- Heizblock
- Voltmeter
- Blotkammer
- Wippschüttler
- Falcondreher
- Aufnahmegerät

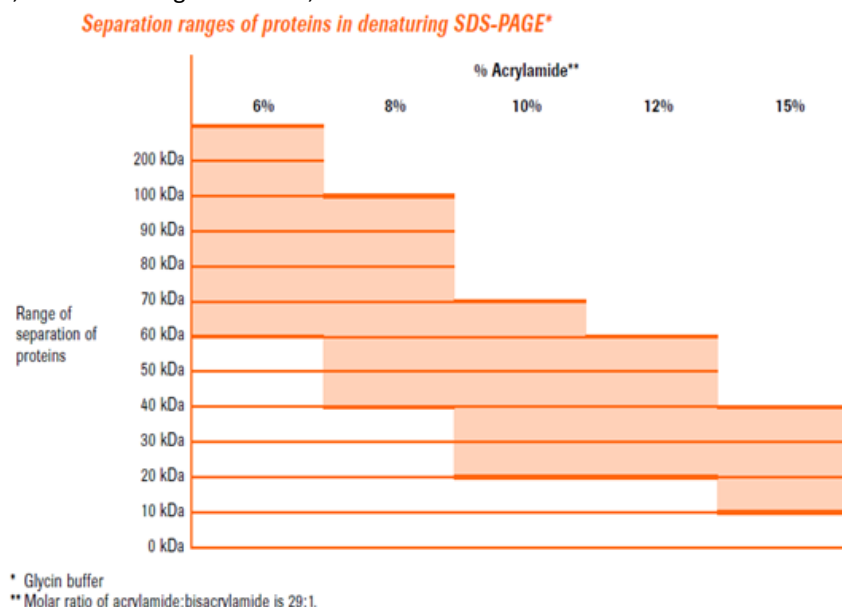
## 3. Lösungen

- 10x- SDS- Laufpuffer (1 Liter)  
250mM Tris base (MW=121,14g/mol Sigma T6066-5KG)  
1,9M Glycin (MW= 75,05g/mol Sigma 3908.3)  
1,5% SDS aus Pellets (MW=288,38g/mol Roth CN30.3)
- 5x SDS-reduzierender Probenpuffer (20 ml)  
1,5M Tris base (MW=121,14g/mol T6066-5KG) (pH=6,8)  
2% SDS aus Pellets (MW=288,38g/mol Roth CN30.3)  
10% Glycerin (MW=92,09g/mol Roth 3783.2)  
0,01% Bromphenolblau Na-Salz (MW=691,9g/mol Roth A512.1)  
5%  $\beta$ -Mercaptoethanol (MW=78,13g/mol Roth 4227.3)  
für nicht reduzierenden Puffer  $\beta$ - Mercaptoethanol weglassen
- Lower Tris (1 Liter)  
1,5M Tris base (MW=121,14g/mol Sigma T6066-5KG) (pH=8,8)  
0,4% SDS aus Pellets (288,38g/mol Roth CN30.3)
- Upper Tris (1 Liter)  
0,5M Tris base (MW=121,14g/mol Sigma T6066-5KG) (pH=6,8)  
0,4% SDS aus Pellets (MW=288,38g/mol Roth CN30.3)
- Acrylamid Rotipherese Gel30 (Roth 3029.1)
- APS (40%)

- 4g Ammoniumperoxodisulfat (MW=228,20g/mol Roth, 9592.1) in 10 ml steriles Reinstwasser lösen
- 1 ml Aliquots einfrieren bei -20°C
- TEMED (Roth, 2367.2)
- Proteinmarker prestained für Western Blot, Biozym ProSieve Quadcolor 4,6-300kDa, 830537
- Glycerin (100%)
- 70% Ethanol
- 10x-Transferpuffer für 2 Liter
- 192mM Glycine (MW= 75,05g/mol Sigma, 3908.3)
- 25mM Tris base (MW=121,14g/mol Sigma, 6066-5KG)
- Für 1x Transferpuffer 20% Methanol zugeben
- zu färbende Primärantikörper und entsprechende HRP-gekoppelte Sekundärantikörper
- Blockierlösung (5% w/v Milchpulver in TBST)
- 10x TBS-Puffer
- 25 mM Tris base (MW=121,14g/mol Sigma, 6066-5KG) (pH=7,6)
- 150mM NaCl (MW=75,44g/mol Roth, HN00.3)
- 1x TBS-Puffer+ 0,05% Tween
- Detection Reagents 1 + 2 (Thermo 32106)

#### 4. Durchführung

- Pro Gel 2 Glasscheiben sowie Spacer mit VE-Wasser spülen und mit 70% EtOH reinigen. Wird nur 1 Gel benötigt Dummy verwenden
- Zusammenbau der Gelapparatur:
  - Spacer zwischen den Gläsern positionieren.
  - Basisplatte mit den Füßen nach oben stellen, weiße Stifte aufdrehen.
  - Beide Gläser gleichzeitig in Plattenhalterung geben, dabei zeigt Glas mit Ohen nach hinten.
  - Flügelschrauben der Plattenhaltung festdrehen, dabei auf gerade Ausrichtung der Spacer achten.
  - Plattenhalterung entnehmen und Basisplatte umdrehen, Silikonstreifen zeigen jetzt nach oben.
  - Plattenhalterung einsetzen, weiße Stifte einschieben und in dieselbe Richtung nach unten drehen.
  - Dichtigkeit kann mit VE-Wasser überprüft werden
- 10 ml Trenngel ansetzen, ausreichend für 2 Gele. Prozentigkeit ist abhängig von Proteingröße.
- 4,95 ml Sammelgel ansetzen, ausreichend für 2 Gele





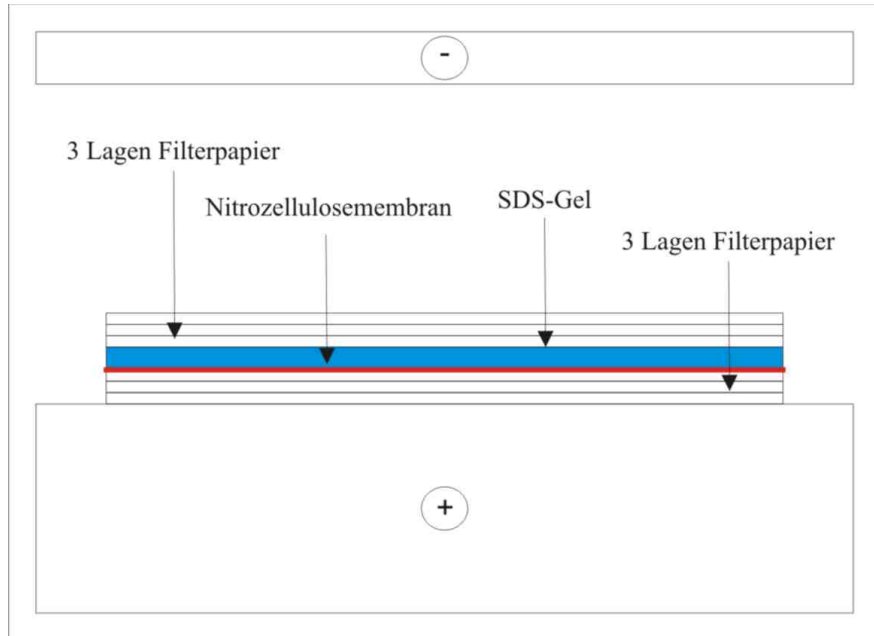
	Sammelgel(5%)	Trenngel (8%)	Trenngel(10%)	Trenngel(12%)
Upper Tris	1,25 ml	-----	-----	-----
Lower Tris	-----	2,5 ml	2,5 ml	2,5 ml
Acrylamid	0,5 ml	2,7 ml	3,3 ml	4 ml
Wasser	3,2 ml	3,1 ml	2,2 ml	1,5 ml
Glycerin	-----	2 ml	2 ml	2 ml
APS 40%	12 µl	14 µl	14 µl	14 µl
TEMED	12 µl	14 µl	14 µl	14 µl

- Reagenzien in dieser Reihenfolge pipettieren, vor Zugabe von APS und nach Zugabe von TEMED vortexen, zügig arbeiten
- Erst Trenngel ansetzen, während Trenngel auspolymerisiert Sammelgel ansetzen
- Trenngel mit Pasteurpipette aufnehmen und in den Zwischenraum der Gläser füllen, bis er zu 2/3 gefüllt ist
- Mit VE-Wasser auffüllen, damit Trenngel gerade Abschlusslinie bildet.
- Auspolymerisieren abwarten, ca. 10 Min
- VE-Wasser abnehmen, ggf. mit Hilfe von Filterpapier
- Sammelgel bis zu den Ohren einfüllen, zügig den Kamm gerade einschieben
- Auspolymerisieren abwarten, ca. 15 Min
- Plattenhalterung von Basisplatte nehmen und in Gelwann einhängen
- Gelwanne bis zur Fülllinie mit 1x SDS-Laufpuffer füllen, auch Zwischenraum zwischen den Gelen füllen
- Kamm entfernen
- Pro Geltasche können 20 µl, max. 30 µl Probe eingesetzt werden
- Probe mit 5x Ladepuffer versetzen, so dass Ladepuffer mit Probe auf 1x Ladepuffer verdünnt wird
- Proben aufkochen, 5 Min bei 95°C (Heizblock) und abzentrifugieren
- Taschen beladen, pro Gel eine Lane mit 5 µl Marker befüllen
- Deckel aufsetzen und an Stromquelle anschließen
- 1 Gel wird bei 25 mA für 1 Stunde laufen gelassen, Volt und Wattzahl maximal stellen (400 V, 50 Watt). Bei 2 Gelen in der Gelkammer entsprechen 50 mA
- Gel stoppen, wenn die Lämmli-Bande auf Höhe des unteren roten Dichtungsgummi ist
- Sammelgel entfernen

#### Blotting

- Pro Gel 6x Whatman-Paper, 1x Blotting Membran auf die Größe des Trenngels zuschneiden
- Blotkammer mit Transferpuffer befeuchten, Whatman-Paper, Gel und Membran in Transferpuffer tränken
- Aufbau Blot:
  - 3x Whatman-Paper
  - Blotting Membran
  - das Gel
  - 3x Whatman-Paper
- Mit einer Pasteurpipette fest über den Stapel rollen, um dazwischen liegende Luftblasen zu entfernen
- Deckel der Blotkammer mit Transferpuffer befeuchten und Kammer schließen
- Dauer des Blottings sowie Stromstärke sind abhängig vom Protein, standardmäßig folgende Einstellungen verwenden:
  - Dauer: 1 - 1,5h (immer das rechte Voltmeter peQLab EV202 verwenden!)
  - Stromstärke: 3mA /cm<sup>2</sup> (ca. 150mA /kleines Gel)

- Volt auf Maximum (sollte sich nach dem Einschalten nicht über 15V einrichten!)
- Wenn der Marker auf die Membran übertragen wurde, war das Blotten erfolgreich



#### Antikörperfärbung

- Blot mind. 1h in Blockierlösung blocken
- Primärantikörper in 5-10 mL Blockierlösung oder TBST verdünnen
- Blots mit der oberen Seite nach innen in die Falcons rollen und auf einem Falcondreher inkubieren (entweder 1-2h bei RT oder ÜN bei 4°C)
- Blots 3x in TBST-Puffer unter Schütteln waschen
- Vor dem Entwickeln sollte das Aufnahmegerät bereit sein! (siehe Bemerkungen)
- HRP-gekoppelte Sekundärantikörper in 5-10 mL Blockierlösung oder TBST in Falcons verdünnen, Blots 1h bei RT inkubieren

#### Entwickeln

- Blots 3x mit TBST-Puffer waschen
- Auf einem Stück Frischhaltefolie die Entwicklungslösung mischen: 2 mL Lösung pro Blot (1mL von Detection Reagent 1 (Peroxide Solution); 1mL vom Detection Reagent 2 (Luminol Enhancer Solution)). Unbedingt vermeiden, Tropfen von der einen in die andere Flasche zu übertragen! Immer frische Spitzen verwenden.
- Blot mit der Oberseite nach unten in die Lösung auf der Frischhaltefolie legen, ½ - 1min entwickeln lassen
- Blot mit der Oberseite nach oben auf den Einschub des Aufnahmegerätes legen. Luftblasen mit dem Finger wegstreichen
- Marker mit einem Kuli nachzeichnen
- Aufnahmegerät schließen, Geräteeinstellung kontrollieren, siehe Bemerkungen.
- Durchführung Western Blot-Aufnahme:
  - bei geschlossener Klappe „Acquire“ auswählen, es öffnet sich neues Fenster
  - „Movie Mode“ auswählen, mit „Go“ starten.
  - Lichtbildaufnahme: bei leicht geöffneter Klappe auf „Acquire“ → „Live“ bzw. nochmals „Acquire“

#### 5. Bemerkungen

- Blot nur mit Handschuhen anfassen!

- Das gesamte Protokoll sollte mit Handschuhen durchgeführt werden. Besonders wichtig ist dies beim Handling der Membran; andernfalls sind nach dem Entwickeln Fingerabdrücke zu sehen.
- Antikörper können in Blockierlösung oder in PBS- verdünnt und bei -4°C gelagert werden, zumindest so lange bis die Milch sauer wird oder man gibt Na-azid 10% (1:200) zu
- Ladekontrollen können verwendet werden, um einheitliche Beladung der Geltaschen nachzuweisen. Färben und Entwickeln kann gemeinsam mit dem Zielantikörper erfolgen, hier muss auf nicht-überlappende Größe von Ladekontroll- und Zielprotein geachtet werden. Alternativ kann Blot nach dem Entwickeln gewaschen und ein zweites Mal gefärbt werden
- Das Aufnahmegerät muss zum Entwickeln heruntergekühlt sein. Es empfiehlt sich, es mindestens 1h vor Benutzung bereits einzuschalten; ist die Software gestartet, kühlt das Gerät schneller. An Mehrfachsteckdose hängen Aufnahmegerät und PC, am Gerät selbst muss zusätzlicher Schalter eingeschaltet werden.
- Einstellungen Aufnahmegerät:
  - Blende: An der Kamera den unteren nummerierten Ring drehen, so dass 0,95 an der Markierung des mittleren Rings liegt
  - Filter: auf Filter Wheel Position 1 einstellen (rote Leuchtanzeige am Gerät)
  - Fokus: Eine Visitenkarte oä. auf den Einschub (höchste Position) legen. Im Live-Modus die Kamera am geriffelten oberen Ring scharf stellen
  - Software
    - Movie Mode: Belichtungszeit kann hier eingestellt werden. Auf Desktop liegt Datei mit Standardeinstellung: 6 frames à 30 Sekunden
    - Excitation: None
    - Emission: Chemi
- Nach Schließen des Aufnahme Fensters öffnen sich automatisch die Bilder zum Abspeichern

## 1. Materials

- Tweezers
- Coverslips
- Glass slides
- Polyethylene-foil 75x25mm (Heraeus 64712818)

## 2. Equipment

- Hard-metal knife
- Rotational microtome (Leica RM-2255)
- Fume hood
- Press

## 3. Solutions

- Deionized H<sub>2</sub>O (ddH<sub>2</sub>O)

## 4. Chemicals

- Xylenes (Roth, A513.1)
- Ethanol 30%, 60% (Roth 34209271)
- 2-Methoxyethylacetate (2-MEA) (Merck 8.06061.2500)
- Acetone (Sigma 32201-2.5 L)

## 5. Protocol

### Cutting slices

- Carefully transfer and install hard-metal knife into rotational microscope.
- Before starting to cut slices, wet surface of polymer block with 30% EtOH to soften polymer block. This step can be repeated several times during cutting.
- Transfer slices on glass slides.
- Add 60% EtOH on top of cut slices allowing the polymer slice to flatten.
- Cover glass slide with PE foil and roll over the foil with the help of a 50 ml Falcon to press the slices onto the glass slides.
- Remove excess EtOH from slides.
- Stack all glass slides and place them into press and tighten screw to apply pressure on the slides.
- Dry slides at 50°C overnight, but **readjust screw on press after approximately 2 h of incubation!**
- after cooling down to room temperature (overnight), loosen the screw and remove PE foil from slides

### Deplastification of 5-7 µm slices resulting from Technovit 9100

Repetitions	Duration	Chemicals
2	20 min	Xylenes
2	20 min	2-MEA
2	5 min	Acetone
1	5 min	ddH <sub>2</sub> O

## 6. Annotations

- Use deplastificated slides directly with staining protocols (rehydration is not necessary).
- Slices or sections thicker than 10 µm can't be deplastificated completely. Instead, the duration of all the deplastification steps is halved, so that only the surface is deplastificated. This way, the stainings will work, but won't be as colorful as with completely deplastificated slices.
- 2-MEA is permanently toxic to female reproduction (<http://www.gifte.de/Chemikalien/2-methoxyethylacetat.htm>).

## 1. Materialien

- 6-Well Platten oder Zellkulturschalen (60,1 cm<sup>2</sup>)
- sterile Einmalpipetten
- sterile Pipettenspitzen mit Filter
- sterile Reaktionsgefäße 1,5 ml
- 50 ml Tubes
- 0,45 µm Filter

## 2. Geräte

- Sicherheitswerkbank S1+S2
- Brutschrank (37°C, 5% CO<sub>2</sub>)
- Wasserbad
- Fluoreszenzmikroskop mit Filter für GFP bzw. RFP
- Vortexer
- Pipetten

## 3. Lösungen

- DMEM Zellkulturmedium mit 10% FCS
- DMEM Medium, serumfrei
- DMEM Zellkulturmedium mit 30% FCS
- Plasmid DNA (lentiviraler Vektor, Verpackungsvektor, Hüllprotein-Vektor), Lagerung bei -20°C
- Transfektionsreagenz z.B. X-treme GENE9 Reagenz von Roche (1 ml # 06 365 787 001), Lagerung bei +4°C  
z.B. PEI

## 4. Durchführung

### Aussäen der virusproduzierenden HEK 293T Zellen (max. p15-20)

- Zellen sollten eine Konfluenz von 70-80% erreichen
- eine Kontrolle (ohne Zugabe von DNA) mitlaufen lassen

für 6 Well (9,6 cm<sup>2</sup>) bei 1 Tag Wachstum → 2x10<sup>5</sup> Zellen aussäen mit 2 ml Medium  
für Schale (60,1 cm<sup>2</sup>) bei 3 Tagen Wachstum → 5x10<sup>5</sup> Zellen aussäen mit 10 ml Medium

### Tag 1 - Transfektion am Beispiel von X-treme GENE9

Reagenz: X-treme GENE9 von Roche

Mengen: berechnet für ein 6-Well (→ für eine 60,1 cm<sup>2</sup> Schale dann die 6-fache Menge einsetzen)

Verhältnis: DNA in µg : 1  
Reagenz in µl : 3

Molares Verhältnis: lentiviraler Vektor : 1 → 0,58 µg pGIPZΔeco(shRNA) GFP/RFP (11774 bp)  
Verpackungsvektor : 2 → 1,15 µg psPAX2 (10703 bp)  
Hüllprotein-Vektor: 1 → 0,27 µg pMD2.G (5824 bp)  
2,00 µg

Finales Volumen: 200 µl

- Durchführung:
- serumfreies Medium (200 µl abzüglich µl an DNA-Mix) in sterile Eppis pipettieren
  - 6 µl X-treme GENE9 (auf RT bringen und vor Gebrauch vorsichtig vortexen) dazupipettieren
  - vorsichtig vortexen
  - DNA als Mix (verdünnt in kl. Menge serumfreien Medium) dazupipettieren
  - vorsichtig vortexen

→ **ab hier S2!!**

- Inkubation 25 Min. bei RT
- inzwischen frisches Medium (10% FCS) auf HEK 293T Zellen geben
- DNA/Reagenz-Mix mit einer 1000 µl Filterspitze nochmals resuspendieren und tröpfchenweise auf die Zellen pipettieren
- Platte /Schale vorsichtig schwenken
- ü.N. 37°C inkubieren

### **Tag 2 - Mediumwechsel**

Medium mit 30% FCS auf Zellen geben um Virusproduktion anzuregen (für 48 h)

### **Tag 3 - Bilder aufnehmen, wenn Reporter gen (wie z.B. GFP) vorhanden**

### **Tag 4 - Virusernte**

Virusüberstand mit steriler Spritze abnehmen und Zellen mittels - 0,45 µM Filter (mit geringer Proteinbindung) oder  
- Zentrifugation bei 2000 rpm abtrennen

Die Zielzellen nach Möglichkeit sofort infizieren und/oder Virus in Aliquots bei -80°C lagern. Wiederholtes Einfrieren und Auftauen des Virus vermeiden!

## **5. Bemerkungen**

Das Herstellen von Lentiviren ist nur unter der Sicherheitswerkbank im 2. Stock, Raum 204 erlaubt und infizierte Zellen dürfen auch nur dort im Brutschrank stehen.

Die Lagerung von Viren bei -80°C ist nur im 2. Stock, Raum 209 möglich.

Folgendes ist zu beachten:

- das Labor darf während der S2-Arbeiten nicht von anderen Personen betreten werden
- bei Arbeiten mit Lentiviren ist Mundschutz zu tragen
- es dürfen nur Einmalpipetten verwendet werden
- Pipettenspitzen mit Filter verwenden
- Abfallsäcke müssen mit S2 gekennzeichnet sein
- Flüssigabfall in Glasflaschen pipettieren, mit Autoklavierband versehen und als S2 kennzeichnen
- den Arbeitsplatz nach Beendigung der Arbeit mit viruzidem Mittel (z.B. Descosept AF) gründlich desinfizieren
- Well-Plates nur in Wannen in den Brutschrank stellen



## 1. Materialien

- sterile Pipetten 5/10/25 ml
- sterile Pasteurpipetten, lang
- sterile Zellkulturflasche
- steriles Zentrifugenröhrchen 15 ml bzw. 50 ml

## 2. Geräte

- Sterilbank
- Brutschrank (37 °C/5 % CO<sub>2</sub>)
- Wasserbad (37 °C)
- Pipettierhilfe
- Absaugeinrichtung
- Zentrifuge
- Zellzählgerät
- Mikroskop

## 3. Lösungen

- PBS<sup>-</sup> / EDTA-Pufferlösung (siehe SOP)
- Trypsin/EDTA (siehe SOP)
- Caco-2-Kulturmedium (siehe SOP): MEM (Minimum Essential Medium Earle von Promocell mit stabilem Glutamin; # C-75220) supplementiert mit:
  - 20 % (v/v) FCS
  - 1 % (v/v) Na-Pyruvat
  - 1 % (v/v) NEAA (Non essential aminoacids)
- FCS

## 4. Durchführung

Die benötigten Lösungen wie PBS- / EDTA-Pufferlösung, FCS und geeignetes Zellkulturmedium werden bei 37 °C im Wasserbad angewärmt. Das Passagieren der Zellen wird wie folgt durchgeführt:

- Zellkulturmedium aus der Kulturflasche absaugen.
- Zellkulturflasche mit PBS- / EDTA-Lösung spülen (kleine Flasche 25 cm<sup>2</sup>: 2 ml, mittlere Flasche 75 cm<sup>2</sup>: 4 ml, große Flasche 175 cm<sup>2</sup>: 8 ml) und wieder absaugen.
- PBS<sup>-</sup> / EDTA-Lösung in die Kulturflasche pipettieren (T 25: 2 ml, T 75: 4 ml, T 175: 8 ml) und für max. 10 min im Brutschrank inkubieren, absaugen (Vorsicht! Zellen können sich bereits ablösen!)
- Trypsin/EDTA zugeben (T 25: 2 ml, T 75: 4 ml, T 175: 8 ml), im Brutschrank für max. 3 min inkubieren.
- Zellen unter Beobachtung (gegebenenfalls unter dem Mikroskop) durch Klopfen vollständig ablösen.
- Enzymreaktion durch Zugabe von FCS (10 %) abstoppen.
- Zellen mit einer Pipette vorsichtig resuspendieren und in ein 50 ml Zentrifugenröhrchen überführen, Zellkulturflasche mit PBS<sup>-</sup> / EDTA-Pufferlösung spülen, um alle Zellen zu überführen.
- Zellen bei 1000 rpm für 5 min abzentrifugieren und Überstand absaugen.
- Zellpellet in definiertem Volumen des geeigneten Zellkulturmediums gut resuspendieren (kleine Flasche 25 cm<sup>2</sup>: 2 ml, mittlere Flasche 75 cm<sup>2</sup>: 3 ml, große Flasche 175 cm<sup>2</sup>: 5 ml)
- 10 µl entnehmen und Zellzahlbestimmung mit Zellzählgerät vornehmen.
- Aussaat der Zellen je nach Bedarf in eine / mehrere Zellkulturflasche/n (T75: 0,7x10<sup>6</sup> Zellen/ T150: 1,4x10<sup>6</sup> Zellen)
- Volumen des Zellkulturmediums auf 3 ml (kleine Flasche: 25 cm<sup>2</sup>), 12 ml (mittlere Flasche: 75 cm<sup>2</sup>) bzw. 25 ml (große Flasche: 175 cm<sup>2</sup>) ergänzen und Zellkulturen zur Weiterkultivierung im Brutschrank inkubieren.

## 5. Bemerkungen

- Caco-2-Zellen werden bei 80 % Konfluenz passagiert (2 Mal pro Woche).



## 1. Materialien

- Sterile Glaspasteurpipetten
- Sterile Glaspipetten
- Eppendorfpipetten mit dazugehörigen Tips
- Weiße 96-Wellplatte
- Neubauerzählkammer

## 2. Geräte

- Tecan Infinite M200
- Laminarflow
- Brutschrank (37°C, 5%CO<sub>2</sub>)
- Wasserbad
- Zentrifuge
- Absaugeinrichtung
- Mikroskop

## 3. Lösungen

- PBS-/EDTA
- PBS+
- Trypsin/EDTA
- FCS
- Kultivierungsmedium der verwendeten Zellen
- Celltiter-Glo Reagenz

## 4. Durchführung

- Zellen in einer Dichte von 5-7x10<sup>3</sup>Zellen/ Well aussäen(je nach Zellart), 3Wells/Bedingung
- Inkubation im Brutschrank für 4Tage
- Am Tag 4 Medium absaugen und zu testende Substanzen auf die Zellen geben(immer Positivkontrolle und Negativkontrolle sowie Leerwert mitführen)
- Vorbereiten des Celltiter-Glo Reagenz, dazu die 10ml Reagenz (weißes Fläschchen) in das Lyophilisat (braunes Fläschchen mit gelbem Deckel) pipetieren ( in diesem Zustand bei -20°C Lagerung wiederverwertbar)
- Tecan Infinite M200 einschalten und Programm vorbereiten
  - 2min Schütteln
  - 10min Inkubation
  - Lumineszens (Label1,keine Abschwächung, Integrationszeit 1000ms, Ruhezeit 0ms)
- Nach gewünschter Inkubation, Substanzen absaugen
- Mit PBS+ 1x waschen
- 100µl Zellkultur-Medium in die gewünschten Wells pipetieren
- 100µl Celltiter-Glo Reagens je Well hinzufügen
- Messung →2min Schütteln
  - 10min Inkubation
  - Lumineszens (Label1, keine Abschwächung, Integrationszeit 1000ms, Ruhezeit 0ms)

## 5. Bemerkungen

- Zellen werden während der Messung lysiert und können somit nicht weiterkultiviert werden